NUCLEAR POWER PLANT AKKUYU

Basic report for «Akkuyu» NPP site

Units 1, 2, 3, 4

AKU.C.010.&.&&&&&.&&&&.002.HC.0004

Revision 1

Moscow,

May 2013

AKKUYU NPP POWER GENERATION JOINT STOCK COMPANY

AKKUYU NGS
ELEKTRİK ÜRETİM ANONİM ŞİRKETİ
Farabi Sokak No: 27 Çankaya-ANKARA
Tel: (0312) 442 60 00 Fax: (0312) 442 60 16
Hitit Vergi Dairesi 031 054 6698 (3)

General Director AKKUYU NPP JSC

_____A.E. Superfin

«17» 05 2013

NUCLEAR POWER PLANT AKKUYU

Basic report for «Akkuyu» NPPsite

Units 1, 2, 3, 4

AKU.C.010.&.&&&&&.&&&&.002.HC.0004

Revision1

Volume 2

Director of Planning and Design Branch JSC
"Concern Rosenergoatom"

_____S.V. Egorov

«15» 05 2013

Technical Director of
AKKUYU NPP JSC

_____A.M. Afrov

«15» 05 2013

Moscow,

May 2013

NUCLEAR POWER PLANT AKKUYU

Basic report for «Akkuyu» NPP site

Units 1, 2, 3, 4

AKU.C.010.&.&&&&&.&&&&.002.HC.0004

Revision 1

Volume 2

Head of Technical Regulation Division

_____I.M. Kogay

«__15__» ____05____2013

Head of Operation Division

_____V.V. Vdovin

«__15__» ____05____2013

Chief Specialist for design solutions

_____A.V. Abramov

«__15__» ____05____2013

Moscow,

May 2013

NUCLEAR POWER PLANT AKKUYU

Basic report for «Akkuyu» NPP site

Units 1, 2, 3, 4

AKU.C.010.&.&&&&&.&&&&.002.HC.0004

Revision 1

Volume 2

Deputy Director

_____I.V. Novak

«_14_» _____05_____2013

Design Chief Engineer

_____I.V. Ivanchenko

«_14_» _____05_____2013

Head Specialist

_____V.I. Dorofeev

«_14_» _____05_____2013

Moscow,

May 2013

BASIC REPORT CONTENTS

APPENDICES

GENERAL CONTENTS OF THE VOLUME 2

LIST OF TABLES

LIST OF FIGURES

ABBREVIATIONS ACCEPTED

Akkuyu NPP	Akkuyu Nuclear Power Plant
ATH	Seismological Institute, National Observatory of Athens (NOA), Greece
BCIS	Bureau Central International de Seismologie
BU	Boğaziçi University, Istanbul
CAFZ	Central Anatolian Fault Zone
CGS	Coast and Geodetic Survey of the United States, NEIS, USA
CMT	Centroid Moment Tensor
CSEM	Centre Sismologique Euro-Mediterraneen
DDA	General Directorate of Disaster Affairs, Ankara, Turkey
DSHA	Deterministic Seismic Hazard Analysis
DSI	General Directorate of State Hydraulic Works, Ankara
DST	Dead Sea Transform
DUSS	Department of Geology, Faculty of Sciences, Damascus University, Syria
EAF	Eastern Anatolian Fault
EERC	Earthquake Engineering Research Center
EFZ	Eskişehir Fault Zone
EHB	Engdahl, van der Hilst and Buland
EIE	General Directorate of Electrical Power Resources Survey and Development Administration, Ankara
FADL	Field Daily Activity Logs
FBFZ	Fethiye-Burdur Fault Zone
FZ	Fault Zone
GCMT	Global Centroid Moment Tensor Project
GII	Geophysical Institute of Israel
GIS	Geographic Information System
GM	Geomagnetic
GMPE	Ground Motion Prediction Equations
GMRT	Global Multi-Resolution Topography
GPS	Global Positioning System
GRAL	National Centre for Geophysical Research, Beirut, Lebanon
HLW	National Research Institute for Astronomy and Geophysics, Helwan

HRVD	Department of Geological Sciences, Harvard University
IAEA	International Atomic Energy Agency
IASPEI	International Association for Seismology and Physics of the Earth Interior
IMST	Institute of Marine Science and Technology
IPRG	Institute for Petroleum Research and Geophysics, Israel
IRIS	Incorporated Research Institutions for Seismology
ISC	International Seismological Centre
ISCJB	International Seismological Centre (own determinations using JB tables)
ISK	Kandilli Observatory and Earthquake Research Institute, Boğaziçi University (BU KOERI). Istanbul, Turkey
ISN	Iraqi Meteorological and Seismology Organization, Iraq
ISS	International Seismological Summary, UK
JSO	Jordan Seismological Observatory. Natural Resources Authority, Jordan
KOERI	Kandilli Observatory and Earthquake Research Institute
KSA	Observatoire de Ksara, Zahle, Lebanon
MED_R	MedNet Regional Centroid - Moment Tensors INGV Italy
METU	Middle East Technical University
MOS	Geophysical Institute-Russian Academy of Science, Obninsk
MTA	Mineral Research and Exploration of Turkey
NAFZ	North Anatolian Fault Zone
NEAF	North East Anatolian Fault
NEHRP	National Earthquake Hazards Reduction Program (USA)
NEIC	National Earthquake Information Center
NEIS	National Earthquake Information Service
NGA	Next Generation Attenuation
NIC	Geological Survey Department (GSD), Cyprus
NPP	Nuclear Power Plant
NSSC	National Syrian Seismological Center, Syria
PGA	Peak Ground Acceleration
PSA	Peak Spectral Acceleration
PSD	Power Spectral Density

PSDM	Pre-Stack Depth Migration
PSHA	Probabilistic Seismic Hazard Analysis
PSTM	Pre-Stack Time Migration
PUL	Pulkovo, Russia
R	Resistivity
RQD	Rock Quality Designation
RYD	King Saud University, Riyadh, Saudi Arabia
SCR	Stable Continental Regions
SHAP	Seismic Hazard Analysis Program
SNSN	King Abdulaziz City for Science and Technology, Saudi National Seismic Network, Saudi Arabia
SSG	Specific Safety Guide
TAEK	Turkiye Atom Enerjisi Kurumu (Turkish Atomic Energy Authority)
TEH	Geophysical Institute, Tehran University, Iran
TGFZ	Tuzgölü Fault Zone
THE	University of Thessaloniki, Greece
USGS	United States Geological Survey
WPNS	WorleyParsons Nuclear Services
ZUR	Schweizerischer Erdbebendienst, Institut fur Geophysik, ETH, Switzerland
ZUR_R	Zurich Moment Tensors, Swiss Seismological Service ETH ETH

6. GEOLOGY, GEOPHYSICS AND SEISMOLOGY

6.1 REGIONAL AND NEAR REGIONAL STUDIES

6.1.1 REGIONAL TECTONICS AND GEOLOGICAL STRUCTURE

6.1.1.1 GENERAL TECTONICS AND GEODYNAMIC FRAMEWORK

Turkey lies along the Eastern Mediterranean sector of the seismically active and tectonically complex Alpine-Himalayan orogenic belt. The active tectonics of Turkey is the consequence of the convergence between the African, Arabian plates in the south and the Eurasian plate in the north. As a result of the convergence the Anatolian region represents a crush zone that consists of numerous blocks forming a crustal mosaic in between (6/101], Figure 6/1.1).

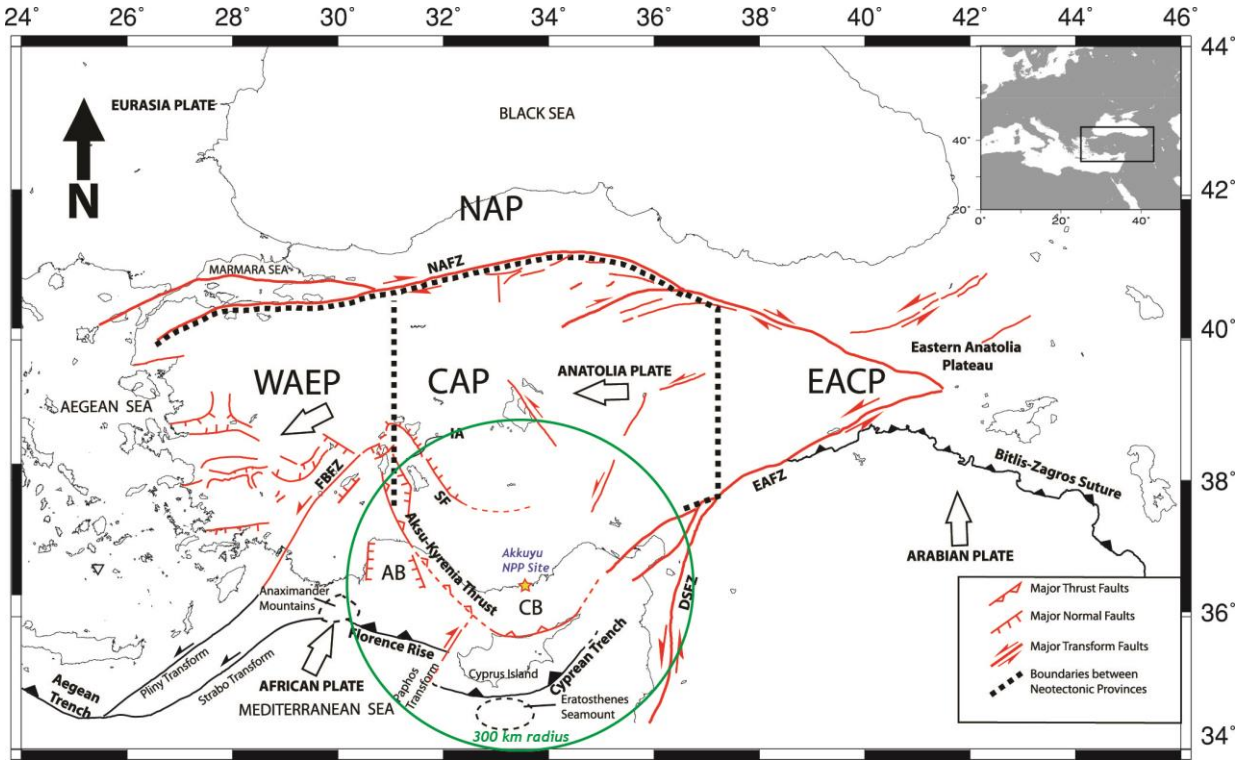

Figure 6/1.1 – Major tectonic and geological features of Turkey. The thick white arrows show the motion directions of the associated plates with respect to Eurasia. The approximate boundaries between zones of different tectonic deformation styles (different tectonic provinces) are indicated with thick dashed lines. These provinces are EACP, Eastern Anatolian Contractional Province; CAP, Central Anatolian Province; WAEP, Western Anatolian Extensional Province; NAP, North Anatolian Province. NAFZ, North Anatolian Fault Zone; EAFZ, East Anatolian Fault Zone; DSFZ, Dead Sea Fault Zone; FBFZ, Fethiye-Burdur Fault Zone; SF, Sultandağ Fault; IA, Isparta Angle; AB, Antalya Basin; CB, Cilicia Basin. ([6/32], modified)

The active crustal deformation pattern reveals two N-S trending compression or crustal shortening: one between the eastern Black Sea and the Arabian plate and the other between the western Black Sea and the Isparta Angle. Since the Black Sea has oceanic lithosphere, it is actually a separate plate. However it can be considered as a block, because the Black Sea is a trapped

oceanic basin that cannot move freely within the Eurasian Plate. The North Anatolian Fault (NAFZ), East Anatolian Fault (EAFZ), Thrace Fault (SF), Hellenic Trench, Cyprian Trench, Dead Sea Fault (DSFZ), and the Bitlis – Zagros Suture Zone form major active tectonic boundaries between these blocks and the plates in the eastern Mediterranean (Figure 6/1.1).

As a result of the convergence between the Arabian and Eurasian Plates continental collision takes place along the Bitlis Suture Zone and the Anatolian Block moves westward along the NAF and EAF relative to the Eurasian Plate[6/101; 6/102; 6/120; 6/152 and 6/200]. GPS measurements indicate slip rates of 24±1 mm/yr. and 9±2 mm/yr. for the NAF and EAF respectively, and a counterclockwise rotation for the Anatolian Block [6/149 and 6/189]. The NAF runs sub-parallel to the Black Sea coast and it surrounds the southern Black Sea margin together with the Thrace Fault Zone and the North East Anatolian Faults (NEAF). The interface between the oceanic lithosphere at the leading edge of the northward moving African Plate in the eastern Mediterranean Sea and the deforming Aegean-Anatolian continental lithosphere forms the northward dipping Hellenic and Cyprian subduction zones in the south (Figure 6/1.1). Since there is a velocity differentiation between the northward motion of the African and the Arabian Plates (10mm/yr and 18 mm/yr, respectively), this difference is accommodated along the sinistral strike-slip Dead Sea Fault that forms the plate boundary between the African and the Arabian Plates.

Geodynamic Framework of the Eastern Mediterranean

The Eastern Mediterranean is commonly interpreted as a relic of the Neothethys Ocean [6/2, 6/207 and 6/92], whose original passive margins are still preserved to the east and to the south in the Levantine and Herodotus basins (Figure 6/1.2).

In the Eastern Mediterranean, active geodynamic processes are basically influenced by three large plates (African, Arabian and Eurasian) and several minor ones (Anatolia, Sinai, Aegean and Adria).

To the north, it is dominated by the northeast-directed subduction of the African plate under the Crete and Cyprus trenches (Figure 6/1.2). It is noteworthy that, whereas thinner oceanic lithosphere is currently subducting under Crete, a thicker continental margin is subducting into the Cyprus trench [6/191]. The Aegean Sea formed in a back-arc setting by thinning of a variety of tectonic units, which were mainly emplaced during the Upper Cretaceous–Paleocene convergence-collision processes [6/33 and 6/190].

According to [6/2], the Hellenic subduction system was active at least since the Late Cretaceous and the back-arc rift developed later. Furthermore, it is noteworthy that despite the long-lasting formation of the Aegean basin (ca. 40 Ma), the extension rate is relatively low, so that no oceanic crust was generated. This area is currently undergoing a widespread regional extension, which can be dated back to the Eocene–Early Miocene [6/63 and 6/124].

The subduction of the African plate under the Crete trench is marked by seismic and volcanic belts, which display a well-defined Benioff zone extending down to about 160-180 km (USGS Earthquake Catalogue, http://neic.usgs.gov/neis/epic) [6/137]. Earthquake focal mechanisms indicate down-dip extension in the slab [6/180]. The angle of the subduction is about 16°, and tends to flatten beneath NE–SW cross sections (i.e. the direction of the subduction parallel to the relative plate motions). The slab dip increases (up to 30–40°) moving southward, where the subduction is oblique or in lateral ramp.

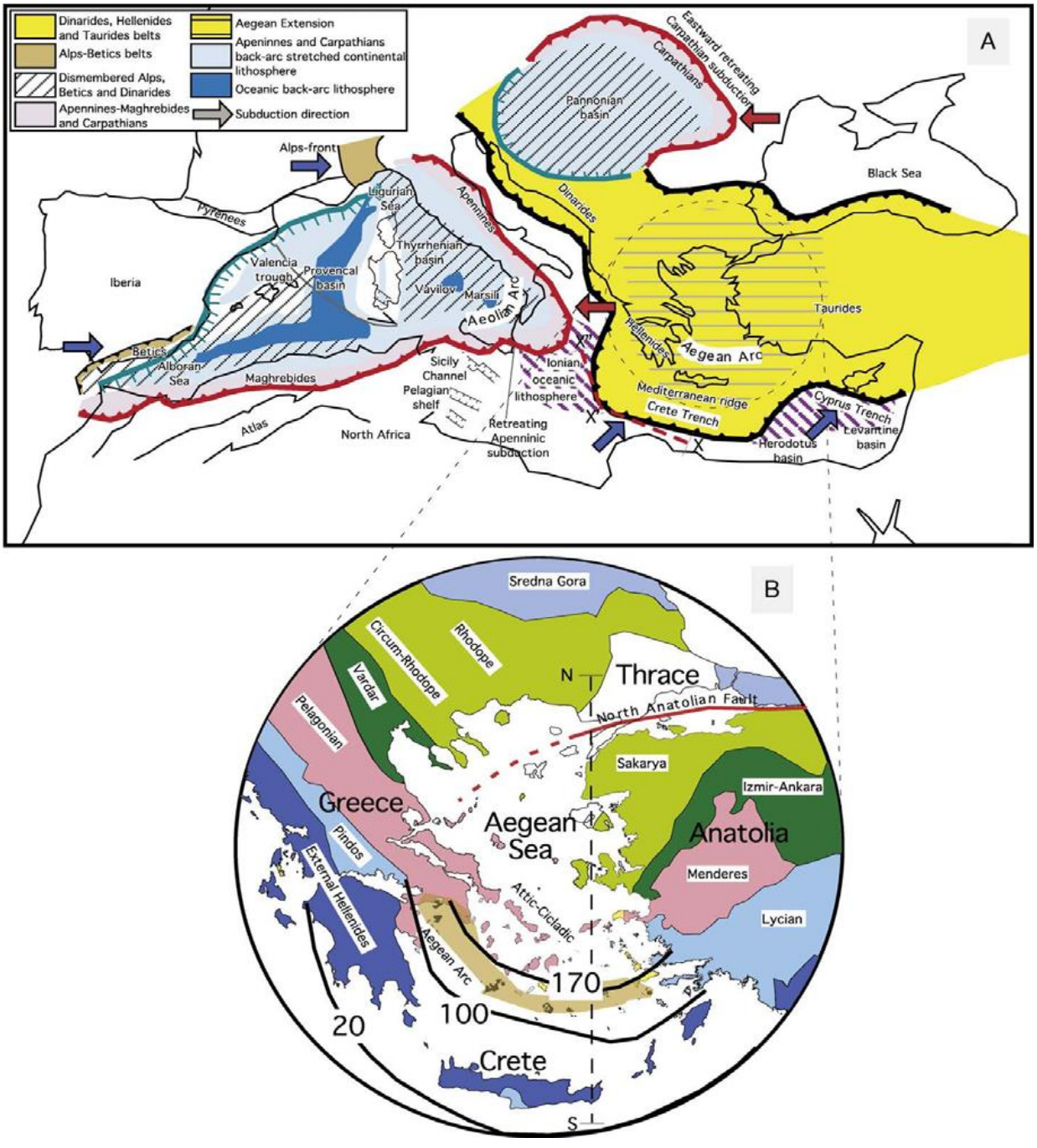

Figure 6/1.2 – Schematic view of the geodynamic framework of the Mediterranean region, [6/2]

Allmendiger (2007) [6/9] and Özeren and Holt (2010) [6/176] using numerous GPS measurements have modeled the active tectonic deformations in Turkey and surrounding regions and produced strain rate maps (Figure 6/1.3).

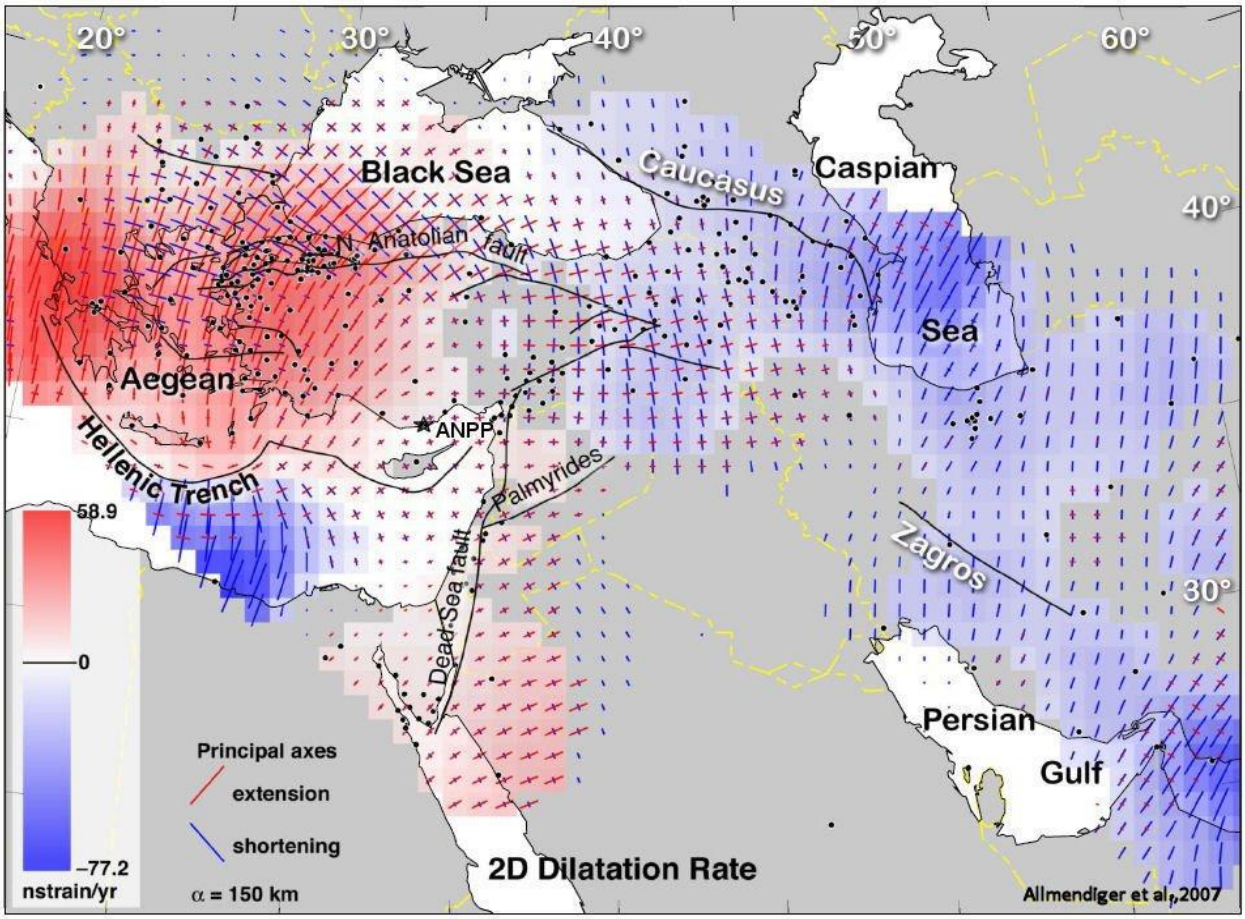

Figure 6/1.3 – The strain rate map of Turkey and surrounding regions [6/9]

These maps indicate that the most pronounced deformation takes place along the North Anatolian and East Anatolian Fault Zones that form the tectonic boundaries of the Anatolian block. These maps also clearly show that eastern Turkey is mainly dominated by compressional deformation as a result of the still ongoing continental convergence between the Arabian and Eurasian Plates along the Bitlis-Zagros Thrust zone and the effects of this convergence is transmitted all the way up north to the Caucasus region. On the other hand the Aegean region is mainly dominated by extensional deformation mainly as a result of the slab pull back along the Aegean subduction zone. The Akkuyu region is the least strained area in Turkey which may partially explain why it was selected for the construction of a nuclear power plant (Figure 6/1.3).

6.1.2 DESCRIPTION OF REGIONAL GEOLOGICAL STRUCTURES

The Anatolian block and its surroundings are neotectonically dominated by the following major structures (Figure 6/1.4):

- Hellenic Trench
- the Antalya and Cilicia basins;
- the Isparta Angle;
- the Tuzgölü and İnönü-Eskişehir Fault Systems (Central Taurus)
- the Central Anatolian Fault Zone (CAFZ) including Ecemiş and Namrun fault zones;
- the Adana Basin;
- the East Anatolian Fault Zone (EAFZ);
- the Cyprus Trench;
- the Dead Sea Rift.

6.1.2.1 HELLENIC TRENCH

The Hellenic Trench subduction zone (including Hellenic and Cyprian Trenches) is part of the larger boundary zone between the Eurasian, African and Arabian plates (Figure 6/1.4). Its origin is linked to the northward motion of the African (Nubian) plate since Oligocene-lower Miocene time [6/233 and references therein].

The most prominent features are a series of linear, seafloor escarpments with more than 2 km of individual relief (trenches). Three NE-SW striking trenches (Ptolemy, Pliny and Strabo trenches) were developed in the eastern part of the trench, with high-angle dips to the southeast. A fourth trench that crosses the floor of the south and central Ionian Sea, strikes on average NW-SE and dips to the southwest. According to Kreemer and Chamot Rooke [6/139] the Pliny and Strabo trenches accommodate 21-23 mm/yr. On the western side, the relative plate motion is accommodated by right-lateral shear along the Cephalonia transform fault (20 ± 1 mm/yr, [6/201]).

Subduction of the oceanic lithosphere is sub-horizontal offshore of Cyrenaica and dips gently to the island of Gavdos, where it plunges beneath Crete, defining a Benioff zone: according to Papazachos [6/180], focal mechanisms of earthquakes along the plate interface show mostly reverse faulting south of Crete and a mixture of reverse-oblique mechanisms at intermediate depths. The former type of faulting is due to N-S (across the trench) compression, the latter is the result of E-W (along the trench) compression at intermediate depths (50-170 km). According to the seismological database, dips are prevalently ranging between 40° and 70°.

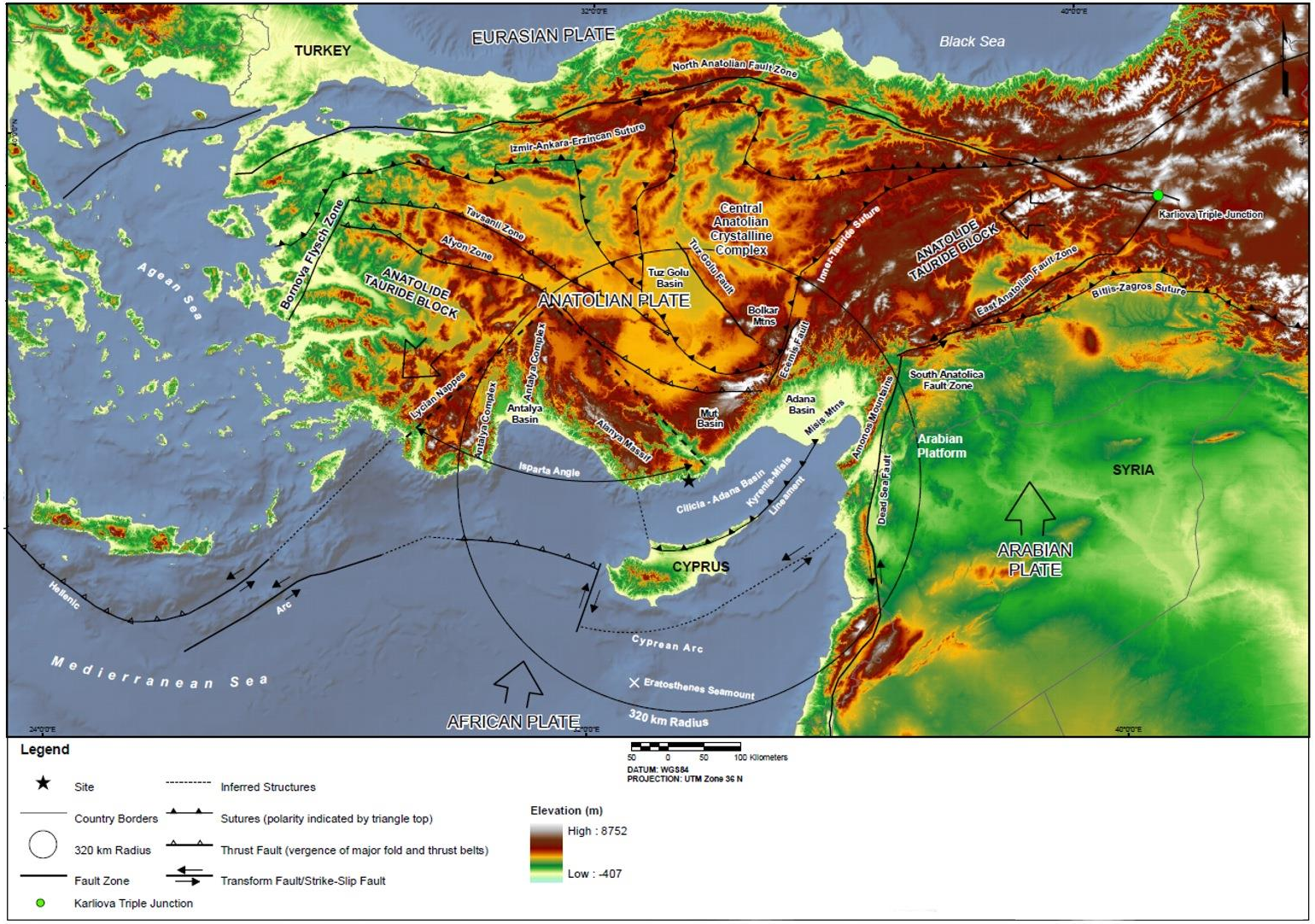

Figure 6/1.4 – Major geotectonic structures in the Akkuyu regional area and surroundings (from [6/38; 6/46; 6/59; 6/60; 6/61; 6/122; 6/1; 6/171; 6/191; 6/211])

With respect to the seismicity associated with the Hellenic Trench, according to Ambraseys [6/12], the largest recent earthquakes did not exceed M = 7.3 in the last century. However, it has to be noted that historical and archaeological studies have suggested that earthquakes which occurred near Crete in 365 AD and 1303 AD [6/100] have been much larger than any Hellenic Trench earthquake that occurred in the last century, in agreement with convergent margins similar to the Hellenic Trench that can commonly produce M > 8 earthquakes [6/105].

The eastern flank of the V-shaped eastern sector of Hellenic Trench is characterized by the presence of the Pliny and Strabo trenches controlled by left-lateral transpressive faults.

At the junction of the Hellenic and Cyprus Trenches are located the Anaximander Mountains that form an area of pronounced seafloor relief. They are bordered to the west by the deep Rhodes Basin (with depths up to 4485 m) and by the shallower (~2600 m) Antalya Basin to the east. The Anaximander Mountains are composed of three distinct seamounts i.e. Anaximander in the west, Anaximenes in the south, and Anaxagoras in the east [6/228].

6.1.2.2 ANTALYA AND CILICIA BASINS

Four seismically determined stratigraphic units have been identified by the authors of Marine Geology special issue n. 221 published in 2005, e.g. [6/145] in the Antalya and Cilicia Basins (Figure 6/1.4).

Unit 1- Plio-Quaternary. Unit 1 is composed of siliciclastic successions of Plio-Quaternary age. The base of this unit is marked by a strong and distinctive reflector, identified in the eastern Mediterranean as the "M-reflector". This Unit is thickest along the central axes of both the Inner and Outer Cilicia basins, and sharply thins toward the Kyrenia Range and the south-western Turkish coast.

Unit 2 – Miocene (Messinian). Unit 2 is composed predominantly of halite alternating with lesser quantities of anhydrite and limestone, and is correlated with the Messinian evaporites.

Unit 3 – Miocene (pre-Messinian). Unit 3 is subdivided into two major seismic stratigraphic subunits. Subunit 3A is composed of fluvio-deltaic successions of mainly Tortonian age; Subunit 3B is mainly composed of middle Miocene turbidite successions.

Unit 4 - Cretaceous–Eocene. The Unit constitutes the acoustic basement in the Adana-Cilicia basin and consists of a diverse collection of regional lithostratigraphic units ranging from the lower Mesozoic to upper Oligocene.

The southern margin of the Antalya basin is bounded by the Florence Rise, the northern boundary of the Mediterranean Ridge. According to Kopf [6/138] and Wdowinski [6/235], the Mediterranean Ridge is affected by reverse faulting and associated earthquakes, under the influence of the active compression to the north (along the Aegean–Cyprus Trench). In fact, seismic profiles

show clear thrust structures (reverse faults) in the deformation front of the accretionary wedge. The seismicity record is characterized by reverse faulting focal mechanisms as well as NW-SE and NE-SW trending strike-slip faults. The convergence rate increases northwestwards from Cyprus to Anaximander Seamount and is in the range of 9-14mm/yr [6/235].

The Cilicia Basin

The Cilicia basin complex is an arcuate and contiguous structure; in detail, two distinct physiographic and structural domains can be distinguished [6/7]:

a) the E–W trending Outer Cilicia Basin, subdivided in three minor domains (southern basin, salt-cored fold belt and northern basin);

b) the NE–SW trending Inner Cilicia Basin and its inland extension, the Adana Basin.

In 1977-1978 MTA (Dr. Boztaş) has carried out a geological and geophysical study of the Cilicia Basin for TEK (Turkish Electricity Authority) [6/39]. This study was based on 6 new seismic lines, two recorded roughly parallel to the Turkish coast and four orthogonal to it: in total, 625 km of seismic profiling. In addition, the results of the cruises of Evans, Mathews and Woodside in 1972/1974 (so-called Shackleton expeditions) were reviewed, where capable faulting in the area had been pointed out for the first time. The purpose was to verify if:

c) there was an equivalent of the North Cyprian fault zone along the Turkish coast;

d) the WNW trending graben structures in the Adana Basin extended towards Akkuyu;

e) the Alanya-Morfu ridge was a faulted block.

Another aim was to provide further information for a better understanding of the broad tectonic setting and geological evolution of the northeastern Mediterranean Basin.

The main results are summarized below:

f) There is a strong reflector on all lines, very likely corresponding to the Tertiary underneath the Messinian evaporites.

g) A thick sequence of Plio-Quaternary sediments fill the basin south of Adana Basin, likely due to the feeding from the Seyhan and Ceyhan rivers.

h) There is an east-west trending graben.

i) In the Cilicia trough there is a system of normal growth-type faults near the Cyprus coast and paralleling it.

j) More toward the center of the basin, a system of deformed sediments elongated in the east-west direction is attributed to diapirism.

k) On the western side of the Cilicia Basin, along the Morfu-Alanya "range", there are active faults with relative throw at the sea floor of less than 60 m; tentatively, a north-south trend is reconstructed for them.

Aksu [6/7] has analyzed 4500 km of multi-channel seismic reflection profiles collected in 1991-92 by the Institute of Marine Science and Technology (IMST - Dokuz Eylül University) and by Turkish Petroleum Corporation. IMST has provided also 1500 km of single-channel seismic reflection profiles.

The analysis of seismic profiles [6/7] has revealed a complex tectonic setting with coexistence of contractional, extensional and transcurrent domains.

Outer Cilicia Basin

The Outer Cilicia Basin is bounded by the Anamur-Kormakiti Zone to the west and Inner Cilicia basin slope to the NE.

The E–W trending basin in the northern sector of Outer Cilicia basin (*Northern Basin)* is situated immediately south of the Turkish coastline and extends southward to the salt-cored fold belt. It is 30–35 km wide, which contains a relatively undisturbed Plio-Quaternary succession.

According to Aksu [6/7], close to the Turkish margin the Basin has a complex architecture dominated by three major systems of extensional faults: 1) a zone of NE–SW trending faults defines the marine extension of the Ecemiş fault zone, 2) a zone of NE–SW trending faults marks the marine extension of the Kozan fault zone, and 3) an E–W trending fault system controls the architecture of the northern margin of the Outer Cilicia Basin. No evidence of Plio-Quaternary reverse faulting exists along the margin of the continental shelf. There are only normal faults which do not appear to cut through the Miocene reflectors. These would be the same faults found by Gökçen [6/95].

Anamur–Kormakiti zone

The Anamur–Kormakiti zone separates the Outer Cilicia Basin in the East from the Antalya Basin in the west.

More recent activity seems to have the marine extension of the Kozan Fault Zone, a NE–SW trending 15 km wide belt delineated by many closely spaced high-angle faults. The westernmost fault is a prominent feature south of the Göksu delta, where it creates a 100–150 meters step on the sea-floor, marking the shelf-edge. Toward the northeast, this fault loses its sea-floor expression as it becomes progressively buried under the Pleistocene deltaic successions of the Seyhan, Ceyhan, Tarsus, and Göksu rivers. However, the inboard portion of the fault system can readily be traced northeast toward the Inner Cilicia and Adana basins [6/7]. The Kozan Fault Zone is described in a separate section later in this report.

6.1.2.3 ISPARTA ANGLE

The Isparta Angle is a north-convex triangular-shaped region which delineates the north-western inland extension of the marine Antalya Basin (it is bounded to the west by the Lycian Nappes and to the east by the Beyşehir, Hoyran and Hadım Nappes (Figure 6/1.4). During the Miocene, the western limb of the Isparta angle, including the Beydağlari carbonate massif experienced a 30° counter clockwise rotation, whereas the eastern limb experienced a 40° clockwise rotation since the Eocene ([6/130; 6/184] and references therein).

The Fethiye–Burdur Fault Zone [6/24], a wide zone characterized by sinistral strike-slip faults with considerable normal dip-slip component, defines the western margin of the Isparta Angle. The FBFZ is defined by NE–SW trending major faults with numerous NW–SE trending shorter faults representing extensional features in a 50km wide shear zone [6/114; 6/231 and 6/103]. Several medium to large earthquakes with different fault plane solutions occurred in this zone. Some authors identified this FZ as a prominent left lateral shear zone. 1957, M= 7.1 Fethiye earthquake and other historical earthquakes (417 and 7th century AD, along Cybra Fault) show evidences of left lateral motion [6/114] and according to Barka and Reilinger [6/24] this left-lateral motion is corroborated with GPS measurements showing a movement of at least 15 mm/yr. Focal mechanism of 1914, M=7 and 1971, M= 6.2 Burdur earthquakes instead indicate normal motion predominantly. October 3, 1914 Burdur M= 6.2earthquake is associated with a 23 km fault rupture along the southeast coast of the Burdur Lake [6/85]. Oblique slip normal fault controlled the margins of several extensional basins.

Detailed studies of the tectonically active depression called Karamık Graben have been conducted by Çiçek and Koçyiğit [6/49]. It has two graben infills separated by an angular unconformity: (a) a deformed graben infill of Late Early Miocene-Middle Pliocene age, and (b) an undeformed neotectonic infill of Plio- Quaternary age. These two graben infills reveal an episodic history for the Karamık Graben, and a Plio- Quaternary age for the extensional neotectonic period in the Isparta Angle. According to these authors the northern border fault was reactivated by the Mw=6.5 Çay earthquake (February, 3rd 2002).

Two extensional phases (phase-I and phase-II extensional periods) interrupted by an intervening short-term contractional phase are recognized [6/135] also in Suhut graben, whose margins are controlled by oblique-slip capable normal faults.

6.1.2.4 CENTRAL TAURUS

In this section the most relevant geological structures located in Central Taurus mountain ranges and in particular the vicinity of the so called Tuzgölü basin are described (Figure 6/1.4).

This is the largest basin in Central Anatolia, located in the Kırşehir block. It is characterized by three major depressions: (1) the Southern Aksaray Depression, which is covered by younger volcanic rocks, and is the largest and least explored area; (2) the Ereğli Depression; (3) the Sultanhanı Depression. According to the gravity and aeromagnetic anomaly maps and their upward continuation [6/21], there is no dividing structure or anomaly to separate the major basin into two basins.

The region is surrounded by major tectonic suture and microplatelets, described by Ketin [6/128] and by Şengör [6/199].

Tuzgölü Fault System

The Tuzgölü Fault system is located at the eastern margin of the Tuzgölü basin (Figure 6/1.5). According to Çemen [6/46], this fault system as well as the Yeniceoba and Cihanbeyli faults that bound the western margin of Salt Lake basin, may have been formed as normal faults suggesting extension or strike-slip faults with a normal component of movement indicating a large transtension at the time of their initiation (Late Maastrichtian).

During the Quaternary the Tuzgölü fault was predominantly reactivated as a normal fault with a right lateral strike-slip component. This is evidenced by (1) a major unconformity between the post-Eocene Koçhisar Formation of the Tuzgölü basin and the underlying Eocene rock units; (2) a well-developed rollover anticline observed on seismic reflection profiles; and (3) a right-step along the Tuzgölü fault zone clearly visible in the field.

In 1983 an earthquake occurred at Kosker along the north-westernmost tip of the TGFZ. Recent seismicity is characterized by moderate events, including two Mw=6.0 events (15.12.2000 and 03.02.2002).

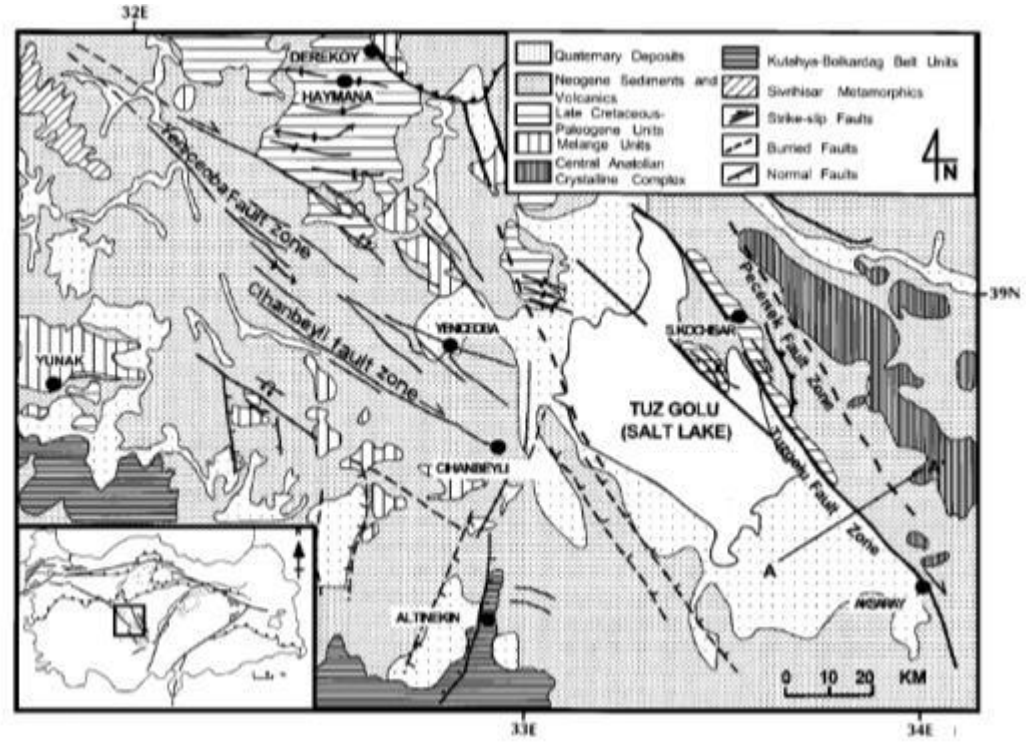

Figure 6/1.5 – Schematic geological map of the Tuzgölü basin and surrounding areas. Source [6/46]

İnönü-Eskişehir Fault System

The İnönü-Eskişehir Fault System (İEFS) is an about 15-25 km wide, 450 km long and NW to WNW trending zone of active deformation (mega shear zone system) characterized mainly by strike-slip faulting [6/198].

The system consists of three fault zones [6/198] (Figure 6/1.6) namely the Alpu Fault Zone (AFZ), the Eskişehir Fault Zone (EFZ) and the Orhaniye Fault Zone (OFZ).

The EFZ constitutes the western to central part of the system. It is made up mostly of N30°W trending right-lateral strike-slip fault segments with normal components. However, the AFZ and OFZ are composed of E-W trending normal and NE to NW trending strike-slip fault segments.

Toward the southeast, this system splays into three fault zones [6/177]. The NW striking Ilıca Fault Zone defines the northern branch of this splay. The middle and southern branches are the Yeniceoba and Cihanbeyli Fault Zones, which also constitute the western boundary of the tectonically active extensional Tuzgölü Basin. The Sultanhan Fault Zone is the southeastern part of the system and also controls the southwestern margin of the Tuzgölü Basin. Structural observations and kinematic analysis of mesoscale faults in the Yeniceoba and Cihanbeyli Fault Zones clearly indicate a two-stage deformation history and kinematic changeover from contraction to extension. N-S compression was responsible for the development of the dextral Yeniceoba Fault Zone. Activity along this structure was superseded by normal faulting driven by NNE-SSW oriented tension that was accompanied by the reactivation of the Yeniceoba Fault Zone and the formation of the Cihanbeyli Fault Zone.

Several strike-slip pull-apart basins occur along the İnönü-Eskişehir Fault System. One of them is the the Mahmudiye-Çifteler-Emirdağ basin. It is an about 25 km wide, 85 km long and NW trending active depression located between Yörükkaracaören and Emirdağ. This basin contains two infills. Older and deformed (tilted and folded) infill, which rests with an angular unconformity on the erosional surfaces of Pre-Miocene metamorphic and nonmetamorphic rocks, consists predominantly of lacustrine carbonates. The younger and undeformed basin infill (neotectonic infill) is composed of Upper Pliocene-Holocene terrace deposits, sandstones, lacustrine mudstone to thin limestones alternation and alluvial fans. Two basin infills separated by an angular unconformity, the deformation pattern of the older basin infill and the active margin-boundary faults in strike-slip nature are indicative of the superimposed character of the Mahmudiye-Çifteler-Emirdağ pull-apart basin [6/198].

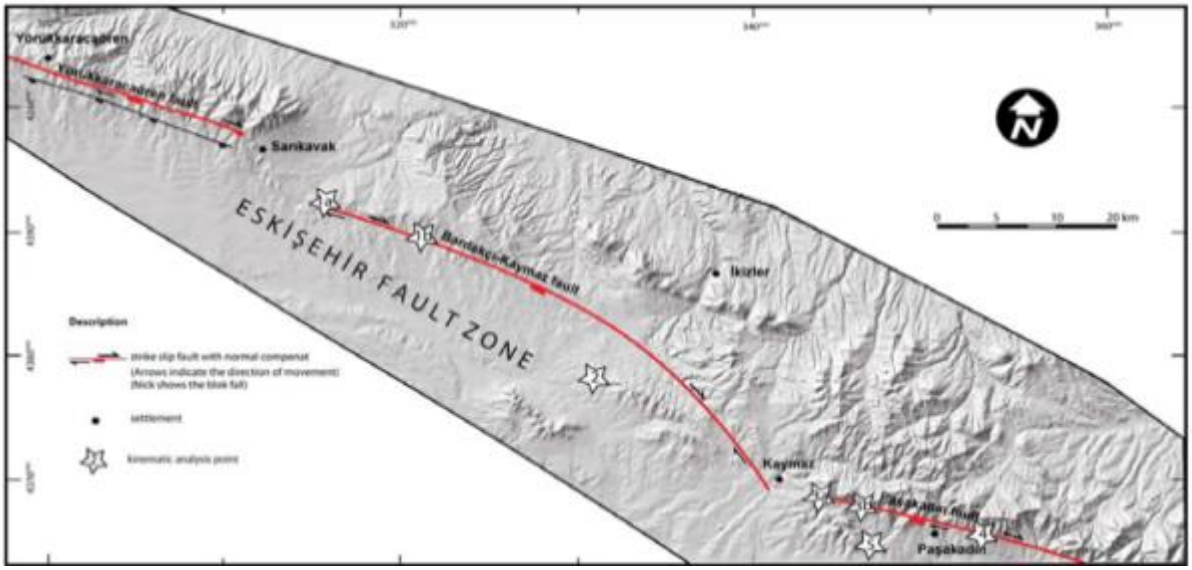

Figure 6/1.6 – The Eskisehir fault zone. Source [6/198]

6.1.2.5 CENTRAL ANATOLIAN FAULT ZONE

The Central Anatolian Fault Zone (CAFZ) is the third longest strike-slip fault in Turkey. It initiates at the north from Düzyayla (Sivas) and runs through Kayseri, Camardı (Niğde); Kamışlı, Pozantı and the Gülek Pass where it finally passes through north of Mersin and reaches Anamur [6/133] (Figure 6/1.7).

With an average trend of N60E, the CAFZ is an approximately 730 km long, and 2 to 80 km wide, active sinistral strike-slip fault. It continues beneath the Mediterranean Sea and determines the boundary of the Antalya and Adana basins as far as to the west of Cyprus (Figure 6/1.7).

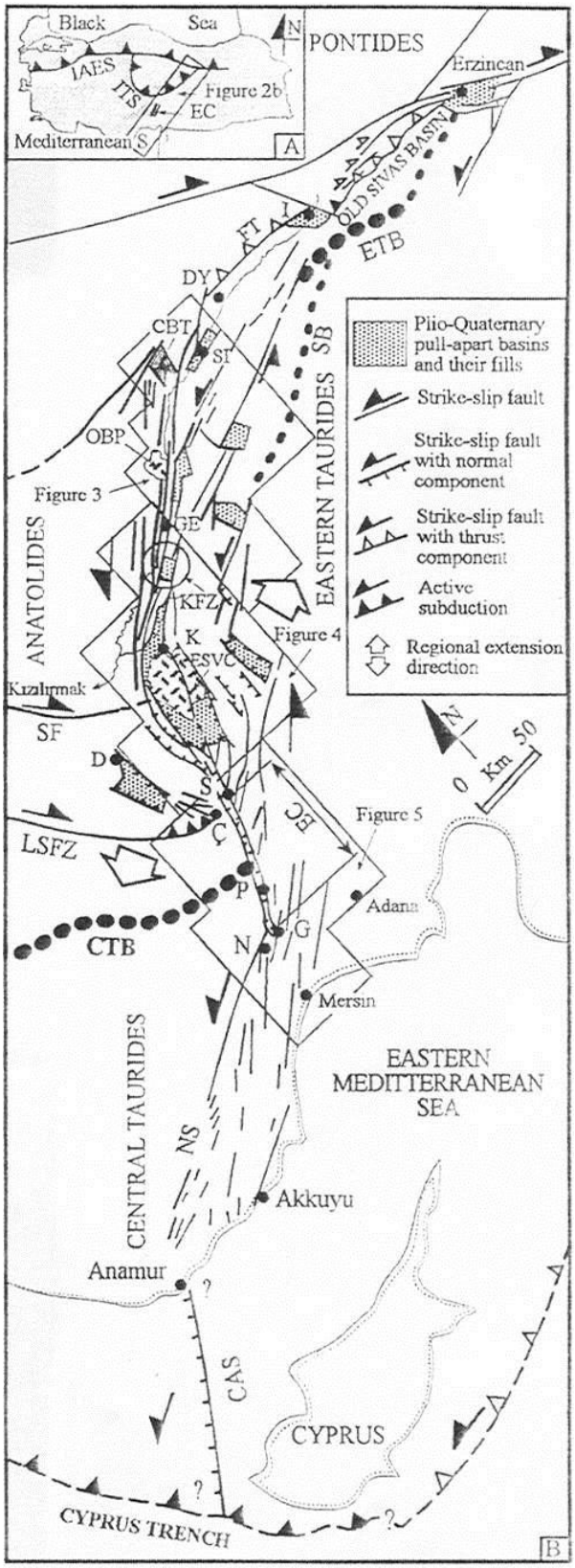

Legend: CAS = Cyprus-Anamur fault segment; CBT= (Cermik-Bakırcıoğlu travertines; CTB = Central Tauride-Anatolide boundary; EC = so-called 'Ecemis Corridor'; ESVC= Erciyes stratovolcano complex; ETB = Eastern Tauride-Anatolide boundary; FT = Frontal thrust of Izmir-Ankara-Erzincan Suture (IAES); ITS = Inner Tauride Suture; KFS = Klzfllrmak Fault Zone; LSFZ = Lake Salt Fault Zone; NATF = North Anatolian Transform Fault; NS = Namrun fault segment; OBP = Orta basaltic plateau; SB = approximate southern boundary of Tertiary Sivas basin; SF = SalandaFault; C = Camardi; D =Derinkuyu; DY = Dtizyayla; E = Erzincan; G = Gtilek: GE = Gemerek: K = Kayseri; N = Namrun; P = Pozanti; S = Sulucaova; SI = Sivas. Arrows show sense of movements on faults

Figure 6/1.7 – The Central Anatolian Fault Zone (after Koçyiğit & Beyhan [6/133]

Since Late Pliocene, the continued westward escape of Anatolia has caused left movement along the CAFZ. As a result of this motion transtensional areas have been formed around left

stepping and southward bending regions of the fault zone. The CAFZ resulted from the reactivation and propagation of an older paleotectonic structure, the so-called “Ecemiş Corridor” [6/247].

Based on geometric discontinuities [6/133] the CAFZ is divided into 24 segments. Each of them is characterized by a number of strike-slip morphotectonic features reflecting recent movement.

According to Kocyigit and Beyhan [6/133], the NE half of the CAFZ can be subdivided into the following segments: Sivas, Kızılırmak, Gemerek-Şarkışla, Erkilet, Yeşilhisar, Kavaktepe-Dikitilitaş, Çamardı-Derinkuyu, Tecer, Dökmetas, Dündarlı-Erciyes, Develi, Samakaya-Yeniköv, Kaynar-Pazarören and Karanfildağ. These segments occur in a 25-80 km wide, 200 km long zone and are connected by a series of short, approximately N-trending oblique slip normal faults and related pull-apart basins. Distinctive neotectonic features occur in this area: Plio-Quaternary terrace conglomerates are elevated and dissected, Plio-Quaternary fissure eruption-induced basaltic plateaus. The Erciyes pull-apart basin is about 35 km wide and 120 km long.

The Çamardı segment of the so-called ”Ecemiş Corridor” was named the Ecemiş fault zone [6/247]. It will be described in a separate section later in this report.

Another 40-45 km long, NE-trending active sinistral strike-slip fault zone was recently detected and named the Kızılırmak Fault Zone [6/115].

The central part of the CAFZ is subdivided into six segments (Demirkazık-Sulucaova, Cevizlik, Kamışlı, Asaryaylası, Akca-Kızılcık and Hamidiye-Fındıklı). A linear depression or rift-like structures occur in the area between the town of Sulucaova to the northeast and the town of Tekir to the southwest: it is approximately 2-8 km wide, 100 km long, and displaces the Tauride Mountain range of tens of kilometers in a sinistral direction.

To the South, the Ayvalı-Tekir segment is about 1 km wide and 20 km long segment: it is an oblique normal fault zone composed by several parallel to sub-parallel faults.

The Namrun segments are about 40 km wide and 200 km long. It consists of numerous parallel to sub-parallel faults which are a few hundred meters to 50 km in length (see next section).

Earlier researchers have reported that the so-called “Ecemiş corridor” terminate around Ardıçlı and Ayvalı villages. However, recent aerial photograph and field studies (Demirtaşlı [6/54], Demirtaşlı and Genç [6/57]) have demonstrated that only the rift-like geomorphology disappears but fault segments either bend westward at 45-60°N or bifurcate into numerous parallel to sub-parallel faults and then collectively run in an average 50°N trending new segment, here called the Namrun segment. Steep linear fault scarps, sinistrally offset stream beds (up to 3.1 km), active landslides and well-preserved slip planes with nearly horizontal slip lines are common field evidences of the Namrun segment. For instance, to the northeast of Darıpınarı village, the Kadıncık River is offset sinistrally by up to 260 m by one of the faults. Moreover, the upstream of the same

river is offset sinistrally by up to 3.1 km by another fault of the Namrun segment. In addition, a dense and linear fault-parallel distribution of micro-earthquakes [6/44] indicates not only its presence but also its activity.

To the South, a possible marine continuation of the CAFZ is still not defined. A remarkable sea bottom escarpment which runs about 32°N occurs along the boundary between the Antalya and Cilicia-Adana basins. It is marked by a sudden break in slope and by a linear distribution of closely spaced bathymetric contours between Anamur and the west of Cyprus. In addition the eastern margin of the Antalya basin displays a steep, straight, morphotectonic pattern along which Miocene deposits are brought against Mesozoic carbonates. This long linear submarine escarpment which is named the Cyprus – Anamur segment may imply that the CAFZ extends from Anamur farther across the Eastern Mediterranean sea floor up to the Cyprian Trench.

Below are reported the descriptions of the most relevant fault zones within the CAFZ.

Sivas Fault Zone

The Sivas Basin is one of the most well-known major Tertiary basins of Anatolia connected with the evolution of the Neotethyan Ocean. It is located in the eastern part of central Anatolia between the Central Anatolian Crystalline Complex (CACC) in the north and Taurides in the south.

It started to form as the product of Late Maastrichtian extensional tectonism in Central Anatolia. Since Early Pliocene, reactivation of the EFZ triggered the development of NE-SW trending transtensional basins on the vast plateau formed during Late Miocene [6/62].

Its southern margin is well defined, while its northern margin is well marked by both the frontal thrust of the Izmir-Ankara-Erzincan Suture and the Sivas to Kizilirmak segments. The frontal thrust is dominated by a south-vergent thrust fault segment although it shows back-thrusting in places. It was named the “Sivas Basin Northern Boundary fault” and interpreted as a left-lateral transpressive fault related to the North Anatolian Fault [6/133].

Ecemiş Fault zone

The Ecemiş fault zone is part of the Central Anatolia Fault Zone. The length of the zone is about 250 km and the width varies between 1 and 6 km.

Recent publications have focused on whether the geomorphology of the EFZ represents the product of active strike-slip [6/133] or glacial scouring of an ancient fault zone which is no longer active [6/240]. According to Koçyiğit and Beyhan [6/133], the offset since Early Quaternary is 3.1 km. According to Jaffey and Robertson [6/122], the Çamardı fan complex is dissected by a “small graben” that is inferred to mark the site of surface breaks induced by historical earthquakes. This feature has been cut numerous times with a total offset in the order of hundreds of meters. Diversion of active stream courses is seen along exposed faults (maximum in the Emli Valley, with

2.4 km of sinistral offset). These observations suggest that a small amount of strike-slip motion (up to 250 m) has occurred since the deposition of the Plio-Quaternary fans. However, this was subordinate to coeval dip-slip faulting. The total sinistral offset of the Ecemiş FZ is inferred to be 60 ±5 km (comparable to that of the NAFZ, larger than that of the EAFZ). [6/122], The activity started probably during Oligocene-Miocene times, 7-20 Ma earlier than NAFZ and EAFZ, mainly as left lateral strike-slip system. During the Plio-Quaternary the slip became mainly extensional creating a system of grabens and half grabens. Left lateral displacement continued into Late Pliocene-Quaternary times, as shown by river offsets on alluvial fans shed from the footwall of the transtensional half grabens [6/122].

The existence of distinct geomorphologic features along active fault segments associated to a relevant seismicity constitutes evidence of the capability of the Ecemiş Fault Zone. The potential formation of pull-apart basins, deflection of streams and morphotectonic evidence prove a dominant left-lateral movement [6/58, 6/133 and 6/122], although the Quaternary activity seems more characterized by a normal extension in the East-west direction [6/122].

Evidence of activity is totally lost between Gülek and Mersin, so that a possibility does exist that this fault merges with the WSW-ENE-trending Namrun FZ as suggested by Koçyiğit and Beyhan [6/133]. According to them, the southern extension of the Central Anatolian Fault Zone should follow the Namrun FZ. Alternatively, some authors (see for example [6/8]) believe the EFZ continues with the same SSW trend, reaching Mersin and then continuing either inland along the coast down to Silifke, or offshore, in the Adana-Cilicia Basin. According to Özel [6/175] the major fault complex that separates the eastern portion of the Cilicia-Adana basin from its central portion is the offshore extension of the Ecemiş Fault; the same offshore fault was already mapped by Gökçen [6/95].

Regarding the inland continuation of the Ecemiş FZ south of Gülek, Dermitaşlı has performed a detailed field reconnaissance study in 2011 and 2012 [6/94] concluding that:

1. There is no possibility that the *Ecemiş Fault Zone may continue southwestward under the Mediterranean Sea to intercept the site area. Detailed geological investigations and geological mapping carried out on this zone proved that it terminates north of Belenköy, 30 km north of Mersin. From this point southwestward we cannot see any prominent fault which may be the southwest continuation of the Ecemiş Fault. There are a few not continuous faults trending N25E affecting only the Karaisalı Formation (Tm2). These faults do not continue in the Middle Miocene clastics (Tm3) and the overlying Tortonian sediments (Tm4: Kuzgun Formation). Therefore they are older than Middle-Late Miocene. Furthermore any fault which is claimed to be the southwestern extension of the Ecemiş Fault should affect the wide spread caliche deposits of Plio-*

Quaternary age existing in the coast between Mersin and Erdemli. These caliche beds have shown no sign of any tectonic activity.

2. Quaternary faulting along the Ecemiş Fault Zone has been observed only at the northern parts of the zone between Pozantı at the south and Demirkazık at the north.

3. Active faults may exist on the southwestern extension of the Yumurtalık Fault near to the southern border of the Cilician Trough. Active faults near the Turkish continental shelf, parallel to the Mersin-Erdemli-Silifke shoreline are not expected, since there is no evidence of long, continuous and permanent faults on the shore and in the mainland trending in this direction. On the other hand seismic surveys carried out between Turkey and Cyprus did not indicate such a fault [6/39].

There has been also much debate as to whether the southern portion of the Ecemiş Fault extends offshore. To definitely clarify this point, in 2011 WorleyParsons [6/244] has made a new interpretation of 7 seismic lines, provided by Turkish Petroleum Corporation, TPAO (seismic reflection lines recorded in 1991-1992), which cross this proposed lineament; actually, these lines have already formed the basis for previous studies [6/7 and 6/175].

The conclusions of the analysis by WorleyParsons [6/244] are:

1. *The submarine channel oriented NNE-SSW, more or less in line with a possible offshore extension of the Ecemiş Fault, is actually to be interpreted as an incision corresponding to an ancient bed of the paleo-Tarsus river, when the coastline was approximately located along its southern edge. This channel most likely is buried under the deltaic sediments outside the circle in the northerly direction towards the present coastline.*
2. *There is some evidence of recent faulting in the area, but it is related to salt diapirism and therefore it is not deep-rooted (i.e., not tectonically driven).*
3. T*he Ecemiş Fault does not have an offshore extension. Instead, it terminates inland north of Mersin and does not reach the coastline. Moreover, it splits into westward branches before merging with the Namrun Fault. The fault geometry further implies that the left-lateral strike-slip behavior of the early Ecemiş Fault now is less dominant and has been transformed to a clockwise rotational motion with east-west extension. …. Based on offshore seismic data, there exists no evidence of the offshore extension of the Ecemiş Fault. Additonally, the early strike-slip character of this inland fault is now less prominent.*

In conclusion the most recent and updated study summarized above has shown that the Ecemiş Fault does not continue offshore. Furthermore, no proven evidence of active strands of the EFZ has been found inland along the coast or near-shore [6/172].

<u>Namrun Fault</u>

The Namrun Fault Zone is the southwestern segment of the Central Anatolian Fault Zone that lies between the east of Gülek and Namrun (Figure 6/1.7 and Appendix B). It is a left-lateral strike-slip fault that splays from the Ecemiş Fault to the north of the Adana basin [6/133 and 6/115].

The Namrun fault zone is formed by a number of fault segments which trend N60-80E and are 4-8 km long. These faults are the Namrun, Çamarası Sebil, Cehennemdere, Alaiye, Tepetaş, Meydan and Cevlik faults. The left lateral offsets seen on the contact with the Tertiary units and on morphological features, the microearthquakes and the fault plane solutions all suggest that these fault strands are active strike-slip faults with considerable normal components.

According to Koçyiğit and Beyhan [6/133], the southern extension of the Central Anatolian Fault Zone follows the Namrun FZ, extending much to the west to reach Anamur on the Mediterranean Sea, from where a long linear submarine escarpment extends further south across the Eastern Mediterranean Sea floor down to the Cyprus Trench. The submarine escarpment is marked by a sudden break in slope and by a linear distribution of closely spaced bathymetric contours. On the other hand, Dermitaşlı (2012), in his report [6/94] specifically devoted to the analysis of the Ecemiş and Namrun Fault Zones, concludes that:

Several new faults with regional importance have *been observed as a result of these regional tectonic investigations. Most of these faults generally trend ENE -WSW direction. All of them are normal faults looking upthrown sides towards north and downthrown sides towards south with steeply dipping fault planes. These step faults can be grouped under a common name of the Namrun Fault Zone.*

However it is also shown that these faults are cut by the Ecemiş Fault Zone ...

When we go towards west away from the Ecemiş Fault zone, the regional importance and intensity of these faults decrease. Northwest of Erdemli, faults such as Yağda and Fındıkpınarı continue only 5 to 10 km in Middle-Upper Miocene limestones with little vertical displacements ...Therefore we can say that the westernmost extension of the Namrun Fault Zone loses its regional importance and intensity.

If the Namrun FZ extends across the region to reach Anamur, then its shortest distance from the site would be about 40 km. However, in the neotectonic map of Turkey reported in Akın and Çiftçi [6/3], the Namrun FZ loses any evidence west of the eastern side of the Mut Basin. Actually, west of it, short fault strands can be recognized following a similar trend, but they lack any direct link with the Namrun FZ and, according to available studies, any evidence of recent activity along them (see also Kozağaç Fault below). The kinematics of these faults appears to have been dominantly of normal type.

The lack of any evidence of a throughgoing fault zone west of the eastern edge of the Mut Basin is the basis in the SHA for limiting to that edge the seismic zone corresponding to the

Namrun FZ. Moreover, it must be stressed that even east of Mut Basin the evidence for Quaternary activity can only be found toward Namrun, very close to the Ecemiş Corridor.

Kozağaç Fault

Between the towns of Mut and Anamur, approximately 36 km NW of the NPP site, a series of short mainly NW trending discontinuous faults are exposed. This fault set is known as the Kozağaç fault system. The faults range from a few km to 40 km in length, and dip 70-80° either NE or SW. Most faults are located either within the Miocene deposits of the Mut basin or at its margins where they define the fault contact between older Jurassic-Cretaceous limestone basement rocks, and younger basin filling deposits. According to studies by Demirtaşlı and Genç [6/57 and 6/55], these are Late Miocene-Pliocene age normal faults with no supporting field or seismic criteria suggesting that the Kozağaç fault set has been recently active [6/75].

6.1.2.6 ADANA BASIN

The Adana basin is nestled between the Taurus Mountains in the north and west and the Misis Mountains in the east (Figure 6/1.4 and Appendix B). To the southwest it merges with the marine Inner Cilicia – Basin. It hosts a 6000 m thick sedimentary succession, spanning Miocene to Recent. The Miocene succession is bounded by exposed pre-Miocene basement rocks of the Taurus Mountains in the north and northwest, and the Misis Mountains in the east.

The following tectonic structures within the Adana Basin are considered relevant for this study:

Göksu Fault

The Göksu Fault zone is a left-lateral strike-slip zone located between the towns of Sariz to the NE and Ceyhan to the ENE [6/181; 6/182]. It is located between the Ecemiş and the Eastern Anatolian Fault Zone, having similar strike and type of movement (left lateral strike-slip). It is approximately 240 km long. The fault zone consists of several short and discontinuous fault segments oriented parallel, subparallel and oblique to the main strand of the zone [6/75]. The Misis-Ceyhan fault, which is thought to have been associated with the 27 June 1998, M=6.3 earthquake in the area, is presumed to be a segment of the Göksu fault [6/235].

The length of the Göksu Fault segments is expected to be in the same order as the adjacent Ecemiş fault. Its distance from the Akkuyu NPP is about 90 km.

Kozan Fault

The Kozan fault is located along the northwestern margin of the Adana basin and has played an important role in its evolution [6/182].

Its trace can only be hypothesized since it is covered by the Upper Miocene – Pliocene deposits. On the surface the zone is expressed as a linear system of south west and south-south-west ruptures. It appears to have strike-slip characteristics with reverse components to accommodate the

uplift of the Taurides. The Kozan Fault is approximately 136 km to the NE at its closest approach to the site.

6.1.2.7 EAST ANATOLIAN FAULT ZONE

The East Anatolian Fault System is an 80 km wide and 700 km long NE-trending and seismically very active sinistral strike-slip fault system [6/20] (Figure 6/1.4). The left-lateral EAF marks the 600 km long strike-slip boundary between the Arabian and Anatolian plates, linking the Dead Sea Fault to the NAF (Figure 6/1.8).

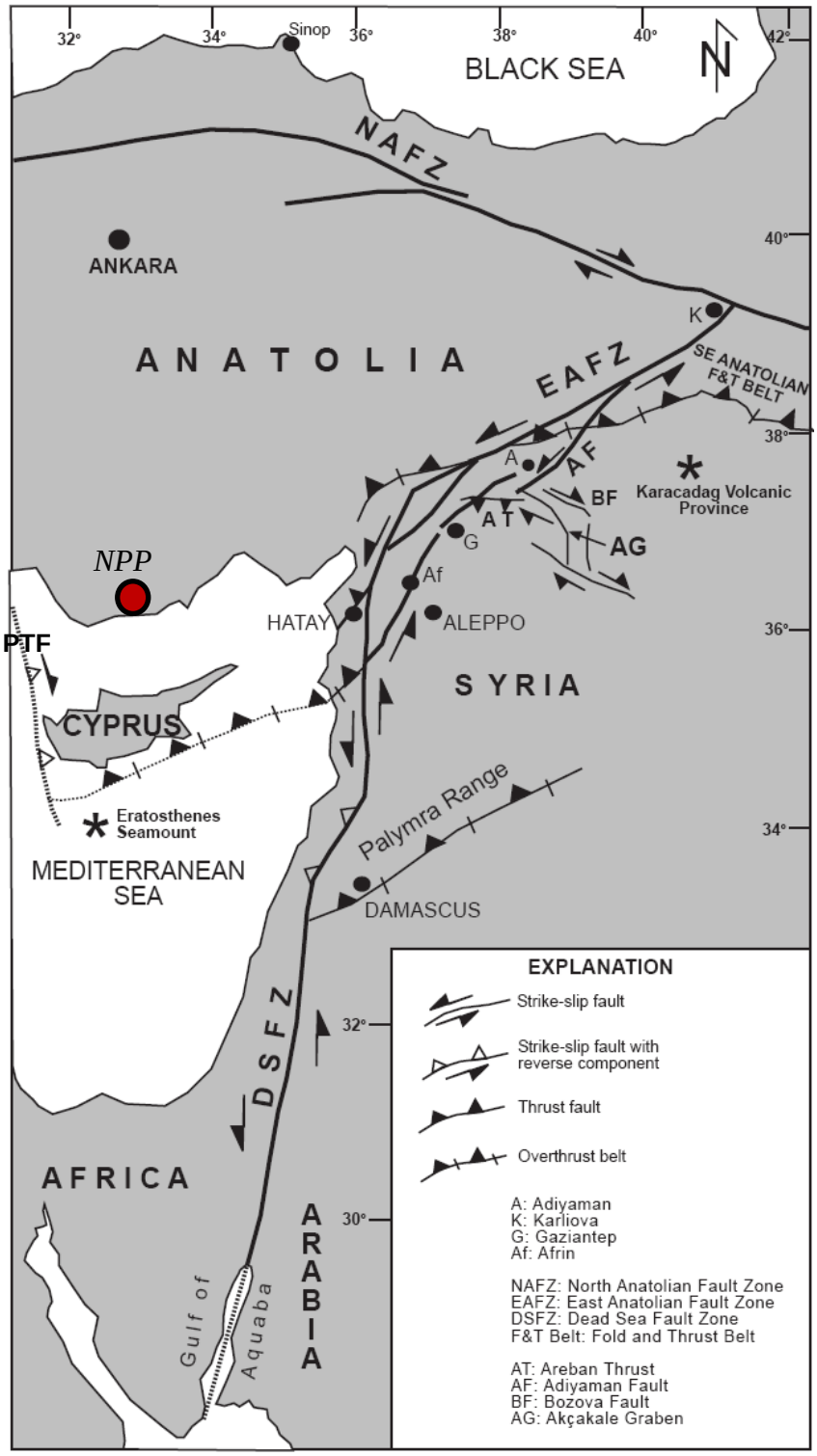

Figure 6/1.8 – The Eastern Anatolian Fault Zone (EAFZ) in the frame of the geodynamic context of Eastern Turkey and Arabia [6/203]

It is located between Karlıova in the northeast and Karataş-Samandağ Counties in the southwest and forms the southeastern outline of the Anatolian platelet. It cuts across and displaces in left lateral direction the Bitlis Suture Zone formed by the final continent-continent collision of the southerly located Arabian plate with the northerly located Eurasian plate.

According to Şengör [6/200], the EAFZ was produced by the Middle Miocene collision of the Eurasian and Arabian plates, and it was extending in the southwest direction across the Amanos mountains and NW margin of the Gulf of Iskenderun during its youthful stage [6/200]. Three major discontinuities have been recognized on the EAF trace: 1) the Bingöl area; 2) the Hazar basin and the Sincik area. There are also many other minor fault discontinuities. This fault zone has ruptured over most of its length during the 19th century by earthquakes of M~7 (e.g. Lake Hazar events in 1874 and 1875). Based on the strike of the segments the EAFZ should consist of six segments [6/195], however Hempton [6/107] defined only five segments based on geometry and behavior while Barka and Kadinsky-Cade [6/23] based on fault geometry and seismic activity, suggested that there may be 14 different segments. The segment between Tuskoğlu and Celikhan has experienced earthquake events on March 2, 1893 (M = 7.1, 45 km depth), December 4, 1905 (M = 6.8, 38 km) and most probably on March 28, 1513 (M = 7.4, 103 km).

The EAF average slip rates are 10-11 mm/yr [6/47 and 6/189], a total offset of 15-30 km [6/195, 6/239 and 6/240] and estimated age of 3-4 Ma. The fault trace is segmented with a maximum recognized segment length of about 100 km [6/161, 6/23 and 6/195]. According to Yilmaz [6/249] about 9 mm/yr left lateral motion occur along the EAFZ.

A number of strike-slip basins are located along the EAFZ. Two basin infills are separated by an intervening angular unconformity. This stratigraphic evidence confirms that the strike-slip neotectonic regime started from Late Pliocene. The strike-slip nature of the fault is confirmed also in the central part of the EAF by focal mechanisms. Nevertheless, active thrust deformation is evidenced to the south of the EAF, at the boundary between the Tauride belt and the Arabian platform by the occurrence of M=6.7 thrust earthquake in Lice in 1975 [6/195; 6/173 and 6/210] and by the geomorphological study of Cowgill [6/52].

6.1.2.8 CYPRIAN TRENCH

The Cyprus (or Cyprian) Trench is a part of the plate boundary between Afro-Arabia and Eurasia in the Eastern Mediterranean (Figure 6/1.4). It has a similar geometry to the Hellenic Trench, but it is shorter and the convergence rate is about two-three times slower. The Hellenic Trench is subjected mainly to subduction, whereas the Cyprian Trench is subjected to subduction, collision and transcurrent tectonic processes. It extends from Anaximander Mountains (west) to

Lebanon coastline and can be divided into three sectors with different types of deformation due to different convergence mode. In the western sector the seismic activity and the gravity field indicate an active northward subduction of oceanic material related to the African Plate beneath the Turkish Plate [6/30]. As suggested by the diffuse seismicity and the distributed concentration of earthquakes, the subduction is probably interrupted at the central segment of the Cyprian Trench due to the collision of the Eratosthenes Seamount, a continental fragment of the African Plate drifting northwards towards Cyprus, which forms a zone of intense deformation. Its impinging on the Cyprian Trench is partly responsible for the uplift of Cyprus [6/146 and 6/104]. The subducted slab is detached [6/89] or it is steep and segmented, perhaps in early detachment phase [6/32]. The depth of earthquakes increases northwards from shallow to intermediate.

According to Papadimitriou & Karakostas [6/178], the seismic activity onshore and offshore the southern coasts of Cyprus Island is primarily caused by slip on faults arranged obliquely to the plate boundary. The three major fault zones that accommodate the majority of the recent seismic activity in this area are the dextral Paphos fault and the Lemessos and Larnaka oblique thrust faults. The Lemessos fault zone, in particular, has been recognized on the basis of the spatial seismicity distribution and supported by previous neotectonic studies and stress orientation. The most recent significant earthquake which occurred is related to Lemessos and Larnaka oblique thrust faults with max rupture length of 24km and displacement of 72cm (24 June 1896 earthquake, M=6.5) [6/178]. The event of 29 September 1918 (M=6.3) occurred east-southeast of Cyprus Island on a fault going parallel to the subduction front. A rupture length of 19 km and an average slip of 52 cm were estimated for this event, which is located far from the major faults [6/178].

The major structural element of western and southern Cyprus is the NE-SW trending dextral transform fault (Paphos Transform Fault (PTF); Figure 6/1.8), associated with intermediate depth seismicity. Associated with this fault is the October 9 1996 (M= 6.8) earthquake. According to Papadimitriou & Karakostas [6/178] this earthquake has produced fault rupture of 30km length and 15km width. The 1996 hypocenter had depth of 76 - 85 km [6/189]. According to Wdowinski [6/234] the NE-SW trending Paphos fault is a tear fault and represents the transition between the western and central segments of the trench. This fault produces large strike-slip earthquakes and has convergence rate of 7-8 mm/yr [6/235].

The northern sector of the island is characterized by Kyrenia fold/thrust belt that preserves evidence of passive and active margin phases, the latter involving both strike-slip and thrust faulting. The uplift of the Kyrenia range occurred in the mid-late Pliocene and continues presently [6/41]. An E-W trending, N dipping normal faulting occurred north to the range [6/7] (see Cilicia basin description above).

According to Cagnan & Tarnican [6/40] the higher Peak Ground Acceleration values obtained for a return period of 475 years for rock conditions, are along the southern coastline of Cyprus, where the expected ground motion is between 0.3 and 0.4 g. The rest of the island is characterized by lower ground motion. The largest earthquakes mostly occurred at the southern and western part of the island, causing damage in Paphos, Limassol, and Famagusta (e.g., the earthquakes of year 342 with magnitude M=7.4, year 1222 with M=6.8, year 1577 with M=6.7, year 1785 with M=7.1, year 1940 with M=6.7, and 1996 with M=6.7 [6/40].

6.1.2.9 DEAD SEA FAULT

The Dead Sea Fault is a N-S trending major tectonic structure which runs from the Taurus Mountains to the Gulf of Aqaba (Figure 6/1.9) and has length of about 1000 km.

Since the Middle Miocene, it accommodates left-lateral motion between the Arabian plate and the Sinai subplate, connecting a region of extensional tectonics in the Red Sea to the Taurus collision zone to the north.

A crustal image across the Dead Sea Transform (DST) has been produced by the DESERT Project. The data indicate that in correspondence to the Araba Fault (AF) which is the southern segment of the DST system, the basement is displaced for several kilometers.

Nevertheless, the Moho depth increases steadily from about 26 km in the Mediterranean to about 39 km in the Jordan highlands, except for the basement below the Araba Valley (Wadi Araba) [6/236]. These Authors conclude that the AF cuts through the crust, becoming a broad zone in the lower crust and even in the mantle. This is in agreement with [6/206] and Rumpker [6/192] which suggest that the DST cuts the whole lithosphere, accommodating the motion between the African and the Arabian plates.

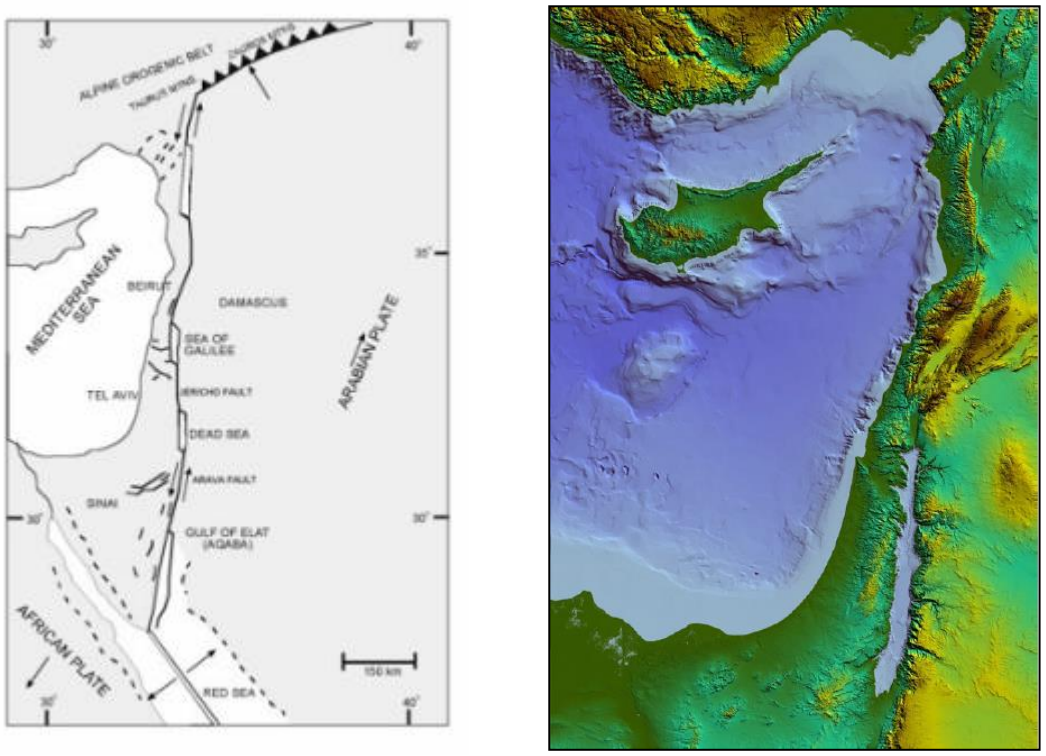

Figure 6/1.9 – The Dead Sea fault is a N-S tectonic lineament running from the Zagros Mts. to the Red Sea. Its geomorphic expression is clearly visible over a Digital Elevation Model

Local geology shows systematic offset of numerous pre-Miocene geological features by approximately 107 km [6/26 and 6/91]. The presence of downthrown blocks and grabens infilled with Quaternary sediments constrains the amount of vertical displacement along the DSF in the order of 3,000 m. Paleoseismic and archeoseismic studies show Holocene and historical activity as left-lateral offsets of natural and manmade structures [6/15, 6/67, 6/132, and 6/167].

Focal mechanisms of moderate to large earthquakes show left-lateral motion along the fault system in general agreement with the location of the active faults based on geological data [6/22; 6/109; 6/132 and 6/167]. According to the seismological database, prevalent dips range between 40° and 75°.

Geodetic measurements are consistent with and confirm the left-lateral slip as well as the slip rate inferred by paleoseismic evidence of 4±1 mm/yr [6/141, 6/142, 6/148, 6/189 and 6/234].

The fault zone consists of en-echelon faults with extensional jogs and pull-apart basins which are associated with releasing bends and pressure ridges. These pull-apart basins have acted like sediment traps, allowing the deposition of clastic and evaporitic sediments.

Archeological and paleoseismological studies have evidenced the co-seismic reactivation of about 100 km long segment of the Dead Sea Fault in historical time (e.g. 749AD, [6/145]), demonstrating that this fault is capable of generating M > 7 earthquakes.

The largest known instrumental earthquake along the Dead Sea Fault zone was located about 100 km south of Aqaba (1995, Mw = 7.3): it produced about 1.6 m of left-lateral slip, along an 80 km fault segment.

6.1.3 NEAR REGIONAL STUDIES

The near regional investigations scale as defined in IAEA SSG-9 [6/113] is an area of at least 25km radius where in addition to the published information and data, site specific investigations are needed which may include field reconnaissance, remote sensing data collection and field investigations as necessary. A summary of the near regional database is presented in this subsection including a description of the the general tectonic units, stratigraphy and hydrogeology. Additional near regional analysis specifically with respect to fault displacement hazard is available in Section 6.6.

6.1.3.1 TECTONIC STRUCTURE OF THE NEAR REGION

The Akkuyu NPP site is located at a distance of some 50 km to the south-west from Silifke and lies at the south of Taurus (Taurides) belt central part, which is limited with two tectonic zones: Ecemiş fault in the east and Hadım tectonic cover in the west. From the north it is limited with the Internal Taurus belt (Figure 6/1.10).

The Central Taurus belt may be divided into the following structural stages:

- autochthonous and parautochtonous platform of carbonates and clastics;
- allochthonous mélange and ophiolite rocks.

Autochtonous and parautochtonous rocks occur between Silifke and Anamur and in the north they are vastly overlaid with post-tectonic marine Middle-Upper Miocene (15 million years) formations. To the east from Anamur they obduct onto metamorphic rocks of Alania massif and its Paleocene-Eocene cover along the NW – SW direction of Hadim tectonic cover. This important tectonic event occurred in Eocene Period (40 million years).

Hadım cover probably is extended in the eastern direction under the Mediterranean Sea, connected with Ecemiş fault of south-west strike, which is one of the important left horizontal displacements, occurred in the upper Eocene. Therefore, Alanya massif [6/181] may be considered as the western bench of the Bitlis massif in the south-east part of Turkey.

Three tectonic regions are identified in the Central Taurus belt between Silifke and Anamur, in particular: the southern, middle and northern. Differentiation of these regions started in Early-Paleozoic Era and was strengthened during Triassic Period.

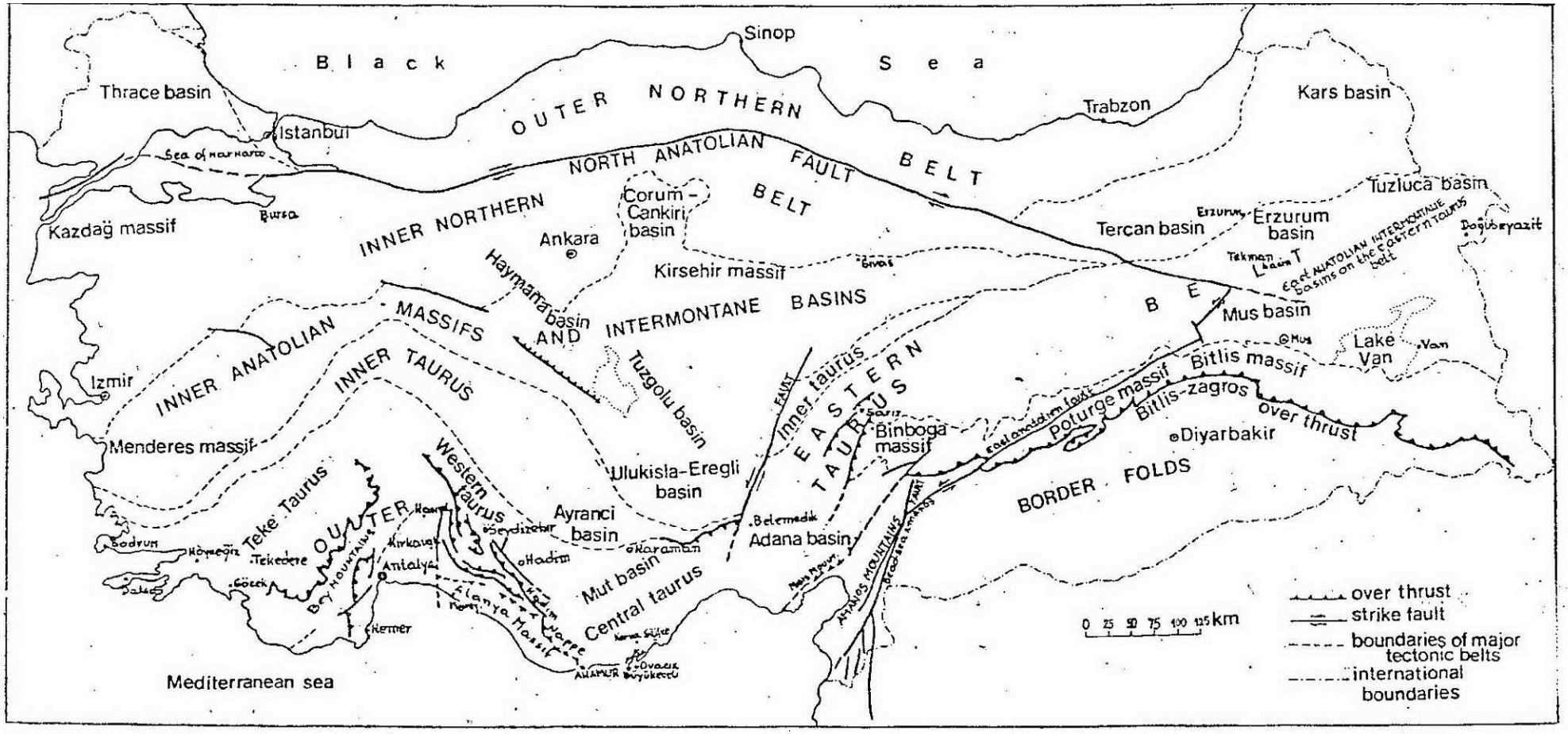

Figure 6/1.10 – General Tectonic Map of Turkey [6/64]

The first stage folding occurred in Late-Permian Period. The second stage was accompanied by overthrust, which occurred in Middle-Late Triassic Period (Eocimmerian Orogeny, Mountain Building processes). In Jurassic-Cretaceous Periods, the platform carbonate deposits covered all three tectonic regions, unconformably bedding onto all ancient deposits. Impacts of Middle and Late-Alpine motions (Lamarian and Pirinean phases) mainly occurred in the middle and north regions, which was confirmed by the ophiolites availability in the north. Molassa basin developed in the middle and northern geotectonic regions, where Lower-Miocene sediments were deposited. The Middle-Miocene marine limestones which are gently bedding, represent a flat surface and are not of tectonic origin.

Orogenic processes throughout the entire Central Taurus belt, including the Akkuyu Province was completed before Miocene.

According to the results of the performed investigations, any evidence of the present-day tectonic formations and active dislocations (faults) have not been discovered in the near region.

Figure 6/1.11 presents a simplified geological map of the major tectonic units of the central Taurus Belt around the Akkuyu NPP site.

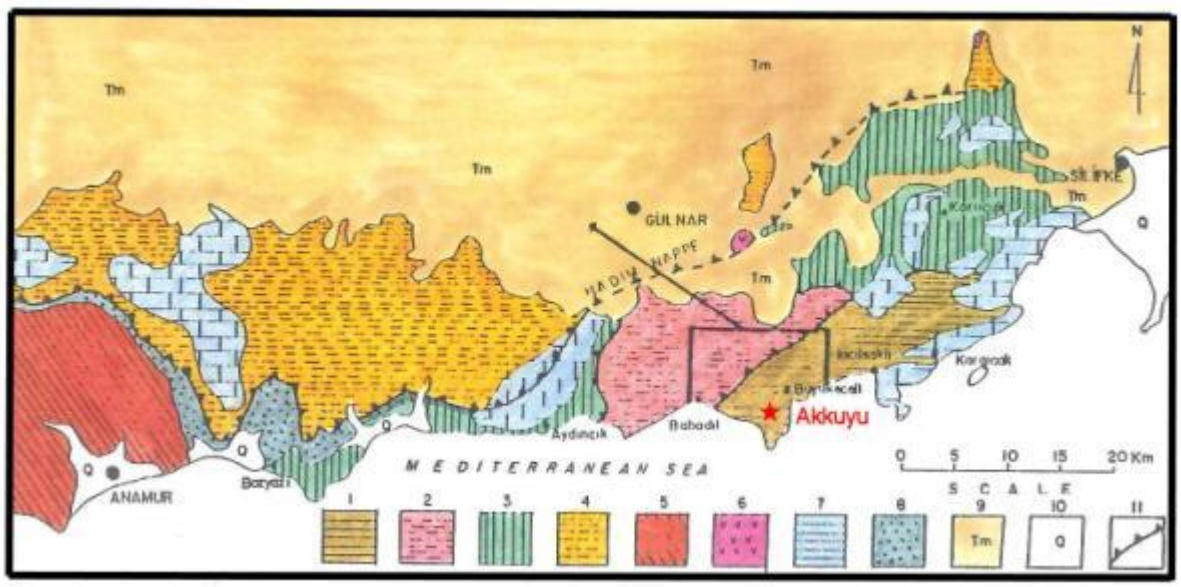

Figure 6/1.11 – Simplified Geological Map of the Major Tectonic Units of the Central Taurus Belt Around the Akkuyu NPP Site. 1-Southern Zone, 2-Intermediate Zone, 3-Northern Zone, 4-Aladağ Unit (Hadım Nappe), 5-Alanya Massif, 6-Ophiolites, 7-Jurassic-Cretaceous Platform Carbonates, 8-Paleocene-Eocene Olistostrome, 9-Marine Miocene, 10-Quaternary Deposits, 11-Thrust [6/57]

Southern region

The Southern region includes a coastal area between Silifke and Ovacık, where Cambrian to Miocene deposits are represented by non-metamorphic sedimentary rocks.

The observed stratigraphic discordances in the southern region are as follows:

- Upper-Devonian Period angular unconformity;
- Upper-Permian Period angular unconformity;
- Lower-Jurassic angular unconformity;
- Angular unconformity from Early-Miocene.

Carboniferous and Late-Permian deposits are absent in the region because of the Early Hercinean orogenesis.Unlike continental Triassic Period of the middle region, Triassic System is represented by marine sediments. There is a transition from the Upper-Permian to Lower-Triassic sediments in the eastern part of the region, while in the western part, in the Akkuyu region, the Upper-Triassic sediments (Kuşyuvasıtepe formation) unconformably overlies the Upper-Permian sediments.

An important low-angle overthrust occurred at the end of the Triassic Period from the north to the south in the middle region where formations obducted onto the southern region rocks.This low-angel overthrust was a result of the Early-Alpine orogenesis and affected all the geotectonic regions in the Central Taurus belt.

Following the strong folding and overthrusting in the Early-Alpine orogenesis, the southern region was covered by the Jurassic-Cretaceous carbonate platform sediments. Middle-Miocene limestone (Silifke formation) unconformably overlays all older rocks in the southern region. A regional uplift occurred at the end of the Miocene and Pliocene and caused inception of uplift and sub-aerial exposition of the Miocene marine sediments. Detritus cones were deposited During Pleistocene-Holocene. The remains of uplifted marine terraces could be observed at the shore around Akkuyu, 10 - 15 m higher than the present sea level which indicates for sea level fluctuations during the Quaternary.

The present-day Quaternary alluvial sediments cover older detritus cones. Coastal sediments and pebbles are formed today at the shore of the southern region. No fault dislocations are evident in the Quaternary sediments.

Middle region

The middle region lies northward from the southern region and is gently thrusted-over from north to south. It consists of a thick alternation of Lower and Middle-Cambrian sediments, represented by limestone, shale and intercalations of conglomerates (Sipahili formation). This formation is overlain by Late-Cambrian to Late-Devonian (Babadıl Group). This formation

(Babadıl Group) was not described separately because it has very small thickness and it is difficult to differentiate it in the field.

The Upper-Cambrian is represented by red quartzitic sands and siltstones similar to the Ovacık formation sediments.

The Silurian Period is represented by graptolitic shales very similar to their analogues in the coastal area (Ovacık and Hırmanlı formations).

The Devonian Period is represented by alternation of limestone, shale and quartzite and is lithologically similar to the Karayar and Sığırcık formations. The discovered brachiopods and corals indicate a Late Devonian age for the upper part of the Babadıl Group.

Possible unconformities may occur between sediments of these groups. Lower-Carboniferous low-thickness limestone and quartzite from Korucuk formation are locally distributed in the region.

The Upper-Permian limestone (Kırtıldağı formation) unconformably occurs above the Babadıl Group, and they are unconformably overlain by the Upper-Triassic red sandstones, shale and conglomerates (Murtçukuru formation). Formations called Dibekli (Early-Jurassic) and Tokmar (Upper-Jurassic – Lower-Cretaceous) which have a strong unconformity occur above the Sipahili formation and the Babadıl Group.

In Tepeköy which is located in the central part of the middle region, the Early-Miocene conglomerates are slightly inclined. Molassa deposition was formed in the middle and northern regions in the Early-Miocene where in the freshwater and lagoons, partially carbonaceous (organic rich) deposits (Çavuşlar formation) were accumulated. They have structures of abrupt decline, turbidite runoffs and faults which could have synsedimentary origin. The Çavuşlar formation is unconformably, overlain by marine limestone of Middle-Miocene Period (Silifke formation). The Silifke formation is subject to minor scale faulting. The Quaternary deposits in the middle region were not affected by faults.

Northern region is located northward from the middle region and obducts from the north to the south. A flat overthrust may have occurred prior to the Upper-Permian transgression (Djulfian). Limestone sedimentation occurred before Kırtıldağı formation, since it unconformably overlies older formations of these two tectonic regions. However, such displacement of Hercynides was to a large degree undistinguished on the background of later manifestations of the Alpine tectonics and flat overthrust.

In the Paleozoic period the development of the northern region is somewhat similar to development of the coastal region before the Carboniferous period. As it was pointed out above, the

Earlier-Carboniferous deposits were still not developed in the southern and middle regions, while they were developed in the northern region.

Outcropping Carboniferous deposits in the northern region could be observed around the Korucuk and İmamuşağı Village near Silifke. The Late-Permian is represented by limestone with thin quartzite inclusions. The Triassic deposits are not represented in the region and Jurassic carbonate deposits unconformably overlie older formations.

The Late-Cretaceous "wild flysch" containing olistostromes and olistoliths of Paleozoic rocks, accordingly overlies the carbonate rocks of the Jurassic-Cretaceous platform. Ophiolites were displaced along this "wild flysch" in the Late-Maastrichtian – Early-Paleocene period, while accumulation of carbonate sediments continued in the southern region's platform where Cretaceous-Paleocene Hayvandağı limestone was deposited. This convincingly proves that ophiolite mélange rocks which moved from the north overlie the north region "wild flysch".

6.1.3.2 STRATIGRAPHIC DESCRIPTION OF THE NEAR REGION

The geology of the coastal region is formed by Plio-Quaternary deposits overlying the Miocene basement from Mersin City to Göksu Delta. From Göksu to the east, the adjacent coastal region is dominated by Paleozoic age rocky coast with small pockets of alluvium and pocket beaches near the mouths of small ephemeral streams (Figure 6/1.12).

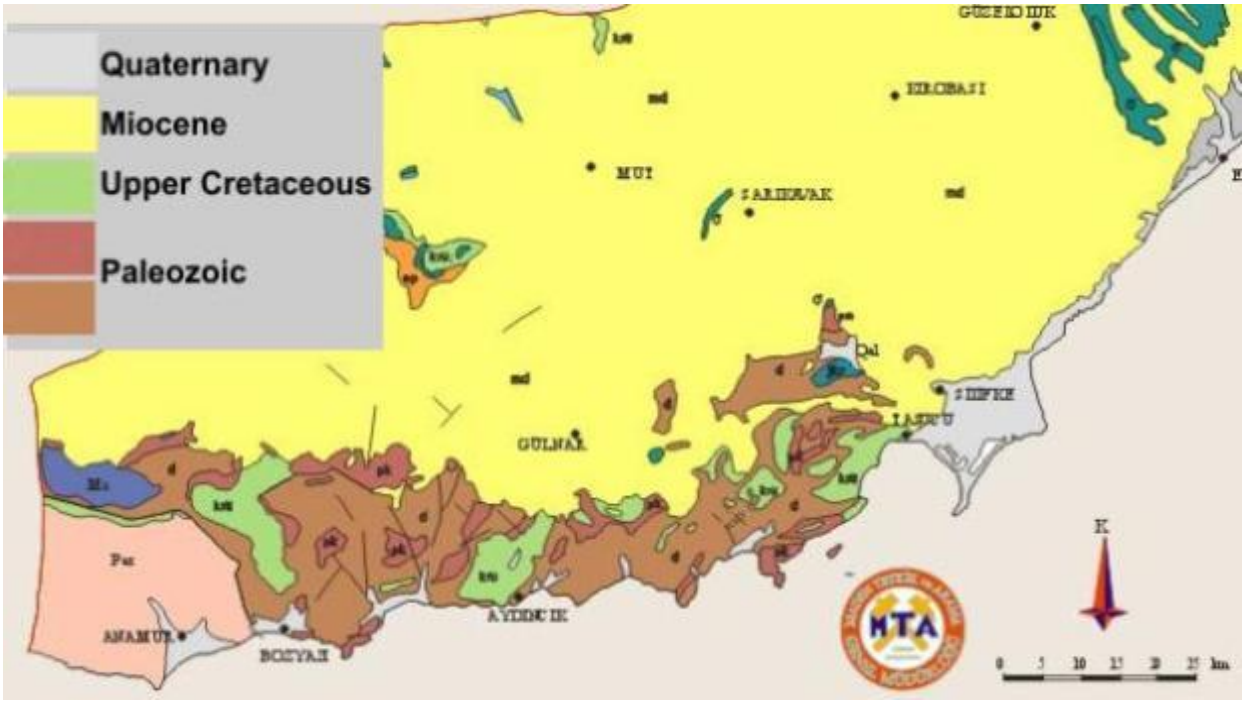

Figure 6/1.12– The geologic map of the area [6/172]

Akkuyu NPP site is located in the Southern tectonic region. The geological map in 1:25000 scale is provided in Appendix E. Geological map in 1: 5000 scale is provided in Appendix F.

Geological profiles are provided in Appendix G. Stratigraphic section of the western part of the Southern Region is provided in Appendix H.

Geological structure of the near region starting from Cambrian System and ending with Quaternary deposits is given below.

Cambrian System

Lower Department

Hacıishaklı Formation

In the lower part of the section Hacıishaklı formation is represented by pink, cross-bedded quarzites. The middle part consists of pink, greenish siltstones, medium-bedded. The upper part of the formation consists of white cross-bedded quarzites.

The thickness of the Hacıishaklı formation is 100 m.

Middle Department

Ovacıkışıklı Formation

The Ovacıkışıklı formation is represented by dark-grey with trilobite fossils and pink carbonate wackestones. The thickness of the formation is 75 m.

Upper Department

Ovacık Formation

The Ovacık formation outcrops north of Hacıishaklı Village which is situated at the southern part of the Ovacık Bay, 15 km east of the Akkuyu NPP site. The Ovacık Formation has been subdivided into three members. The lower and middle members belong to Upper Cambrian age and the upper member to Ordovician age.

The lower member of the formation includes pink-colored, medium-bedded nodular limestone and buff to green-coloured siltstone and silty shale intercalations. Silty micaceous shales contain small inarticulate brachiopoda which belong to a family indicating a Cambrian-Ordovician age.

Pink nodular limestone intercalations yield conodonts and small brachiopods indicating uppermost Cambrian.

The middle member of the Ovacık Formation is composed of red and greyish-green colored silt-stones and buff colored quartzitic sandstones. Siltstones contain specularite veinlets. Micro-cross- lamination is common in siltstones. Sandstones are cross-bedded. Near the Akkuyu Site at Taşlık Hill these varicoloured siltstones outcrop under the late Permian Limestones of the Kırtıldağı Formation. This indicates that before the late Permian, block faulting took place that brought the Ovacık Formation next to the Büyükeceli Formation.

Ordovician System

Lower, Middle Department

Ovacık Formation

The upper member of the Ovacık Formation is composed of olive green, silty shales containing Ordovician graptolites such as Dydymograptus sp. and Tetragrapthus sp. Fine grained, cross- laminated sandstone inter beds with erosional bases and sole marks increase towards the top. Cone-in-cone structures, fucoids, worm tracks and burrowings are the typical sedimentary structures of the upper member.

The Ovacık Formation has been deposited on an open marine shelf below wave base. Sandy layers are interpreted as turbiditic intercalations.

The thickness of the Ovacık Formation is 400 m. It is conformably underlain by the OvacıkIşıklı Limestone and is conformably overlain by the Eğripınar Formation.

Silurian System

Lower Department

Eğripınar Formation

The Eğripınar Formation is named after Eğripınar Village which is situated to the north of Ovacık Bay. The type section (the sequence of strata identified as the original sequence for a location or area; the standard against which other stratigraphy of parts of the area are compared. Also known as section) of the formation lies 1 km west of the village.

The Eğripınar Formation has been subdivided into two members. The lower member is composed of yellow to buff-colored, thick-bedded, arkosic conglomerates and sandstones containing well-rounded quartz pebbles. Local channeling and cross-bedding can be seen. No fossils have been obtained from the lower member. Pebbly sandstones and conglomerates are intercalated with siltstones.

A siltstone-shale member has been discriminated at the upper part of the formation. A few sandstone beds containing erosional basis and flute casts exist at the top of the upper member.

The thickness of the Eğripınar Formation is 125 m.

Hırmanlı Formation

Outcrops of the Hırmanlı Formation can be seen 40 km south-west of Silifke, around Hırmanlı Village.

The Hırmanlı Formation is mainly composed of very thin-bedded, laminated, black shales containing the following graptolites indicating Early Silurian: Monograptus, Climacograptus and Rastrites.

The thickness of the formation is 100 m. The Hırmanlı Formation conformably overlies the Eğripinar Formation.

The Hırmanlı Formation was deposited in a restricted basin.

Late Silurian – Early Devonian Periods

Karayar Formation

The name of this formation is taken from the locality which is known as Karayar on the highway between Silifke and Anamur, 6 km west of Hacıishaklı Village.

In Karayar the lower 200 m of the Karayar Formation is composed of dark-coloured, evenly-bedded limestones (calciturbidites) and black shales. The upper 150 m of the formation consists of bluish-gray, medium-bedded nodular limestones which are followed by brownish-gray thick-bedded partly laminated silty and sandy limestone with brachiopods and crinoids. Shale samples taken from the middle part of the formation yielded miospores indicating a Late Silurian age.

In the upper part of the Karayar Formation thick-bedded limestone is predominant with brachiopods and corals of Early Devonian age. The thickness of the Karayar Formation is approximately 350 m. It conformably overlies the Hırmanlı Formation.

Devonian System

Lower Department

Sığırcık (D_3) Formation

The type section of the Sığırcık Formation is evident in Sığırcık Village, 48 km west of Silifke. A reference section of this formation can also be seen along the Silifke-Anamur highway between Haciishaklı и Büyükeceli Village.

The Sığırcık Formation is composed of limestone and quartzite alternation at the base and quartzite, dolomite and shale alternation and conglomerates at the top. Shale intercalations are more common at the base. The quartzite is white to yellowish, locally brick-colored cross-bedded, and ripple marked.

Limestone is medium to thick-bedded, dark grey to buff, biogenic, full of crinoids, corals and brachiopods. The dolomite is grey, thick to medium-bedded unfossiliferous. Shale interbeds in the upper part of the formation are red coloured and nonfossiliferous and may indicate subaerial exposure.

The Sığırcık Formation conformably overlies the Karayar Formation. Crinoids, brachiopods and corals collected from the Sığırcık Formation indicate an Early Devonian age.

The Sığırcık Formation has been deposited in a very shallow water environment. Red coloured shales and conglomerates with a red mudstone matrix in the upper part of the formation may indicate to a regression and continental deposition for the upper part of the Sığırcık Formation.

Middle Department

Büyükeceli (D_2, members 1-8) Formation

The type section of the Büyükeceli Formation is 1 km south of Büyükeceli Village, 50 km west of Silifke, on the roadcut of the Silifke-Anamur highway. The formation has been subdivided into eight members described in Section 6.3.1.

The total thickness of the Büyükeceli Formation is approximately 630 m. The thickness of the formation gradually decreases towards east. At Akdere Village which is 25 km to the east of the type section, the thickness of the Büyükeceli Formation drops to 40 m.

Fossils collected from the Büyükeceli Formation such as Disphyllum Goldfussi, Calceola Sandalina and Amphipora Ramoza indicate to Middle Devonian Age.

The felump structures and megabreccia sheets which are common in the lower half of the formation from member Db2 to member Db6 indicate synsedimentary tectonic movements. The upper half of the formation composed of Db7 and Db8 were deposited under rather stable shelf conditions.

Upper Department

Akdere Formation

The type section of the Akdere Formation is in Akdere Village which is situated 30 km southwest of Silifke.

The Akdere Formation is composed of biohermal limestone and quartzitic sandstone, siltstone and shale alternations.

The biohermal limestone is dark gray, partly sandy, dolomitic and highly fossiliferous. The quartzitic sandstone is white to pink, intercalated with reddish brown to buff coloured siltstone and olive-gray shale. A few oolitic iron ore (hematite) beds exist in the middle part of the formation. The top of each biohermal limestone shows to some extent iron encrusting which might indicate cessation of deposition and beginning of lagoonal conditions.

The Akdere Formation is easily recognizable in the field, due to its reddish-brown to buff color. It conformably overlies the Büyükeceli Formation.

Fossils such as Disphyllum caesoitosum, Hexagonaria sp., Thamhooora sp., Cyphoterrorhynchus gr. and arpaehsis collected from the Akdere Formation indicate a late Devonian age.

Akdere Formation might have been deposited in an open shelf and possibly backreef and lagoonal conditions. Fluctiations of sea level might give rise to alternation of reefs and iron bearing lagoonal sandstones and shales.

Permian System

Kırtıldağı Formation

In the Southern region, the Kırtıldağı Formation outcrops around the Akkuyu site forming the highest hills such as Gökdegik, Kizilin, Çarkgedik, Taşlıburun and Taşlık hills. Near the Akkuyu NPP site, the Kırtıldağı Formation unconformably overlies the Akdere Formation starting with 20 m thickness, dark grey, medium to thick-bedded lime mudstone and foraminiferal wackestone, which is conformably overlain by 25 m of pink, cross-bedded quartzit. Fossils collected from the lower limestone unit yielded Early Late Permian age, such as Pachyphlaina sp., Staffella sp., Pseudovermigoella sp., Polydioxedina.

The middle part of the Kırtıldağı Formation in the Southern region is represented by highly fossiliferous, gray, well-bedded foraminiferal wackestone with packstone intercalations. The limestone is rich in brachiopods, corals, gastropods and especially in foraminifers indicating Late Permian age such as: Mizzia Velebitana, Permocalculus sp. and Geinitzina.

The second limestone unit is conformably overlain by pink, cross-bedded quartzitic sandstone which grades upward into dark gray, thick-bedded partly dolomitic wackestone. Dolomite intercalations increase towards the top of the formation. The upper part of formation is characterized with typical stromatolithic bedding.

Everywhere in the Southern region the Kırtıldağı Formation unconformably overlies the Akdere Formation, except north of Taşlık Hill where it is underlain by the quartzitic sandstone member of the Ovacık Formation. This situation may indicate to a Pre-Late Permian faulting.

Triassic System

Kargıcak Formation

The type section of the Kargıcak Formation lies 20 km northeast of the Akkuyu NPP site and 1 km west of the Kargıcak Village. At the type section the Kargıcak Formation starts with yellowish gray to maroon, varicoloured marls with bluish gray, thin-bedded, partly oolitic grainstone and wackestone interbeds. Oolitic grainstone interbeds include dwarf gastropods called Naticella sp. Microfauna obtained from limestones and marls such as Ammodiskus sp., Meandrospira sp. indicate Early Triassic age for the lower part of the Kargıcak Formation.

Varicoloured marls with thin limestone interbeds are conformably overlain by gray, thick-bedded dolomitic limestones and dolomites. The following microfossils were obtained from the dolomitic limestones indicating middle Triassic age: Citaella Iulis Silva and Agathamina sp.

The total thickness of the Kargıcak Formation is 250 m. Locally a thin boxite horizon may occur at the top of the Kargıcak Formation.

The Kargıcak Formation does not outcrop near the Akkuyu NPP site.

Kuşyuvasıtepe Formation

The type section of the Kuşyuvasıtepe Formation is 2 km south of Akkuyu. It also outcrops east of Hacıishaklı Village. The Kuşyuvasıtepe Formation is composed mainly of white thick-bedded, very fine grained mudstone and wackestone with occasional chert nodules. A thin basal conglomerate has been observed only at Kizilin hill where white, well-bedded cherty wackestone is overlain by gray, wavy bedded, partly nodular, politic grainstone with abundant crinoids.

The thickness of the Kuşyuvasıtepe Formation is 150 m. At the type section hear Akkuyu it unconformably overlies the Kırtıldağı Formation. It is the youngest Mesozoic rock unit outcropping in the Akkuyu region and it is unconformably overlain only by Quaternary deposits.

The following fossils were obtained from the Kugyuvasitepe Formation indicating to Middle-Late Triassic age: Endothyra cf, Kupferi, Endothyronella Wirzi.

Jurasstic System

Lower Department

Dibekli Formation

The Dibekli Formation is named after the Dibekli Village which is situated 20 km northeast of the Akkuyu NPP site. Dibekli Formation locally starts with a basal conglomerate which is overlain by dark gray, well bedded lime-mudstones and wackestones. Slope breccias and intraformational conglomerates are common at the base. At the top of the Dibekli Formation oolitic and oncolithic grainstones and packstones are intercalated with oolitic iron beds and iron stained quartzitic sandstones. These beds are distinguished from the remaining part of the Dibekli Formation to form the Isiklikiziltepe Member.

Dibekli Formation is developed largely in the eastern part of the Southern Region where it unconformably overlies either the Kargıcak or the Kuşyuvasıtepe Formation. It does not exist in the Akkuyu region, possibly because of uplifting and erosion which took place after the Triassic. Only the upper part of the Dibekli Formation exists in the Middle Region where it unconformably overlies all the older rock units. In the type section the following microfossiIs were obtained from the Dibekli Formation indicating Early Jurassic age: Mayncine termieri, Paleodasycladus medius,

Taumatoporella sp., Ammobaculites sp., Orbitopsella praecursor, Lituosepta reacoarensis, Tetrataxis cf. conica, Haurania amiji, Pseudocuclamina sp., Reophax sp., Pseudocyclamina lituus Trocholina sp.

The maximum thickness of the Dibekli Formation cropping out in the Middle Region is 30 m.

The Dibekli Formation was deposited on the edge of a carbonate platform.

Tokmar Formation

The type section of the Tokmar Formation lies 1 km south of Tokmar Village which is situated 25 km southwest of Silifke.

Tokmar Formation starts with light gray, thick to medium bedded dolomites and dolomitic limes-intones which are overlain by white coloured well-bedded carbonate muds tone and wackestones. A very thick-bedded to massive, white, partly pseudoolitic biomicrite bed overlying the dolomitic lower part of the Tokmar Formation can easily be recognized in the type section and serves as a marker horizon for the Tokmar Formation which outcrops in all geotectonic regions. However, Tokmar Formation does not exist in the Akkuyu area probably due to erosion. The thickness of the Tokmar Formation is 700 m.

Tokmar Formation unconformably overlies the Dibekli Formation and the other older rock units in all geotectonic zones. The following microfossils were obtained from the Tokmar Formation indicating to Middle-Late Jurassic to Lower Cretaceous age: Pfenderina Neocomiensis and Kurnubia Palesiniensis.

The Tokmar Formation was deposited on an open carbonate shelf.

Cretaceous – Paleocene Period

Hayvandağı Formation

The name of the Hayvandağı Formation has been taken from the hill which is called Hayvandağı situated 2 km east of Hırmanlı Village.

Hayvandagı Formation is mainly composed of white coloured, medium to thick-bedded wackestone. Locally a basal conglomerate may exist at the base of the Hayvandağı Formation. It unconformably overlies all the other rock units older than Late Cretaceous including the formations of lower Paleozoic age.

Thickness of the Hayvandağı Formation is about 200 m.

The following fossils were obtained from the base of the Hayvandagi Formation indicating to Late Cretaceous: Globotruncana arca, G. Stuarti, G. Conica.

From the upper part of the Hayvandağı Formation the following fossils were obtained indicating to Paleocene age: Gavelinells sp and Miscellenes sp.

Neocene period

Miocene

Silifke Formation

Silifke Formation does not exist in the southern region around the Akkuyu NPP site. The nearest outcrop of the Silifke Formation in the southern region east of the site is in Boğsak Village where the Silifke Formation unconformably overlies the Tokmar Formation.

Pliocene-Quartenary Period

Plio-Quaternary breccias

Talus breccias of old alluvial fans with peculiar red cement outcrop under the young alluvium of a small creek at the Akkuyu site and on a slope 500 m north of the site overlaying members of Büyükeceli formation and Akdere formation.

They also occur along the shore 3 km west of the site, southwest of Karacadollugu Hill. They consist of pebbles, cobbles and boulders mainly of the Büyükeceli, Akdere and Kırtıldağı Formations.

Clasts of the talus breccias are not sorted. They are strongly cemented with a peculiar red limy material. Outcrop patterns and lithologic characteristics indicate that talus breccias have been deposited under subaerial conditions over this flat topography, transported by small creeks or accumulated by the direct influence of the gravity. They are assumed to have been deposited during early Quaternary or even Pliocene times since they are overlain by recent Quaternary alluvium.

They have been subjected to Karstic processes. Solution cavities of breccias are filled with caliche and clay which might have been deposited by Karstic waters.

Quaternary System

Recent Alluvium Fans

Alluvial fans occur in the mapped area where small streams run out on to the coast. They show an initial dip of 5 - 10° degrees towards the south and they mainly consist of conglomerates with coarse sandstone intercalations. Boulder and cobble size clasts of conglomerates are strongly cemented by red limy matrix.

Recent alluvial fans exist in the Akkuyu NPP site unconformably overlying Plio-Quaternary breccias.

It is supposed that the age of the recent alluvial fan of Akkuyu site may very between 5000 and 10 000 years.

Calichi

Calichi deposits are very common along the coasts of the Mediterranean Sea. In the area under investigation calichi beds have been deposited on the Aksaz bay and along the coast line1 km north of Kuşyuvası Hill.

The formation of calichi results from the effect of evaporation. Fissures and cracks which are very common in calichi deposits should not be considered as tectonic features. They are synsedimentary in origin.

Some calichi beds are formed as a cluster of tubes. There is a hole inside each tube through which limy sea water rises up by capillary movement due to evaporation and is deposited as $CaCO_3$ at the top of the tube. Consequently, cubiform calichi deposits grow upwards as a cluster of tubes. This is a common phenomena which have taken place along the shore north of Kuşyuvası Hill. Three steps of calichi deposits indicate that the sea level was 2 - 3 m higher than it is now when the first calichi terrace was formed some 4000-5000 years ago.

Neither calichi deposits nor recent alluvial fans show any evidence of faulting.

6.1.3.3 HYDROGEOLOGICAL CONDITIONS OF THE AKKUYU NPP NEAR REGION

The following water-bearing strata can be identified under the hydro-geological map of 1/500000, Adana sheet (Figures 6/1.13, 6/1.14 and in Appendix J), in the Akkuyu region:

- quaternary water-beating strata in unlithified deposits, highly water-abundant with specific capacities more than 2 l/sec/m (K_1);
- locally-spread quaternary water-bearing strata in unlithified deposits, highly water-abundant with specific capacities from 0.5 up to 2 l/sec/m (K_1);
- non-productive water-bearing strata of the Permian-Carbonic age (pK_1) with specific capacities less than 0.1 l/sec/m;
- non-productive water-bearing strata of the Devonian age (d_2) with specific capacities less than 0.1 l/sec.

The quaternary water-bearing strata are mainly developed in the river valleys. As to the Akkuyu NPP region the alluvial water-bearing strata are located in the Sipahili river valley (7km to the west from the NPP site) and Büyükeceli (2.5km to the east from the NPP site) as a belt of 400-1.000m wide.

Sands and gravel and pebble deposits represent the water-containing rocks. Thickness of deposits varies from 40 up to 100m.

The filtering parameters identified by pumping tests are as follows:

- for alluvial deposits of the Sipahili river the specific capacity was 13 – 80 l/sec/m, water transmissivity T = 1500 – 8500 m^2/day;
- for alluvial deposits of the Büyükeceli river the specific capacity was 0.89 l/sec/m, water transmissivity T = 100 – 180 m^2/day.

The ground water level changes from 2.5 down to 3.5m in the valley of the Büyükeceli and up to 2m in the Sipahili valley.

The ground water flow in the Sipahili valley during the year is directed to the Mediterranean Sea. In the Büyükeceli valley the ground water flow is directed to the Mediterranean Sea in winter time, and in summer its direction can change due to water pumping from isolated wells.

The alluvial horizons are being recharged from infiltration of precipitation as well as seepage from rivers along their entire length.

The alluvium ground water chemically is alkaline moderately hard with mainly ions of Calcium, Magnesium and bicarbonate.

The alluvial water-bearing strata of these rivers are being used for local water supply via operational wells.

Under the investigation findings of 1973 the affirmed reserve of the ground water amounts to $0.8x10^6m^3$/year in the Büyükeceli valley and $2.6x10^6m^3$/year in the Sipahili valley.

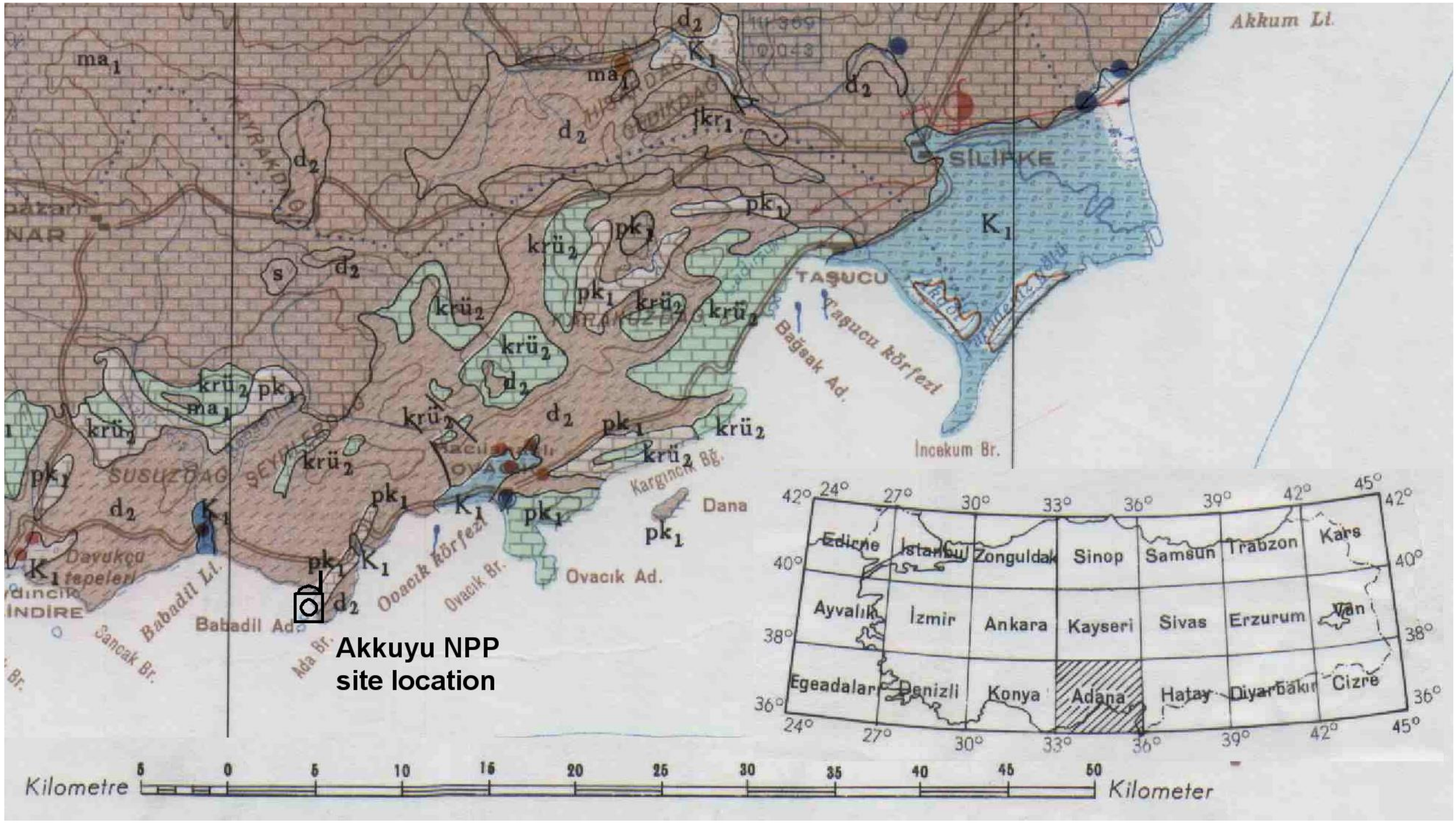

DSİ 1970 - Hydrogeological Map of Turkey (scale:1/500.000) - Adana sheet

Figure 6/1.13 – Hydro-geological map of the Akkuyu NPP region (from the map of 1/500000)

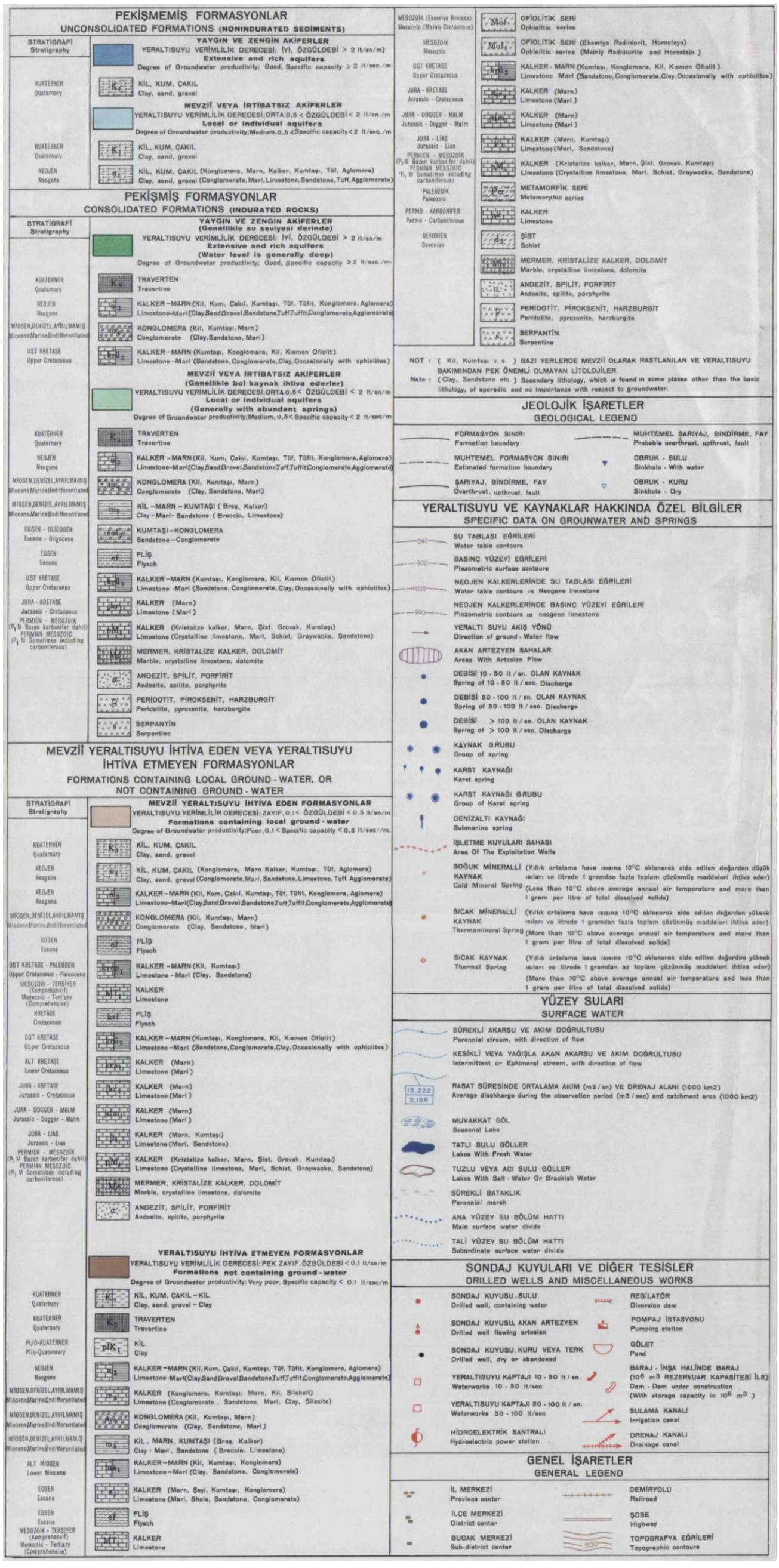

DSİ 1970 - Hydrogeological Map of Turkey (scale:1/500.000) - Adana sheet

Figure 6/1.14 – Legend to the hydro-geological map

The water-bearing strata attributed to carbonate rocks of the Paleozoic, Mesozoic and Cainozoic, used to have anisotropic hydraulic properties. The rocks themselves have no porous structure and conductivity. However, ground waters are retained in fissures filled with microfragmental soil which occurred in the result of tectonic movements and in cavities emerged due to karstification. After accumulation in a certain system it emerges as springs with different capacities (for instance, submarine springs in the Ovacik valley) [6/212].

The submarine springs in the Ovacik valley are located at a distance of 25 – 30km to the north-east from the Akkuyu NPP site and have karst origin. Capacities of the inspected springs were from 0.3 up 8m^3/sec [6/212].

In some places there are small springs resulted from contact of a formation and along the entire shore. The most important springs with fresh water are located in the NPP region:

- Aksaz springs located at a distance of 1.5km to the west from Akkuyu, capacity around 1 – 2 l/sec;
- Kocaşli spring located to the east from the settlement of Kocaşli and with discharge rate from 5 l/sec (dry season) up to 400 l/sec (winter);
- Soguksu springs located to the west from the settlement of Gilindere with discharge rate from 1,120 up to 7,931 l/sec.

In conclusion it is worthwhile to note, that:

- a set of Paleozoic rocks, which cover a large area in the Akkuyu NPP vicinity, under the existing data is not suitable for water supply purposes as the ground water in these deposits have insignificant discharge rates.
- the carbonate rocks of the Jurassic-Cretaceous and Miocene ages contain waters. But the karst sources with discharge rates 0.3 – 8 m^3/sec formed by the formations are located at a distance of 25 – 50 km from the Akkuyu site.
- Sipahili and Büyükeceli valleys nearby Akkuyu contain ground water in the alluvial deposits. The discharge of a well in the Büyükeceli valley is 5 – 6 l/sec, in the Sipahili valley – 40 l/sec. But these strata located only in the valleys of the mentioned rivers.

6.2 SITE VICINITY SURVEY

According to IAEA SSG-9 [6/113] site vicinity studies should cover a geographical area typically not less than 5 km in radius. In addition to providing a yet more detailed database for this smaller area, the objective of these investigations is to define in greater detail the neotectonic history of the faults, especially for determining the potential for and rate of fault displacement at the site (fault capability), and to identify conditions of potential geological instability of the site area.

This section provides some details on the offshore geophysical, geological and geomorphological investigations and the studies performed in the site vicinity to account for earth related hazards. In addition, Section 6.6 provides detailed fault displacement hazard assessment with emphasis on the site specific investigations performed in the site vicinity to demonstrate that there is no potential for surface faulting at the site.

6.2.1 MARINE GEOPHYSICAL SURVEY

The seafloor morphology of the Northeastern Mediterranean is largely controlled by tectonic features and high sediment input from large rivers [6/8].

Cilician Basin is bordered by the coastal strip from Anamur to Mersin to the north, the Iskenderun Basin to the east, the Antalya Basin to the west and Kyrenia Mountains in Cyprus to the south. The sedimentation in Cilician Basin is mainly controlled by four majors rivers; Ceyhan, Seyhan, Tarsus and Göksu rivers. The Akkuyu NPP site is located in the northern part of the Cilician Basin, to the west of the Göksu River (Figure 6/2.1).

Figure 6/2.1 – North Eastern Mediterranean and Akkuyu (Images from Google Earth)

6.2.1.1 SEISMIC SURVEY IN 2011

A high resolution seismic survey was conducted offshore Akkuyu in 2011 [6/74]. Location map of seismic profiles is given in Figure 6/2.2. The seismic data obtained from the study area were interpreted using the seismic stratigraphic principles [6/45]. Seismic reflection profiles revealed the existence of an erosional surface separating a seismic unit and the acoustic basement.

A reflector (Reflector R) with high amplitude is observed in all seismic profiles. There is no prominent reflector beneath this surface. The strong reflector (Reflector R) forms the upper surface of this basement rock unit.

In the late glacial maximum, sea level was about 125 meter below the present sea level (Fairbanks 1987). During this glacial age all the shelf areas of the Mediterranean Sea were exposed to subaerial erosion and excavated by rivers and streams. Therefore, it is thought that the reflector R is an erosional surface which was formed during the lowstand of sea level before the latest rise.

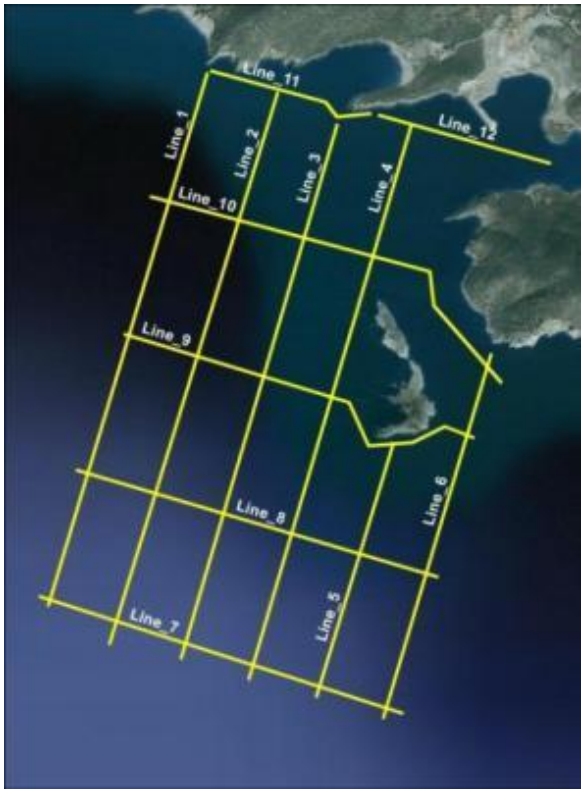

Figure 6/2.2 – Location Map of the Subbottom Profiles Collected in the Study Area [6/74].

A seismic unit (Unit A) on the reflector R has been defined in the seismic profiles. It has been deposited during the Flandrian transgression following the glacial maximum. The upper surface of the Unit A represents the present sea floor. It is difficult to define the internal configuration of Unit A because of the thin deposition. It is observed in some places that the internal reflectors of this unit are typically semi-continuous parallel reflections.

The thickness of Unit A is calculated where the reflector R is present. Near the shoreline, the reflector R cannot be observed because of the lack of penetration due to thick Unit A deposits. The distribution map of the Unit A thickness in milliseconds (msec) is represented in Figure 6/2.3.

Some representative seismic sections along profile lines 5 – 7 are given in Figures 6/2.4 to 6/2.6.

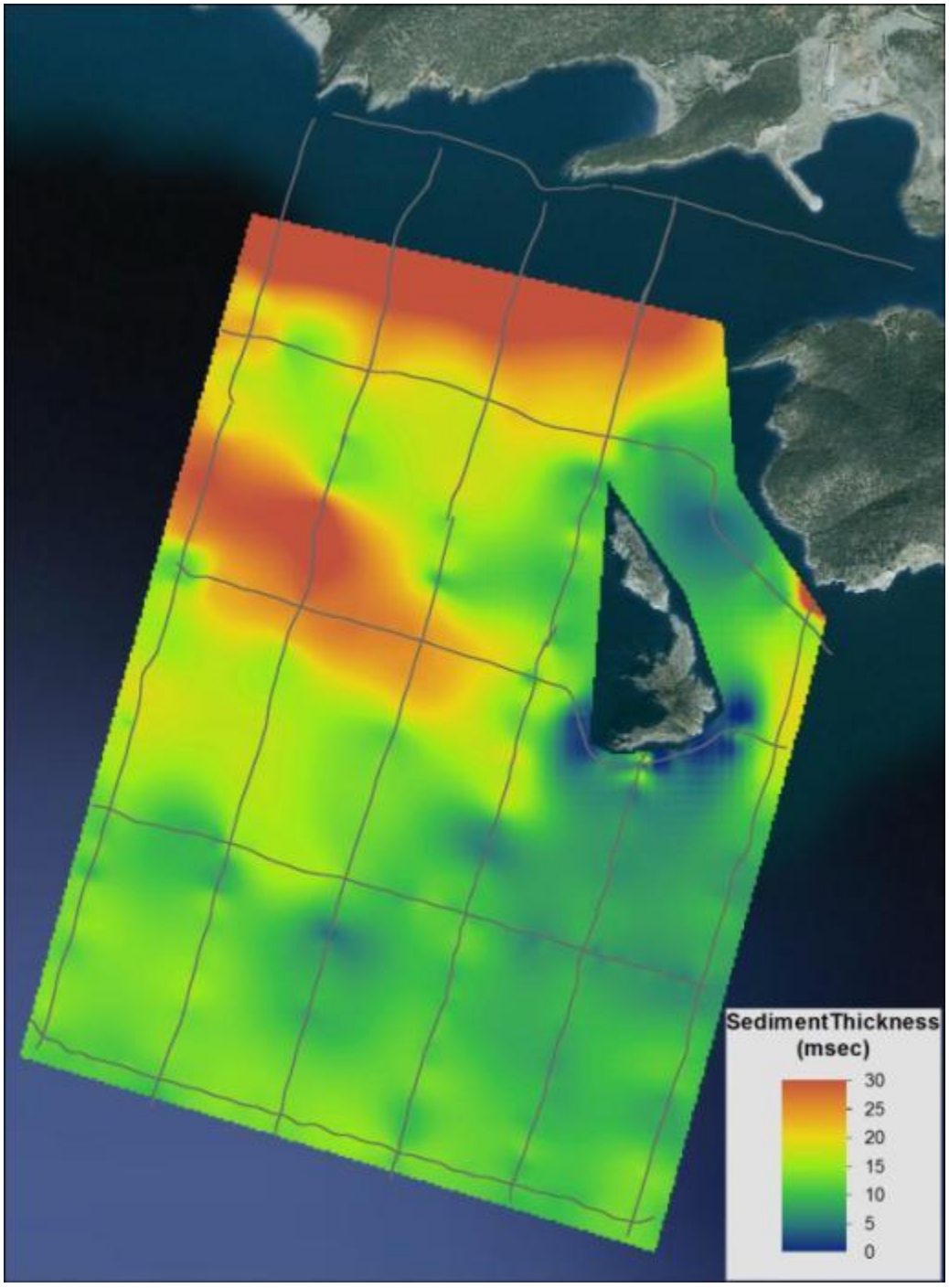

Figure 6/2.3 – Thickness map of the Unit A in milliseconds

In the text the thickness values are given in meter (m) taking a seismic velocity of 1500 m/s for time-to-depth conversions, providing minimum estimates of unit sediment thickness.

The sedimentation is limited in the study area because of the lack of a significant source of sediment and an accommodation place. The distribution of Unit A is controlled mainly by the seafloor morphology and it is best developed along the coast. It is limited or almost non-existed in the areas around the islands (Figure 6/2.3).

It becomes thinner seaward in the study area, as observed on the profiles Line 1 to 6. It is almost disappearing at Line 9 because of the extensions of the island's rock (Figure 6/2.2). It thickens in the near shore region due to relatively greater fluvial sediment supply. It reaches its maximum value of 23m at the northern coast of the study area.

According to the results of marine seismic survey done in 2011 within the Akkuyu NPP sea area, it can be concluded that the dominant factor on sediment thickness distribution is paleo-relief of the shelf. Reflector R forms the upper surface of the basement rock unit.

A local channel like feature which is almost parallel to the coast is observed in the thickness map and seismic profiles (Figure 6/2.3). The thickness of Unit A in this channel has a range between 7 m and 14 m.

This channel can be the result of excavation of a river or a faulting activity. Because of the lack of seismic penetration to the basement rock, the fault is not observed clearly on the seismic profiles. The fault, if it exists, at this location does not deform the recent sediment deposits, so it is concluded that it is a feature with no recent activity. Figures 6/2.4 to 6/2.6 provide the interpretation of seismic lines 5 – 7.

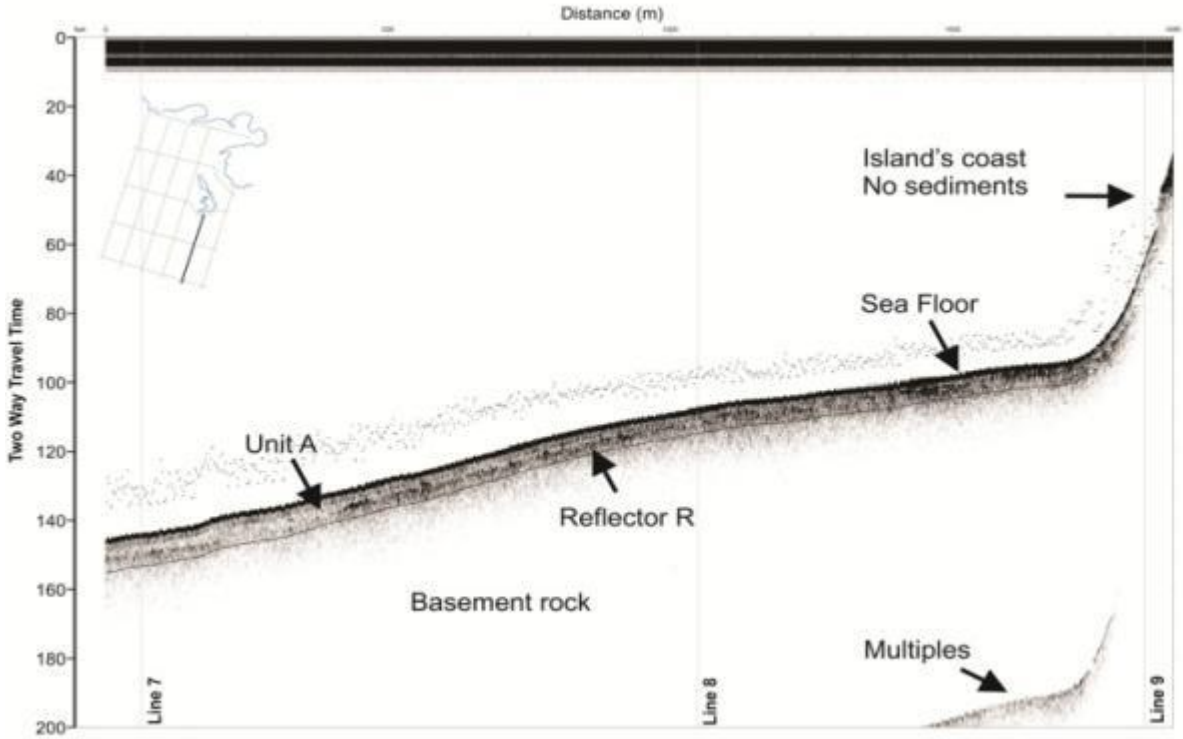

Figure 6/2.4 – Seismic Interpretation of Line 5

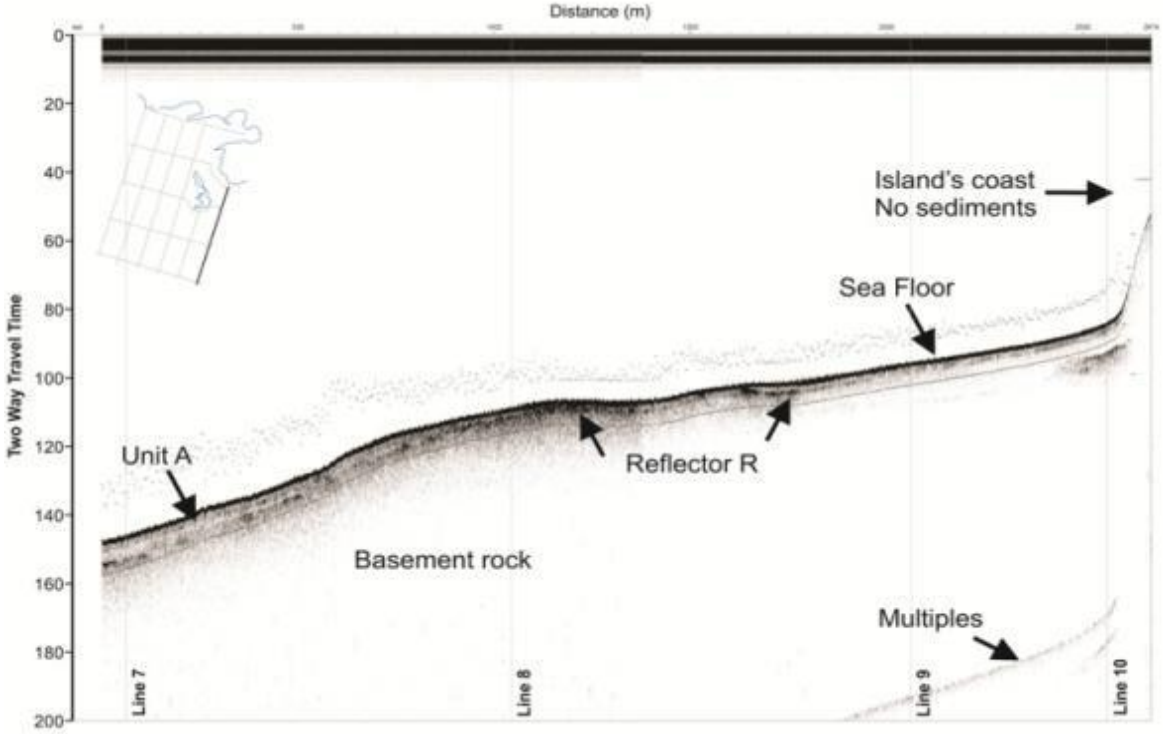

Figure 6/2.5 – Seismic Interpretation of Line 6

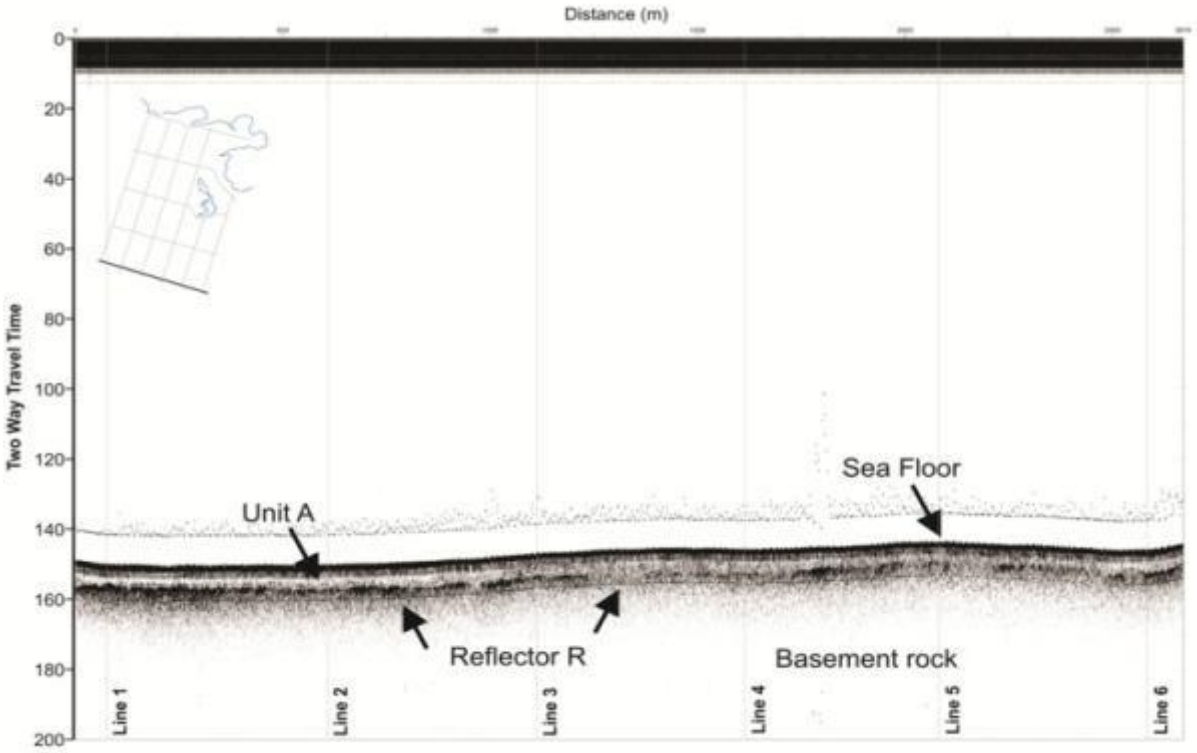

Figure 6/2.6 – Seismic Interpretation of Line 7

6.2.1.2 MARINE GEOPHYSICAL SURVEY IN 2012

In 2012 marine seismoacoustic survey was performed in order to study geotectonic features of the Cilician Basin in the Mediterranean Sea.

The survey was done 30 km east from the Akkuyu NPP site along six profiles covering an area of about 55x60km (more than 2700km^2) adjacent to the Southern Turkish shore by Silifke.

The main objective of the 2D Multi-channel Marine Sparker Survey was to identify the main structural-tectonic elements of the Cilician Basin that can be considered as seismogenic in the seismic hazard assessment of the Akkuyu NPP site.

The Study area lies within the Cilician Basin contiguous to the onshore Adana Basin–offshore Cilicia Basin. These two basins lie just to the north of the boundary of the Eurasian and Africa plates (Figure 6/2.7).

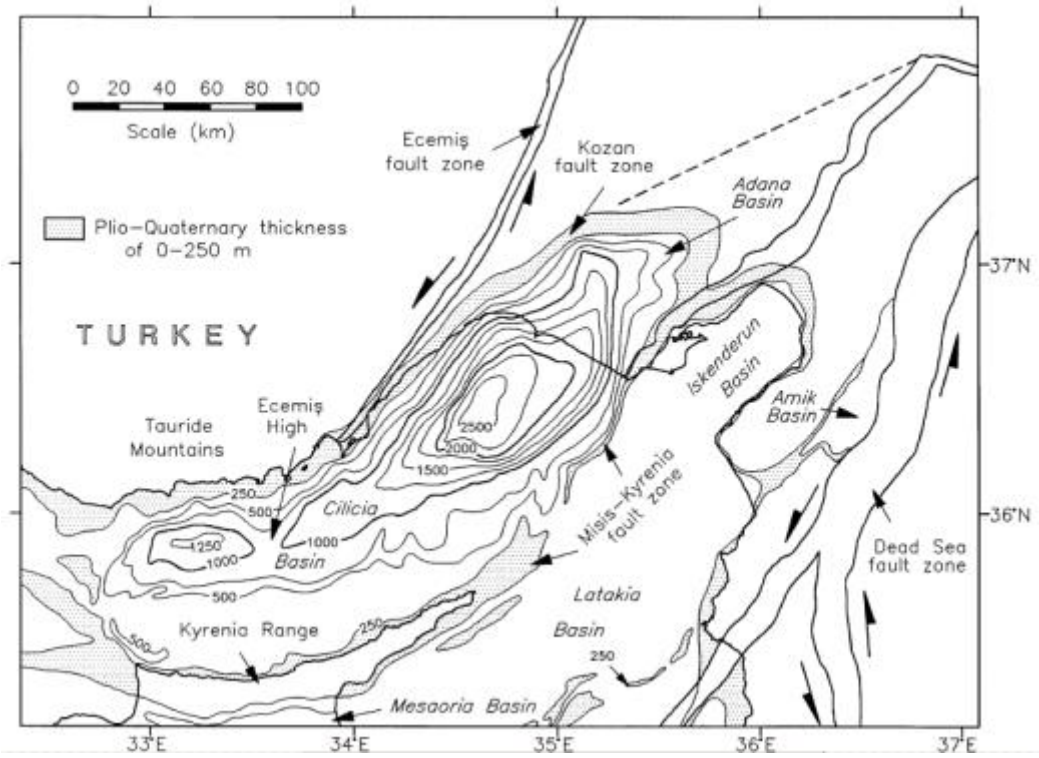

Figure 6/2.7 – Map Showing The Plio-Quaternary Thickness and Major Structural Framework of the Adana-Cilicia Basin [6/8]

The geology of the adjacent coastal region of the study area is dominated by Plio-Quaternary deposits (see Figure 6/2.7) overlying the Late Tertiary (mainly Miocene) limestones, marls, sandstones and conglomerates. The Plio-Quaternary deposits are characterized by terrace deposits, alluvium, slope debris, alluvial fans and travertine [6/172]. The Cilicia Basin can be divided into an E–W trending deeper Outer Cilicia Basin in the west and a NE–SW trending shallower Inner Cilicia Basin in the northeast. The Adana Basin in the northeast represents the onshore extension of the marine Cilicia Basin. Four rivers (Seyhan, Ceyhan, Tarsus, and Göksu)

provide most of the siliciclastic input into the Cilicia–Adana basin complex; Seyhan, Ceyhan, and Tarsus Rivers form a major deltaic complex that occupies the Adana Basin [6/8].

The Plio-Quaternary is expressed in the oil exploration seismic data as a regularly reflective package of acoustically strong and continuous composed of siliciclastic successions of Plio-Quaternary age. The base of this unit is marked by a strong and distinctive reflector, identified in the eastern Mediterranean as the M-reflector. This unit is thickest along the central axes of both the Inner and Outer Cilicia basins, and sharply thins toward the Kyrenia Range and the southwestern Turkish coast. In the southern Adana and Inner Cilicia basins, this unit is characterized by a prograding wedge of deltaic sediments, which reaches its maximum thickness of ~ 2500 ms immediately seaward of the present-day mouths of Seyhan and Tarsus Rivers. In the Inner Cilicia Basin, a predominantly transparent subunit with weak and discontinuous parallel reflections occurs at the base of the Plio-Quaternary succession, and is correlated with the early Pliocene.

The Miocene (Messinian) is generally characterized by a low reflectivity package with weak and often discontinuous reflections, although in the Outer Cilicia Basin, the succession has a stratified appearance delineated by discrete continuous reflectors with a corrugated geometry. It is readily distinguished by its strongly reflective top reflector (M reflector) and its less reflective and more discontinuous base. This unit is composed predominantly of halite alternating with lesser quantities of anhydrite and limestone, and is correlated with the Messinian evaporites. It is missing, or very thin, near the Turkish margin of the basin complex. In the northwestern Outer Cilicia Basin, a strongly reflective package of conformable parallel reflectors occurs as distinct mound-shaped bodies, correlated with Messinian-bedded pebblestone, sandstone, gypsiferous, and fossiliferous limestone successions. In the central portion of the basin, the seismic facies shows a clear lateral transition to the low reflectivity halite dominated succession typical of the local Messinian.

The **Miocene (pre-Messinian**) underlies the M-reflector and the Messinian evaporites when present. This unit is subdivided into two major seismic stratigraphic subunits.

The upper subunit is characterized by lower frequency rhythmic reflections, showing good lateral continuity. Data from the exploration wells show that it is composed of fluvio-deltaic successions of mainly Tortonian age. The base of the unit is a prominent, but discontinuous, reflector that locally represents an unconformity. In the northwestern Outer Cilicia Basin, a thick strongly parallel reflective package underlies the mound-shaped deposits of the Messinian. This seismic unit extends as a south thinning wedge below the evaporite-dominated succession of Messinian age;

The lower sub-unit of the pre-Messinian consists of high frequency, continuous, rhythmic reflectors, mainly composed of middle Miocene turbidite succession.

According to [6/8] the deposition of the Miocene successions in the Cilicia–Adana basin complex occurred within a foredeep, south of the arcuate Tauride fold–thrust belt. The entire region became emergent during the Messinian salinity crisis, and up to 1000 m of evaporites were deposited in the Cilicia and southern Adana basins. Stratigraphic and structural relationships demonstrated that the late Plio-Quaternary Cilicia–Adana basin complex evolved as an asymmetric piggy-back basin on the hanging wall of the large south-verging Misis–Kyrenia thrust culmination.

On the Misis–Kyrenia segment of the culmination, thrust activity ceased in early Messinian, whereas on the Kyrenia segment, it continued to the present. The shift in the kinematics is expressed by the development of the NE–SW trending steep faults with extensional separations bounding the Plio-Quaternary depocentre in the Adana and Inner Cilicia basins.

Progressive westward displacement of the Tauride block within the Aegean–Anatolian microplate created a localized transtensional regime within the Inner Cilicia and Adana basins. The northern basin-bounding fault system, including the Kozan fault in the Cilicia Basin, is a set of large antithetic structures linked to the master faults.

A major antithetic structure started activity in the lower Pliocene separated the Sourthern and northern sections of the Outer Cilicia basin, with a northward migration of the locus of the depocentre, also accompanied by a 900 ms drop in the depth of the M-reflector.

Two major fault zones may extend through the surveyed area, the Ecemiş Fault Zone and the Kozan Fault Zone (see 6.1.2.5 and 6.1.2.6 sections)

The Kozan Fault zone corresponds to the 200 km long Kozan-Mersin section of the fault zone. It is covered by the Upper Miocene-Pliocene deposits, therefore, its trace could only be identified by the help of the data obtained from the boreholes drilled in the Adana basin. It is seen that some of the earthquake epicenters are aligned parallel with its trace.

Four horizons within the Plio-Quaternary sequence were tentatively interpreted across all profiles. This interpretation is a coarse representation of the seismic-stratigraphy of the surveyed area. The relationship between the shape and extent of the sediment bodies and the separation of the seismic profiles does not allow for clear correlation of the seismic units across the major depositional domains (continental shelf, slope, abyssal plains and canyon troughs). Nevertheless, these horizons are locally consistent and serve as geometrical markers for the interpretation of the major faults, the key objective of this survey.

The predominant characteristics of the seismic units are given in Table 6/2.1.

Table 6/2.1 – The Predominant Characteristics of the Seismic Units

Unit	Acoustic facies	Internal configuration
1	Generally high amplitudes on the bottom, locally loss of amplitude to the top; good lateral continuity	Generally parallel. Sometimes chaotic near fault zones. Sigmoid and chaotic near the shelf.
2a	High to Medium amplitude; alternating strong and weak reflections in the prograding bodies near the continental shelf. Good lateral continuity	Sigmoid and oblique progradational bodies, sometimes chaotic. Parallel offshore . Common channels features towards offshore.
2b	Medium to low amplitude; good continuity	Sigmoid and oblique progradational bodies, sometimes chaotic. Parallel offshore
3	Low amplitude; weak continuity;	Parallel. Poor internal reflections, mainly chaotic. Flat surface, sometimes slightly undulating.

The methodology of the performed marine geophysical survey allows providing for a depth of survey of no less than 100m if the thickness of the marine bottom sediments is more than 25 m and determination accuracy of layer bedding boundaries of 0.5m to 1.0m.

The survey was conducted along the grid shown in Figure 6/2.8.

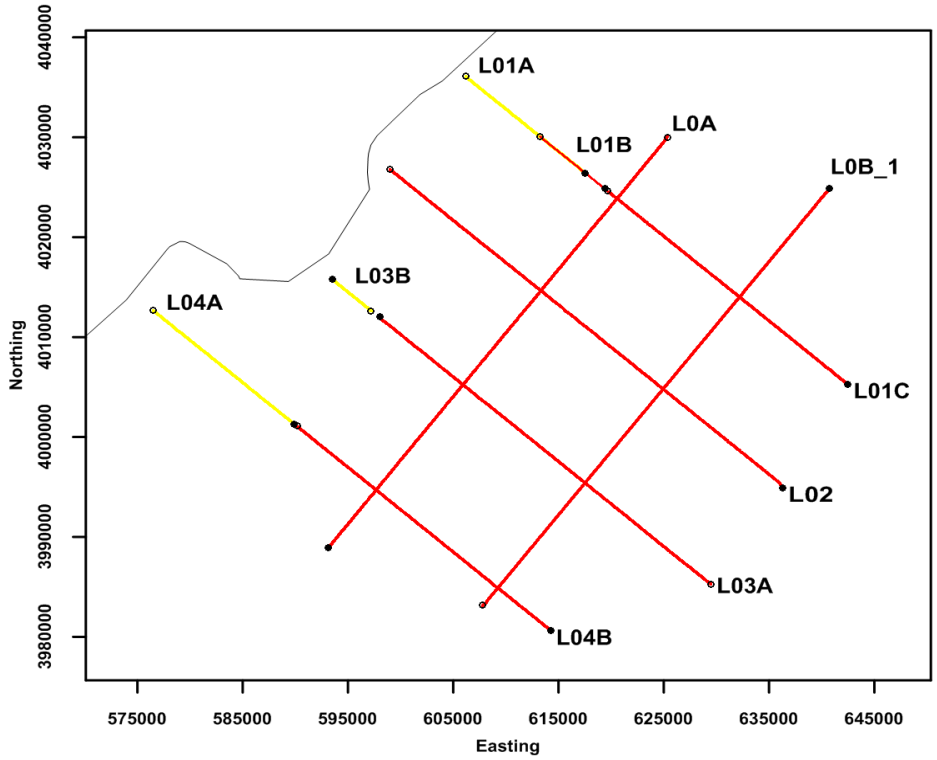

Figure 6/2.8 – Layout of marine geophysical survey in 2012. Survey Grid: Yellow Lines - Shallow Water Profiles; Red Lines - Deep Water Profiles; Open Circle - Start Of Line; Black Circle - End Of Line.

The survey grid comprises six, 50km long profiles, arranged in four main lines, perpendicular to the shore at 12km spacing and two tie lines parallel to the shore, 15km apart.

Orientation of the main lines is 130° - 310° N, and orientation of the tie lines is 040° - 220° N.

The survey water depths varied significantly, between 10m and 970m, from the shallow near shore continental shelf to the deeper Cilician basin offshore.

In order to optimize the acquisition parameters to the changing depths, the lines were split into shallow and deep water segments, 3 shallow water segments and 7 deep water segments.

In total, 10 profiles were acquired and processed for a total linear distance of 309km.

The conclusions of the survey point out that all major deformation features affecting the seabed and/or the Plio-quaternary sediments present in the multichannel sparker profiles were identified and, where possible, correlated with the available bathymetric data.

6.2.2 GEOMORPHOLOGY AND RELIEF OF THE SITE VICINITY

The highest points in the combined watershed area were Kizilin Hill (269.8 m) at east, Taşlık Hill (221 m) at west, Taşlıburun Hill (171 m) at far west and Kuşyuvası Hill (197 m) at the south and a number of topographical highs without names.

The general morphology of the area was characterized by a gradual and continuous increase of elevation from coastal planes towards inland (Figure 6/2.9). The highlands and footslopes were incised by streams creating a moderate to steep topography (Figure 6/2.10).

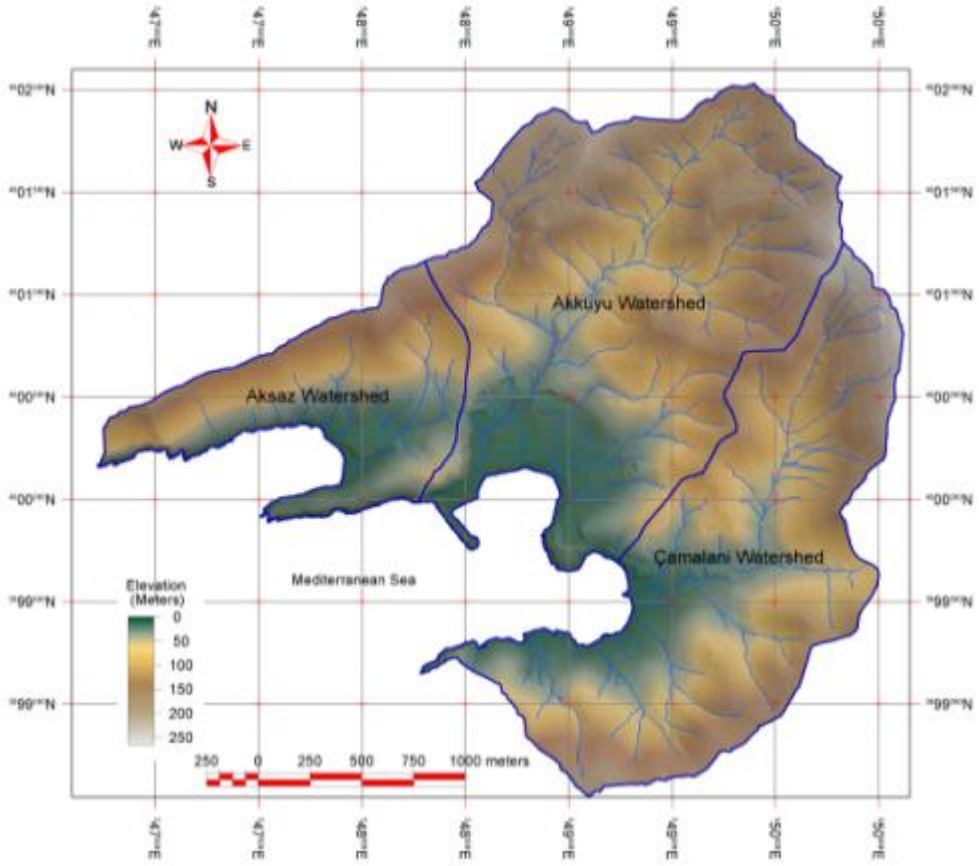

Figure 6/2.9 – Digital Elevation Model of the Project Area Watershed

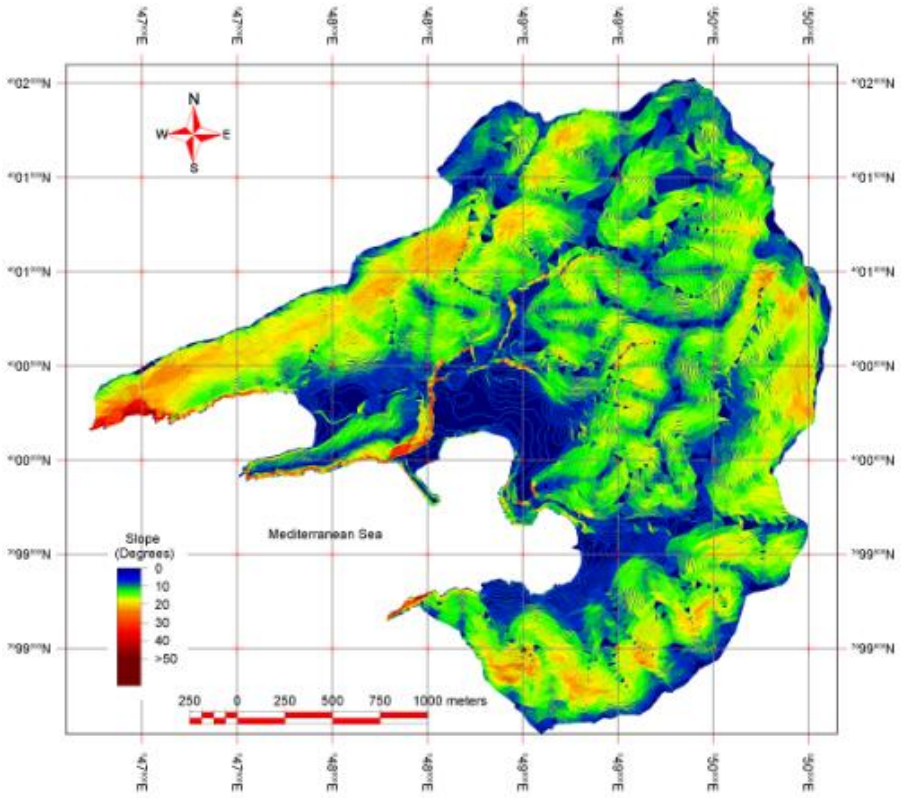

Figure 6/2.10 – Slope Map of the Project Area Watershed

All three bays have their individual coastal plains. However the coastal plains were altered significantly by human activity. In Aksaz Bay significant spoil piles (5 - 8 m in thickness) are present, covering old valleys extending the plain in higher unnatural elevations for coastal deposits.

On the other hand the major activity was at Akkuyu Bay, significant excavation yielded in a approximately 800 meter long scarp at immediate east of the Inceburun Hill, a flat surface (~300x300m) east of Inceburun Hill, and a spoil pile (~400x200m) east of Akkuyu Bay, and even shoreline had been altered by sea fillings for about approximately 100 m.

In Çamalanı Bay, an excavation area was observed in the border in between Akkuyu and Çamalanı watersheds near the coast and spoil piles were used to change the shoreline. Furthermore not only in the coastal areas but also further inland there were many spoil piles around the major roads as islands which change the topography. Within the frame of the engineering-geological survey a map of engineering-geological zoning in scale 1:1000 was compiled, where boundaries of man-made soils were determined.

Natural assemblages of mixtures of pine trees and wild olive trees were the major landcover type throughout the catchments. The canopy coverage of these assemblages ranged from moderate to dense. There exists no significant preference among the tree types for any particular type of lithology present in the area. Even at top of old spoil piles (~30 years) pine trees were growing naturally. However the natural sandy beaches at coastal plains and previously excavated surfaces had sparse vegetation cover.

In all through three catchments no major mappable scale karstic geomorphological units were observed. However in trench sections or cross sections created by excavations, meso scale karsts and their infilling reddish “terra-rossa” were observed.

6.2.3 STRUCTURAL GEOLOGY

In the region, the main folding and overthrusting events occurred prior to Early Jurassic due to Early-Alpine orogeny and orogenic processes throughout the entire Central Taurus belt ceased before Miocene which is followed by a regional uplift during Late Miocene – Pliocene times.

At the Akkuyu NPP site vicinity, Devonian age Büyükeceli and Akdere formations display a highly deformed structure (Figure 6/2.11). Figure 6/2.12 presents photo of excavations on the southern side of Inceburun Hill, this photo clearly shows that the Büyükeceli Formation is characterized by series of folds and faults.

Figure 6/2.11 – Close-Up Photo of Deformation of Member Db7 of the Büyükeceli Formation

Figure 6/2.12 – Photo Mosaic of the Southern Section of the Multi-Level Cut Slope at the South of Inceburun Hill

Unconformities

In the site vicinity, an angular unconformity have been identified between Kırtıldağı (Upper Permian) and Akdere (Middle Devonian) formations and also another between Devonian age bedrocks (Akdere and Büyükeceli formations) and Quaternary deposits.

Folds

In the region, folding developed in connection with Variscan and Alpine orogenic movements.

Near Akkuyu NPP site, fold axes trend WSW-ENE and W-E directions which are consistent with overthrusting identified in the north.

The ENE-WSW trending Akkuyu Anticline, which is displaced by shear faults, is one of the prominent structures of the area.

According to the previous microtectonic analysis, the original fold axis B0 (060°/0°) was rotated to B1 (065°/10° NE) suggesting that the Akkuyu Anticline was initially formed during Variscan orogeny and later affected by Alpine orogeny.

The Akkuyu Anticline is accompanied by the Akkuyu Syncline to the north. The southern part of Synclyne is displaced by the Akkuyu Fault.

Faults

Various kinds of faults have been identified in the previous studies [6/56]. Additional fault investigations were conducted in 2011 to study the tectonic nature of the major faults and the potential for their activity in Quaternary period.

Taşlık Overthrust

The fault trends NE-SW for a distance of 4 km, about 1 km north of Akkuyu site (immediate north of the mapped area). Along the Taşlık Overthrust various members of the Büyükeceli Formation have been thrusted over the Kırtıldağı Formation from SE to NW. At the north of Aksaz Bay, the orientation of the fault plane is measured as 050°/45°SE [6/56].

Field evidences suggest that the fault had been formed during Early-Alpine orogeny. The Taşlık Overthrust, which is displaced by the Aksaz Fault, is accepted as a dead fault.

Akkuyu Fault

This is a dip slip (normal) fault with latitudinal strike dipping 60^{o} N.

Akkuyu Fault is located in the northern part of the site and is the second largest fault after Taşlık Overthrust (extending for a distance of 1 km) in the site vicinity.

To the west, the Akkuyu Fault was offset by the Aksaz Fault. Based on borehole investigations made in the Aksaz alluvium, Demirtaşlı [6/56] argued that the displaced section of the Akkuyu Fault continued under the Aksaz alluvium.

The performed investigations showed that Akkuyu Fault did not have tectonic impact on Quaternary breccia sediments.

Aksaz Fault

The NNW-SSE trending Aksaz Fault dips towards ENE offsetting both the Akkuyu Fault and the Taşlık Overthrust. The fault is a thrust fault with a strike-slip component where Büyükeceli Formation was thrusted on to the Akdere Formation. In the south, the fault was covered by the Quaternary alluvium of the Aksaz Bay, now by artificial fill. Based on the previous borehole and

trench observations, it was concluded that the fault is not active [6/56]. This was also demonstrated by the works carried out in 2011.

Unnamed Thrust Fault

The unnamed thrust fault has meridian extension and is dipping towards east and has a total length of 500 m.

Along this fault, the oldest members of the Büyükeceli Formation have been thrusted over the Akdere Formation from east to west. The fault is cut by the Taşlık Overthrust in the north and by Akkuyu Fault in the south. Therefore, it has been assumed to be older than both of them.

Tear Faults

Presence of tear faults is quite typical for the territory of the site. They are trending NNW-SSE or NNE-SSW directions offsetting the axis of Akkuyu Anticline and marker horizons (Db3 and Db5) of the Büyükeceli Formation

Tear faults trending in NNE-SSW direction are more distinguishable as compared with the others. They display right or left lateral strike-slip movements.

They are likely to be formed during Early Alpine orogeny as tear faults associated with folding and overthrusting. In the site, some of them are covered partly by Quaternary deposits and newly formed artificial fill and do not show any recent fault activity.

Normal Faults

During the field campaign, several small scale normal faults were also observed along the cut slopes of the Akkuyu NPP site. These WSW-ENE trending faults are dipping 40 - 60° towards north and display minor offsets that occur within the Büyükeceli Formation. Absence of any active morphotectonic signature related to these fault suggests that they are recently inactive. A photograph showing example of such faulting is provided in Figure 6/2.13.

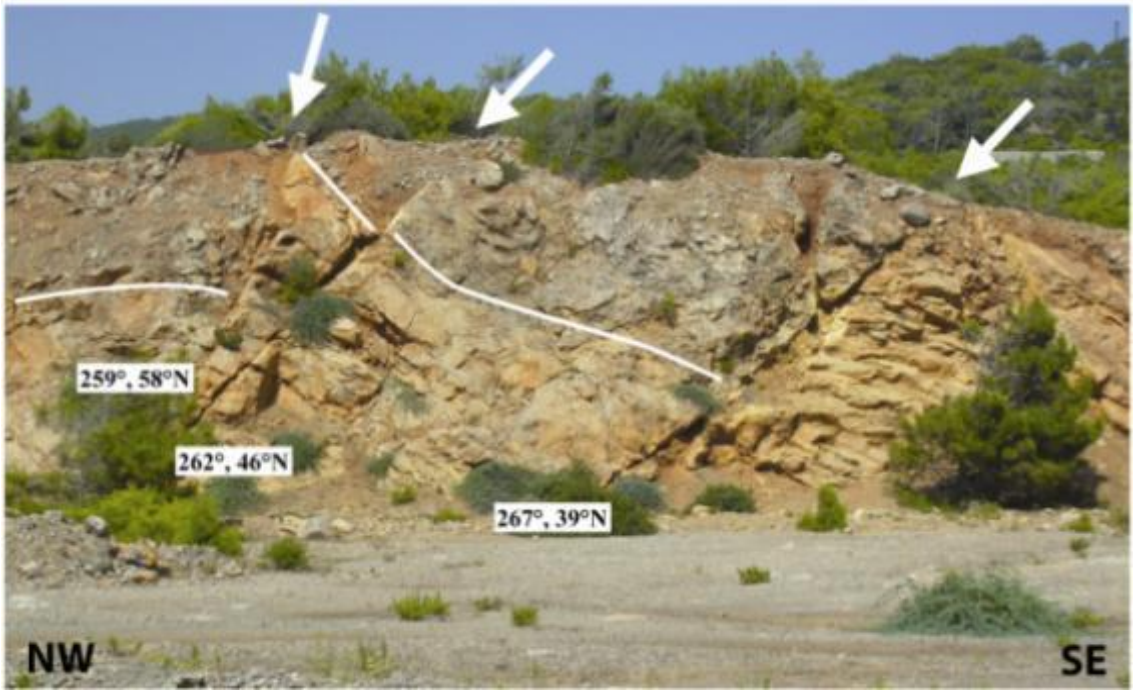

Figure 6/2.13 – Photograph Showing Normal Faults Observed at the Road Cut Between Akkuyu and Çamalanı Bay

In whole, description of paleoseismological trenches and other investigations, including borehole studies that were carried out at the territory with 1 km from the site radius, did not reveal any sign of seismic displacements of active faults. More information specifically justifying that there are no capable faults within the Akkuyu NPP site vicinity is provided in Section 6.6.

Joints

Previously, MTA team had collected extensive data from joint sets affecting the different members of the Büyükeceli Formation near the Akkuyu NPP site and found two longitudinal (046°/72°NW - 050°/66°SE), three diagonal (000°/74°W - 103°/58SW - 020°/80°SE) and one cross (150°/62°SW) joint sets [6/56] (Figure 6/2.14).

The conclusion was made, that starting from Pliocene age (1-2 million years ago) the Akkuyu NPP site is tectonically passive. Residual seismic deformations have not been detected within the site.

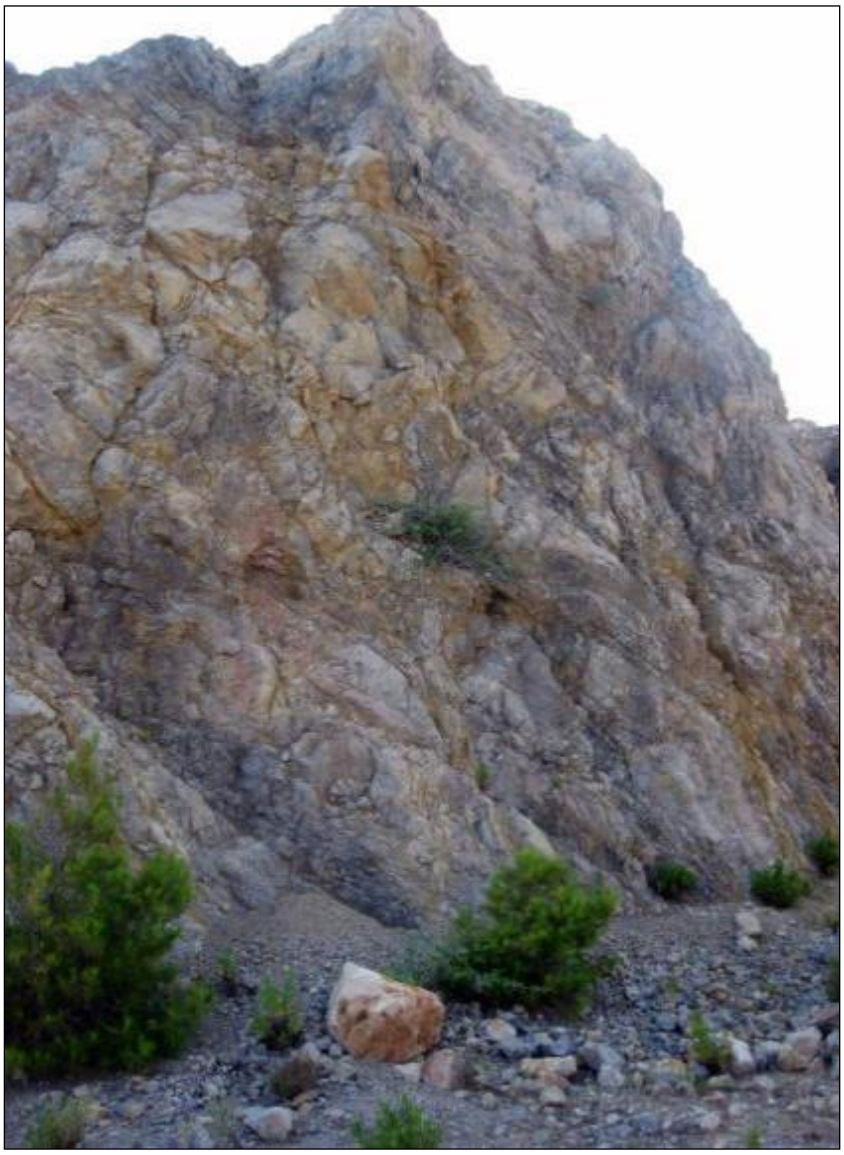

Figure 6/2.14 – Fractures developed within dolomitic limestone of the Büyükeceli Formation

6.2.4 MICROSEISMIC INVESTIGATIONS

In the period from 1977 to 1988 three cycles of instrumental investigations of micro-earthquakes were carried out in the surroundings of Akkuyu NPP (Section 6.4). At the stage of 2011 survey, a local network, consisting of 13 seismic stations was arranged in the near site area. Information of the network configuration, type of seismic stations is given in Section 6.4. Results of monitoring (list of micro earthquakes), including those obtained in 2011, are given in Appendix L.

6.2.5 DATA ON HAZARDOUS GEOLOGICAL PHENOMENA

The following geological phenomena will be discussed for the Akkuyu NPP site.

Landslide Processes

The Akkuyu NPP site is located in surroundings of hills up to 200 m high. A mountain relief was formed in folding epochs. Natural angles of slopes are approximately 35°. In 1983 (Detailed Site Investigations Report) the Kuşyuvası and Taşlık hills, and also Akkuyu mountain ridge were investigated in the course of detailed examination of the Akkuyu NPP site aimed at determining strata bedding orientation. These studies have revealed that a risk of landslide at the Kuşyuvası hill is absent due to the bedding orientation (deep into a slope) of the strata. The Akkuyu mountain ridge formed by the Büyükeceli formation is supported by the intrinsic geological strata bedding. The stability studies rthat were made for the Taşlık Hill also demonstrated its stability.

Karstification

The possibility of carbonate solution, i.e. of the development of karst forms depends on the following conditions:

l) Lithology (presence of soluble carbonate rocks);

m) Fracturing of a carbonaceous rock mass;

n) Distinct climatic and groundwater conditions.

Karstification is strongest in pure fine-grained limestone and under the influence of a large amount of precipitation and/or movement of CO_2-rich groundwater. The coarser or the more argillaceous the limestones are, the more indistinct becomes the development of karst. The same is valid for increasing the dolomite content in the limestone layers. The famous Dinaric karst terrains are restricted to limestone formations with almost uniform composition of over 90 % $CaCO_2$ [6/108]. The same may be observed for the pure Miocene limestones, approximately 55 km east of Akkuyu where karst cavities of considerable size called Heaven and Hell are touristic attractions.

From the latter, it has been concluded that in the geologic past the climatic conditions of Akkuyu were favorable to create karst phenomena and since the Büyükeceli Formation is predominantly of calcareous composition the investigation of the degree and extent of karstification in the bedrock has been one of the main objectives of the geotechnical investigations performed at the site.

Concerning the two geological assumptions (a) and (b) mentioned above it is clear that the bedrock at the site belongs mainly to the subunits Db2, Db3 and Db4 of the Büyükeceli Formation and only the topmost surficial layers are formed by other deposits. The Db2 to Db4 layers are, however, predominantly built up by dolomites and synsedimentary breccias with varying quartz,

clay and/or lime content (data obtained by petrographic analysis of rock samples). Concerning the lithological criteria governing mainly the degree of karstification it can therefore be stated that due to its mineralogical composition the rock mass concerned is not susceptible to carbonate solution.

Presence of faults in the Akkuyu region (b), which together with a continuous groundwater flow toward the sea (c) may be the reason for the development of small karstic features observed at boring cores or along borehole walls monitored with TV-camera.

Basically, there are two types of karst phenomena observed:

- Small spheroid cavities with diameter up to 1 – 2 cm, the so-called pea-karst. It occurs in calcite-bearing carbonate rock but also in altered dolomite down to a depth of 30 - 40 m below ground surface either as single "peas" or, more frequently, crowded in certain rock horizons. This carbonate solution phenomenon is of negligible importance for any type of geotechnical considerations;
- The second type is related with the widening of pre-existing discontinuities in the rock mass along bedding planes or along joints or fractures. These karstic openings are enlarged up to a few cm locally. The opening width of the majority of joints or fractures, slightly or not enlarged by carbonate solution, is in the order of millimeters. According to TV-investigations the frequency of occurrence and the size of carbonate solution phenomena are decreasing with depth. They are distinct to intensive down to 20 – 30 m below ground surface, but in depths of 35 – 40 m only slight to no karst signs are observed.

It should, however, be pointed out that within the NPP site area or even where the Büyükeceli Formation is cropping out within the site region, the surface morphology has nothing common with known karst terrains. Subterraneous karst is always accompanied by specific geomorphologic features and forms, e.g. karens, jamas, dolines, mogotes, sinking brooks, etc. Such features determine the typical landscape character of classical karst or, vice-versa, the absence of those characteristics is a strong indication for the minor karstification potential of the Büyükeceli Formation.

Cave-like escarpments along the generally steep shore at Akkuyu might be quoted to question the above argument. However, thorough investigations of these bluffy sections along the Inceburun peninsula have shown that these "caves" are genetically associated with the intersection of major faults (e.g. Aksaz fault) and that this rock material is preferably washed out by sea wave erosion. So far, this is not indicative for the absence of associated karst but these concave bluff

sections are only encountered along the side of the shore orientated toward the main wind direction, i.e. where abrasion is strongest, and never along the leeward side, for example along the north shore of Inceburun peninsula though also here such intersections of faults exist. Moreover, on the fault planes exposed in the cave-like escarpments, no coating by secondary calcite can be observed as usually encountered in karst cavities.

A further strong, if not the strongest indication for the non-existence of a well-developed subterraneous karstic system in the Büyükeceli Formation is the steep gradient of groundwater table toward the sea in particular during the rainy season and subsequent months. If there would be a karstic system of any significance the groundwater table would adjust to sea level within a relatively short time period.

A further reason for the low degree of karstification may be that the subsurface salt-water front inclined approximately 60° toward north along the shore line of the Akkuyu NPP site would suppress groundwater flow toward the sea, i.e. below the mean sea level stationary groundwater conditions can be assumed. With respect to the groundwater chemistry such conditions do not allow for mix-corrosion which is the most important carbonate solution process within the phreatic zone.

The relatively low permeability of rock mass determined by borehole head tests and pumping tests also indicates the existence of only small solution-widened openings of joints and other planes thus confirming the supposed little carbonate solution activity within the Büyükeceli Formation.

Other Weathering Processes

Physical weathering conditions such as impact of sunbeams, temperature drop, mechanical-biological weathering are able to influence the state of the Akkuyu NPP site rocks, but are less significant compared to karst and at present are partially active only in the top strata.

Nevertheless, physical impacts of water and wind, probably, to a certain degree decrease the rock strength properties. Weathering, being a long-term process may cause significant changes in the strength properties due to displacement of rock particles accompanied not only by worse deformation characteristics, but also possible reorientation of stress planes. The latter may cause processes of fracturing and opening planes within the limits of outcropped bedrock. Similar consequences relative to parallel to the surface jointing fractures are explained by temperature changes during Pleistocene Age and/or daily temperature changes nowadays.

It is believed, that similar processes, associated with further subrosion, have formed sub-horizontal fractures with a length of several meters and width up to 30 cm. Such manifestations were discovered in the trench investigations.

At deeper levels the influence of mechanical and chemical weathering decreases abruptly.

6.3 SITE AREA INVESTIGATIONS

6.3.1 GEOLOGICAL STRUCTURE OF THE SITE

Lithostratigraphic units outcropping on the surface of Akkuyu NPP site (within 1 km) include:

- Büyükeceli Formation (Middle Devonian period, 385 - 398 million years);
- Akdere Formation (late Devonian period, 359 - 385 million years);
- Kırtıldağı Formation (Permian period, 251 - 299 million years);
- Breccia of Pliocene-Quaternary (0 - 5.3 million years);
- Quaternary sediments (0 - 2.6 million years old) presented by alluvial fans, proluvial, colluvial deposits and caliche.

Geological map of the site in 1:2000 scale and profiles are given in Appendix K.

Owing to the symmetric structure of sediments composing the Büyükeceli formation in the site region, it was possible to make formation lithological separation into eight members.

Member 1 (Db1). This member is the Büyükeceli formation basement and is not outcropped within the Akkuyu site. It consists of basal conglomerate of 5 - 10 m. thick. The pebbles of the conglomerate are polygenic mostly consisting of the pebbles of the Sığırcık Formation. Filler is presented by unconsolidated sandstone and silty mudstone. A stack is characterized by frequent fractures and is subjected to severe weathering.

Member 2 (Db2). Db2 is divided into three parts. The lower part is presented by bluish gray, thick bedded carbonate wackestone of 40 m thickness with abundant corals such as Disphyllum Goldfussj and Calceola Sandalina.

Carbonate wackestone layers contain thin layers of brecciated limestone. The lower part is moderately fractured and less prone to karst formation in comparison with the middle and upper parts of the member.

The middle layer consists of light gray, thin bedded, laminated calcilutites show slump structures, 20 m thick megabreccia zone can be observed in the middle part. The fragments ranged in megabreccia size from pebbles to boulders. Megabreccia is cemented partly by clay and partly by sand filler. Megabreccia is inhomogeneously expressed laterally and is of consedimentary origin.

The middle complex is often highly fractured. Because of its characteristics it is subject to karst formation more significant than the bottom of the member.

The upper part of Db2 is made up of dark gray, thick to medium bedded, dolomitic wackestone with thin bedded yellowish gray shale intervals The layers of dolomite wackestone are

characterized by frequent fractures. Shales are fragile and highly fractured. While drilling at different depths down to a depth of 60 meters dolomite sand in the upper complex of caverns is often encountered.

The total thickness of Db2 is 150 m. It outcrops extensively in the core of the Akkuyu anticline trending in NE-SW direction.

Member 3 (Db3). Db3 consists of white massive, cross-bedded quartzitic sand stone of 1 m thickness. Although this thin marker horizon of the Büyükeceli Formation shows considerable lateral extension in the investigated area, stratigraphic pinch-outs and local lensing exist. Together with the Amphiflora horizon (Db6) it has been used as a marker bed to establish major structural features in the area.

Member 4 (Db4). Light gray, thin to medium bedded, laminated calcilutites forms the major constituent of Db4. A few mega breccia horizons exist in the Db4, mainly consisting of the clasts of quartzitic sandstone of Db3 and limestone blocks of Db2. Slump structures and chaotic appearance of the megabreccias in Db4 indicate that synsedimentary tectonics were active during sedimentation of this member. No fossils have been found in Db4.

Member 5 (Db5). Dark gray, thick-bedded, partly dolomitic and breccia ted wackestone with a very distinctive and peculiar stromatoporoid named Amphipora Ramoza make up Db5. Because of its unique fossil content and lithology Db5 has been used as a marker horizon to deliniate structures in the area. Apart from stratigraphic pinch-outs and nonexistence for very short distances in a few localities, the Amphipora beds show considerable lateral extension in the investigated area. Nowhere in the mapped area two or more successive Amphipora beds have been observed. The maximum thickness of Db5 is 2 meters.

Member 6 (Db6). Db6 is composed mainly of mega breccia sheets including limestone clasts and boulder of Amphipora beds and light gray, medium- bedded, partly dolomitic, waekestone intercalations. Individual clasts of Amphipora bed in the megabreccia sheets range from pebbles to angular 25x75 cm or larger blocks. Mega breccias are poorly sorted and heterogeneous. No obvious grading has been observed. The long axis of the big boulders and cobbles are more or less parallel with the bedding plane of the underlying limestone. No fossils have been found in the wackestones overlying and underlying the megabreccia sheets.

Member 7 (Db7). Db7 starts with white to pink, medium-bedded quartzitic sandstone beds which are overlain by dark, medium-bedded bluish-gray, highly bituminous gastropod wackestone with crinoids and bryozoas. Dark-gray, thin-bedded fissile shales and dark gray, bituminous limestone are intercalated with white to pink, cross-bedded, quartzitic sandstone. Stromatolites exist in the lower and middle part of the member. At the top, pink to rusty coloured wackestone beds

with abundant ryozoans and gastropods form a marker horizon. The total thickness of Db7 is 150 m. Apart from one locality near Akkuyu Village, no slump structures and megabreccias have been observed in Db7 which may have been deposited in a very shallow open shelf.

Member 8 (Db8). The last member of the Büyükeceli Formation is composed mainly of dark gray, thick-bedded, highly fossilifeous dolomitic wackestones and dolomites, with abundant corals, gastropods and brachiopods. It is overlaid by Adkere formation. The thickness of Db8 is 150 m.

The total thickness of the Büyükeceli Formation is approximately 630 m. Towards the East, thickness, of the formation gradually decreases. At Akdere Village, which is 25 km East of the type section, the thickness of the Büyükeceli drops to 40 m.

Fossils collected from the Büyükeceli Formation such as Disphyllum Goldfussi, Calceola Sandalina and Amphipora Ramoza indicate to Middle Devonian Age.

The felump structures and megabreccia sheets which are common in the lower half of the formation from Member Db2 to Member Db6 indicate synsedimentary tectonic movements. The upper half of the formation composed of Member Db7 and Db8 were deposited under rather stable shelf conditions.

Upper Department

Akdere Formation

The type section of the formation is in the Akdere village, which is located 30 km east of the Akkuyu NPP site. The Akdere Formation is composed of biothermal limestones intercalated with quartzitic sandstones, siltstones and shales. The formation starts with a marker horizon consisting of dark-to-bluish gray, medium-to-thick bedded wackestone containing abundant gastropods. At the Akkuyu site area, the formation is exposed just north of the Akkuyu Fault where it is strongly sheared and jointed. The thickness of the Akdere Formation is about 250 m at its type locality. The formation is unconformably overlain by the Kırtıldağı Formation.

Permian System

Kırtıldağı Formation

The formation crops out along the southern part of the Çamalanı Bay area. It starts with 20 m thick, dark gray, medium bedded foraminiferal wackestone, followed by pink, cross-bedded quartzite. Dark, bluish gray, medium-to-thick bedded foraminiferal wackestones with packstone intercalations form the middle and upper members of the Kırtıldağı Formation.

Pliocene-Quaternary Deposits

Talus Breccia

They are observed locally under Late Quaternary alluviums as consolidated with reddish carbonate cement and partly at sections characterized by high slopes as slope wash deposits. They consist of pebbles, cobbles and boulders of Büyükeceli and Akdere formations. Clasts of the talus breccia are unsorted. The thickness varies significantly within short distances and rarely exceeds 1m.

Quaternary Deposits

Alluvial Fans

They exist along the streams crossing the site and possibly Late Quaternary (Holocene) in age. They consist of loosely cemented and unsorted 1 to 3 m thick conglomerates with sandstone intercalations. During recent excavations, alluvial deposits previously reaching the shore have been removed or covered by spoil piles at Akkuyu Bay and partly at Aksaz Bay and Çamalanı Bay. Prior to recent excavations, trench and borings of MTA team at Aksaz Bay characterized the alluvial cover as 120 cm top soil and 3 m silty clay with increasing pebbles at the bottom.

Beach Sediments and Calichi

Quaternary beach sediments which are composed of loose aggregate of unlithified sand size particles are exposed at Aksaz Bay and Çamalanı Bay whereas covered by spoil piles at Akkuyu Bay. In the investigation area, lime rich Calichi deposits formed due to evaporation causing upward motion of sea water by capillary action through the cracks of beach rocks, are mainly observed at Aksaz Bay.

Soil Cover

It is the youngest geological unit containing organic reddish-brown soil and sandy-silt deposits with rock fragments. Thickness is highly variable and rarely exceeds 1 m.

Excavated surfaces and filled sections

During the past several decades, Akkuyu NPP site have been heavily altered due to extensive excavations carried out at the site. For this reason, the artificially altered topography is classified into two which comprise excavated surface and fill. Excavated surface refers to the scraped and smoothened bedrock whereas fill refers to the filled and covered site by extracted material from the excavations. Ancient coast line taken from earlier topographic data also allowed the identification of sea fill from land. Mapping of bedrocks at the excavated surface was not possible since it was covered with very thin gravel which was scattered around. Therefore both excavated surfaces and fill sites are mapped as separate units on the revised geologic map of the Akkuyu NPP site.

Geological map of the site in 1:2000 scale updated upon results of engineering-geological survey in 2011 is presented in Appendix K.

6.3.2 HYDROGEOLOGICAL CONDITIONS OF THE NPP SITE

6.3.2.1 STAGES OF HYDRO-GEOLOGICAL STUDIES

The study of Akkuyu NPP site conditions (including hydro-geological conditions) began in 1975 soon after this site had been selected by the Turkish Electricity Transmission Corporation (TEK).

The purpose was to assess the subsoil conditions of NPP's buildings and structures focusing on the following:

- soils bearing tests, including determination of their static and dynamic loads and the necessity of waterproofing;
- studying the construction pits parameters, including Method Statement development, determination of the pit walls stability and dewatering techniques;
- studying the structure, geotechnical and hydro-geological characteristics of soils;
- analyzing the possibility of using the excavated soils as construction materials.

All works have been carried out in compliance with USA standards (Guide 1.132 and 1.138), International Society for Rock Minerals (ISRM) in terms of the guidelines for studying the rock grounds and the guidelines of the International Atomic Energy Agency (IAEA).

The study consisted of three stages.

The first stage in 1975 included assessing by TEK the overall suitability of the site for construction of the Nuclear Power Plant.

During the second stage – June 1976 - July 1978 the study was carried out by the geotechnical department of the earthquake engineering study institute and Bogazici University Kandilli Observatory and Earthquake Research Institute [6/34]. The site general geotechnical conditions were studied at this stage. The results of the study indicated the need for an in-depth assessment of these parameters.

The third stage was performed from September 1980 to April 1982. The Engineering Department of EMCH+BERGER BERNE Ltd, Switzerland (ENG) and engineers of GONCER AYALP ENGINEERING COMPANY, Ankara (GAMB) took part in the geotechnical studies supervised by the Turkish NPP Technical Consortium.

The drill works and field identification procedures of soils were carried out by the Turkish State Hydraulic Works (DSI) company. This company was also responsible for the laboratory analyses of soils and water samples, except for the rocks petrology studies which were performed by the Mineral Research and Exploration Institute of Turkey (MTA). It took only three stages of the study to drill 81 exploratory holes 10 to 180 m deep and of 3800m overall length.

GAMB also carried out geological engineering and hydro-geological studies of Akkuyu II site (Çamalanı) and assessment of the ground water deposits to use them as a water supply source for the needs of the nuclear power plant [6/220].

Within the hydro-geological studies all three stages included assessment of the groundwater level regime, transmissibility of the water-bearing soils, groundwater temperature regime and chemical composition.

Both, in Akkuyu and in Çamalanı sites, the ground water level was regularly monitored. At the Akkuyu site the level of groundwater was measured starting from September 1976 to January 1978, and also from November 1980 to October 1981. 30 piezometers were installed with measurement frequency of once a week. In Çamalanı region the groundwater level was measured in the period of April 1984 to August 1985 and the results of measurements were shown in METU report (1986) [6/155]. Therefore, groundwater level variations – both, long-term (seasonal) and short-term - were accurately monitored at both sites.

Water injection, slug tests and pumping tests were used to assess the values of the water-bearing rocks permeability.

The expedition in 1979 (see Tezcan et al., 1979) [6/229] carried out the field permeability tests and Lefranc test to determine the in-situ permeability of subsoil at Akkuyu NPP site. A single packer was used in the hydro-geological tests. Pressure ranges were selected as 3-6-10-6-3 kgf/cm2. For each pressure step the test was repeated twice for a constant period of time – 5 minutes.

In Lefranc test water is injected into the well under constant water head. Permeability factor is found through measuring the amount of water needed to maintain constant water head in the well.

In total, 180 slug tests and injections were made, as well as 13 single and 2 group pumping tests.

TEK report (1983) [6/222], based on geological and geotechnical data, specifies three different layers in the water-bearing rocks. They include: upper layer (T-layer) composed of alluvium and other quaternary deposits; bed-rock upper layer (U-layer) composed of the bed-rock crushed zone underlaying the T-layer, and bed-rock lower layer (L-layer) which practically has no significant deformations and/or fractures.

The following K factors are suggested as the design values of permeability:

- for T-layer above average sea level K= 21.6 m/day;
- for U-layer above average sea level K= 6.9 m/day;
- for L-layer K= 1.7 m/day.

In 1986 METU carried out trial hydro-geological study in the area of Çamalanı bay. The study was aimed at defining the aquifers types and their properties, defining the direction and speed of the groundwater flow, assessing the groundwater variation causes, hydraulic parameters of aquifers, anisotropic factor, groundwater quality, and also studying the contact area between fresh and marine water [6/155].

In 2011 Akkuyu NPP site environmental conditions study was resumed. In 2011-2012 the Turkish company ENVY carried out 18 single pumping tests, provided piezometric system consisting of 33 piezometers and is currently monitoring the regimes: the level, temperature and chemical regimes of groundwater are being studied.

6.3.2.2 DESCRIPTION OF AQUIFERS

Akkuyu site and the region in whole feature rather complicated hydro-geological conditions and have a number of specific conditions peculiar to the territories composed of karsting rocks and influenced by structural setting.

Groundwater is found in porous stratum, in secondary crevices of fractures and solution channels. Secondary porosity of fractures and solution channels is formed due to the carbonate rocks that can be met in the region. Despite the fact that their initial porosity is rather low, each carbonate formation in the region, due to karstification and fracturing, potentially may contain groundwater. The borehole logs indicate that all formations of Akdere and Büyükeceli group are fractured and contain cavities. Apart from fractures and solution channels, the unstable zones are composed of breccia, and similar crushed materials are a good medium to contain groundwater. The youngest (breccia) deposits at lower depths also contain groundwater, though heir volume is rather limited.

Although all geological formations may contain groundwater, it is difficult to say that they all form one and the same aquifer. The fractures and solution channels may form local water-bearing zones separately from the whole system of groundwater circulation.

The groundwater of Akkuyu NPP site to the known depth is composed of Quaternary deposits, Permian system upper rocks (Kirtildağı system) and medium and upper Devon (Akdere and Büyükeceli systems).

Three water-bearing formations may be identified in the investigated geological section:

- Quaternary aquifer;
- Kirtildağı aquifer;
- Büyükeceli and Akdere formations aquifer.

The quaternary aquifer is found along the coast and at the sites, where land-planning works were made. The stratum is composed of various quaternary deposits (alluvium, marine, anthropogenic). The thickness of quaternary deposits varies from 1.0 m to 28.0 m. The thickness of aerated zone varies from 0.0 to 8.0 m.

Water-bearing rocks are composed of sands of various grain size and gravel-pebble deposits containing clay. The aquifer thickness varies from 0.2m to 8.1 m. The aquifer is unconfined, penetrated to the depth of 0.0m to 8.0m, with absolute elevations from 0.00 to 4.54 (0.00 – Mediterranean Sea level).

The aquifer transmissibility varies from 100 m2/day to 180 m2/day, specific capacity – 0.89 l/s/m. The permeability of rock (hydraulic conductivity coefficient) is within 2.8 – 37.5 m/day [6/222].

The aquifer is recharged through infiltration of rainfall, temporary streams and from adjacent and underlying aquifers. Water from the aquifer is discharged into Mediterranean Sea.

The aquifer mainly contains calcium-bicarbonate fresh waters. Their use is limited in the region and they are mainly used to supply water for the agricultural needs from the irrigation wells and captured springs. The springs discharge is up to 0.5 l/s.

Kirtildağı system aquifer is found on a limited area and is penetrated by single wells in the north-west and south-east parts of the territory. Penetrated thickness of deposits varies from 24.5m to167.0 m.

The water-bearing rocks are composed of limestones, quartz rocks and sedimentary carbonate rocks. The aquifer penetrated thickness to the south-east of the territory is 11.0 – 18.5 m, the levels are penetrated at the depths of 11.5 to 24.0 m with absolute elevations of 0.89 – 7.67.

In the north-west of the territory where elevations are significantly higher (100.00 - 180.00), the levels are penetrated at the depths of 20.0 m to 113.6 m with absolute elevations of 20.27 – 167.39; however the origin of these waters is not clear, perhaps they arise from the drilling fluids.

This aquifer is confined and free-flowing. The clays which are found in the upper part of Akdere system form an impermeable barrier between Akdere and Kirtildağı formations [6/155]. The aquifer in this site remains practically unstudied. Detailed studies on this aquifer shall be carried out during the next stage.

The aquifer of Büyükeceli and Akdere Devonian systems can be found on the most part of the territory. Büyükeceli deposits are composed of the intercalated limestones, dolomitic limestones, megabreccia, argillites and quartz sands. Akdere deposits are composed of intercalated limestones, lime argillites, dolomitic limestones, sands, aleurites, sedimentary carbonate rocks, clays and argillites. The penetrated thickness of deposits lies within 2.5 – 143.8 m range.

In those sites, where the aquifer is not overlain by youngest beds, it is the first aquifer from the surface. In the areas of quaternary deposits the aquifer is overlaid with recent beds, however it is connected with them through the cross-flows. The aquifer is confined and unconfined.

The penetrated thickness of Devon aquifer varies from 0.6m (well № 6b) to 116.5 m (well № 194) depths; the levels are penetrated at 1.5 m to 102.7 m depths with absolute elevations of 0.05 to 9.95. In this elevations range there lies a common aquifer with one groundwater surface.

However, it should be noted that approximately in 20 % of the drilled wells the levels are set much higher, but it is unclear whether this aquifer is composed of the drilling fluids or the wells penetrate the localized groundwater aquifers in the separated fractures and channels. During trial pumping test in 6 wells at high altitude, the water was pumped out for several (7-35) minutes in spite of the very low flow rate (speed).

The aquifer hydro-geological parameters were determined using various methods. Thus, the results of the slug tests indicate that the hydraulic conductivity coefficient (Kf) varies from 0.008 to 17.3 m/day while the value of 0.8 to 1.8 m/day prevails. The results of single pumping tests show that the transmissibility coefficient does not exceed 0.8 m/day [6/222]. According to the hydro-geological tests and Lefranc test carried out in 1979, the hydraulic conductivity coefficient is within the range of 6.0m/day to less than 0.009 m/day. The log tests and interval testing of the soils' water-absorbing capacity through water injection showed average flow speed values from 0.0684 to 0.029 m/day, and transmissibility coefficient was from 1.33m/day to 0.58 m/day [6/155]. The results of the single pumping tests carried out in 2012 [6/77] show that the hydraulic conductivity coefficient varies from 0.48 m/day to 3.37 m/day.

Such wide range of hydraulic conductivity gives evidence of the heterogeneity and high anisotropy of the aquifer.

The ground water of the Devonian deposits can be classified as water of double porosity.

The aquifer is recharged due to the rainfall infiltration and, possibly, due to the cross-flows between beds. The water is discharged into Mediterranean Sea and, presumably, into the lower aquifers.

The groundwater of the complex mainly includes calcium-magnesium hydro-carbonate fresh pH-neutral waters.

Water samples taken from the coastal wells exhibit high contents of Na+ and Cl- ions due to the sea water intrusion. In terms of their chemical composition these waters may be classified as sodium-calcium chloride-hydro-carbonate waters.

6.3.2.3 FILTRATION PROPERTIES OF WATER-BEARING MATERIAL ON THE BASIS OF SINGLE WELL PUMPING TESTS, PERFORMED IN 2012

Twelve single well pumping tests were performed in 2012 [6/77], of which 6 failed, due to immediate drying up of the well.

The list of wells where single well pumping tests failed is given in Table 6/3.1.

Table 6/3.1 – List of wells, dried up during single well pumping tests

Well number	Coordinates, m		Wellhead elevation, m	Well depth, m	Depth up to ground water level, m	Ground water level elevation, m	Water column height, m
	X	Y					
54	548440.400	4002113.910	76.50	76.00	71.00	5.50	5.00
65	547931.700	4002010.430	53.81	55.00	47.98	5.83	7.02
67	548136.090	4002009.730	57.27	61.00	53.78	3.49	7.22
71	548526.790	4002015.860	53.78	55.00	46.38	7.40	8.62
78	549216.840	4002017.940	62.95	68.00	42.00	20.95	26.00
419	549219.060	4001263.890	31.89	45.00	21.00	10.89	24.00

Based on single well pumping tests the hydrogeological parameters of water bearing horizon water-bearing materials were defined. The hydraulic characteristics obtained during single well pumping tests [6/77] are given in Table 6/3.2.

Table 6/3.2 – Hydraulic characteristics of water-bearing materials based on single well pumping tests

Well number	Coordinates, m		Index of tested materials	Water-bearing materials	Well head elevation, m	Takeoff spot elevation, m	Well depth, m	Static level elevation, m	Dynamic level elevation, m	Drawdown, m	Discharge, Q, l/sec	Specific Discharge Q, l/sec	Water transmissibility T, $m^{2/day}$	Hydraulic conductivity coefficient kf, m/day	Storage coefficient μ* (S)	Specific yield μ* (Sy)
	X	Y														
127	548277.110	4001819.240	Db2	Dolomite limestone	16.80	17.10	36.00	1.67	-7.80	9.47	2.66	0.28	10.39	0.52	0.00520	0.21
131	548479.860	4001817.920	Db2	Dolomite limestone, breccias	24.71	24.96	44.00	1.80	-7.36	9.16	1.25	0.14	9.59	0.48	0.01300	0.23
159	548629.340	4001766.930	Db2	Dolomite limestone, breccias	7.65	7.93	30.00	1.58	-7.70	9.28	3.38	0.36	23.56	1.18	0.00190	0.02
207	549030.650	4001721.800	Db7	Dolomite limestone	8.20	8.47	30.00	0.99	-9.83	10.82	3.20	0.30	12.74	0.64	0.00047	0.31
319	549031.340	4001520.150	Db7	Dolomite limestone, calcareous loamy marl	7.10	7.55	30.00	0.38	-5.60	5.98	3.82	0.64	28.24	1.41	0.00478	0.40
472	549586.910	4000875.120	Da	Dolomite limestone, calcareous loamy marl	28.66	28.91	40.00	0.81	-2.04	2.85	3.07	1.08	67.31	3.37	0.00998	0.07
											Avaerage value	**0.47**	**25.31**	**1.27**	**0.00589**	**0.21**
											Max	**1.08**	**67.31**	**3.37**	**0.01300**	**0.40**
											Min	**0.14**	**9.59**	**0.48**	**0.00047**	**0.02**

6.3.2.4 GROUND WATER DYNAMICS

Hydrogeological network, which includes 33 observation wells equipped with fluid level recorders (piezometer), exists currently at Akkuyu site (4, 4A, 4B, 6, 6A, 6B, 9, 12, 12A, 15, 15A, 15B, 16, 16A, 16B, 29, 49, 52, 56, 61, 63, 92, 97, 101, 113, 132, 253, 269, 273, 372, 462, 488, 502), for which complex of observations on levels, temperatures and basic elements of ground water chemical composition are made.

All the piezometers are equipped at Devonian water horizon.

6.3.2.4.1 LEVEL REGIME

The ground water levels for the observation period from October 2011 to February 2013 was at the absolute depth marks 0.12 – 11.23 (exception being wells No 56 and 502, which, probably, open-up isolated water-bearing horizons at higher levels, and well No 63, where there is wide scatter of values from 2.59 to 33.21).

Dependency diagram of levels from distance to sea is given in Figure 6/3.1.

The amplitude of level variation changes from 0.77 to 5.01, constituting on an average 2.68 m. The maximum, minimal and average values of ground water levels and amplitude of their variations are given in Table 6/3.3.

Ground water level change amplitude in low-water season and high-water season based on materials of monitoring observations of the previous years [6/34] can reach 6 meters.

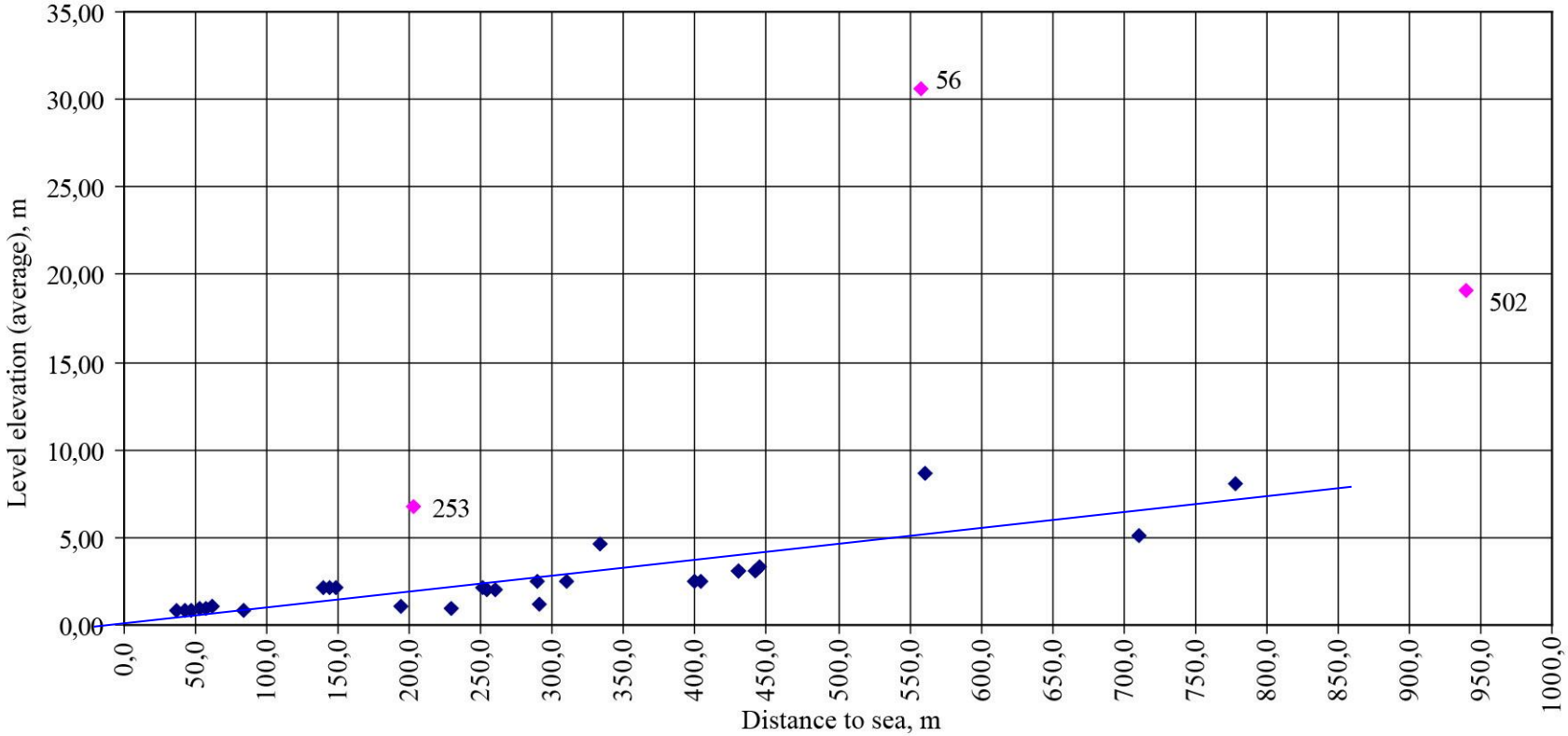

Figure 6/3.1 – Dependency diagram of levels from distance to sea

Table 6/3.3 Maximum, minimal and average values of ground water levels and amplitude of their variations for observation period

Piezometer No	Coordinates, m		Groundwater elevation, m			Amplitude A, m
	X	Y	Average	Max	Min	
4	4001806.000	547946.000	2.18	3.99	1.35	2.64
4A	4001803.000	547942.000	2.17	3.95	1.04	2.91
4B	4001800.000	547938.000	2.17	3.92	1.08	2.84
6	4001993.000	548733.000	3.07	6.00	1.91	4.09
6A	4002003.000	548732.000	3.09	6.07	1.93	4.14
6B	4001998.000	548732.000	3.11	5.95	1.13	4.82
9	4001787.000	548365.000	2.51	4.84	1.66	3.18
12	4001791.000	548965.000	2.02	3.82	0.75	3.07
12A	4001795.000	548968.000	2.04	3.78	0.85	2.93
15	4001595.000	548577.000	1.02	2.34	0.34	2.00
15A	4001589.000	548577.000	0.93	2.27	0.46	1.81
15B	4001584.000	548577.000	0.91	2.24	0.44	1.80
16	4001624.000	548793.000	0.88	1.68	0.12	1.56
16A	4001619.000	548793.000	0.83	1.69	0.39	1.30
16B	4001614.000	548793.000	0.83	1.61	0.40	1.21
29	4002318.634	548927.916	8.03	11.23	6.41	4.82
49	4002113.031	547920.066	-	dry	dry	-
52	4002123.014	548228.151	8.66	9.33	8.05	1.28
56	4002109.607	548623.261	30.62*	33.19*	29.39*	3.80*
61	4002135.970	549126.937	5.08	7.78	2.77	5.01
63	4001994.666	547735.845	16.96*	33.21*	2.59*	30.62*
92	4001940.091	549103.217	3.31	4.89	2.36	2.53
97	4001864.620	548031.590	2.15	3.72	1.55	2.17
101	4001868.340	548230.650	2.49	4.51	1.71	2.80
113	4001875.415	548826.413	2.54	5.11	1.79	3.32
132	4001816.410	548531.190	2.55	5.44	1.74	3.70
253	4001616.513	548282.447	6.80*	9.24*	5.67*	3.57*
269	4001621.658	549131.705	0.90	1.84	0.61	1.23
273	4001560.810	547981.932	0.78	1.24	0.47	0.77
372	4001421.116	549238.468	4.59	7.44	3.34	4.10
462	4000974.550	549582.700	1.21	2.17	0.86	1.31
488	4001885.216	547582.978	1.11	1.48	0.60	0.88
502	4001095.965	550204.443	19.09*	21.50*	18.43*	3.07*
Note - Rejected values are marked by *sign (well 63) and not taking part in the calculation (56, 253 and 502)						

Underground water level variability patterns in the water bearing horizon, confined to deposits of Büyükeceli and Akdere formations, are shown in Figure 6/3.2.

It is seen from the graphs that the level regime is formed under the influence of climatic factors, and probably tides. The variations of ground water level are directly related to seasonal changes in quantity of atmospheric precipitation. The maximum levels are in January-March viz. period of maximum atmospheric precipitation, minimum during June-September i.e. dry period. The histograms of total monthly precipitation by weather stations Anamur and Near Gate are given in Figure 6/3.3.

Based on regime observations infiltration value was preliminarily calculated. At levelled, relatively flat sections of the territory, the infiltration feed value constitutes about 40% of the quantity of atmospheric precipitation, at steeper terrain - 6-10%.

The following formula has been used for calculations (Lebedev, 1989):

$$\Delta N^{+} = \mu \Delta H^{+} \qquad (6/3\text{-}1),$$

where

ΔN^{+} – thickness of the infiltration recharge stratum, m;

μ – water yield coefficient (an average value is used, which results from pump-down processing findings for 2012, See Table 6/3.2);

ΔH^{+} – level increase value, m (result obtained from the monitoring observation diagrams).

A proportion is formed and the percentage of infiltration due to the volume of precipitation is calculated based on the obtained infiltration recharge value and knowing the precipitation depth. These calculations are rough and will be specified during the next stages.

In Figure 6/3.4 the hydrogeological map is shown with ground water hydroisobaths, confined to rocks of Büyükeceli and Akdere formations. Data on wells nos 56, 63, 253 and 502 were not considered when constructing hydroisobaths.

As seen, ground water has general slope of surface towards the regional drain viz. Mediterranean Sea. Flow gradient changes from 0.020 – 0.006.

At present it is impossible to assess the depth of active water exchange (ground water relatively intense circulation zone from zones of their feed to drain zones), conduct stratification (change in vertical permeability) of hydrogeological section, i.e. define the real 3D structure of ground water filtration flow. All necessary data related to the abovementioned issues will be studied during next stages of engineering surveys.

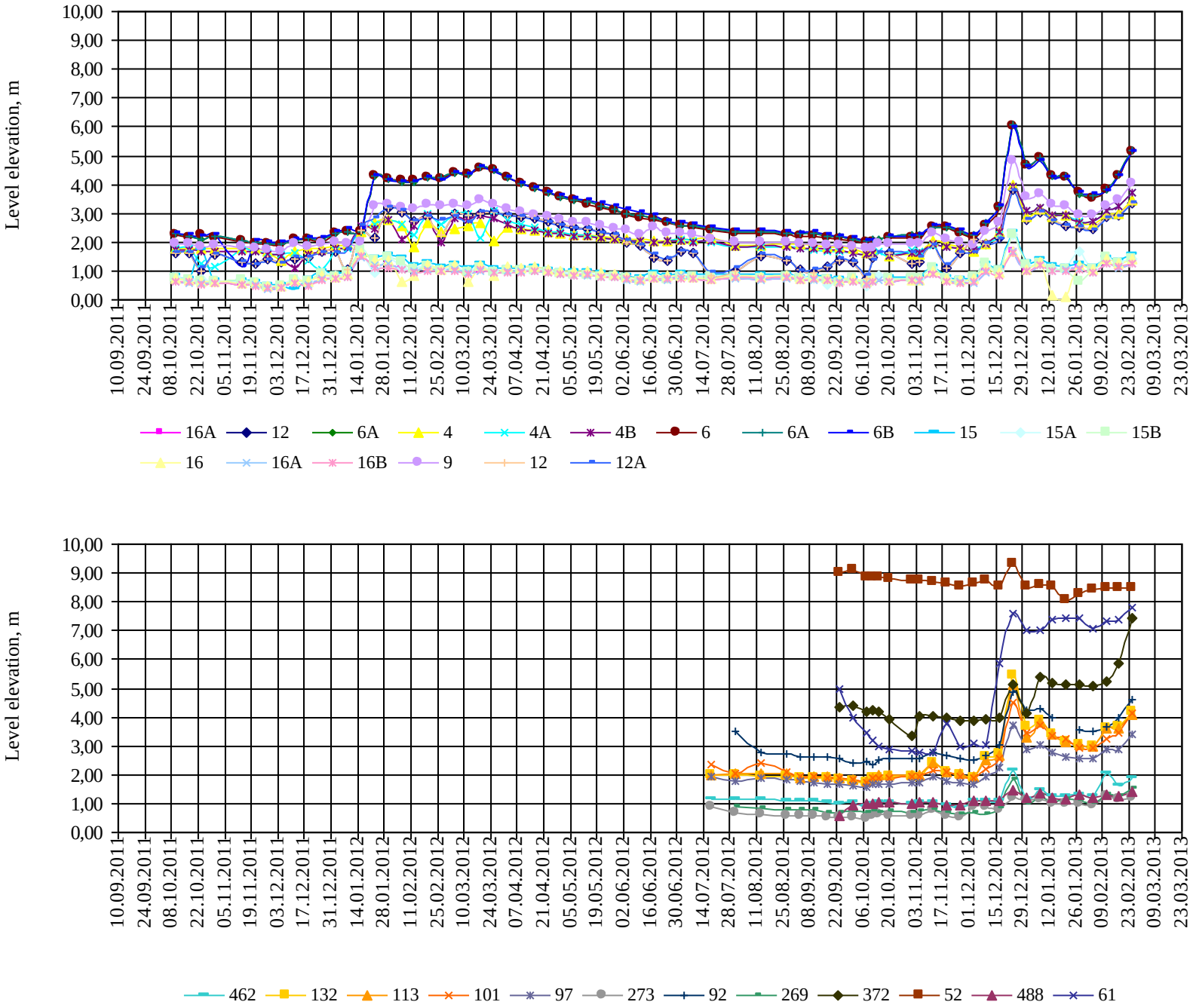

Figure 6/3.2 – Ground water level variation graphs in deposits of Büyükeceli and Akdere formations.

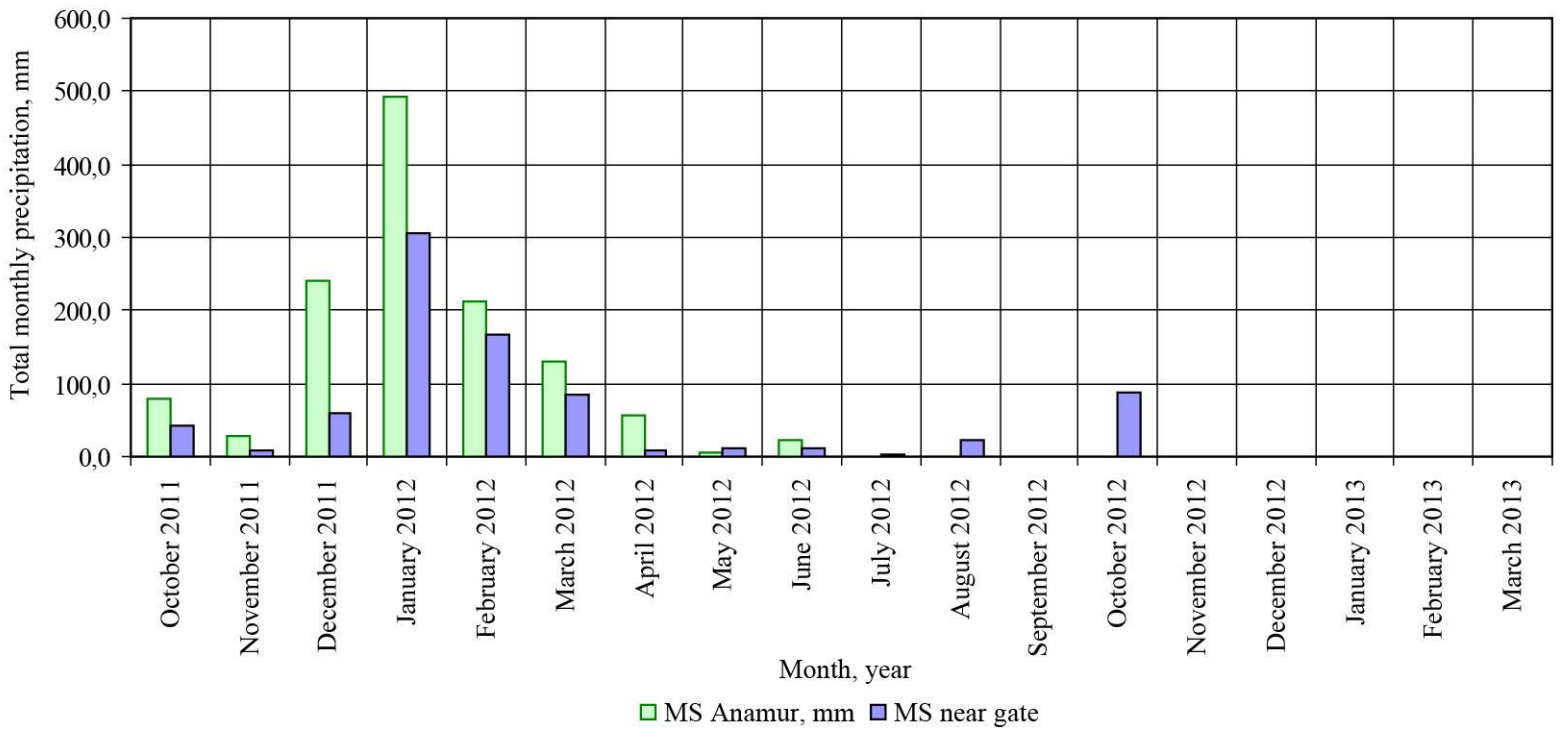

Note - MS - meteo station

Figure 6/3.3 – Histogram of total monthly precipitation

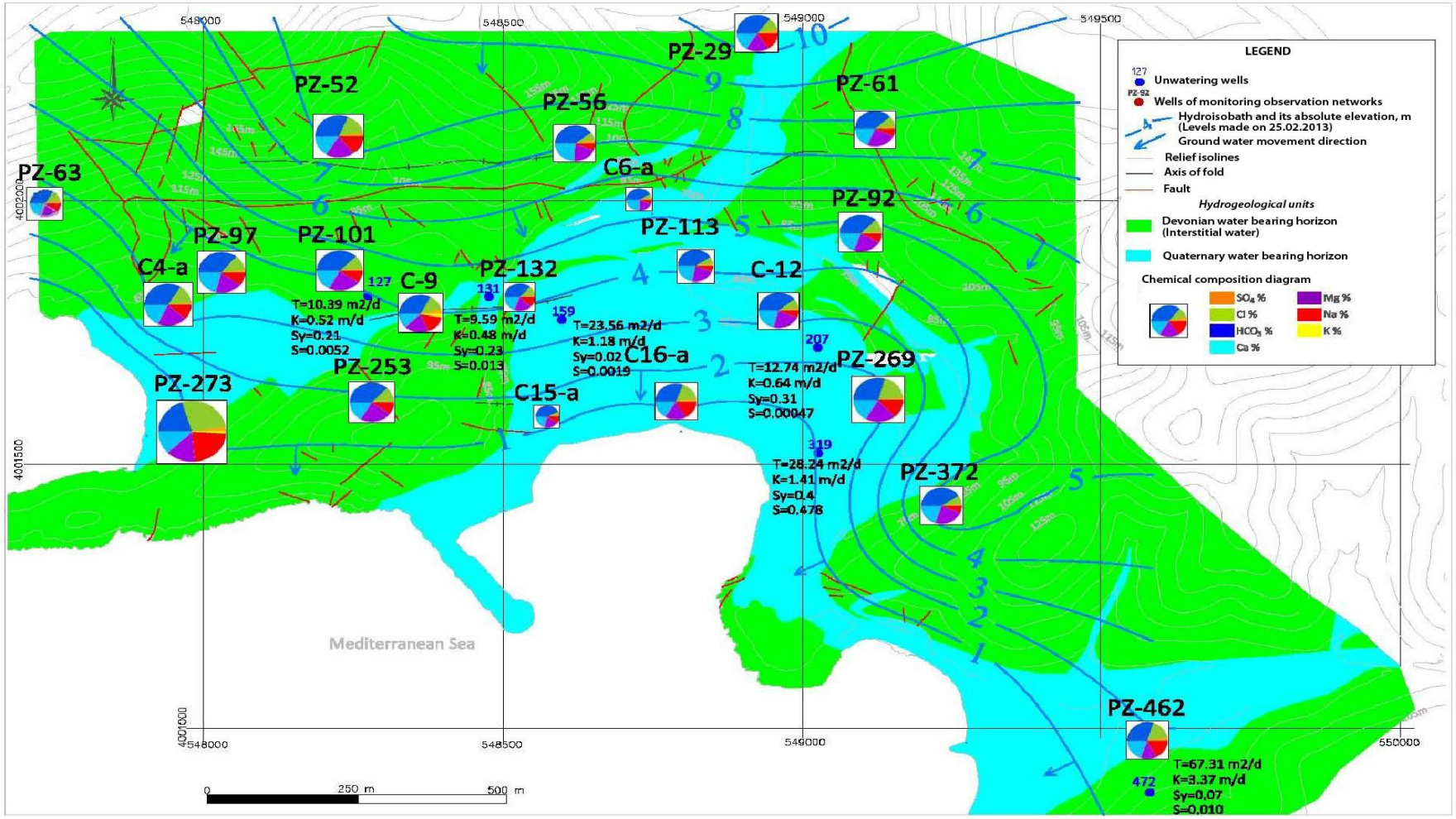

Note: Hydroisobaths were performed for Devonian waterbearing aquifer

Figure 6/3.4 – Hydrogeological contour map of site (scale 1:10 000)

6.3.2.4.2 GROUND WATER TEMPERATURE REGIME

For the observation period from October 2011 to February 2013 ground water temperature of Devonian water horizon changed from 14.9 to 27.6 °C, on an average constituting 22.4 °C. Amplitude of temperature variations changes from 0.3 (well No 56) to 12.7 °C (well No 273), constituting on an average 4.6 °C.

The maximum, minimum and average values of ground water temperature and amplitude of their variations are given in Table 6/3.4.

The highest temperature variations were noted in well No 273, located at the Aksaz Bay Coast. Based on geophysical works, performed at the site, this site is distinguished by considerable cleavage of water bearing material and intrusion of sea water is observed there [6/77]. Probably, such variation of water temperature at this site is related to this circumstance.

Similar temperature variations was also observed at other onshore well that is explained by air and sea temperature instability.

Table 6/3.4 The maximum, minimum and average values of ground water temperature and amplitude of their variations for observation period

Piezometer No	Coordinates, m		Water temperature, °C			Amplitude A, °C
	X	Y	Average	Max	Min	
4	4001806.000	547946.000	22.7	25.6	19.9	5.7
4A	4001803.000	547942.000	22.6	25.1	20.0	5.1
4B	4001800.000	547938.000	22.5	25.6	20.1	5.5
6	4001993.000	548733.000	22.6	26.8	19.2	7.6
6A	4002003.000	548732.000	22.5	26.4	19.4	7.0
6B	4001998.000	548732.000	22.4	26.7	19.6	7.1
9	4001787.000	548365.000	21.9	25.8	19.1	6.7
12	4001791.000	548965.000	22.2	26.8	19.1	7.7
12A	4001795.000	548968.000	22.2	26.6	19.8	6.8
15	4001595.000	548577.000	22.9	26.1	19.4	6.7
15A	4001589.000	548577.000	22.8	26.5	19.1	7.4
15B	4001584.000	548577.000	22.7	25.6	19.1	6.5
16	4001624.000	548793.000	22.4	26.3	19.3	7.0
16A	4001619.000	548793.000	22.2	24.5	19.3	5.2
16B	4001614.000	548793.000	22.0	24.4	18.6	5.8
29	4002318.634	548927.916	20.6	21.2	20.3	0.9
49	4002113.031	547920.066	22.8	dry	dry	dry
52	4002123.014	548228.151	22.5	22.8	22.4	0.4
56	4002109.607	548623.261	22.5	22.6	22.3	0.3

Piezometer No	Coordinates, m		Water temperature, °C			Amplitude A, °C
	X	Y	Average	Max	Min	
61	4002135.970	549126.937	21.7	21.9	21.5	0.4
63	4001994.666	547735.845	23.3	23.5	22.3	1.2
92	4001940.091	549103.217	21.9	25.4	21.3	4.1
97	4001864.620	548031.590	23.5	25.9	23.0	2.9
101	4001868.340	548230.650	22.8	25.4	22.1	3.3
113	4001875.415	548826.413	22.9	25.0	22.4	2.6
132	4001816.410	548531.190	24.1	25.9	20.7	5.2
253	4001616.513	548282.447	21.4	25.4	20.8	4.6
269	4001621.658	549131.705	22.7	25.2	22.1	3.1
273	4001560.810	547981.932	22.1	27.6	14.9	12.7
372	4001421.116	549238.468	21.2	21.5	20.0	1.5
462	4000974.550	549582.700	21.9	25.4	21.3	4.1
488	4001885.216	547582.978	23.3	23.6	23.1	0.5
502	4001095.965	550204.443	20.9	21.4	20.5	0.9

Ground water temperature variation graphs are given in Figure 6/3.5.

As seen from the graphs, the maximum values of temperature are during the hot months (June-September/October), minimum - for the cold and rainy months (January-April).

Ground water levels and temperature are in inverse proportion i.e. the higher the level, the lesser the temperature.

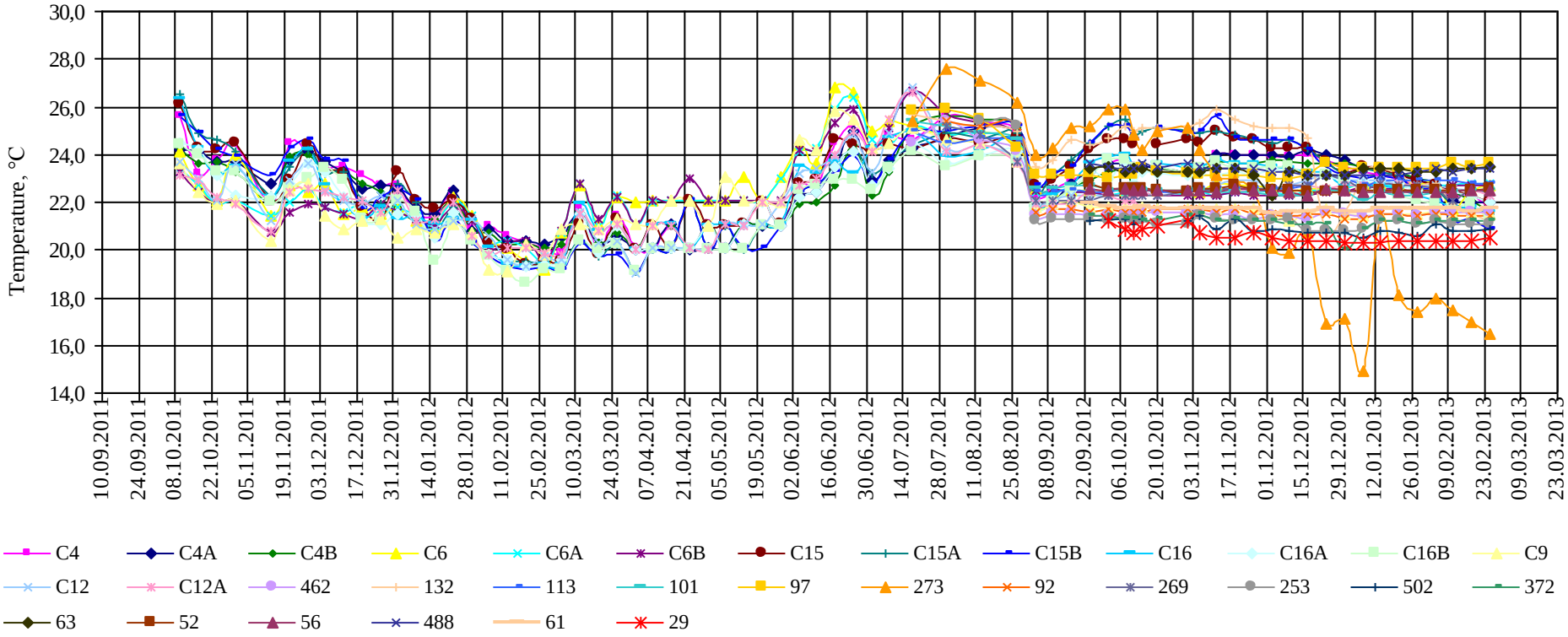

Figure 6/3.5 – Ground water temperature variation graphs

6.3.2.4.3 GROUND WATER CHEMICAL COMPOSITION

For the observation period 96 water samples were taken from the piezometric network well.

By chemical composition Devonian water bearing horizon water is primarily hydro carbonate and chloride- hydro carbonate of mixed cation composition calcareous, potable with mineral content 0.3 - 1.0 g/l (on an average 0.7 g/l). In separate samples, taken from the wells, located in the coastal zone, the water becomes hydro carbonate-chloride and chloride sodium-calcium and sodium, salty with mineral content 1.1 - 3.0 g/l (on an average 1.7 g/l). Average chemical composition diagrams are given in Figure 6/3.6.

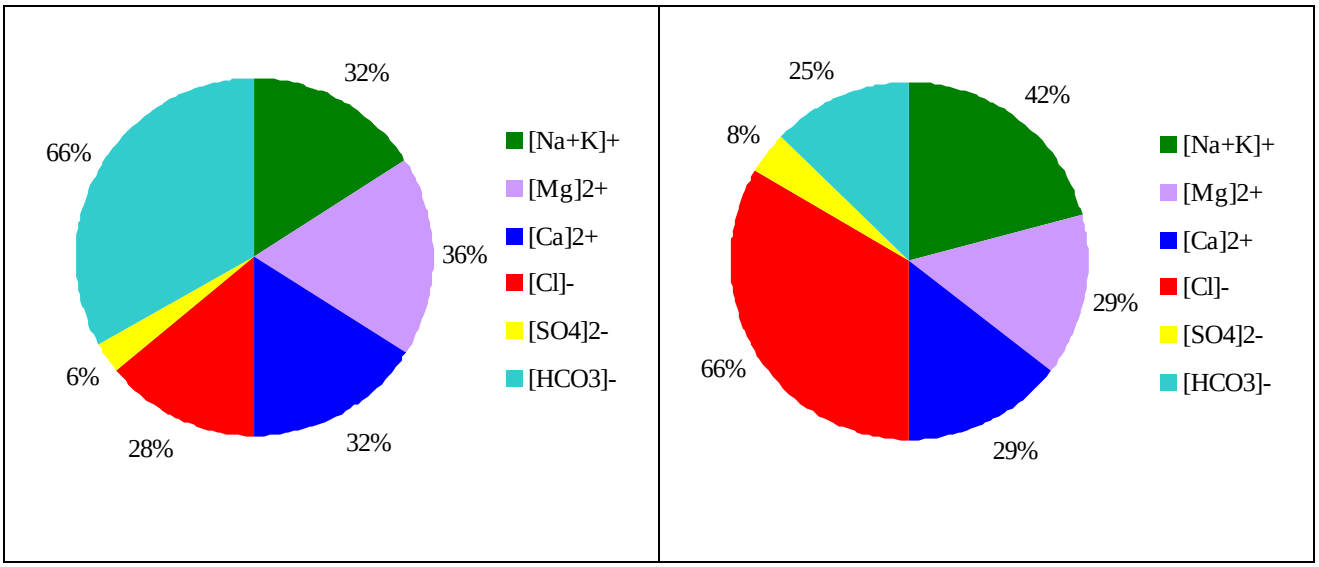

A) B)

Figure 6/3.6 – Ground water chemical composition diagrams (A - main territory, B- coastal zone)

pH value varies from 6.81 to 8.16, constituting on an average 7.29 (neutral water).

The presence of ions NO_2- and NO_3- is noted almost in all the samples, and in certain samples their content goes up to 7.3 mg/l (NO_2-) and 67,3 mg/l (NO_3-). Increased content of these ions certify about anthropogenic pollution. Fe ions are also present in some samples.

Ground water of the horizon in relation to concrete of normal permeability is non-aggressive by pH, HCO_3- content and aggressive carbon dioxide.

In relation to cable lead sheathing water is poorly (75%) and medium aggressive (25%) by pH and total hardness and from poorly aggressive to high aggressive by NO_3- content.

In relation to cable aluminium sheathing water is poorly (75%) and medium aggressive (25%) by pH , primarily highly aggressive (85%) by Cl- ion content, non-aggressive (40%) and poorly aggressive (60%) by Fe ion content (Fe^{2+}+Fe^{3+}).

6.3.2.5 HYDROGEOLOGICAL ENVIRONMENT MATHEMATICAL MODEL DEVELOPMENT

Possibility of more complete account of the complicated hydrogeological conditions and a complex of various factors of the technogenic intervention impacting infiltration features determines efficiency of the hydrogeological modelling as an investigation method.

Development of the filtration model includes several stages:

Schematization of hydrogeological conditions, which consists of:

Spatial model break-down;

Definition of external and internal model boundaries and boundary conditions. Hydrodynamic boundaries and their physical and mathematical representation in numerical scheme are to be selected given the general hydrodynamic situation, maps available (topographic, geological, underground water depth-to-water maps etc.);

Determination of profile boundaries (specified via absolute marks of the bottom and roof of each calculated stratum);

Filtration parameters of water-bearing materials (taken based on the hydrogeological information available with due consideration of the findings of the works accomplished both during the previous years and today);

Hydraulic relationship of the water-bearing horizons (taken at the model through assigning a vertical filtration coefficient Kz);

Infiltration recharge (in the model it is set as infiltration recharge intensity for calculation of which information on monthly precipitation depth in the region of work is used, besides information about superficial and groundwater flows is also used).

The findings of the engineering geological investigations, testing for underground waters inflow, laboratory research, data of monitoring observations of the groundwater levels accomplished both earlier and in 2011-2012 have been used during schematization of the geological and hydrogeological conditions of the Akkuyu NPP site.

2. Inverse modeling (model calibration). Calibration of the infiltration model is being performed by comparing model rated heads with observation data of the groundwater levels per boreholes. The budget of water discharge is additionally being controlled. To reach a satisfactory coincidence of model heads with the observation data the inverse problem is being resolved, when the filtration parameters of calculated strata are being specified as well as the amount of infiltration recharge.

3. Numerical solution of the filtration problem can be obtained thanks to the Visual MODFLOW software package. The filtration problem is being solved by the conjugate gradients

method providing the most reliable outcomes. The map of the natural head distribution in the water-bearing horizons under study is a result of the filtration problem.

4. The MODPATH software is being used for detailed study of the filtration flow structure. The filtration flow data obtained allow rather accurate track the movement of the maximum concentration front and define locations for control points when solving the migration problem.

6.3.2.6 RADIONUCLIDE MIGRATION IN GROUND WATER

The radionuclide migration occurring with the ground water much determines the sanitary and radiation conditions of the aqueous medium in the NPP area.

The radionuclide migration means heat and mass transfer in the ground water.

The convective transport resulted from hydraulic transportation of water particles by the filtering flow is a main radionuclide migration in case of transfer of polluted solutions into the water-bearing horizon.

The next migration mechanism is a hydro-dispersion (planned), which causes dilution of the concentration fronts and exit of pollution beyond the area limits by averaged paths of water particles along the lines of fluid flows countering the pollution source. The lateral (profile) hydro-dispersion along with the vertical velocity component is in charge of the "carrying" pollution through flow depth. The radionuclide sorption and their radioactive decay aggravate their convective hydro-dispersion transport.

The model of radionuclide transfer by the ground water is based on the solution of flow [6/169]:

$$\frac{\partial C}{\partial t} = \frac{\partial}{\partial x_i}\left[D_{ij} \frac{\partial}{\partial x_j}\left(\frac{C}{\rho K_d + \vartheta} \right) - V_i \frac{C}{\rho K_d + \vartheta} \right] - \lambda (C - C^m) + Q , \qquad (6/3\text{-}1)$$

where: C – total concentration, Ci/m^3;

C^m – concentration of parent radionuclide;

ϑ – moisture content, dimensionless parameter; in saturation conditions $\vartheta = n_a$, where n_a – active porosity;

ρ – dry soil density, kg/m^3,

K_d – distribution coefficient, m^3/kg;

V_i – filtering flow (Darcy velocity), m/sec;

D_{ij} – coefficient of dispersion, m^2/sec; $D_{ij}=D^*+D^{ij}$, где D^* – efficient coefficient of dispersion, D^{ij} – coefficient of hydrodynamic dispersion, $D^{ij}=\alpha_t|V|\delta_{ij}/\vartheta+(\alpha_l-\alpha_t)V_iV_j/|V|/\vartheta$; δ_{ij}- – Kronecker symbol, α_l – longitudinal and α_t – lateral dispersion, m;

λ – decay constant, l/sec (for radioactive elements);

Q – velocity rate of pollution ingress and velocity of irreversible transfer of admixture into non-exchanged form (settling out into insoluble residue), Bq/m^3/sec;

t – time, sec.

Depending on dimension of a problem *i* or *j* should be assigned. For 3-dimensional option *i* or *j* is equal: 1 for X horizontal axis, 2 of Y axis and 3 for downward Z vertical axis.

All members of the equation (6/3-1) are migration parameters.

Assignment of the migration parameters is based on the findings of laboratory and field investigations.

The main migration medium parameter, which controls intensity of the convective substance transportation in water-bearing stratum, is its capacity: as for chemically neutral components this is an active porosity, fracturing (n_a).

Calculations of radionuclide migration require determination of soil sorption properties forming the site (soils of aeration zone, water-absorbing and water-resisting rocks). Determination of sorption properties should be done in specialized laboratories. The rock sorption property is characterized by the volume capacity coefficient (VCC), which defined the number of mg-eq cations absorbed by 1gr of the tested specimen, and distribution coefficient (Dc), which represents radionuclide concentration ratio in rock to its equilibrium volume content in solution contacting the said rock specimen.

The main filtering parameters necessary for calculation of the ground water pollution are the following:

- Hydraulic conductivity coefficient of the aeration zone rocks;
- Deficit of saturation of the aeration zone rocks;
- Hydraulic conductivity coefficient of water-bearing rocks;
- Water loss of water-bearing rocks;
- Conductance of water-bearing hoziron;
- Volume of infiltration recharge;
- Capacity of aeration zone;
- Flow gradients;
- Filtration rate.

Forecast evaluations are being provided regarding the migration conditions of the following radionuclides: Strontium ^{90}Sr, Cesium ^{137}Cs and Cobalt ^{60}Co (plant-nature radionuclides). In presence of NPP waste salts (sodium nitrates of 100gr/l concentration) sands demonstrate low or practical lack of Strontium-90 absorption, but absorption of Cesium-137 in the same conditions is significant. Therefore the main radionuclide of the wastes, Cesium-137, will be not much mobile even in case of liquid waste influx into the environment.

Further the migration of Strontium-90 is to be only calculated for its large migration capacity and extremely hazardous.

The developed filtration model allows evaluating effects of the NPP beyond-design accident, related with scenarios of influx of radionuclides into the water-bearing stratum.

6.3.2.7 INTERRELATION OF HYDROGEOLOGICAL CONDITIONS WITH KARSTIFICATION

Karstification is one of the important aspects able to influence the water conducting and capacitance properties of the water-bearing stratum.

The report [6/56] prepared by Demirtaşlı group in 1982 provides detailed data about karst development on the NPP site territory.

Under [6/56] the bed rocks mainly consisting of the carbon-bearing solid rocks subject to corrosion and karstification. But mapping of the surface and trench investigations as well as geotectonic drilling, investigations with tele-viewer, geophysical observations, geo-electric prospecting, microgravimetric and seismic investigations have proved that the karstification rate in Büyükeceli formation is not big.

Two types of karst caverns have been found out during the investigations. The bigger and intensive karst formations are at the contact of the upper Büyükeceli formation with the located above Pliocene-Quaternary breccia and in the breccia itself. These openings are up to 30cm wide and up to 15m long. These karst caverns used to be filled with the red soil (soil of ред-rust color, brown clay or calcareous deposits). Caverns of similar type and dimensions have been found out in the most upper part of the Büyükeceli formation.

The second type of karst phenomenon in rocks of the Büyükeceli formation manifests itself as cavernosity and should be attributed to the so called “peakarst”. These are karst caverns of dimensions from 1 up to 10cm, and the dimension and degree of these karst formations decline with the depth. In faulting karstification is possible at the depth of 20-30m, but the finding of the geo-technical drilling and TV observation proved that the rate of karst formation below 30m is low or there are none.

Low permeability of solid rocks, identified based on the injection into the bore holes and further pumping tests, also indicates the low number of pores and caverns in the rock, thus confirming the low activity of carbonaceous leaching of the Büyükeceli formation.

Based on the geophysical investigation results of 2012 [6/78] about 300 karst occurrences have been identified, around 75% of these caverns are thinner than 2m and around 20% only are below the ground water level. The found caverns are mainly filled with the sandy and loamy material. Deeper karst formations are nearby important structural geological elements.

So it is possible to make the following conclusions: karstification in the Büyükeceli formation does not much stimulate increase of the water-bearing horizon capacity; the accumulative capacity of the water-bearing horizon is mainly determined by availability of pores, fissures, faults and crushing zones. The stratum permeability can grow due to open karst caverns; caverns filled with the sandy and loamy material can either diminish permeability or does not greatly impact it.

Nevertheless it is worthwhile to note that the karst available in the region can play an important role forming the ground water regime and budget of Akkuyu NPP since the Akkuyu site can be a part of the uniform system of underground water circulation. So an additional set of investigations within the water shed and along its boundaries is required.

6.3.3 SOIL/ROCK PROPERTIES OF THE AKKUYU NPP SITE

6.3.3.1 PHYSICAL-MECHANICAL PROPERTIES OF SOILS/ROCKS BASED ON RESULTS OF PREVIOUS INVESTIGATIONS

Engineering-geological conditions and the physical and mechanical properties of the Akkuyu NPP site soils/rocks according to the results of geological engineering survey performed in the period 1976-1982 are available in [6/223].

In the Akkuyu NPP site the following deposits can be seen: Quaternary sediments of alluvial and eluvial-deluvial genesis, as well as soil-vegetation deposits that locally overlie the bedrock of the Middle Devonian Büyükeceli formation, represented mainly by sedimentary rock and semi-carbonate sedimentary rocks (dolomite limestone, dolomites). Bedrock deposits are characterized by inclined bedding, heterogenic composition, varying degrees of preservation, fracturing and weathering.

According to the performed studies, taking into account the genesis, lithological composition and physical-mechanical properties of the soils within the site three main geotechnical strata were identified:

- Upper layer (T-layer);
- Bedrock basement upper layer (U-layer);

– Bedrock basement bottom layer (L-layer).

The main geotechnical parameters of the layers are given in Table 6/3.5.

It should be noted that from geological and geotechnical point of view two different layers, namely a "top layer" (T-layer) and bedrock are easily recognizable.

The separation of the Büyükeceli formation related bedrock on distinct geotechnical layers required significant detailed analysis, since the properties of the bedrock as a whole are defined by the rock itself and by the degree of preservation, fracturing, heterogeneity of the rocks, as well as the intensity of bedrock weathering and karst development.

From a geotechnical point of view the bedrock of Büyükeceli formation is divided into two layers: a layer weakened by decompression zone of highly fractured, weathered bedrock designated as “The top layer of bedrock” (U-layer) and sub-base intact bedrock, designated as “The bottom layer of bedrock" (L-layer).

The boundary between these layers is more apparent than clearly expressed, but the performed field and laboratory studies have confirmed its existence.

In determining the layer of the studied bedrock to the U-or L-layer a number of criteria have been taken into account. These criteria can be divided by their importance in two categories:

– criteria of the first order, taking into account the frequency of the location of fractures, the values of permeability and the velocity of longitudinal waves (Vp).

– criteria of the second order, taking into account the rock quality index (RQD), degree of weathering, the speed of drilling, casing length, the modulus of deformation obtained by the results of pressuremeter tests and apparent resistance of the rock.

The upper layer (T-layer)

The upper layer was defined in Quaternary sediments of alluvial and eluviual-deluvial genesis and also in soil-vegetation layer. T-layer locally overlies the site rock basement of Middle Devonian Büyükeceli formation and have uneven distribution of sandy-clayey soils with inclusions of organic admixtures.

The layer thickness varies from 0 to 4.5 m.

The top layer of bedrock (U-layer)

The top layer of bedrock (U-layer) is allocated to the bedrock deposits of Middle Devonian Büyükeceli formation and characterizes a zone of attenuation, decompressing, faulting, bedrock fracturing and lies on the surface or locally under the T-layer deposits.

The deposits are sedimentary rock and semi-carbonate rocks, mainly dolomite limestone, dolomite, veined calcite with interlayers of marl, shale, sandstone, with lenses of quartzite.

As part of U-layer in the upper part, well cemented carbonate breccias of presumably pre-Quaternary age have been detected. Because of the lime content in the cement, breccia is strongly exposed to the carbonates and is characterized by the presence of small cavities and caverns filled by calcareous sandy-clayey material. Thickness of breccia is 1 - 4.8 m

The bottom layer of bedrock (L-layer)

The bottom layer of bedrock (L-layer) was determined in deposits of Middle Devonian Büyükeceli formation and is characterized by intact (parent) rocks, overlain by deposits of U-layer.

The deposits are sedimentary rock and semi-carbonate rocks, mainly dolomite limestone, dolomite, veined calcite with interlayers of marl, shale, clay and stone-like clay, sandstone with lenses of quartzite. L-Layer thickness was estimated as about 200 m.

The Aksaz plain alluvial sediments

The Aksaz plain is bedded westward from the site (boreholes No 84, 85, 88 and 89). Its geotechnical conditions were interesting, since at that time it was planned that the cooling water discharge structure will cross the plain.

This layer is presented by alluvial clay deposits, clay silt with sand and gravel, partially with organic remains, silt sand, alluvial gravel and crushed stone.

It should be noted that the currently available information about the mechanical properties of Aksaz alluvium is not enough to develop detailed geotechnical characteristics. Therefore, the data shown in Table 6/3.5, gives only approximate estimates for the geotechnical properties of these deposits.

Table 6/3.5 – Main Geotechnical Characteristics and Physical-Mechanical Parameters of the Defined Layers, [6/223]

Geotechnical layer	Fracture frequency	Rock quality index, RQD, %	Density, ρ, g/cm^3	Angle of internal friction, φ, ...°	Specific cohesion, C, kPa	Deformation modulus, E, MPa	Dynamic shear modulus, G, MPa	Poisson's ratio, μ	Permeability coefficient, $k \cdot 10^{-4}$, m/s
T-layer	-	0	1.70-2.00	28-38	0-20	5-30*	-	-	-
U-layer	≥ 15/m	10.5	2.25-2.60	20-35	0-200	1000-3000 (locally ≥ 20)	1600-2500	0.35-0.40	1.5-3.5 above msl 0.5-1.5 below msl
L-layer	7-≥15/m	21.2	2.50-2.75	30-45	0-500	2500-5000 (locally ≥ 800)	5000-5400	0.30-0.40	0.09-05
The Aksaz plain alluvial sediments	-	-	1.50-1.90	20-38	0-10	3-7*	-	-	-
** Value of deformation modulus marked with * is given per compression test results*									

6.3.3.2 PHYSICAL AND MECHANICAL PROPERTIES OF SOILS/ROCKS BASED ON RESULTS OF ENGINEERING-GEOLOGICAL SURVEY IN 2011

The upper soil layer in the area covered by the pre-design engineering-geological survey is dominated by Quaternary deposits (alluvial and eluvial-deluvial deposits, deposits of soil-vegetation layer and man-made artificial formations), overlying basement rock of Akdere and Büyükeceli formations, related to Upper- and Middle-Devonian periods.

Bedrock deposits are predominantly represented by sedimentary carbonate rocks and semi-rocks with inclined bedding, irregular structure, non-uniform integrity, fracturing and weathering.

Although, a considerable amount of pre-design engineering-geological investigations have been performed, due to the site complexity, it was not possible to spatially and lithologically differentiate (specify engineering-geological layers and elements) the units of Büyükeceli and Akdere formations. For that reason physical and mechanical properties are given for the lithological dissimilarities encountered during the drilling.

As a result of the drilling, field geotechnical survey and laboratory studies, physical and mechanical properties were obtained for 10 lithological dissimilarities.

The Rock Quality Designation (RQD, %) distribution with depth attributable to each lithological variety is given in Table 6/3.6.

Table 6/3.6 – RQD Distribution in Boreholes

Lithology	Borehole No.	Rock Quality Designation RQD, %			
		0 - 25	25 - 50	50 - 75	75 - 100
(2) Dolomitic limestone	C-1	100	-	-	-
	C-2	52	9	27	12
	C-3	52	48	-	-
	C-4	-	25	-	75
	C-5	72	23	2	3
	C-6	45	35	20	-
	C-8	81	19	-	-
	C-10	66	34	-	-
	C-11	83	17	-	-
	C-12	100	-	-	-
	C-13	100	-	-	-
	C-14	63	31	6	-

Lithology	Borehole No.	Rock Quality Designation RQD, %			
		0 - 25	25 - 50	50 - 75	75 - 100
	C-15	80	20	-	-
	C-16	35	50	15	-
	C-17	100	-	-	-
	C-18	83	17	36	-
	C-19	6	14	54	54
	C-20	8	8	-	30
(3) Megabreccia	C-3	100	-	-	-
	C-4	18	82	-	-
	C-6	-	97	3	-
	C-8	66	34	-	-
	C-10	76	13	11	-
	C-11	32	68	-	-
	C-13	55	40	5	-
	C-14	-	100	-	-
	C-15	50	38	9	2
	C-16	-	24	76	-
	C-19	-	100	-	-
	C-20	-	36	32	32
(4) Mudstone	C-3	100	-	-	-
	C-4	100	-	-	-
	C-18	100	-	-	-
	C-19	69	-	31	-
(5) Wackestone	C-4	-	-	100	-
	C-6	29	15	19	37
	C-19	-	14	43	40
(6) Quarzitic sandstone	C-4	76	24	46	-
	C-6	-	100	-	-
	C-8	100	-	-	-
	C-14	69	-	31	-
(7) Wackestone/Mudstone	C-14	-	41	59	-
	C-19	15	26	37	22

Lithology	Borehole No.	Rock Quality Designation RQD, %			
		0 - 25	25 - 50	50 - 75	75 - 100
(8) Cavity filling	C-4	36	-	64	-
	C-17	100	-	-	-
(9) Crushed zone	C-3	100	-	-	-
	C-7	100	-	-	-
	C-8	100	-	-	-
	C-9	100	-	-	-
	C-12	100	-	-	-
	C-14	100	-	-	-
	C-17	100	-	-	-
	C-18	100	-	-	-
	C-16	100	-	-	-
(10) Dolomictic limestone-breccia intercalation	C-7	24	35	32	9

Values of Menard modulus of elasticity from the results of the pressuremeter tests are given in Table 6/3.7.

Table 6/3.7 – Menard Modulus of Elasticity of the Units

Lithology	Borehole	Em, MPa
Fill 1	C-12	722
	C-17	30 - 35
Dolomitic limestone 2	C-5	Upper levels: 292 - 800
		At depth: 1140 - 8319
	C-10	7365 - 19795
	C-11	Highly weathered parts: 20 - 995
		Slightly and moderately weathered parts:1576 - 9698
	C-12	715 - 2980
	C-17	152
	C-18	1400 - 5100
Breccia/megabreccia 3	C-10	300 - 9850
	C-11	690 - 1550
Crushed zone 9	C-5	20 - 25
	C-7	50 - 450
	C-12	20 - 570
	C-18	200 - 220

Pressuremeter Deformation Modulus vs. Elevation Graph is shown in Figure 6/3.7.

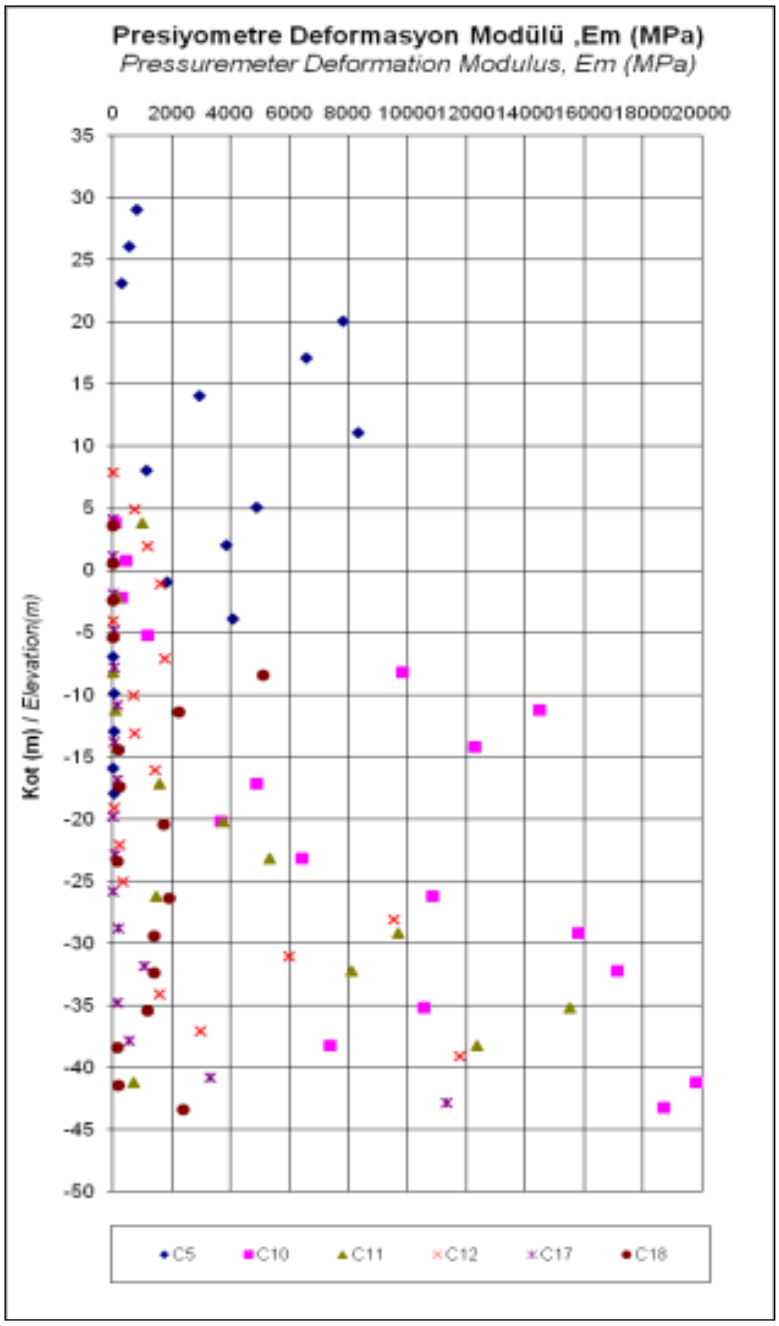

Figure 6/3.7 – Pressuremeter Deformation Modulus Vs. Elevation Graph

Results of laboratory tests of physical-mechanical properties of soils for each lithological variety are given in Table 6/3.8.

Table 6/3.8 – Test Results

Lithology	Uniaxial compression strength σc, MPa	Unit weight ρ, kN/m3 (air-dried)	Cohesion c, MPa	Angle of friction, ° (degree)	Young's Modulus E, MPa	Poisson's Ratio μ	Corrected point load index Ip (50), MPa
Fill (1)	-	-	-	-	-	-	2.20
Dolomitic limestone (2)	5-40	22.90-29.43	0-23	39-41	3068.97-17066.12	0.11-0.26	0.28-8.19
Megabreccia(3)	9.27-65.93	24.70-28.10	16-23	35-36	4341.46-12552.94	0.26-0.35	0.12-6.60
Mudstone (4)	56.15-83.43	26.04-27.12	-	-	-	-	0.69-9.69
Wackestone (5)	23.82-53.08	25.38-27.10	-	-	17890.16	0.16	0.90-6.11
Quartzitic sandstone (6)	36.92	25.60-26.50	-	-	-	-	2.09-2.78
Wackestone/mudstone (7)	11.49-63.40	25.99-28.73	-	-	1887.10	0.21	0.96-7.04
Cavity filling (8)	-	-	-	-	-	-	0.27
Crushed zone (9)	-	-	-	-	-	-	-
Dolomitic limestone-breccia intercalation (10)	-	-	-	-	-	-	-

6.3.3.3 SOIL/ROCK PROPERTIES BASED ON GEOPHYSICAL DATA

Seismic, electric, gravitational and magnetic properties of rocks together with mechanical properties of soils in natural conditions have been studied in the past 40 years.

6.3.3.3.1 SEISMIC SOIL/ROCK PROPERTIES

Seismic properties according to the present-day data

Seismic characteristics of soil/rock profile were studies at the current stage in 2011-2012 using both surface and borehole methods [6/77].

The following surface methods were used:

- seismic prospecting using RWM for determination of compressional seismic waves (V_p);
- seismic prospecting using multichannel analysis of surface waves (MASW) together with analysis of microseisms for determination of seismic shear waves (V_s).
- the following boreholes methods for studying the seismic properties were used:
- Sonic logging;
- PS-logging.

The seismic wave velocities based on surface methods

The results of the seismic prospecting through surface methods are available in [6/33, 6/70].

Seismic prospecting using RWM is carried out along profiles with 5 m offset between the sensors. The studied depths are up to 30÷40 m from ground level.

The V_p velocity is determined by the RWM. The results are presented in the form of seismic cross-sections along each profile.

The V_s velocities were determined using the MASW together with microseisms (ReMi). This has been done for each geophone location.

According to the V_p distribution the Akkuyu NPP site could be described as follows.

The rocks at the northwestern part of the studied area are characterized by V_p in the range from 600 to 3700 m/s. The V_p in the Aksaz Bay area and in the northern part of the NPP site varies from 770 to 3700 m/s.

In Çamalanı Bay the V_p is within the range 800 to 3800 m/s.

The Büyükeceli formation which will be used as a foundation of the structures is characterized by V_p in the range from 800 to 3800 m/s.

In general, according to the surface seismic survey results 3 to 4 seismic layers can be recognized.

The upper layer and in some places also the second from the top layer do not follow certain direction. These two layers correspond to loose Quaternary deposits or artificial soils, which are not found everywhere at the site.

The bedrock is characterized by high velocity of wave propagation, which according to the surface methods varies from 300 to 3000 m/s (V_s) and from 1000 to 4000 m/s (V_p).

Two bedrock layers are clearly identified.

The upper part of the bedrock is more fractured with different weathering degree is characterized by low velocities observed in zones of tectonic disturbances and highly fractured zones.

The lower layer on the seismic profiles corresponds to relatively undisturbed bedrock and is characterized by V_p from 3300 to 3900 m/s and V_s from 1600 to 2300 m/s.

There is a rough surface of the refracting seismic boundary and the clear manifestation of disturbances along the seismic sections are controlled by structural and tectonic disturbances or geological boundaries.

The dynamic parameters of the soil/rock strata based on seismic wave velocities according to the surface prospecting are presented for each profile in tabular form in [6/33, 6/70].

In general, well-conserved bedrocks are characterized by high velocities of seismic waves.

Lower velocities are observed where the rocks are fractured and weathered which mainly occur in the zones of tectonic disturbances.

Dynamic parameters according to borehole geophysical studies

Seismic characteristics of soils/rocks were studied in boreholes by two methods:

- Sonic Logging;
- PS Logging.

Seismic properties according to sonic logging data

Field materials of sonic logging are available in [6/34, 6/35].

Based on the sonic logging the compressional and shear seismic wave propagation velocities V_p and V_s, Young modulus Ed and shear modulus Gd and Poisson ratio μ were determined.

Sonic logging has been done in uncased intervals in boreholes, the upper, most fractured intervals, which had undergone weathering, were not studied because they were cased.

Therefore, only conserved intervals of bedrocks can be characterized based on sonic logging.

Intervals from 5 to 30 m were cased in different boreholes.

According to the sonic logging elastic wave velocities in layer of conserved bedrock vary in the rages: V_p from 3700 to 6400 m/s and V_s from 1400 to 3500 m/s.

The average propagation elastic wave velocities in conserved bedrock according to the sonic logging are: V_p ca. 4000 m/s and V_s ca. 2000 m/s.

Dynamic properties according to PS Logging

Based on PS logging the propagation velocities V_p and V_s were determined in 20 boreholes in 2011 and in 74 boreholes in 2012. Complete description of the method and results are available in reports [6/36, 6/37, 6/70].

The maximum depth of investigation varied from 50 to 130 m.

By PS logging the whole length of borehole has been studied including upper fractured part corresponding to weathering zone of bedrocks.

Based on the seismic wave propagation velocities the dynamic parameters of soils/rocks in each borehole were calculated. Results of determinations of V_p, V_s, and dynamic elastic modulus and shear modulus, and Poisson ratio are available in [6/70].

The character of wave propagation confirms once again that it depends on the conservation degree of bedrocks, which is conditioned predominantly by the weathering.

Figure 6/3.8 presents the seismic cross-sections of V_s along W-E direction through the projected reactor buildings based on PS logging (a) and on surface survey by ReMi/MASW method (b).

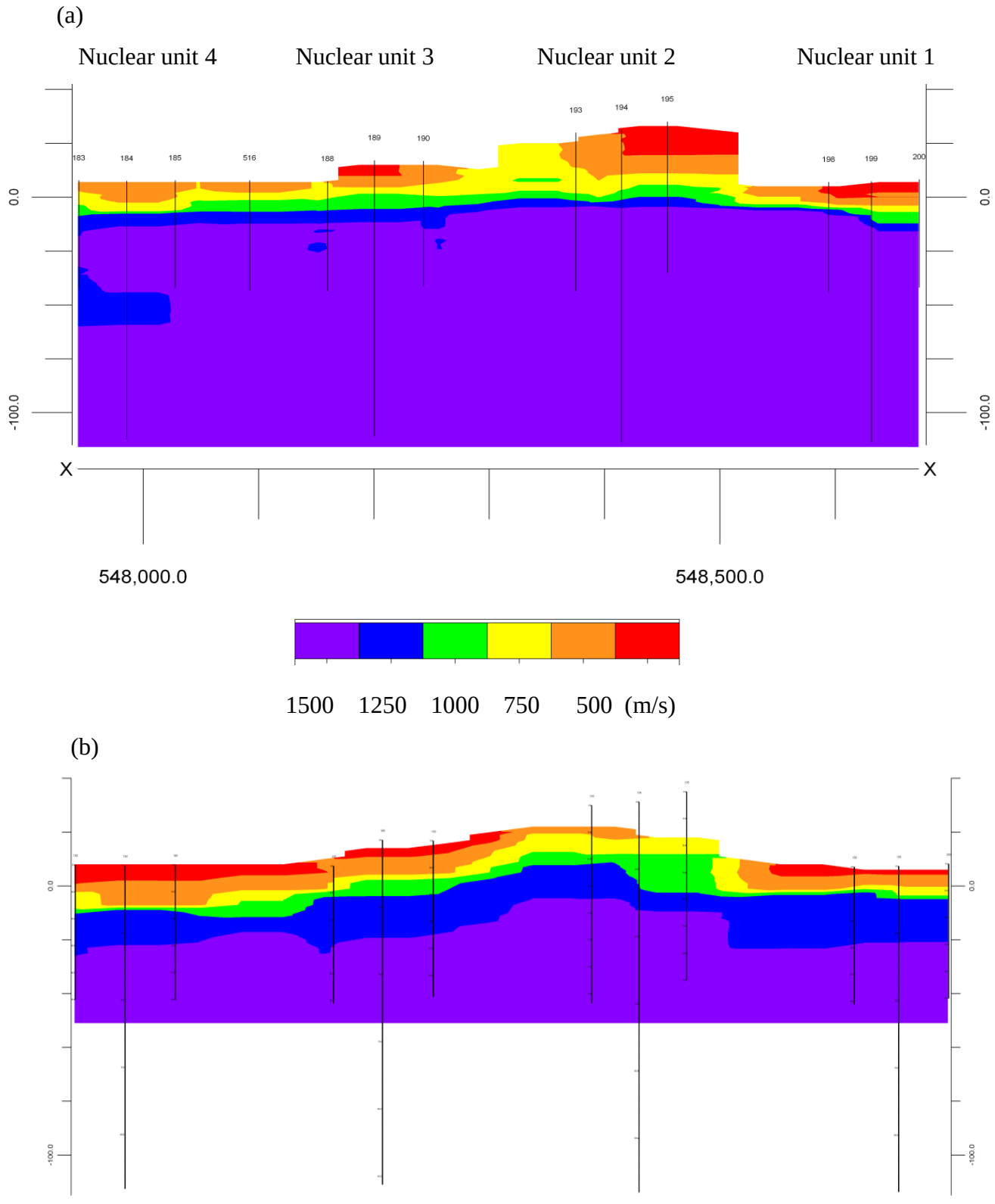

Figurre 6/3.8 – Seismic cross-section through reactor compatments using V_s-waves in WE direction: (a) *PS*-logging data; (b) *ReMi/MASW* data.

Currently, the bedrock at the base of the site is nonuniformly covered by artificial backfill of various thicknesses reaching 8 m.

Bedrock deposits are characterized by sloping, bedding, heterogeneity of composition and various degrees of preservation, fracturing, and weathering.

Soils composing the upper part of the cross-section (recent artificial backfill, alluvial deposits and weathered bedrock) are characterized by very low seismic wave propagation velocities.

According to MASW/ReMi data, artificial soils spread in the area of nuclear units 1, 4, and partly 3 are characterized by V_s values in the range 300÷500 m/s. The upper part of the weathered bedrock is also characterized by low V_s values in the order of 450 ÷ 850 m/s. Beach sand deposits occurring locally in the Aksaz Bay can indicate even lower values.

In general, a regular increase of V_p and V_s values with the increase of depth has been observed in the vertical cross-sections.

Three general layers (zones) are distinguished by seismic properties in the vertical cross-section. They are indicated in Table 6/3.9.

Table 6/3.9 – Seismic properties of rocks of the Akkuyu NPP site in the vertical cross-section

Vertical zoning	Soil description	Elastic wave velocities, m/s	
		V_p	V_s
Upper layer	Artificial (bulk) soils, alluvial deposits, highly weathered bedrock	1100÷2800	200÷1100
Medium layer	Weathered, highly fractured bedrock	2900÷4400	1100÷2000
Lower layer	Slightly fractured bedrock	4500÷6400	2000÷3200

The thickness of these layers varies at the site.

The thickness of the upper layer which is characterized by the lowest velocities, changes from the surface to 15-16 m depth at the location of unit 4, where the depth of the base of the upper layer reaches 8 m.

The thickness of the medium layer varies from 25 to 45 m in different areas. The largest thickness is observed at the location of units 3 and 4, where the lower boundary of this layer reaches values of 80÷90 m.

The lower layer corresponding to the slightly fractured bedrock is studied to depth of about 130 m. Its thickness varies from 50 to 70 m at different site areas depending on the topography.

The results of the present stage investigations performed in 2011 – 2012, confirm the seismic properties obtained from previous investigations.

The following conslusions could be made:

- there is a clear trend in the distribution of the seismic properties of soils/rocks in vertical direction;
- the characteristics of elastic wave propagation confirm their dependence on the degree of preservation of the bedrock conditional primarily on the degree of weathering and fracturing of the rocks;
- the intense weathering reflects in changes of the seismic properties not only in the vertical direction but laterelly as well. This is typical for rocks near major tectonic disturbances and fold axes.

Determination of Vs30 parameter

According to data from surface and borehole geophysical studies, the mean values of V_s for the upper 30 m of the soil/rock profile have ben determined [6/36, 6/37, 6/78].

The V_s30 parameter is largely influenced by the seismic properties of the most upper layer in the cross-section.

As the artificial soils and the weathered bedrock indicate different thicknesses at various parts of the site, a very wide range of variation in the mean values of V_s30 at free surface (the surface of relief) has been observed at different points of the site.

Based upon all surface and borehole investigations performed in 2011 and 2012 generalized V_s30 values were determined for Akkuyu NPP site.

The following methodological bases were used for determination of the V_s30 representation of the site:

- Based on consensus expert judgment, certain sets of measurements were screened out due to their location of the measurements (e.g. only

measurements within the area of interest remain for further analysis). Furthermore, older (prior to 2011) measurements were similarly screened out.

- Each group assigned weights to the methodologies on the basis of the following factors:

– Adequacy of the methodology for the particular application;

– Adequacy of the execution of the process in the field (for the associated measurements);

– Adequacy of the interpretation of the results (for the associated measurements);

– Number of measurements associated with the methodology;

– Adequacy of the location of the measurements;

- All groups had equal voting weights in the generation of the composite weight to be used for the V_s30 determination.
- The weighted mean of the standard deviations were calculated through weighting of the variances (i.e. square of the standard deviation) because σ itself is not a linear operator.
- For each methodology (P-S logging, microtremor, Remi/MASW) a composite mean and the standard deviation of V_s30 is derived from data sets which have not been screened out. For example, the P-S logging had the pair (μps , σps).
- The V_s30 results were derived based on the composite weights representing the consolidated V_s30 estimates for use in the Seismic Hazard Assessment study.

Figure 6/3. shows the territory of nuclear units 1, 2, 3, and 4 that was considered in the analysis of V_s30.

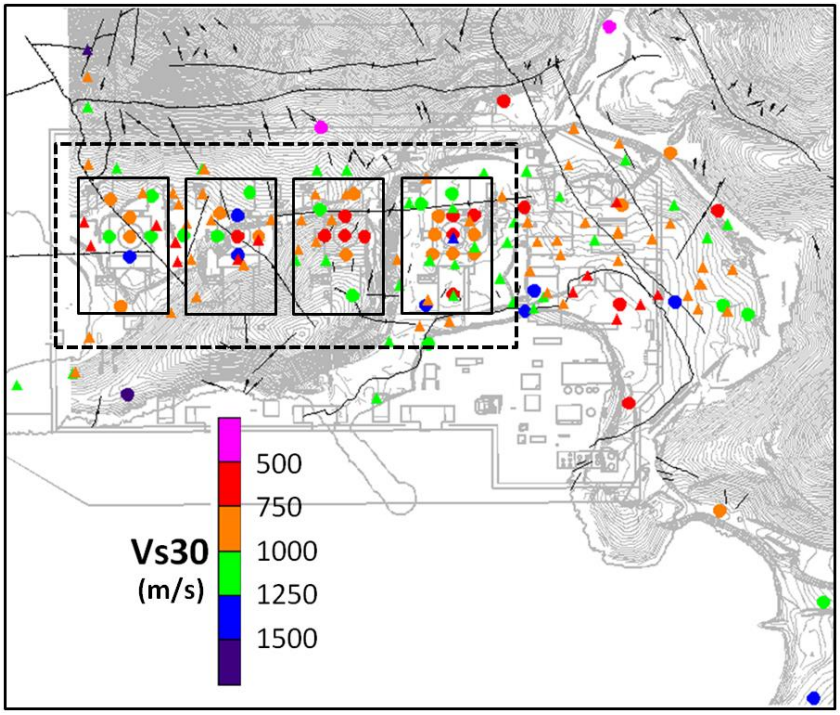

Circle is: PS-logging, triangular is ReMi/MASW method
Squares indicate units 1, 2, 3, and 4

Figure 6/3.9 – Location map of Vs30 studies in Akkuyu NPP site

Following this methodology and taking into account the actual V_s30 estimates generated from the different methods, the following generalized V_s30 result has been calculated:

V_s30=1038 m/s with standard deviation of 266 m/s.

This result is considered as the site reference V_s30 value which represents the area of nuclear units 1, 2, 3 and 4 in the current free field conditions.

Characteristics of the site depending on seismic properties

Given the local seismic characteristics and according to paragraph 3.1 of IAEA NS-G-3.6 [6/72], the Akkuyu NPP site can be classified as a site of type 2, for which the velocity of shear wave propagation V_s in the medium directly below the foundation base in natural conditions is within 1100m/s>V_s>300m/s.

Presently, the site is covered by unevenly distributed artificial fill with varying thickness reaching 8 meters. Bedrock deposits are characterized by inclined bedding, heterogeneity of composition, varying degrees of preservation, fracturing and weathering. Because of that, there is considerable variability of the free field (at existent topography) V_s30 estimates from one point to the other in the area under consideration.

Moreover, there will be considerable grading and leveling activities at the site, which will definitely affect the current soil/rock profile.

Therefore, the selection of the input data (in terms of seismic properties) used in the seismic hazard assessment of Akkuyu NPP site were based on the the international requirements in practical way.

According to paragraph 3.8 IAEA NS-G-3.6 [6/72] “Depending on engineering practices, the input ground motion may be representative of the ground surface motion either on the site or at a hard outcrop”.

Therefore, the design basis seismic ground motion is being developed for “bedrock conditions”, for which the shear wave average velocity for 30 m thickness is more than 1100 m/s.

According to paragraph 11.16 of IAEA SSG-9 [6/113] “The output specification should specify the control points (e.g. depths at the site) for which near surface hazard results are obtained. Usually, the control points include the ground surface and key embedment depths (e.g. foundation levels) for structures and components. The specified control points should be sufficient to develop adequate input(s) for soil–structure interaction analyses”.

For Akkuyu NPP site the control point of nuclear units 1 and 2 correspond to the existing free field conditions.

At the location of nuclear unit 1, the absolute elevation of the free surface has a mean value of 7,2 m.

At the location of nuclear unit 2, the absolute elevation of the free surface has a mean value of 31 m.

At the locations of nuclear units 3 and 4 the control points, for which the condition $V_s30 >$ 1100 m/s is fulfilled are located at different depths within the soil/rock profile.

The control points correspond to the absolute elevations of + 10.8 m (approximately corresponding to average depth of 6,2 m from the surface) for the nuclear unit 3, and +3.2 m (approximately corresponding to average depth of 5,0 m from the surface) for the nuclear unit 4.

The seismic design will be performed with account taken of the dynamic properties of the engineered fill that will be used for site grading and levelling and the ground motion for “bedrock conditions” for each NPP unit and main construction separately using the procedures of one-dimensional site response analysis.

6.3.3.3.2 ELECTRICAL PROPERTIES OF SITE SOILS

6.3.3.3.2.1 ELECTRICAL PROPERTIES BASED ON RESULTS OF PREVIOUSLY PERFORMED INVESTIGATIONS

Site soil electrical properties were investigated at survey stages 1 and 2 [6/66 and 6/164].

Stage 1 involved surface investigation with the use of vertical electrical sounding (VES) technique, with semi-spacing AB/2 = 300 m and electro logging in 6 boreholes, located on the lines of VES profiles.

Based on the results two resistivity sections were arranged for profiles К-1 and К-2, representing the variance in profile electrical resistance to a depth of 100 m [6/66].

Based on the electrical logging results [6/123 and 6/219], logs are plotted to represent the depth-depending variations in electrical resistance and spontaneous polarization potential in each borehole. The logs did not undergo any quantitative interpretation, i. e. resistivity values (ρn, Ohm·m), as well as relative values P = ρn/ρw (where ρw – water resistance in the borehole), were not determined. The interpretation was essentially qualitative one.

As far as electrical properties are concerned, three intervals are distinguished in the section.

The first 10 - 12 m thick interval from the surface level is characterized with low resistivity.

Second interval with 20 - 25 m thickness located below the first one is essentially characterized with high resistivity values in the range: 250 to 650 Ohm·m. Layers with lower resistivity may be found within this interval.

The third depth interval, located approximately at depth greater than 30 m is characterized with considerably lower resistivity. In the upper part of the section ρn value of 150 - 200 Ohm·m is observed, with resistivity decreasing with the increasing the depth reaching as low as 20 - 70 Ohm·m and even lower in some areas at depths 50 to 100 m.

The results of the surface electrical prospecting and electrical logging led to the interpretation for the presence of large open fracturing zone unfilled with clayey substance in depth range 35 - 55 m.

Electrical prospecting was performed in survey stage 2 as well.

Surface electrical sounding was performed with the use of symmetrical Winner installation with electrode spacing: 5, 10, 15, 20 and 50 m, and electric logging in boreholes.

Apparent resistance ρ_k maps were plotted for the above mentioned semi-spacings, corresponding to particular investigation depth.

Resistivity sections were constructed for seven profiles to depth 50 to 100 m.

A decrease in the apparent resistance as the depth increases, particularly, towards the sea is observed. Such decrease is especially sharp below depth levels 20 - 30 m from the sea level. At such depth, ρ_k value decreases. This is probably due to high salinity and very low resistance of seawater, filling the rock mass caverns and open cracks. This is why the results expressed as apparent resistance (ρ_k) measured values, observed below 20 m depth, are not typical for the actual electrical properties of the rock i.e. they only qualitatively characterize the fracturing of the entire mass.

According to investigation stage 2 results, the NPP site bedrock is characterized with resistivity within the range 50 to 700 Ohm·m. Comparing the results of stages 1 and 2, one should bear in mind that the field works were performed in different months of the year. The winter period (November to February) coincides with rainy season when groundwater level may be considerably higher than the one observed in summer time, and salinity may vary depth-wise.

At stage 2, three anomalous zones of relatively low (50 to 150 Ohm·m) resistance are distinguished in ρ_n maps. Such zones are related to more intensive fracturing and water saturation or to the filling of fractures with clayey substance.

Based on the results of the electric logging performed at investigation stages 1 and 2, no large caverns or cavities have been detected in the bedrock.

6.3.3.3.2.2 ELECTRICAL PROPERTIES BASED ON RESULTS OF RECENT INVESTIGATIONS

The electric resistance of the rocks is characterized based on the results of two methods: electrical prospecting via vertical electrical sounding (VES) and 2D profiling (2D-Resistivity or electric tomography).

A complete description of the methodology and results of the works (including) VES curves are available in the original reports [6/73 and 6/69].

Groundwater has an essential affect to the specific electrical resistance values.

As moving away from the seashore inside the land, the salty water affect is replaced by fresher groundwater affect, which results in higher electrical resistance values.

In some places salty water affect is also observed in the deeper parts of the sections. The higher differentiation of geoelectrical sections by electrical resistance is also observed both in VES sections, and in 2D inversion sections.

Within the site area the lateral and vertical changes of the specific electrical resistance (SER) values are connected with the presence of faults and structural tectonic boundaries in the bedrock.

Preserved bedrock is characterized with high SER values. Low resistance values observed in the bedrock are connected with jointing and weathering of rocks, effect of seawater and groundwater filling rock fractures, as well as fault zones or other tectonic disturbances.

The effect of the east-west strike Akkuyu fault is evident at the northern part of the site.

The ρa values grow with increasing the depth.

Water specific electrical resistance in boreholes varies in the range of 1000 - 1200 μS/cm.

In some boreholes, where salty seawater penetration is observed, liquid electrical conductivity reaches levels within 10 000 - 30 000 μS/cm.

Figure 6/3.10 presents the integrated results of the surface geophysical works.

The areas of the profiles where anomalies related with disturbances in the homogeneity of electrical or seismic properties of the rocks have been noticed are shown with different colors. The SER summarized data are available in Report [6/73].

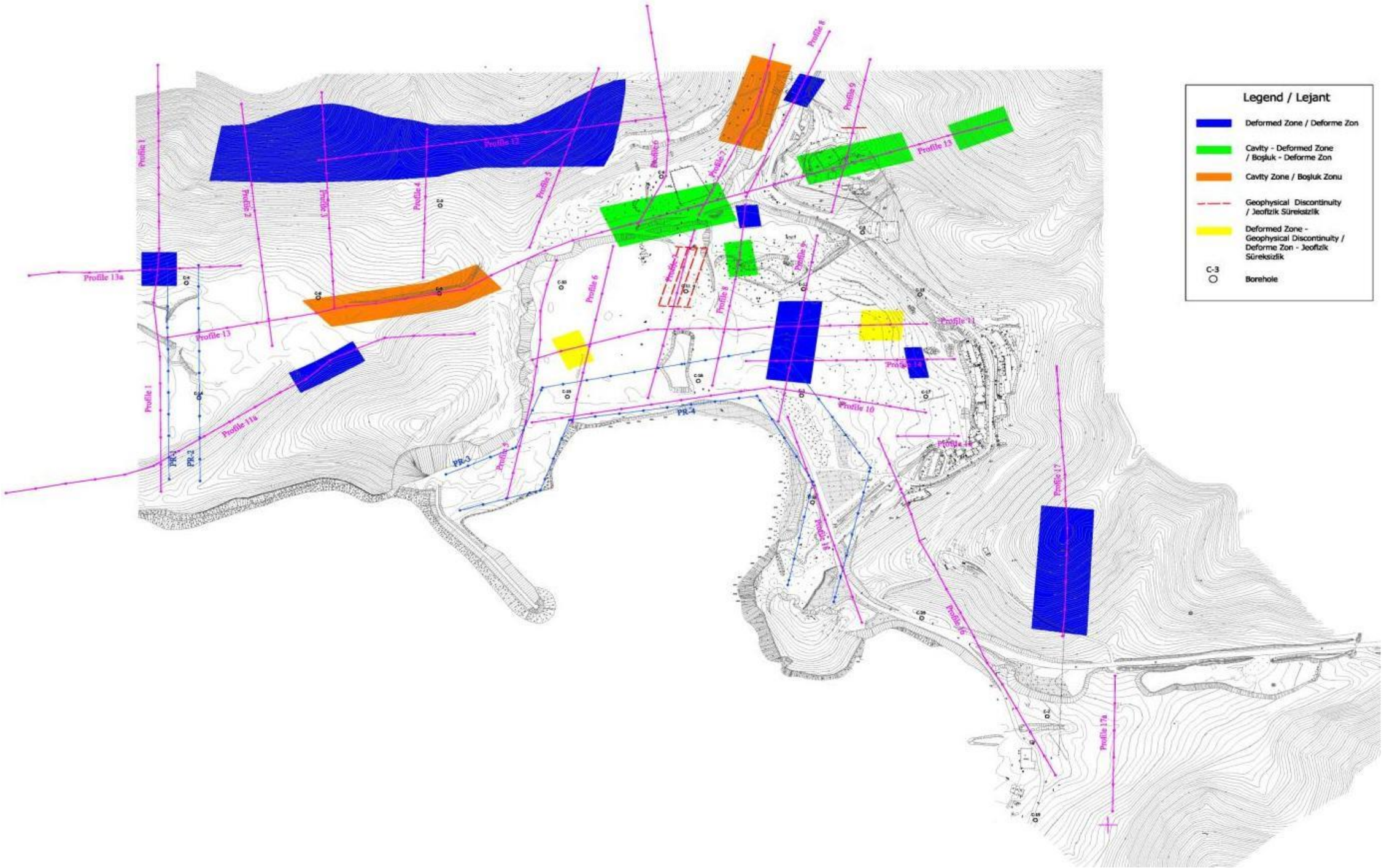

Figure 6/3.10 – Anomalous Areas of Profiles, Distinguished Based on the Results of Integrated Geophysical Studies

6.3.3.3.3 DENSITY AND POROSITY OF IN-SITU SOILS

In-situ density and porosity of soils have been determined based on the results of borehole geophysical studies. The density was determined by means of density gamma-gamma-logging data and the total porosity using sonic logging data.

The porosity values were determined for the depth intervals where clayey minerals are not available in rocks' composition, i.e. in places where the natural gamma radiation values are minimal [6/71].

Total porosity of preserved carbonate rocks is low and varies between 1-9 % and 3-4 % in average [6/71]. As for the mineralogical density, for dolomites it was accepted equal to 2.87 g/cm^3.

The density of rock, in geological descriptions of so called "dolomitic limestone", which does not include intercalations of any clayey minerals, varies in the range from 2.80 to 2.89 g/cm^3.

Water density in boreholes is accepted equal to 1 g/cm^3 for boreholes with water specific electrical conductivity of 1000 μS/cm and equal to 1.1 g/cm^3 for electrical conductivity higher 10000 μS/cm.

The in-situ porosity and density values acquired for carbonate rocks correspond to the values of these parameters determined on core samples in laboratory conditions.

Density in-situ of the rocks, described by the geologists as "dolomitic limestone", without clayey filler, measured in boreholes via density gamma-gamma-logging method, vary between 2.80 - 2.89 g/cm^3. In fact such high density does not normally correspond to that rock variety. Limestone density in average should normally be about 2.79 g/cm^3.

It is possible that density values obtained per logging data are overestimated because the effect of the borehole conditions were not explicitly taken into account (in particular, presence of water in borehole during logging, diameter of borehole etc.).

6.3.3.3.4 GRAVIMETRIC ANOMALIES

Surface gravimetric survey was performed at stage 2 of Akkuyu NPP site investigation [6/34 and 6/160].

The survey was performed in a geodetically controlled exploration grid with 20 m spacing, with the spacing decreasing to 10 m towards the site center. The control survey covered up to 20 % of the whole set of observation points.

Sensitivity of the gravimeter was 0.01 mgal.

"Free-air" (i. e. with no correction for local topography) maps of anomalies have been plotted, as well as simple Bouguer anomaly maps for specified value of intermediate layer density

of 2.35 g/cm^3 and full Bouguer anomaly map for specified value of intermediate layer density of 2.5 g/cm^3.

The intermediate layer density value was specified from logging results.

The correction for local topography was introduced with maximum error 0.007 mgal. Bouguer anomaly values are given with maximum error not exceeding 0.025 mgal.

In the Bouguer anomaly map, several anomalies are distinguished for intermediate layer with density 2.35 g/cm^3. Such anomalies are related to main geologic structures, located, particularly, in the northern and western parts of the site.

Considerable negative anomalies with maximum amplitude 0.3 mgal, extending to 100-150 m, were detected.

Such negative anomalies are caused either by facially substituted rocks of relatively low density (clay or clayey substances) or by karstic structures.

The anomalies were interpreted by means of computer-aided simulation, set to the solving of the direct problem: geologic model building, related theoretical curvature design and comparison of theoretical and actually observed curves.

The direct problem was solved and the two curves (actually observed and theoretical) were compared. As a result were the geological and geophysical models of the bedrock section for two profiles have been constructed [6/34].

According to one of the models, a rectangular layer (lens) is observed in the rock mass of average density 2.62 g/cm^3 along the line of boreholes S33 - S66. The approximate depth of the lens is 10 - 25 m, the density: 1.95 g/cm^3, the approximate thickness: 10 - 12 m and the length: up to 200 m.

Similar anomalies, oriented to the west from borehole S66, are observed in the Bouguer anomaly map.

The location of the largest negative density anomaly in the Bouguer map matches with the location of the lower resistance zone determined by the electric sounding performed in the same area.

The instrument used was not sensitive enough to conclude the presence of cavities when layer thickness exceeded 5 m.

6.3.3.3.5 MAGNETIC FIELD

Geomagnetic survey was carried out along the same profiles as the other surface methods.

Description of the methodology and geomagnetic survey results are available in the original reports [6/73 and 6/69].

The base station, relative to which corrections for magnetic field daily variations were introduced, is located in the geomagnetic observatory in Iznik, Bursa (Bogazici University, Kandilli Observatory and Geophysical Department of Earthquakes Investigation Institute, Geomagnetic Laboratory). The coordinates of Geomagnetic Laboratory in Iznik are 40.50º N and 29.73º E.

A measurement unit of the outcome magnetic field is nanoTesla (nT).

The noise affected data were removed from the total magnetic field, after which a contour map was plotted, converted into a map of magnetic anomalies, presented in Figure 6/3.11.

When comparing the map of the magnetic anomalies (Figure 6/3.11) with the results of surface studies (Figure 6/3.10), it is clear, that the magnetic field anomalous areas correspond to the zones, distinguished based on electric prospecting or seismic survey.

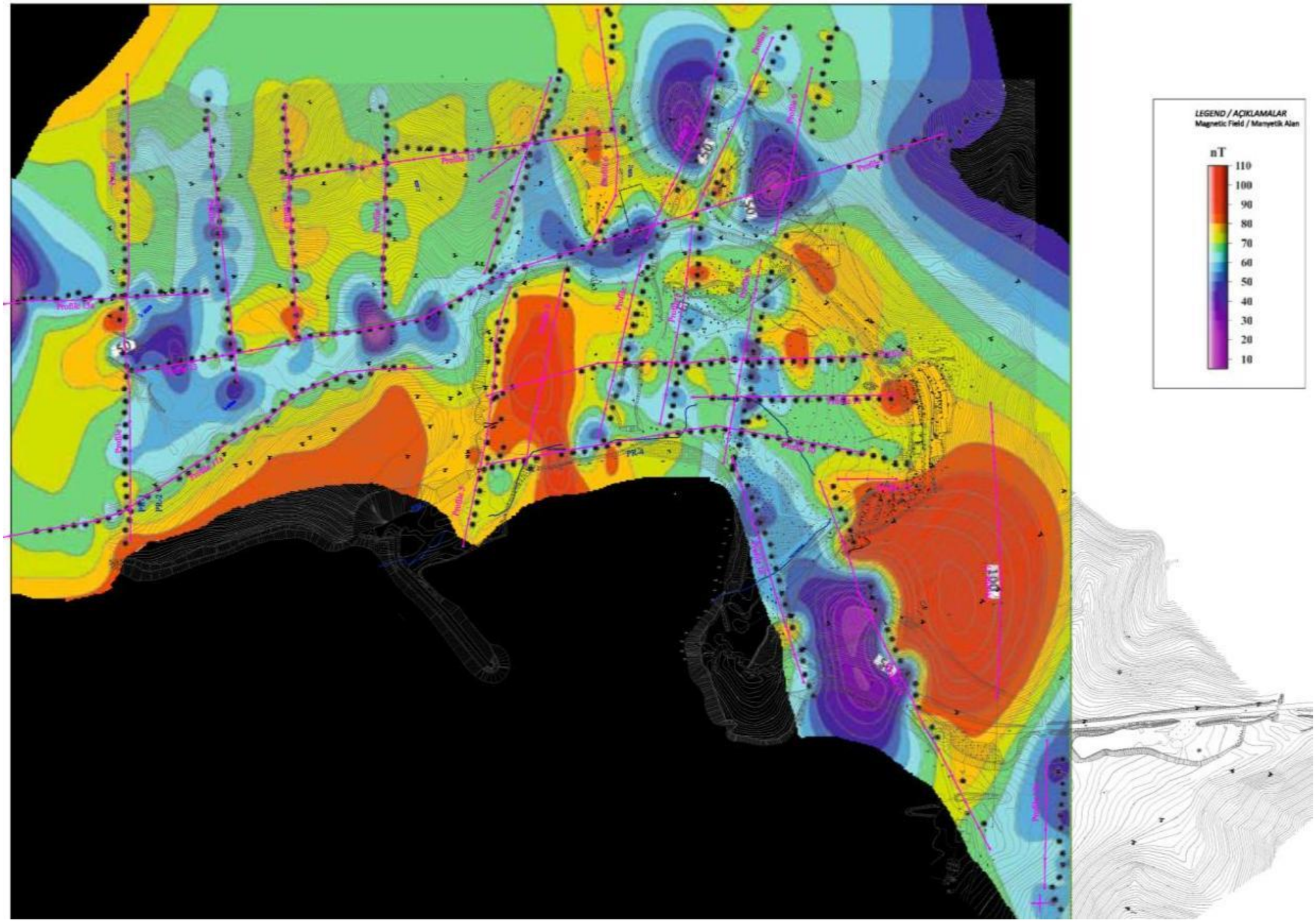

Figure 6/3.11 – Map of Magnetic Anomalies

6.3.3.3.6 STUDY OF SITE AMPLIFICATION CHARACTERISTICS

Preliminary assessment of the site amplification characteristics was performed in 2011 by means of instrumental technique (Nakamura method) [6/166] based on the records of microseisms (in terms of acceleration) at two stations (AKK1 and AKK2). The spectral ratio of the Fourier spectrum relation of the horizontal component to the vertical one (H/V) was analyzed for assessment of dynamic characteristics (site response, predominant frequencies and amplification) of near-surface layers. The H/V spectral ratio of microshocks gives the transfer function of the surface layers [6/166].

30 fragments (windows) of the records of microseisms without peaks were selected for calculation of the H/V spectral ratio. Duration of each of the fragments is 40.96 s. DC offset and any trend components were removed from the records. The records were smoothed by 10 % symmetric cosine window. Amplitude Fourier spectra of vertical and horizontal components were calculated for each of the 30 fragments. Amplitude spectra were smoothed by means of five-point Hanning window. The calculations of spectral coefficients H/V for each were made as per the following formula:

$$\mathrm{H/V} = \sqrt{\frac{\mathrm{EW}^2 + NS^2}{2 \cdot UD^2}} \quad ,$$

where - EW – component of EW spectrum, NS – component of NS spectrum, UD – vertical spectrum component.

Summing up of all 30 spectral ratios was carried out for finding the mean spectral ratio.

The spectral ratio relevant to the two stations (AKK1 and AKK2), are given in Figure 6/3.12.

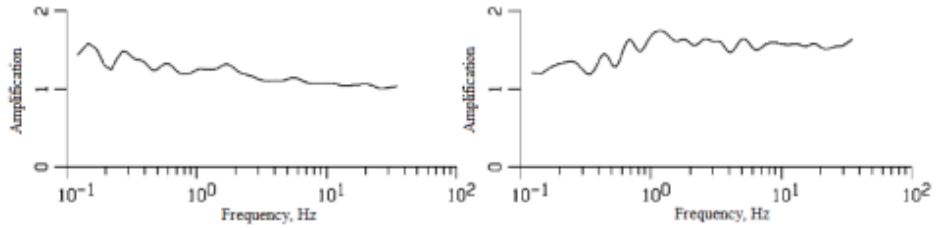

Figure 6/3.12 – Transfer Functions (Site Response), Obtained by Nakamura Method, According to the Records of Microseisms at AKK1 (Left) and AKK2 (Right) Stations

As seen in Figure 6/3.12, transfer functions are close to one which means that amplification at sections under AKK1 and AKK2 stations is insignificant.

An appropriately detailed site response analysis will be performed as part of the seismic hazard analysis for conditions of Vs30 less than 1100 m/s.

6.4 SEISMOLOGICAL INFORMATION

6.4.1 HISTORICAL EARTHQUAKE DATA

The results of historical seismicity investigations in the region at earlier stages of Akkuyu NPP project (before 1990) are available in reports [6/88, 6/84, 6/43 and 6/44].

Within the scope of the Akkuyu NPP project, at the stage of engineering survey renewed in 2011, the historical seismicity data for the area were obtained by the following four research groups: ENVY/BU KOERI (Turkey); WorleyParsons Nuclear Services JSC (USA); Paul C. Rizzo Associates, Inc. (USA); Institute of the Physics of Earth of the Russian Academy of Sciences (Russian Federation).

In the ENVY/BU KOERI survey [6/75] the historical earthquake data, from 2100 BC to 1900 AD, have been collected from all available sources (about 10 compiled regional catalogues). Totally, the list of historical earthquakes of ENVY/BU KOERI includes 380 events which took place within the territory limited by 31°-39 ° N, 28 °-38 ° E. For 271 of these earthquakes the data about their intensity and location are available. Data on historical earthquakes in the area within the coordinates 31-39º N and 28º-38º E, collected by ENVY/BU KOERI, are provided in Appendix M.

Epicenter maps of strong historical earthquakes (2100 BC to 1900 AD, the area is limited by coordinates 31°-39° N, 28°-38° E) according to ENVY/BU KOERI [6/75] are provided in Figure 6/4.1.

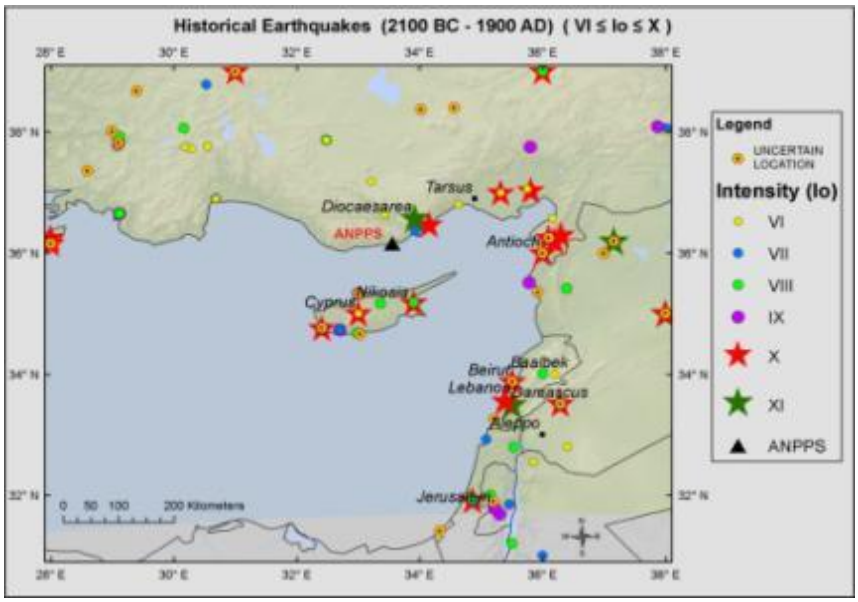

Figure 6/4.1 – Epicenter Map of Strong Earthquakes in the Area

The IPE RAS survey [6/117] utilizes the historical earthquake catalogue developed by ENVY/BU KOERI (380 records) as the basis for the summary catalogue of historical earthquakes. 126 events in the territory within 300 km radius around the site have been analyzed.

It is demonstrated that in the ENVY/BU KOERI catalogue out of 126 pairs of relationships "epicenter intensity-magnitude" 118 pairs are described by the equation:

$$M=0.47I_o+2.55. \quad (6/4\text{-}1)$$

Eight pairs significantly deviate from the regression line. Since these eight events (Figure 6/4.2) are relatively close to the site, all of them have been analyzed.

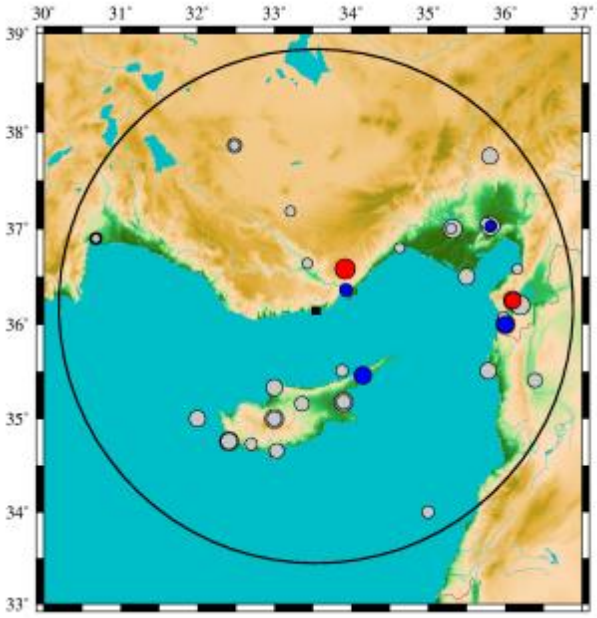

Figure 6/4.2 – Epicenter map of the historical earthquakes based on the ENVY/BU KOERI catalogue. The earthquakes with magnitudes larger (red circles), lower (blue circles), and equal (grey circles) than it follows from equation (6/4-1)

Two of these earthquakes closer than 150 km to the site (earthquake coordinates are taken as per ENVY/BU KOERI catalogue). These events require special care, because they may have some impact on seismic hazard assessment. Some selected significant historical earthquakes are listed and described below [6/13].

AD 97 Diocaesarea

Diocaesarea was completely destroyed together with Nicopolis during the reign of the emperor Nerva. It was the third time that Diocaesarea had to be rebuilt, and this time destruction was total, the imperial government providing 800 pounds of gold for its reconstruction, after which it was renamed Anazarbus. Malalas records that this earthquake happened during the reign of Nerva (18 September 96-25 January 98) and that the emperor died before repairs were complete. Diocaesarea was first called Scynta (or Cyinda) and was destroyed during the time of the Roman consuls (during the first century BC). When rebuilt it was renamed Ciscus. It was destroyed again during the dictatorship of Julius Caesar (49-44 BC), who renamed it Diocaesarea when it was

rebuilt. On this occasion, according to Malalas, the emperor Nerva sent Zarbus to construct a new city on the site, and the new city, which was better than before, was named Anazarbus after Zarbus (Mal. 267/405).

Note: *"During his [Nerva's] reign, Diocaesarea suffered from the wrath of God for the third time, as did Nicopolis and its district. So the emperor sent a Roman senator called Zarbus to rebuild it, giving him eight centenaria. When the senator Zarbus reached Cilicia, and saw the destruction, he put a great amount of energy into reconstructing the town, making it better than it was before: and so the city was named after him as a mark of the citizens' gratitude. He had previously called it Nerva after the name of the emperor." (Mal. 267/405)*

AD 1891, Oct 02, Silifke

An earthquake at 9 h 53 m was felt in Silifke. It lasted for about 20 seconds. It caused no damage (PSB 1307, 10.13).

AD 1891, Oct 29, Mersin

At 21 h 45 m there was a rather violent earthquake at Mersin; it caused no damage (PSB 1307, 11.12).

AD 1891, Nov 03, Mut

A strong earthquake at 5 h 30 m was felt at Kozan and Mut and in the district of Içel (Mersin) in Turkey. There is no evidence that it caused any damage (PBS 1307, 11.20).

AD 1882, Feb 28, Karaman

This earthquake occurred during the afternoon and was felt over a relatively large area. In Adana it caused trees to sway and houses to rock, without damage, and in Limassol there was some panic. The shock seems to have been experienced in Karaman as well, where it damaged the dome of Seki Hamam and houses, but details are not given (PMH 1882, 78.172; Agamennone 1904, 114; Konyalı 1967, 534).

AD 1884, Sep 21 Silifke

On Sunday 9 September (O.S.) at about 6 h 30 m (Turkish time) there was a violent earthquake in Silifke. It caused some damage and the collapse of some walls of the old castle (PTH 1884,12.9).

AD 1895, Nov 23 Karaman

An earthquake, probably originating from Karamania in southern Turkey, caused some damage at Mut, and in particular at Elibaş, Kalpulu and other sites the locations of which are not certain, and it was felt at Nicosia in Cyprus (Lamec 1913, 311; Christofides 1968-1973 sub ann.).

Depth distribution of magnitudes is an essential part of the hazard assessment and therefore, it is better to discuss this topic after completion of instrumental and historical catalogue compilations. But it is also important to consider data on depth distribution of events when compiling historical catalogue.

Magnitude versus depth plot is shown in Figure 6/4.3. Magnitudes below 3 are not shown on the plot, as they do not have significant impact on hazard level. Depths shallower 4 km are also skipped, because overall depth evaluation accuracy in the catalogue is not better than ±5 km.

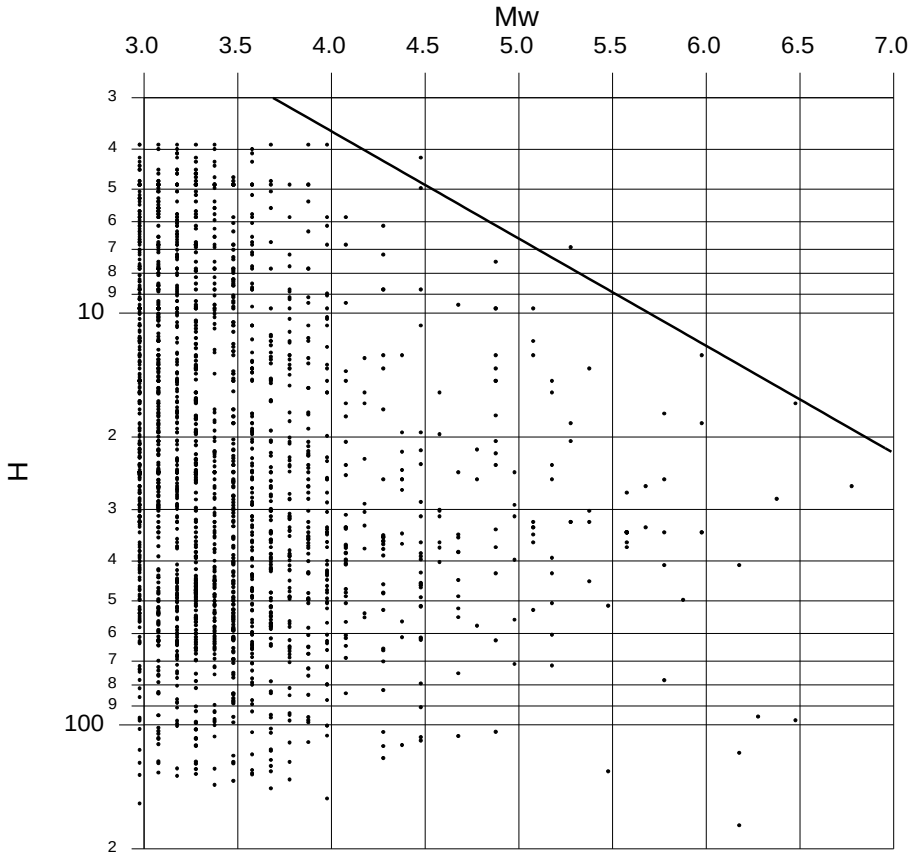

Figure 6/4.3 – Distribution of magnitudes on depth H, km

The line separating data area on the plot is

$$LgH=0.26Mw-0.48 \quad (H\geq 4 \text{ km}) \qquad (6/4\text{-}2)$$

The most essential feature for application of this equation in historical earthquake analysis (when data on event depth are commonly missing) and for further hazard assessment is that

according to the observation data there are no earthquakes with Mw=6 at depth less than 13 km and Mw=6.5 less than 17 km deep.

As for AD 97 Diocaesarea event (No 43 in the ENVY/BU KOERI catalogue), there is certain inconsistency in that Diocaesarea and Nicopolis are combined in one event. In Antic times in Greece, Asia Minor and Middle East at least 5 localities entitled "Nicopolis" were known. The nearest to Diocaesarea was Nicopolis Seleucidis. It was located at ca. 280 km distance from Diocaesarea. It is hard to imagine an earthquake causing total destruction along 280 km path. Possibly, Malalas did not mean that both cities were destroyed simultaneously (suffered from the same earthquake) or maybe the locality name is wrongly recorded. It should be noted that the word "earthquake" (shaking, trembling, etc.) is not mentioned at all – only the wrath of God. What concerns Diocaesarea, its location can be identified without serious problems – it is modern Uzuncaburç located 23 km to the north of Silifke (60 km from the site). The fact that the city was destroyed several times (not necessarily from earthquakes – for example, military actions) does not allow a proper assessment of the construction quality from seismic point of view to be made. Therefore, the intensity assessment IX suggested in the ENVY/BU KOER catalogue is reasonably sufficient.

WP in compilation and preparation of the compiled catalogue also used the historical seismological catalogue for Turkey [6/210]. Epicentral map of historical earthquakes (for the period from 2100 BC to 1963 AD according to [6/210] catalogue) is shown in Figure 6/4.4.

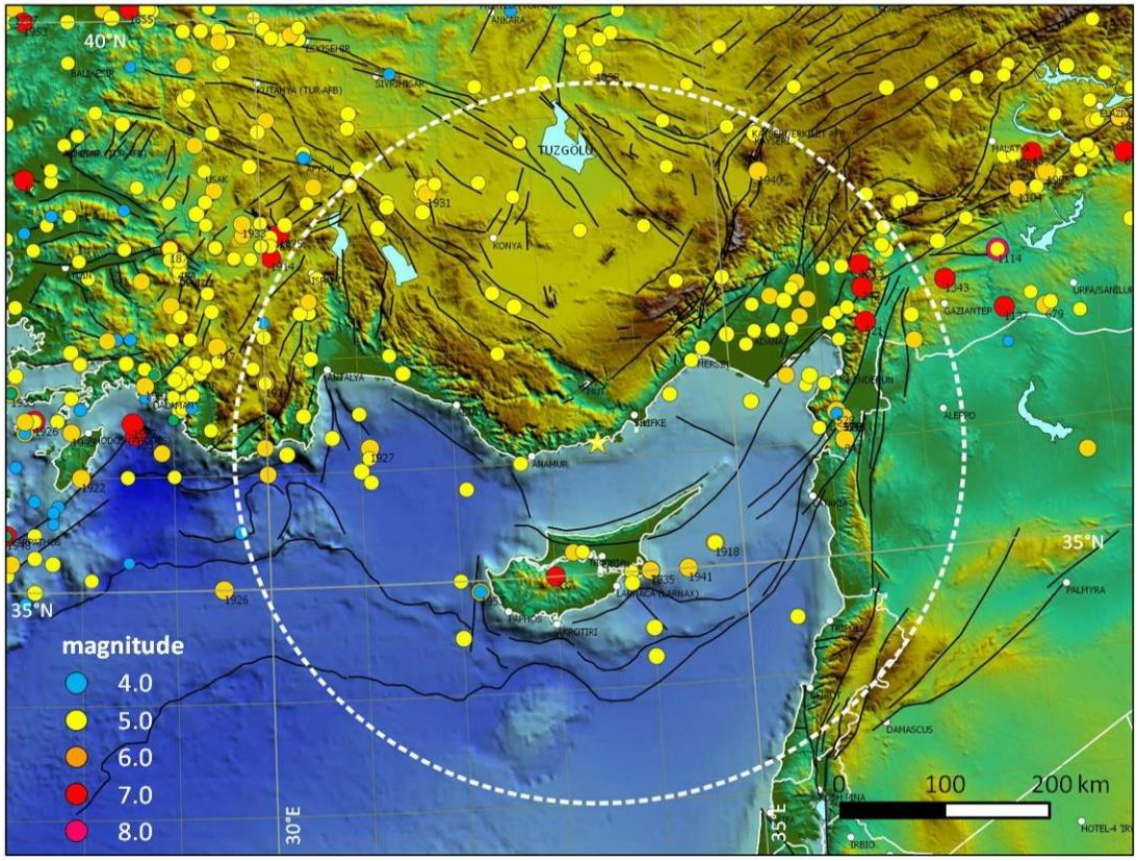

Figure 6/4.4 – Epicentral map of historical earthquakes from [6/210] catalogue

WP revised epicenter location of a historical earthquake in [6/210] catalogue. This event took place in 1213 some 200km away from the site (as per [6/210]). The revision was done because such a strong event could, in WP opinion, influence the seismic hazard assessment for the site because of the relatively high magnitude estimate (M=7.3). Furthermore, in one seismotectonic model proposed by Rizzo, this epicenter was located within the boundaries of the site seismotectonic province.

The earthquake (as reported in the letter written by a soldier to the archbishop of Constantinople in 1213) occurred in Isauria (a region bordering the province of Konya (Iconia) then a very important Seljuk Turkish province. The present day settlement which would correspond to the main city of Isauria is Bozkır on the northern hills of the Taurus Mountains. However, as a more precise location for the observed damage, the letter cites the city of Philadelphia (the present day Alaşehir) several hundred kilometers northwest of Bozkır. In order to clarify the uncertainty with the location of this earthquake a special study has been launched by WorleyParsons. The results show that the event has been misplaced in the historical seismological catalogue [6/210] with most plausible epicenter near Alaşehir which is some 500 km away from the site.

The WP compiled catalogue contains data on 878 historical earthquakes with an intensity not less than 5 points on the MSK-64 scale, and magnitude (M_S), not less than 5.0, which took place

within the territory having co-ordinates 25º-43º N and 25º-45º E. A declustered version of WP historical earthquake catalogue includes 754 records.

The periods of completeness of historical and instrumental earthquakes of different magnitudes in WP compiled catalogue are provided in Table 6/4.1.

Table 6/4.1 – Completeness Periods of Historical Earthquake Catalogue by WP

Magnitude MW	Year of catalogue completeness for 350 km zone
5.0	1921
6.0	1821
7.0	1750
8.0	1160

The summary catalogue of historical and instrumental earthquakes prepared by WP in original and declustered versions is provided in the Appendix M.

The earthquake catalogue presented by Paul C. Rizzo Associates, Inc. (further Rizzo) was compiled from two sources:

- The Earthquake Catalogues for Turkey [6/210];
- The University of Athens (UOA) [6/232].

The catalogue of historical earthquakes prepared by Rizzo in original and declustered versions is provided in Appendix M.

The periods of completeness of the Rizzo catalogue for historical earthquakes (569 events till the year 1900 inclusive) with different magnitudes are provided in Table 6/4.2.

The declustered version of the RIZZO catalogue, which includes historical (until the year 1900 inclusive) earthquakes, totals 404 records.

Table 6/4.2 – Periods of Completeness of the Historical Earthquake Catalogue by Rizzo

Magnitude MW	Catalog Completeness: Alternative 1 – Cumulative Number		Catalog Completeness: Alternative 2 – Stepp (1972)	
	Year	Weight	Year	Weight
> 3	1996	0.5	1999	0.5
> 4	1964	0.5	1968	0.5
>5	1918	0.5	1913	0.5
>6	1896	1.0		
>7	1750	1.0		
>8	1170	1.0		

According to data from compiled earthquake catalogue of Turkey prepared by ENVY/BU KOERI earthquakes with magnitude ≥8 have not been recorded or observed during nearly a

4000-year period. There are no records of such strong events (M≥8) in the IPE RAS catalogue. However, since for historical events there is only intensity data in catalogues, magnitude-intensity conversions have to be used in order to provide for homogenous magnitude scale in the analysis. When applying such conversions in fact, there are 15+ events with Mw estimate ≥7.5 in the Akkuyu project seismological catalogue.

At the present time ENVY/BU KOERI is working on updating and generalization of all the four instrumental and historical catalogues presented by the project participants in 2011. The seismological catalogue in the consolidated report integrates the seismological catalogues analysis of all different parties.

Isoseismal maps for some strong earthquakes in the area within 300 - 350 km from the site, also having a description of macroseismic field, are provided in Figures 6/4.5 - 6/4.9.

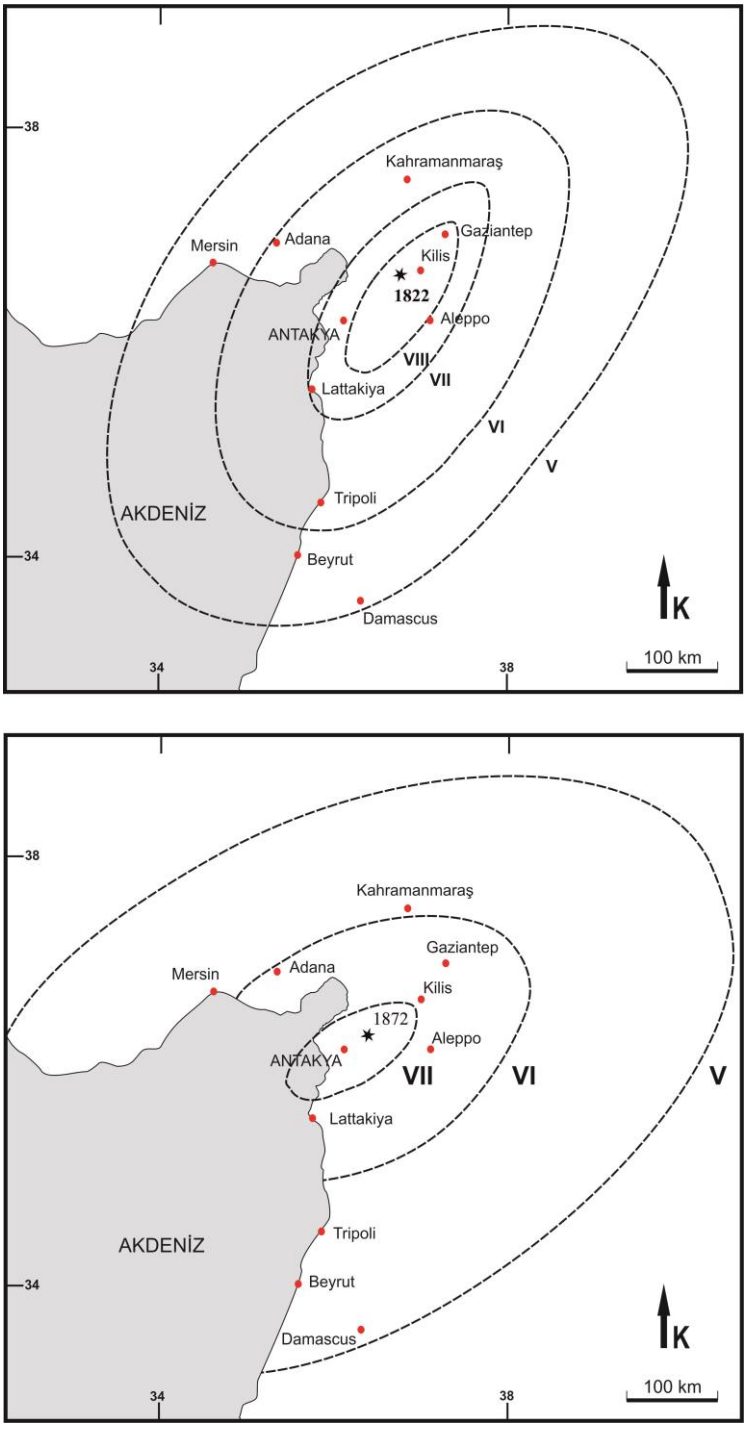

Figure 6/4.5 – Intensity isoline map of 1822 event (M=7.4) and 1872 event (M=7.2), [6/14]

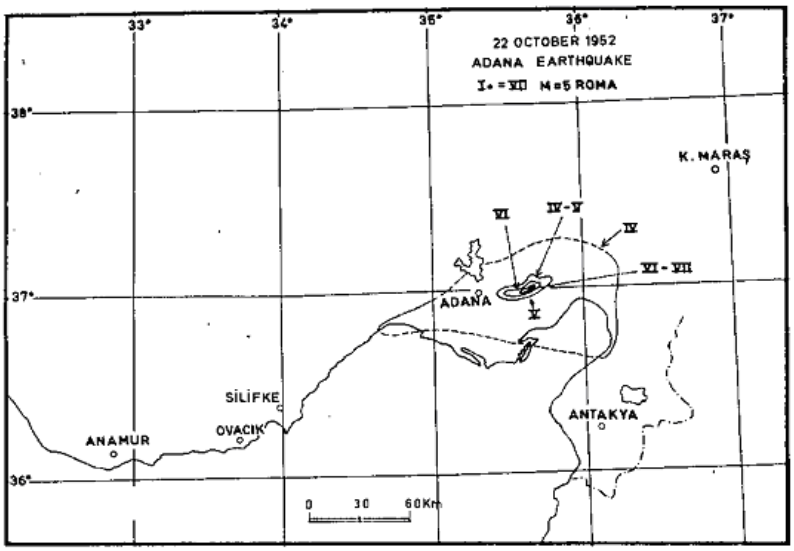

Figure 6/4.6 – Isoseismal Map of 17:00:48,5 October 22, 1952 Earthquake Near Adana; Coordinates of the Epicenter: 37.25º N and 35.65º E; Depth - 70 km; Magnitude MS=5.6; Epicenter Intensity - 7 Points [6/112]

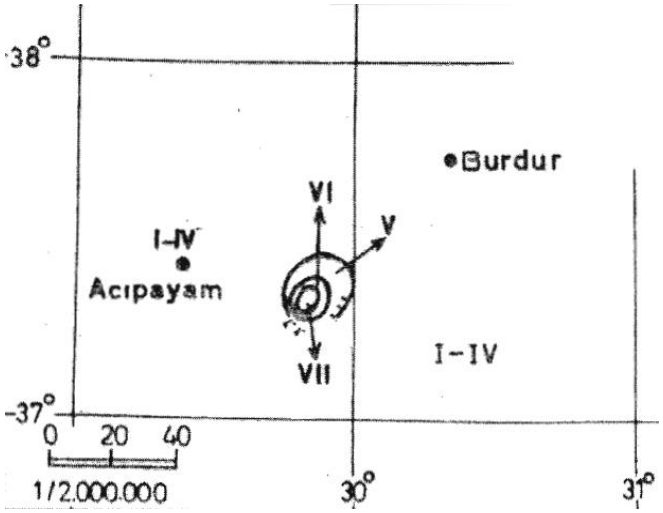

Figure 6/4.7 – Isoseismal Map of November 22, 1963 Earthquake Near Burdur; Coordinates of the Epicenter: 38.07º (37.41º) N and 29.68º (29.89º) E.; Depth - 60 km; Magnitude M_S=5.1 (5.7); Epicenter Intensity - 7 Points [6/112]

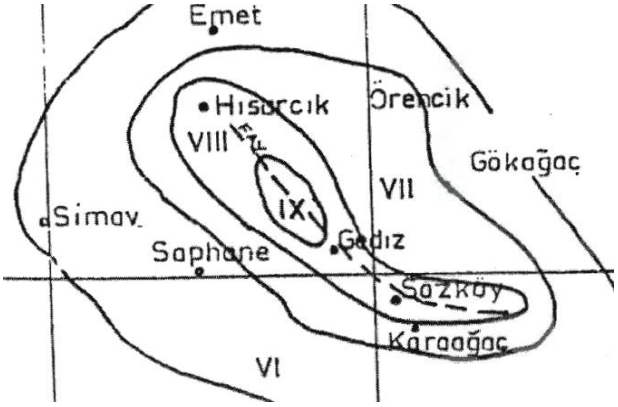

Figure 6/4.8 – Isoseismal Map of 21:02 March 28, 1970 Earthquake Near Gediz; Coordinates of the Epicenter: 39.21º N and 29.51º E.; Depth - 18 km;
Magnitude M_S=7.3; Epicenter Intensity - 9 Points [6/112]

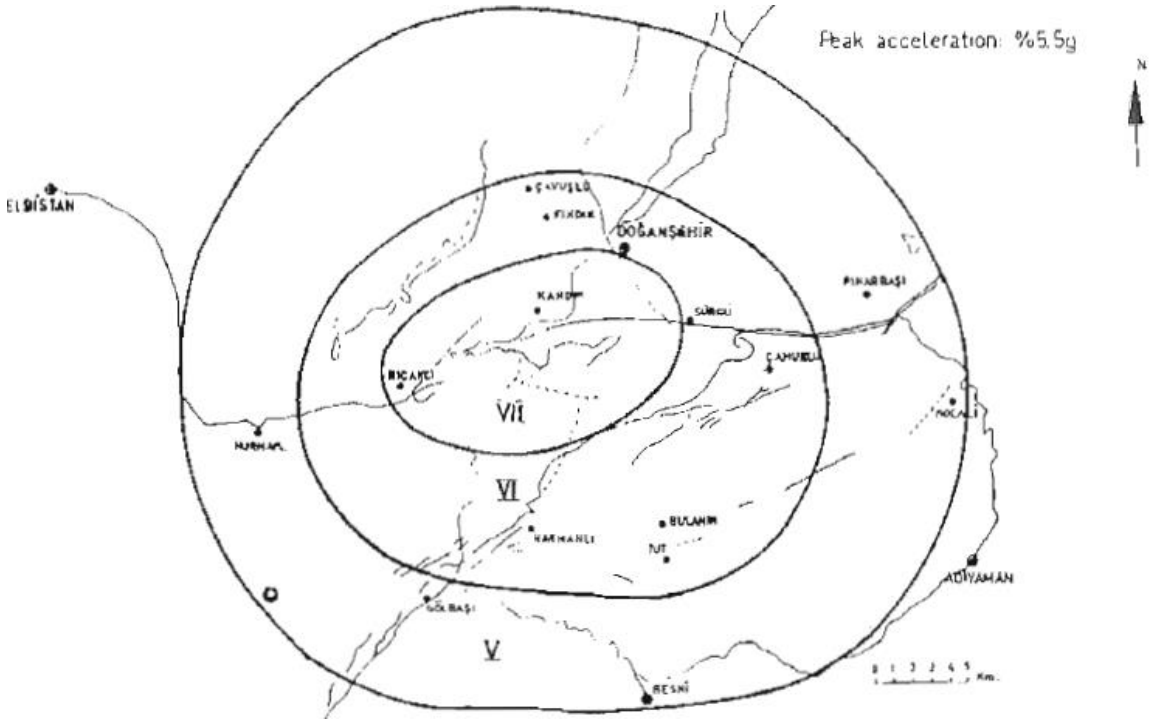

Figure 6/4.9 – Isoseismal Map of 03:35 May 5, 1986 Earthquake Near Malatya-Surgu; Coordinates of the Epicenter: 38.02º N and 37.79º E.; Depth - 4 km; Magnitude M_S=6.0; Epicenter Intensity -7 Points [6/112]

Strong (up to IX-X points MM) historical earthquakes, closest to the Akkuyu NPP site, probably took place in the vicinity of the antique cities of Diocaesarea and Korykos [6/13]. The magnitude attributed to these events was 7.0 - 7.2.

According to the catalogues, no strong seismic events (more than MSK Intensity of 5) were felt nearby or at the Akkuyu site.

For adjustment of parameters of the historical earthquakes nearest to the site (and presence of sources of these events in the region) archeoseismological study in the estimated epicentral zones

near ruins of ancient cities Diocaesarea, Korykos, Olba and Seleukeia was implemented in 2012 [6/82]. The aim of this study was to investigate damages due to historical earthquakes.

The studied region is given in Figure 6/4.10 [6/82].

The study area is on the southern flank of the Taurus Belt. Main geological units in the area are Neogene age limestones and Quaternary deposits. Neogene units consist of resifial limestones called Mut Formation. Limestones including clayey limestone, marl and sandstone bands are well bedded. Beds are gently dipping (between 5° and 10°) towards the Mediterranean Sea. Quaternary deposits consist of loose sediments through the shoreline and alluvial and fluvial deposits in restricted areas (Figure 6/4.11).

Figure 6/4.10 – Locations of ancient sites. GoogleMap and GoogleEarth-Pro software were used for relief image and bathymetry respectively

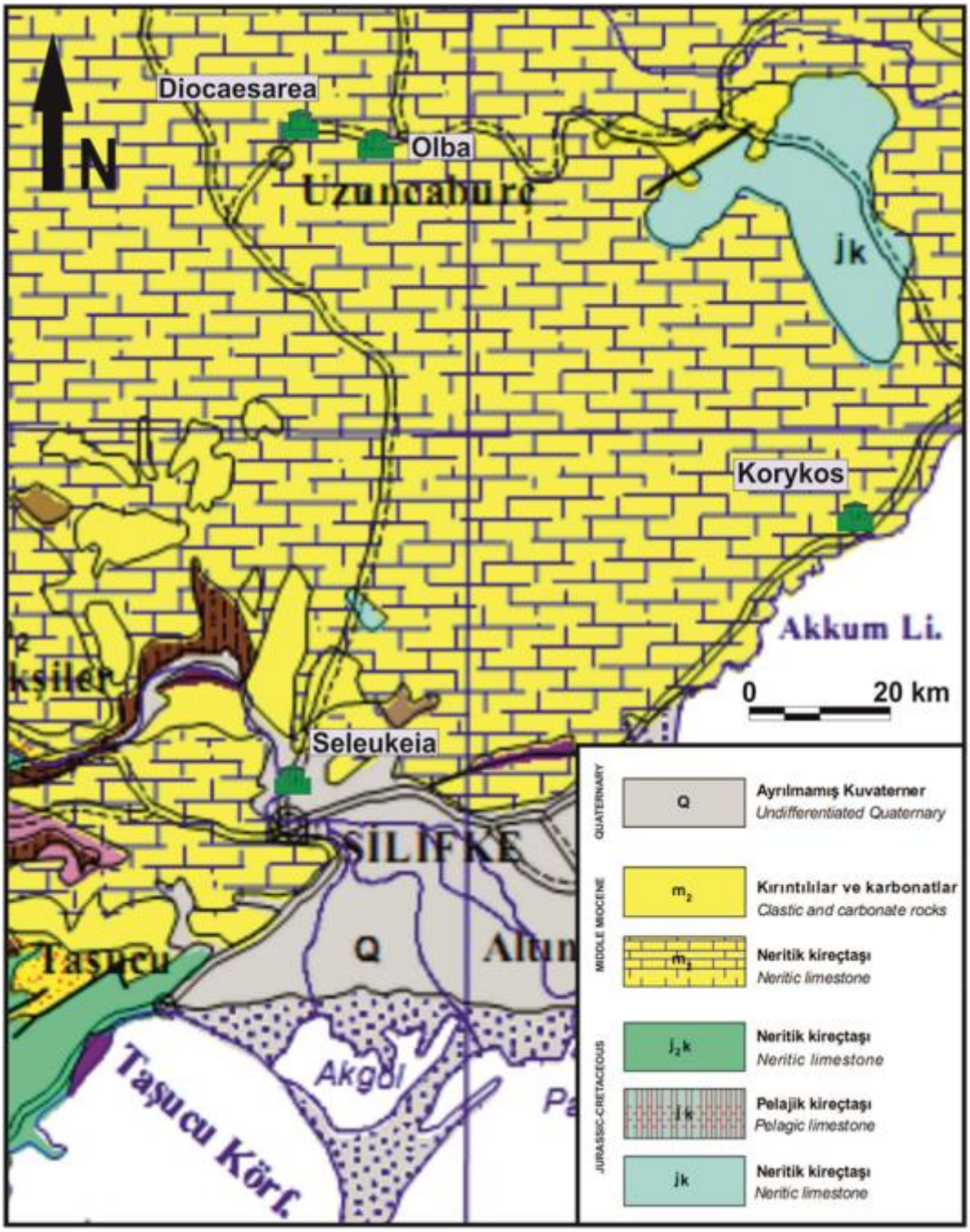

Figure 6/4.11 – Geological map of the study area [6/82]

The ancient sites of Seleukeia and Olba were located both on limestones and Quaternary deposits. Ancient sites of Diocaesarea and Korykos were located on limestone basement rocks.

Seleukeia

Seleukeia and Calycadnus was established in the beginning of 3rd century B.C. by I. Seleukos (one of Alexander the Great's generals) and became part of the Roman Empire around 1st century B.C. Modern town of Silifke was built on the ancient city. Only part of the Temple (2nd century A.D.), a cistern (early Byzantine) and the Roman Bridge over the Göksu River (77 or 78 A.D.) currently exist. About 3 km south of the town, there are ruins of the Saint Thekla church

which was built around middle 5th century A.D. The castle was built at the top of a hill in the western part of the city around 7th century A.D. and it was enlarged in 12th and 13th centuries. Some new buildings were constructed during the Ottoman time.

Diocasearea

Date of ancient ruins in this site goes back 2nd century B.C. but the city was named Diocaseare after the Roman Empire Tiberius (14 – 37 A.D.). The Temple of Zeus and high tower date from the Hellenistic period (2nd century B.C.). Other important buildings mainly date from the 1st to 3rd centuries A.D.: theatre (2nd century), colonnaded street (1st century), parade gate (1st century), fountain (2nd or 3rd century), temple of Tyche (1st century).

Olba

History of Olba goes back at least to the 6th century B.C. but existing ruins date from the Roman period. Roman aqueduct (193 – 211 A.D.) across a valley is one of the remarkable structures in Olba. Nymphaion, theatre, tombs and churches are partly visible in the city center.

Korykos

Korykos was established around the 4th century B.C. Korykos was an important city during the Christian era. The castle was built around the 13th century A.D. The castle and a large cistern are the well preserved structures among ancient buildings. Ruins of churches are visible in east of the castle and north of the Silifke – Mersin highway.

There are other smaller size ancient sites between Seleukeia (Silifke) and Diocaseare (Uzuncaburç). Brief information is given below.

Imbriogon is a small ancient site about 8 km north of Silifke. The ancient site dates from the 2nd century A.D. Absence of Christian construction suggests that it was abandoned before the practice of Christianity. There are temples, tombs and remains of other ancient buildings.

Imamlı ancient site is located on a limestone hill a few kilometers northeast of the modern village of İmamlı. The ancient site is surrounded by a city wall. There are cisterns carved into limestone, tombs and remnants of other ancient buildings.

Işıkkale ancient site comprises ruins of buildings dating from late Roman and early Byzantine times. Although most buildings have collapsed, an early Byzantine basilica is still in good condition.

Buildings in the Karakabaklı ancient site date from the Roman and Byzantine periods. A paved road runs through the ancient site in north – south direction. Some buildings are well preserved at the site.

Tekkadin ancient site is located on a limestone hill close to the modern village of Tekkadın. A church on top of the hill dates from the 5th century A.D. but age of other buildings is probably older.

The ancient city of Aphrodisias is located about 15 km east of the Akkuyu NPP site. It was a harbour city from at least the 6th century B.C. No buildings are visible in the ancient city.

Detailed examination of existing ruins showed damages in ancient sites. Damages are characterized as follows in each ancient site:

- Seleukeia: Column drums were displaced, walls were broken, arches had collapsed, keystones of arches were displaced, walls were collapsed and toppled;
- Diocaesarea: vertical columns deviated from their original positions, walls were cracked, collapsed and tilted, blocks were displaced and rotated, columns were displaced;
- Olba: Walls were collapsed, blocks were broken, displaced and rotated, walls were cracked and extended;
- Korykos: Walls were cracked, collapsed and toppled, keystones of arches were displaced, blocks were rotated;
- Imbriogon: Walls were collapsed and extended, blocks were broken, rotated and displaced;
- İmamlı, Işıkkale, Karakabaklı, Paslı, Mezgitkalesi, Ovacık: Walls were collapsed, keystones of arches were displaced, blocks were broken, displaced and rotated, walls were cracked.

Damages desrbibed above widely spread in the strudied region may be related to ground shaking and are characteristic features for historical earthquakes.

Sopme examples of damages in ancient sites are given below in Figures 6/4.12, 6/4.13, 6/4.14 (all photos are taken from [6/82]).

Figure 6/4.12 – Cracked wall of a church in Korykos, the key-stone of the arch is displaced

Figure 6/4.13 – a) Parade Gate in Diocaseare. View towards west. b) Close up view of top of the eastern blocks. Note rotation and displacement in the left block (blue arrow). Also note dilation between upper blocks (yellow arrow).

Figure 6/4.14 – The Roman aqueduct in Olba. a) U-shaped channel on the aqueduct made of limestone blocks within which water flowed. Note that they are displaced. b) Close up view of the foot of an arch. It was partly collapsed and blocks are cracked.

Technology of active remote sensing based on ground-based laser LIDAR system was used for modeling and measurement of quantitative characteristics of observed damages (rotation angle,

angle of deviation from vertical and horizontal position, azimuth). This technology is based on measuring the travel time of a laser beam from the source to a target. Multiple laser beams sweeping the laser range allow the creation of a three-dimensional (3D) point cloud of the target surface at a millimetre-scale resolution. These point clouds are then commonly converted into triangulated surfaces and used for draping high-resolution digital photographs to create virtual-reality models of the surface. LIDAR is accurate to about 3 mm for a distance of 100 m according to the manufacturers (ILRIS Optech, Figure 6/4.15).

Figure 6/4.15 – The ground based LIDAR system.

Examples of images of the studied objects obtained by LIDAR system are given in Figures 6/4.16 and 6/4.17.

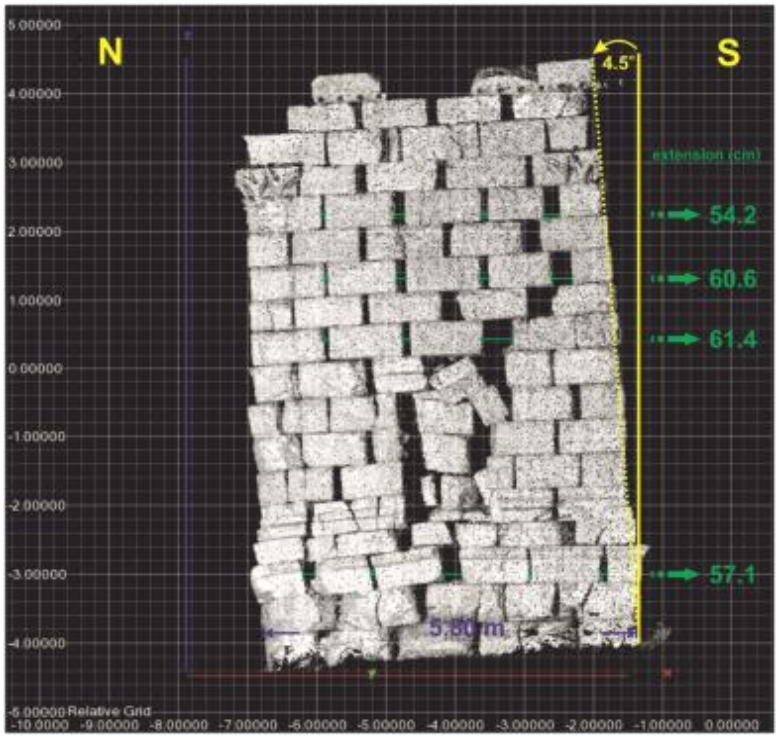

Figure 6/4.16 – LIDAR view of the tomb in Imbriogon (western wall). Amount of extension in the western wall is up 61.4 cm (10% extension)

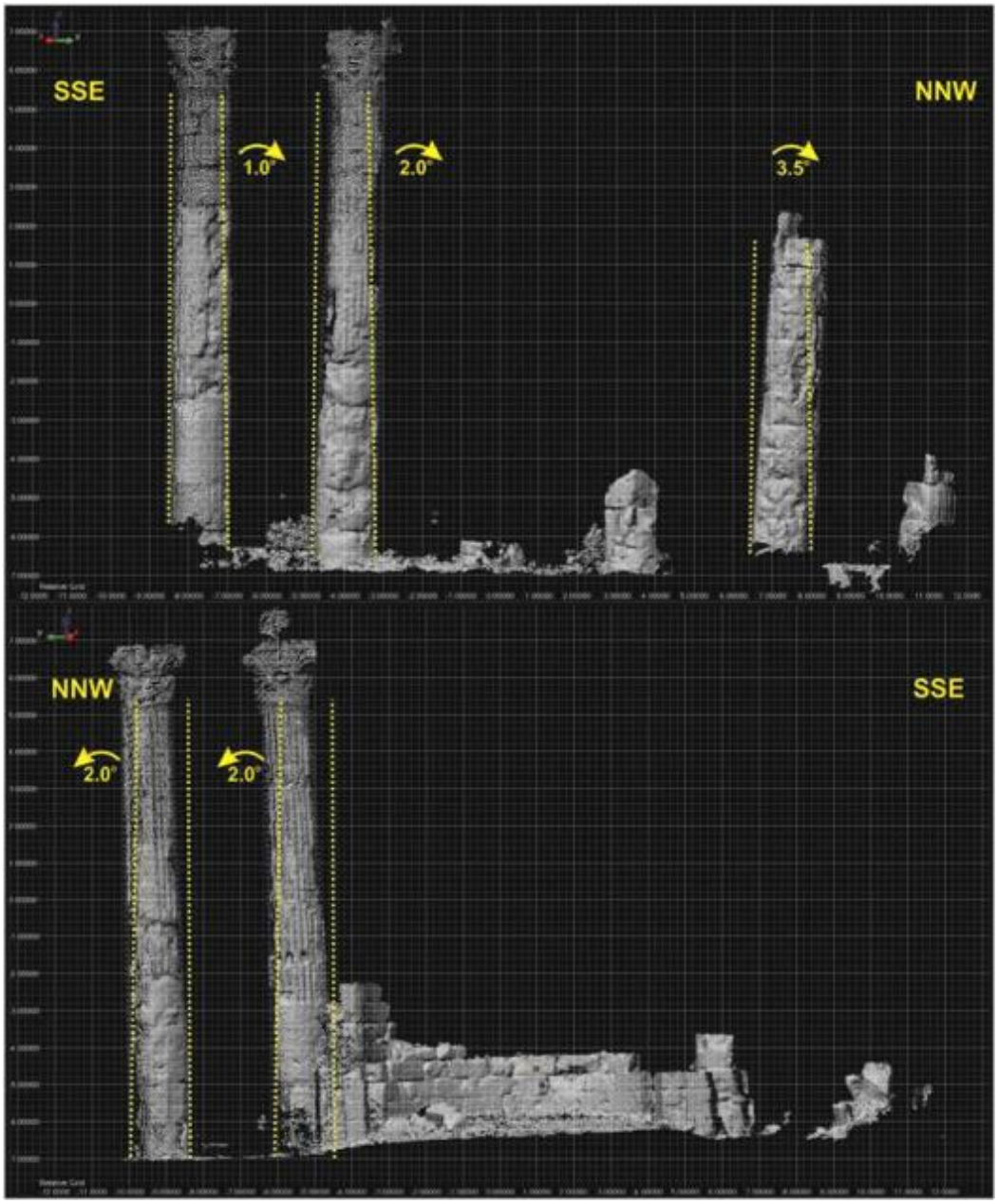

Figure 6/4.17 – 3D LIDAR views of western (a) and eastern (b) sides of the Zeus temple in Diocaesarea. Columns deviated from vertical position in NNW-SSE direction. Amount of deviation from vertical position changes between 1 and 3.5° in northern columns and it is 2° in southern columns.

Ruins of the Roman Temple in Seleukeia and some ancient buildings are located on unconsolidated Quaternary sediments. All ancient buildings in other ancient sites are located on basement limestone rocks. Thus, geological setting of ancient sites eliminates amplification in intensity. Present damage in some ancient ruins is probably cumulative in the existing life of the building. Nevertheless taking into account overall damage in the study area, EMS-98 intensity scale [6/99] and similar damages in archaeological ruins reported from other parts of the world (see Table 4 in [6/82]), deformation is suggested to be observed in ancient ruins in the study area is the result of VIII-IX intensity of shaking.

Figure 6.4/18 summarizes direction of maximum damage (tilting, collapse, extension, deviation from vertical position) based on field observations and LIDAR studies on ruins of large ancient buildings. It is noteworthy that while Roman age buildings were damaged in E-W direction, Hellenistic age buildings were damaged in two different directions (N-S and E-W). This observation may suggest that Hellenistic age buildings experienced two earthquakes; the first earthquake took place before the Roman age buildings were erected in the area and the second one occurred after their construction was completed (after 3rd century A.D.). Considering the historical earthquake account and damages in the study area, it is possible to attribute the first event to the 97 A.D. earthquake and second event to the 4th century earthquakes. Assuming that the travel direction of the seismic waves was N-S and E-W, this relationship suggests that the first event took place either north or south of the study area and the second event took place either east or west of the study area.

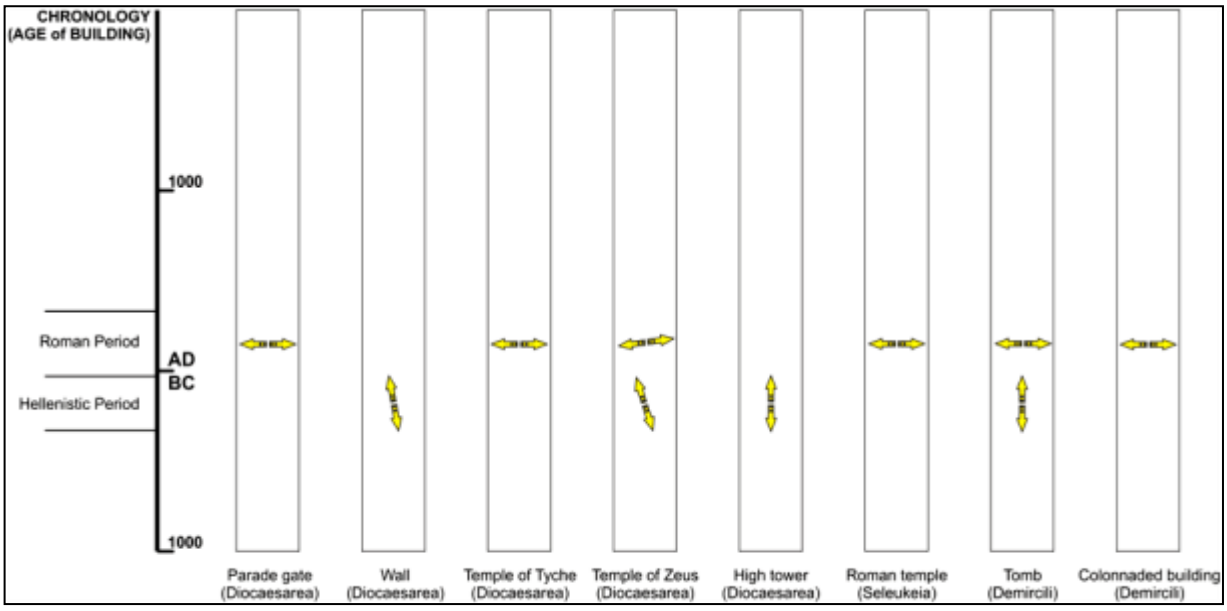

Figure 6/4.18 – Observed and measured directions of damage in ancient ruins of large buildings in the study area

Comparison of the proposed intensity (VIII-IX) with magnitude-intensity tables (Tables 6/4.3 and 6/4.4) suggests at least magnitude 6 earthquakes in the epicentral area.

Table 6/4.3 – Approximate relationship between the magnitude and intensity of an earthquake, with the San Fernando Valley [6/127]

Magnitude	Area felt over, km^2	Distance felt, km	Intensity (maximum expected Modified Mercalli)	Ground motion (average peak horizontal acceleration g=gravity=9.8 m/s^2)
3.0–3.9	1,950	25	II–III	Less than 0.15 g
4.0–4.9	7,800	50	IV–V	0.15–0.04g
5.0–5.9	39,000	110	VI–VII	0.06–0.015g
6.0–6.9	130,000	200	VII–VIII	0.15–0.30g
7.0–7.9	520,000	400	IX–X	0.50–0.60g
8.0–8.9	2,080,000	720	XI–XII	Greater than 0.60g

Table 6/4.4 – Approximate relationship between the magnitude and intensity per USGS data

Magnitude	Typical Maximum Intensity (MMI)
1.0-3.0	I
3.0-3.9	II-III
4.0-4.9	IV-V
5.0-5.9	VI-VII
6.0-6.9	VII-IX
7.0 and higher	IX and higher

According to active fault map of southern Turkey, there is no active fault in the study area. Thus, observed damages in the study area probably resulted from distant sources which require much larger magnitude (at least M=7.0) depending on the distance. For example, intensity distribution of these two events shows that the intensity of the 1822 and 1872 event was V and V - VI in the study area, respectively (Figure 6/4.5). These two events were felt in the study area, however, considering the intensity scale EMS-98 [6/99], it is unlikely that they were responsible for the overall damage. Thereafter as follows from this conclusion it seems reasonable to exclude the 97 and (300-399) events with supposed sources in the area of Diocaesarea and Korikys ancient cities from the catalogues (at least until data is found that will allow the confident determination of the coordinates of these events).

It should be pointed out that the seismic hazard analyses have postulated much higher maximum magnitudes in the seismic source models to the areas mentioned above than those estimated from the historical and archeoseismological research.

6.4.2 INSTRUMENTAL EARTHQUAKE DATA

The study of the Akkuyu NPP instrumental seismicity covers 111 years period from 1900 to 2010, including the first results of the new local seismological monitoring of Akkuyu NPP site (between July 2011 to present).

Instrumental earthquake catalogues were compiled by ENVY/BU KOERI, IPE RAS, WP and Rizzo independently.

There are two agencies operating seismic monitoring network in Turkey. One of them is the Kandilli Observatory Earthquake Research Institute of Bogazici University (BU KOERI). Currently, the network consists of real-time 153 seismic stations compliant with the international standards. In the regional distances of about 300 km from the NPP site, KOERI has installed about 30 seismic stations. The Disaster and Emergency Management Presidency (DEMP) is also operating a seismic monitoring network in the same region.

The distribution of the regional seismic stations operated by the two agencies is shown in Figure 6/4.19.

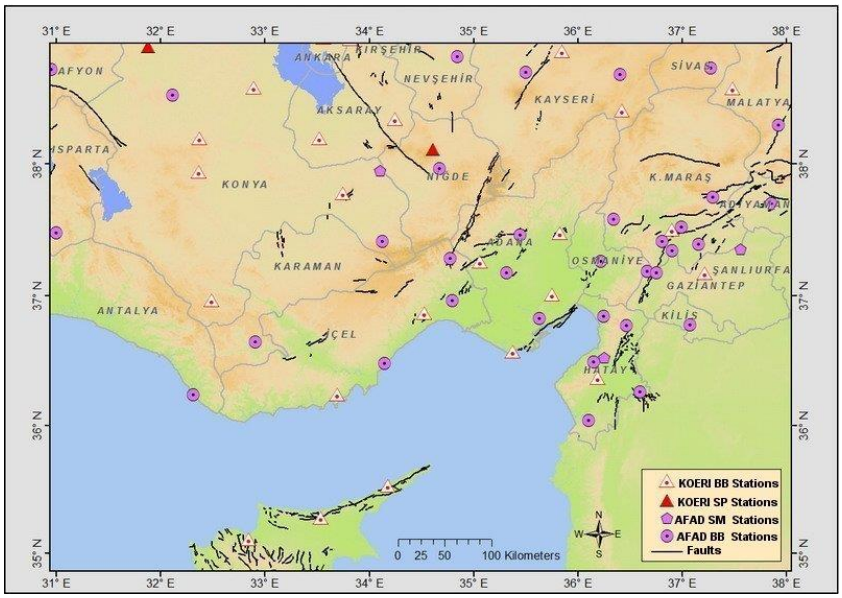

Figure 6/4.19 – The Existing Networks Operated by KOERI and DEMP

IPE RAS instrumental earthquake catalogue is compiled in a spatial frame of 33-39°N, 30-37°E. These frames include an area of more than 300 km radius around the site. The compilation of the IPE RAS catalogue is independent work [6/117].

Information sources of seismological database are presented in Table 6/4.5 and Table 6/4.6.

Table 6/4.5 – Global Scale Sources – International Agencies and Interregional Centers

Agency code	Agency code decoding according the ISC website	Number of records
CSEM	Centre Sismologique Euro-Mediterraneen	8323
ISC	International Seismological Centre (own determinations)	8248
NEIC	National Earthquake Information Center, World Data Center A, USGS	3184
ISCJB	International Seismological Centre (own determinations using JB tables)	1747
MOS	Geophysical Institute-Russian Academy of Science, Obninsk	497
NEIS	National Earthquake Information Service	329
EHB	Data from the Catalogue of Engdahl, van der Hilst and Buland	303
BCIS	Bureau Central International de Sismologie. France	186
ISS	International Seismological Summary, UK	92
USCGS	United State Geological Survey (USGS, GS)	76
IASPE	International Association for Seismology and Physics of the Earth Interior	46
MED_R	MedNet Regional Centroid - Moment Tensors INGV INGV Italy	46
HRVD	Department of Geological Sciences, Harvard University, Cambridge (Now GCMT), USA	43
ZUR_R	Zurich Moment Tensors, Swiss Seismological Service ETH ETH	40
ZUR	Schweizerischer Erdbebendienst, Institut fur Geophysik, ETH, Switzerland	29
GUTE	Data from Gutenberg and Richter, 'Seismicity of the Earth'	18
CGS	Coast and Geodetic Survey of the United States, NEIS, USA	17
GCMT	The Global CMT Project (Previously HRVD) USA	13
EPSI	Data from the EPSI project (EMSC - PI)	12
PUL	Pulkovo, Russia	1
Total amount of records from global scale agencies:		23250

Table 6/4.6 – Regional Scale Sources – National Agencies

Agency code	Agency code decoding according the ISC website	Number of records
ISK	Kandilli Observatory and Earthquake Research Institute, Boğaziçi University (BU KOERI). Istanbul, Turkey	12283
DDA	General Directorate of Disaster Affairs, Ankara, Turkey	5882
GRAL	National Centre for Geophysical Research, Beirut, Lebanon	4560
NIC	Geological Survey Department (GSD), Cyprus	3872
IPRG	Institute for Petroleum Research and Geophysics (former name of GII), Israel	2247
NSSC	National Syrian Seismological Center, Syria	1975
GII	Geophysical Institute of Israel (now IPRG), Israel	1955

Agency code	Agency code decoding according the ISC website	Number of records
JSO	Jordan Seismological Observatory. Natural Resources Authority, Jordan	487
HLW	National Research Institute for Astronomy and Geophysics, Helwan, (NRIAG), Egypt	483
ATH	Seismological Institute, National Observatory of Athens (NOA), Greece	369
GBZT	TÜBITAK, Marmara Research Center, Gebze (TUBI) Turkey	373
THE	University of Thessaloniki, Greece	156
DUSS	Department of Geology, Faculty of Sciences, Damascus University, Syria	73
RYD	King Saud University, Riyadh, Saudi Arabia	69
KSA	Observatoire de Ksara, Zahle, Lebanon	49
SNSN	King Abdulaziz City for Science and Technology, Saudi National Seismic Network, Saudi Arabia	33
TEH	Geophysical Institute, Tehran University, Iran	16
ISN	Iraqi Meteorological and Seismology Organization, Iraq	10
Total amount of records from global scale agencies:		34892

The total number of events in the database is 58142. The total amount of information sources in the database is 38. 20 of these are global scale sources and 18 are regional scale ones. This confirms that regional and local scale sources are both fully represented in the database.

Analysis of tables and epicentral maps from different sources shows that sufficiently complete data on seismicity is available for the region of study. The time period usually recognized as early instrumental is also presented quite well: BCIS (186), ISS (92), USCGS (76), GUTE (18), CGS (17) and PUL (1) accounting for more than 390 records in the time period prior to 1975. Based on the event number (23250) in international seismological sources one can conclude they well control the regional seismicity. Regional centers supply more detailed information (record number 34892). But this happens mostly because regional catalogues include smaller earthquakes. For relatively large earthquakes solutions of international centers are more preferable because when locating the epicenter better azimuthal seismic station coverage is ensured. Highest priority among international sources is given to special projects called for revision of earthquake parameters. Among regional centers highest priority is given to the ISK (Kandilli Observatory and Earthquake Research Institute, Boğaziçi Univ. Istanbul (KOERI), Turkey) catalogue. Territories presented in regional catalogues are partly overlapping. This also serves as an assurance that serious omissions will not happen in the final catalogue.

On the other hand it means that several records from different information sources in the database are related to the one and same earthquake. Distribution of record number occurrences related to the same earthquake in the database is given in Table 6/4.7. From the table it follows that most often (11566 times) there is only one record related to one earthquake. Maximum record number related to an earthquake is 14. There are three such cases in the database.

Table 6/4.7 – Number of records related to the same earthquake and its occurrence

Number of records	Occurrence
1	11566
2	9008
3	3245
4	1129
5	1494
6	415
7	216
8	132
9	70
10	41
11	22
12	24
13	13
14	3

The priority system for sources, which takes into account considerations listed above, is given in Table 6/4.8. This priority system is related only to the hypocentral location. When a record is assessed as having highest priority, it is marked by code P (priority record) in a special field. Naturally, all unique records get this mark automatically. The records having lower priority among the family of records related to the same earthquake, get code C (copies). For example, when there are 14 records in the database related to the same earthquake, code P will be assessed to one of them while the other 13 will get code C. It should be noted that for most of the earthquakes assessing priorities does not affect any parameter because often different agencies supply the same earthquake parameters.

Table 6/4.8 – Priority system for selection of the record from database into the final catalogue

Source code	Priority	Record number in database	Number of priority records (Ð)	Number of low priority records (Ñ)
IASPE	1	46	46	0
EHB	2	303	282	21
ISC	3	8248	7922	326
ISK	4	12283	7915	4368
NEIC	5	3184	680	2504
NEIS	6	329	0	329
DDA	7	5882	2831	3051
GRAL	8	4560	3796	764
CSEM	9	8323	687	7636
GII	10	1955	849	1106
NIC	11	3872	1219	2653
NSSC	12	1975	412	1563
IPRG	13	2247	329	1918
GBZT	14	373	184	189
MOS	15	497	10	487
GUTE	16	18	18	0
ISS	17	92	68	24
KSA	18	49	37	12
BCIS	19	186	32	154
JSO	20	487	26	461
HLW	21	483	24	459
ATH	22	369	10	359
DUSS	23	73	8	65
SNSN	24	33	7	26
THE	25	156	2	154
		Total: 56023	Total: 27394	Total: 28629

Even if only one agency locates an earthquake within the selected spatial frames of the study, the whole record family was included in the database. After priority records were selected, final catalogue was constrained strictly in spatial frames based on the earthquake coordinates reported by high priority record. As a result of this process 26728 earthquakes were deleted which left 27394 in the final catalogue. The last earthquake in the catalogue is dated September 30, 2011.

Homogenized magnitude evaluation

Modern relationships between magnitude and ground motion parameters are based on moment magnitude Mw. It is clear that direct moment magnitude assessments have highest priority with respect to Mw obtained from conversion relationships. There are 4223 direct Mw values reported in the database, which can be immediately transferred into the catalogue. Conversion is required for the other magnitude types using magnitude conversion relationships.

Magnitude *Ms*

In the instrumental catalogue there are no records of earthquakes with magnitude more than 7 (any type of magnitude) in the spatial boundaries of the study. The Ms scale does not saturate in this magnitude range. Therefore, Mw=Ms may be assumed.

Magnitude *Mb*

There is not enough data to construct magnitude conversion relationship between Mw and Mb scales. But well-constrained correlation between Ms and Mb can be elaborated, then using Mw=Ms a Mw estimate could be determined. The most reliable Ms and Mb determinations are reported by the ISC. Totally there are 323 earthquakes, for which the ISC simultaneously reports Ms and Mb (Figure 6/4.20). The whole magnitude range is divided into two parts: lower and higher Mb=4.5. For the interval of magnitudes larger than 4.5 two relationships were compiled – Ms(Mb) (violet line in 6/4-5 relationship), and Mb(Ms) (blue line, relationship 6/4-5)-after which the average between these two was taken (red line, relationship 6/4-6). Corresponding relationships are

$$Ms=1.65Mb-3.60 \quad (Mb\geq 4.5); \qquad (6/4\text{-}5)$$

$$Mb=0.50Ms+2.48 \quad (Ms\geq 4.5); \qquad (6/4\text{-}6)$$

$$Ms=1.83Mb-4.27 \quad (Mb\geq 4.5). \qquad (6/4\text{-}7)$$

Proportionality coefficient between Ms and Mb is 1.83 ± 0.18.

For magnitudes lower than 4.5, proportionality coefficient between Ms and Mb is fixed to 1. The free member is chosen such that using the equation for different magnitude intervals will give the same Ms value for magnitude 4.5

$$Ms=mb-0.50 \quad (mb\leq 4.5). \qquad (6/4\text{-}8)$$

Magnitude *ML*

Relationship between ML and Mb for all determinations in the database (995 in total) is shown in Figure 6/4.21. It is clear from the graph that the same formula for ML to Ms conversion can be used as for Mb to Ms (relationships 6/4-6 and 6/4-7).

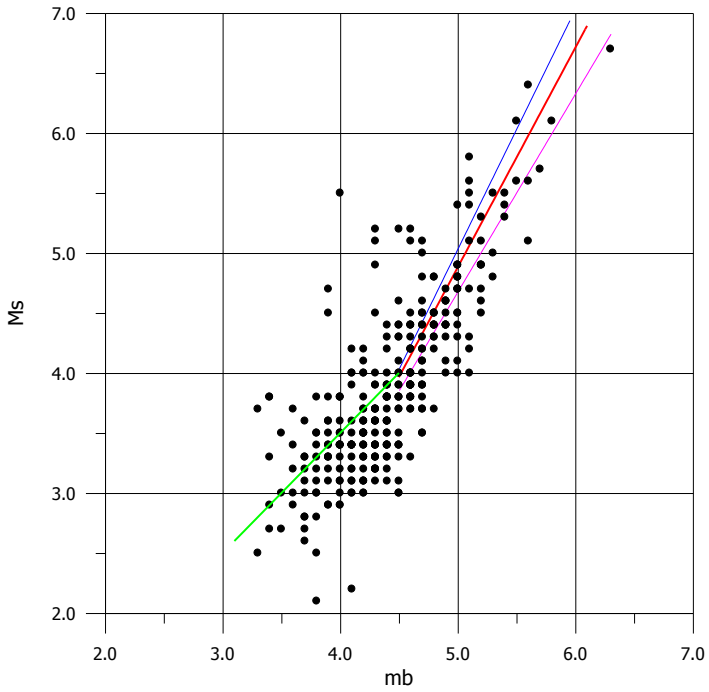

Figure 6/4.20 – Relationship between Ms and Mb Magnitudes Based on ISC Data (323 Determinations). The green line is for Magnitudes Mb not higher than 4.5 (Relationship 6/4-8). The violet line corresponds to the relationship (6/4-5), Blue line – to (6/4-6), and Red line – to (6/4-7)

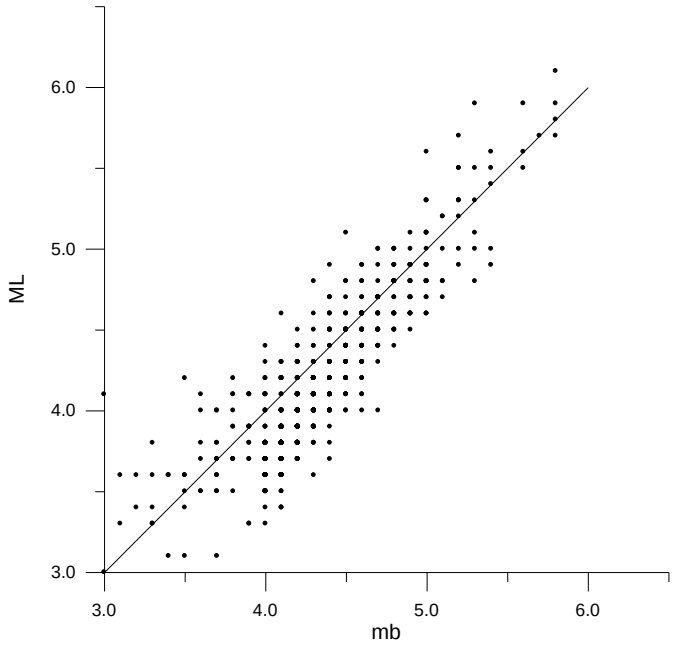

Figure 6/4.21 – Relationship between ML and mb Magnitudes Based on All Available Data from Database (995 Determinations). For Ease of Comparison the Line with Slope 1 is shown

Unknown type

Early instrumental earthquakes (for example from the Gutenberg catalogue), actually are reported in body wave magnitude, but determined using much longer wave periods (10 sec approximately), than it is in case of Mb type magnitude, which is based on 1 sec period. That is

why magnitudes reported as unknown in early instrumental period are close to Ms, which is determined at 20 seconds. Most of the records with unknown magnitude are found in the ISK catalogue (633). Conventionally, it is assumed that they are equal to Ms.

Magnitude *Md*

It is the most frequently reported magnitude type (25006 times) in the database. In order to convert Md events into Mw estimates, first a correlation between Mb and Md has been derived based on data for 212 earthquakes reported in both magnitude types (Figure 6/4.22). There is a 1:1 correlation between Md and Mb for magnitudes less than 5.5 which allow for the same conversion formula to be used for conversion of Md to Ms and Mw respectively (relationships (6/4-7) and (6/4-8). For magnitudes greater than 5.5 direct Mw measurements are available. They have highest priority in the catalogue hence no additional Md conversion was necessary.

Magnitude *Mc*

This magnitude type can not be correlated with any other because there are no cases in the database when Mc is reported together with other magnitude type. Conventionally, it is assumed that it is equal to Mw. This assumption will have impact only on 0.7% of total records in the final catalogue and all of them are small magnitude earthquakes.

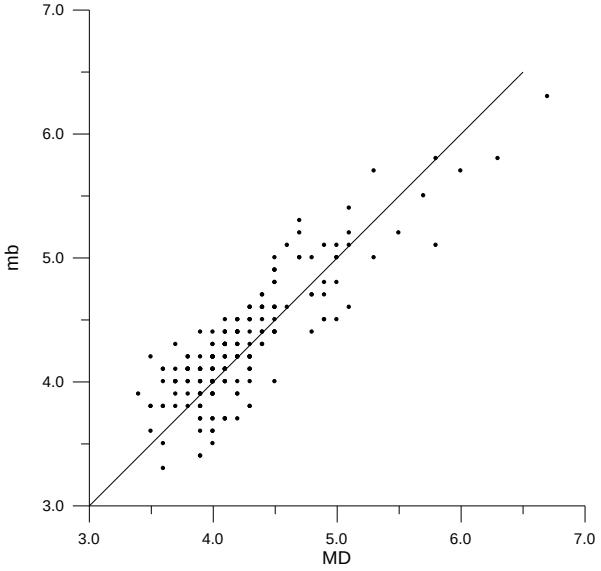

Figure 6/4.22 – Relationship between Md and mb Magnitudes Based on All Available Data from Database (212 Determinations). For Ease of Comparison the Line with Slope 1 is Shown

Therefore, out of 26728 earthquakes in the final IPE catalogue in the study region, 24714 have Mw magnitude determination according to the given conversion procedures. 2014 events are

left without magnitude determinations. Events with a magnitude of M≥2.25 are representative in the IPE RAS instrumental catalogue (for the last 50 years).

Epicenter map of earthquakes is shown in Figure 6/4.23. The circle size on the map is proportional to the magnitude. 300 km circle around the site is indicated (the site is the black square), crosses are for earthquakes without magnitude determination

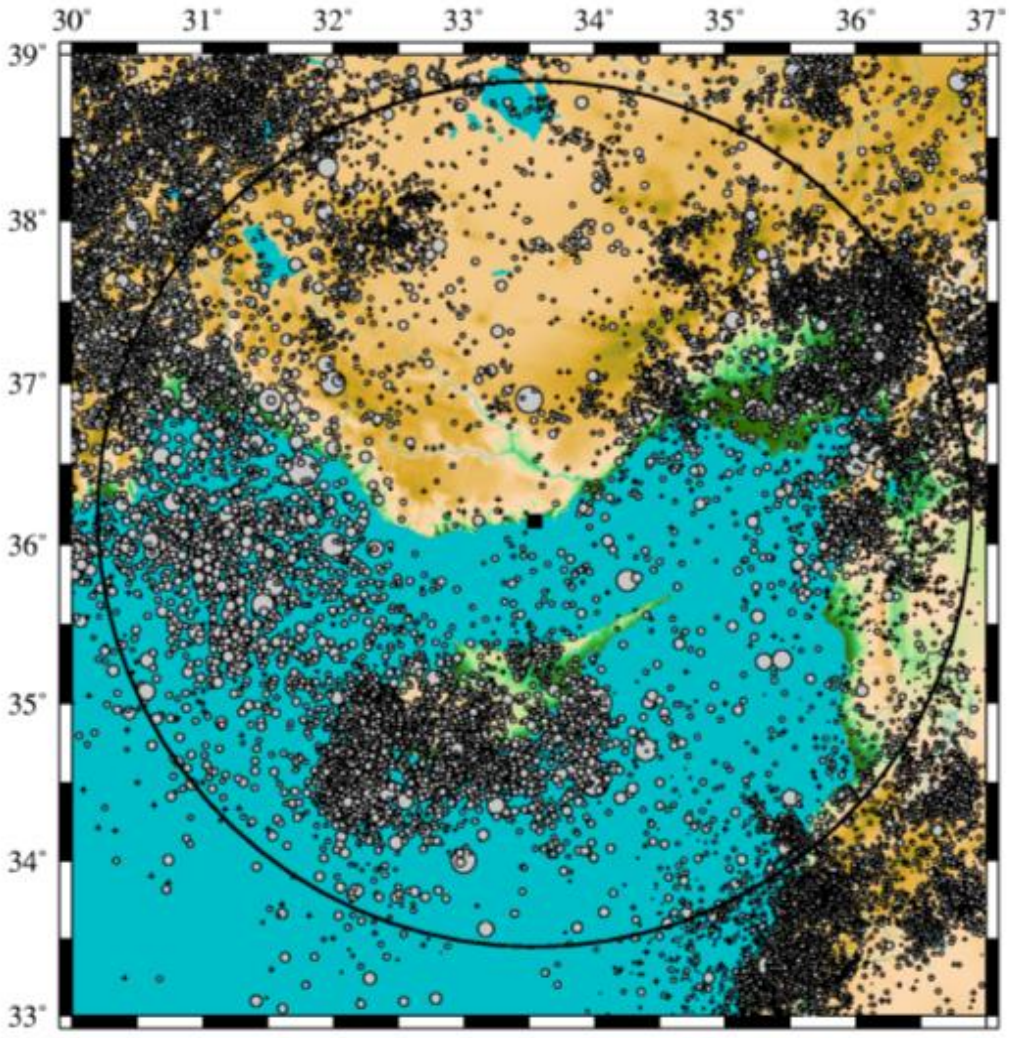

Figure 6/4.23 – Epicenter Map According to the Final Catalogue – 26728 Events

Magnitude depth distribution was presented above (see Figure 6/4.3).

There are two fields to store depths in the IPE RAS catalogue: one is the output of hypocenter location, the other is based on the pP phase arrival. Besides, some depths are marked as preliminary fixed ones. To handle the situation new field was introduced where depths, based on pP phase arrival were put, considering them more reliable, then in free positions were added depths coming from hypocenter solution (fixed depths were ignored). These depths reported were accepted as the best available.

The largest earthquake (Mb=5.5) nearest to the site (Δ=84 km) is the one that occurred in 1970/03/20. The solution and phase data from the ISC webpage for the 1970/03/20 event are reported in Figure 6/4.24, station coverage is shown in Figure 6/4.25.

ISC Comprehensive Bulletin
Event 798219 Turkey

Date	Time	Err	RMS	Latitude	Longitude	Smaj	Smin	Az	Depth	Err	Ndef	Nsta	Gap	mdist	Mdist	Qual	Author
1970/03/20	08:50:04.00	3.70	9.630	36.9000	33.5000	48.82	45.5	90	33.0f		7	7	144	4.00	89.00	m i uk	ISC

(Preliminary determination)

Magnitude	Err	Nsta	Author	OrigID
mb 5.5		1	ISC	1764304

Sta	Dist	EvAz	Phase	Time	TRes	Azim	AzRes	Slow	SRes	Def	SNR	Amp	Per	Qual	Magnitude	ArrID
KSA	3.64	147.0	PN	08:50:54.0	-5.30					T__				__		26208703
KSA	3.64		SN	08:51:56.0						___				__		26208704
CIN	4.38	281.0	PN	08:51:16.0	6.2					T__				__		26208705
KAS	4.47	3.0	PN	08:51:15.0	3.9					T__				__		26208706
ISK	5.41	322.0	PN	08:51:17.9	-6.50					T__				_i		26208707
ISK	5.41		S	08:52:12.0						___				__		26208708
IST	5.43	321.0	PN	08:51:17.0	-7.70					T__				_e		26208709
IST	5.43		S	08:51:28.0						___				__		26208710
PRK	6.16	295.0	PN	08:51:34.0	-1.10					T__				_e		26208711
LAO	89.28	334.0	P	09:03:12.7	15.00					T__				_i	mb 5.5	26208712
LAO	89.28			09:03:22.0						___				_e		26208713

STOP

International Seismological Centre
Pipers Lane, Thatcham, Berkshire
United Kingdom RG19 4NS
+44 (0)1635 861022, voice; +44 (0)1635 872351, fax
admin@isc.ac.uk, e-mail

Figure 6/4.24 – Initial information on 1970/03/20 earthquake based on ISC data

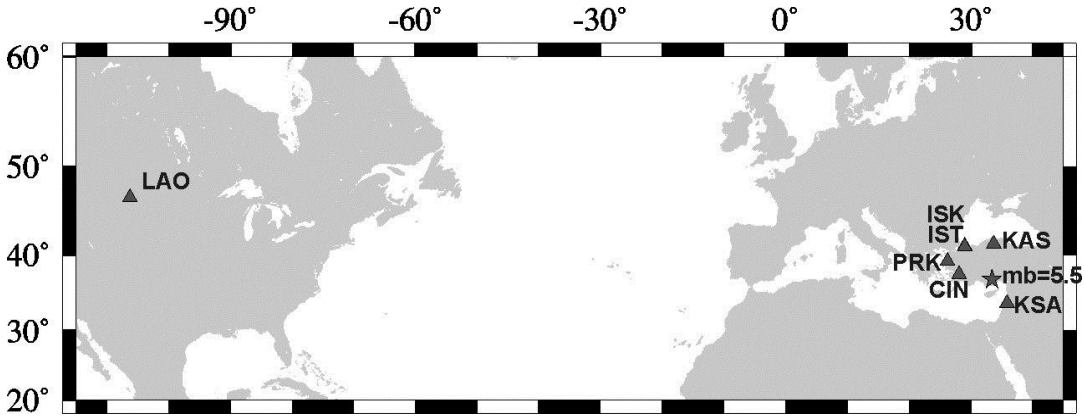

Figure 6/4.25 – Station positions with respect to 1970/03/20 earthquake epicenter

The ISC solution is the only one. This earthquake is not reported by any other agency. The ISC classifies the solution as preliminary (though further versions were not reported). The magnitude is determined based on single station data at Δ=89.28° distance. In such situation the accuracy of magnitude determination can not be evaluated. Both semiaxis of error ellipse are ca. 50 km. IPE-RAS has re-calculated earthquake parameters using phase data reported by the ISC. First, there is an obvious misprint in hours and minutes reported at the IST station for S-wave arrival: it has to be 8h 52m instead of 8h 51m. Second, stations IST and ISK are actually in the same place, therefore there is no sense in taking both of them into calculations. IPE_RAS started with calculations of the hypocenter excluding the ISK station and then – the IST. In final solution, the

one which ensure smaller rms has been kept. Corresponding calculation results of revised solution are given bellow:

```
  date hrmn   sec      lat      long depth   no m    rms  damp erln erlt erdp ic
70 320  850  2.39 3647.71N  33 43.9E  42.0    7 3   4.53 0.000114.3 81.3181.7  3

Origin time error:       9.73

DRMS Values: d=    5.00 km

DRMS:       lon+d     lon-d     lat+d     lat-d   depth+d   depth-d
 DRMS pos    0.01      0.02      0.02      0.02      0.01      0.01

Resolution matrix: k =      0.036

                           Long     Lat   Depth
                  Long    0.955  -0.022  -0.003
                   Lat   -0.022   0.955  -0.001
                 Depth   -0.003  -0.001   0.965

Azimuthal Gap in Station Coverage 148 degrees

stn   dist   azm  ain w phas    calcphs hrmn tsec  t-obs  t-cal    res   wt di
KSA    384 148.6 91.5 1 P   1    PG       850 54.0  51.61  52.67  -1.06 0.75 26
KSA    384 148.6 91.5 4 S   4    SG       851 56.0 113.61  92.70  20.91 0.00  0
KAS    508   0.3 91.1 1 P   1    PG       851 15.0  72.61  68.18   4.42 0.75 20
CIN    509 281.8 91.1 1 P   1    PG       851 16.0  73.61  67.91   5.70 0.75 10
IST    625 320.4 90.9 1 P   1    PG       851 17.0  74.61  82.43  -7.82 0.75  3
IST    625 320.4 90.9 3 S   3    SG       852 28.0 145.61 145.07   0.53 0.25  2
PRK    709 294.8 90.8 1 P   1    PG       851 34.0  91.61  92.91  -1.30 0.75  6
LAO   9945 333.7160.2 3 P   3    sP       9 3 12.7 790.31 790.27   0.03 0.25 33
LAO   9945 333.7160.2 4 P   4    sP       9 3 22.0 799.61 790.27   9.33 0.00  0
```

ISK station was excluded from calculations of the hypocenter

Both variants of solutions – the ISC and revised – are given in Figure 6/4.26. It should be noted that taking into account a small number of stations reporting the earthquake the difference between two variants is very small – it is much smaller than formerly evaluated location errors in each one of both solutions. At the same time, the revised solution seems preferable because of several reasons. First, it takes into account more wave phases; second, the residual time at far station LAO is only 0.03 sec instead of 15 sec, which is clear evidence that solution is much better balanced in the whole data range. Third, in the revised solution the depth (42 km) is not fixed as it is done in the ISC solution. Fourth, and this is maybe the most important reason, the nearest locality is at 15 km distance from the revised epicenter, while this distance is only 2 km from the ISC epicenter. At such small distance, even in case of relatively deep source (in lower horizons of the crust), absence of information on earthquake felt effects is very strange.

As far as the source depth is concerned, relatively deep source depth and location of revised solution is in good agreement with macroseismic data. A rough estimation shows that for 42 km depth and mb=5.5 epicentral intensity is 3-4 degrees; at 15 km distance it is barely felt.

The event itself is very doubtful. The fact that the earthquake with magnitude 5.5 is not recorded by any station further than 700 km from epicenter except only one (LAO, Δ=89.28°), is strange.

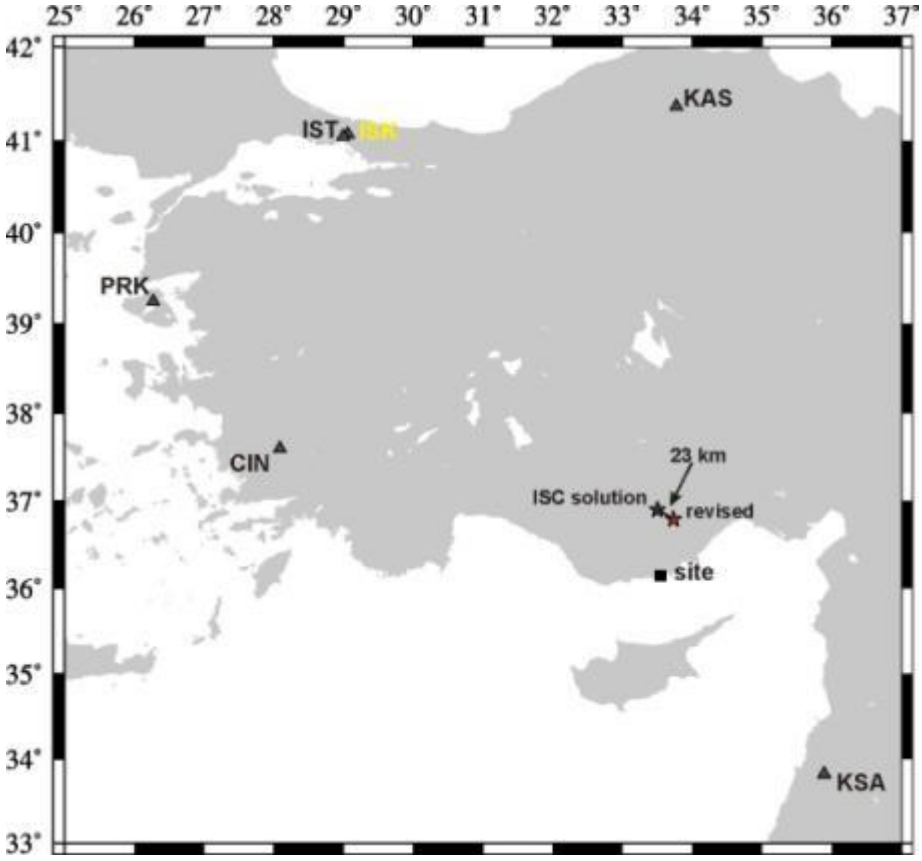

Figure 6/4.26 – 1970/03/20 earthquake. Black star is for ISC solution, red – for the revised solution

After the revision the epicenter is located at 74 km distance from the site, instead of former 84 km. The earthquake hypocenter is 42 km instead of fixed 33 km.

Earthquake source mechanisms

Fault-plane solutions are usually given as orientation of nodal planes and principal stress axes. Parameters of source mechanisms are downloaded from the CMT catalogue [6/106]. The CMT catalogue includes earthquakes starting from 1976 and it is continuously updated. Determinations of fault plane solutions are made using centroid moment method. The solution is searched in form of symmetric seismic moment tensor with zero trace. Mean principal value, which corresponds to intermediate stress axis N, can differ from zero; it can serve as measure of conformity of the solution to double couple source model. In Table 6/4.9 are given solutions for the whole depth and magnitude range within the region 33°-39° N and 30°-37° E. In Figure 6/4.27 are plotted mechanisms of earthquake sources. Numbers in the Figure correspond to numbers in the first column of Table 6/4.9.

Table 6/4.9 – CMT catalogue

N	DATE			TIME (UTC)	EPICENTER				MOMENT		PRINCIPAL AXES									NODAL PLANES					
					LAT	LONG	DEPTH		VAL	EX	T			N			P			1			2		
	YR	MO	DA	HR MIN SEC	deg	deg	km	Mw	Nm		VAL	PL	AZM	VAL	PL	AZM	VAL	PL	AZM	STK	DP	SLIP	STK	DP	SLIP
1	1977	06	01	12:54:51.30	35.790	31.480	58.6	5.6	3.4	17	3.90	36	94	-1.02	54	269	-2.89	2	3	132	64	155	234	67	29
2	1979	05	28	09:27:33.40	35.790	32.020	95.7	5.9	0.9	18	1.05	23	349	-0.20	18	87	-0.85	60	211	48	27	-133	274	71	-71
3	1979	12	28	03:09: 9.70	37.060	36.240	15.0	5.4	1.5	17	1.22	0	96	0.50	90	180	-1.71	0	6	141	90	180	231	90	0
4	1979	12	31	06:21:34.40	36.000	32.010	53.0	5.7	4.2	17	4.34	31	22	-0.32	19	124	-4.03	52	241	67	23	-149	308	79	-70
5	1980	05	02	05:30:59.90	35.99	30.16	15.0	5.8	7.4	17	7.87	37	359	-0.90	3	267	-6.97	53	173	104	8	-72	266	82	-93
6	1981	04	26	14:13:34.50	36.170	31.480	63.0	5.6	3.5	17	3.67	40	22	-0.32	30	263	-3.35	36	148	178	30	4	84	88	120
7	1989	06	24	03:09:58.60	36.280	36.130	15.0	5.1	5.0	16	4.61	17	115	0.86	2	206	-5.47	73	301	203	28	-93	27	62	-88
8	1991	03	11	18:33:47.30	36.750	30.730	122.6	5.1	6.1	16	6.03	66	127	0.16	22	282	-6.19	9	16	131	41	125	268	58	64
9	1991	04	10	01:08:46.40	37.540	35.770	15.0	5.3	1.3	17	1.25	24	104	0.09	19	203	-1.34	59	327	160	27	-136	29	72	-70
10	1991	12	05	20:22: 1.20	36.490	32.270	117.6	5.2	7.1	16	8.23	25	335	-2.37	0	245	-5.86	65	155	66	20	-89	245	70	-90
11	1993	03	22	11:03:50.90	34.740	34.410	15.0	5.4	1.4	17	1.77	60	359	-0.68	18	124	-1.09	23	222	343	27	133	117	71	71
12	1995	02	23	21:03: 7.70	35.020	32.440	15.0	5.9	8.1	17	8.12	55	255	-0.12	16	10	-8.00	30	110	239	21	140	6	77	73
13	1995	05	29	04:58:37.40	34.890	32.630	15.0	5.3	1.1	17	1.17	57	252	-0.11	13	3	-1.06	29	101	224	20	132	0	76	76
14	1996	10	09	13:10:59.60	34.500	32.090	23.0	6.8	1.9	19	2.22	16	4	-0.74	74	178	-1.48	2	274	48	77	170	140	80	13
15	1996	10	10	01:10:24.90	34.580	31.340	19.0	5.7	4.7	17	5.64	33	353	-1.96	52	209	-3.68	18	95	139	53	12	41	80	143
16	1996	10	10	04:54:51.30	34.750	32.030	33.0	5.2	7.1	16	8.74	22	7	-3.30	62	229	-5.44	17	104	147	62	4	55	87	152
17	1996	11	27	00:44:25.90	34.470	32.030	32.6	5.3	1.3	17	1.25	21	19	0.06	46	133	-1.31	36	273	62	48	-168	323	81	-43
18	1997	01	13	10:19:28.30	34.090	31.740	33.0	5.7	4.0	17	3.70	2	323	0.56	73	227	-4.25	17	54	97	76	-11	190	79	-166
19	1997	01	22	17:57:24.40	36.010	35.770	15.0	5.7	4.3	17	5.35	26	104	-2.05	38	352	-3.30	42	219	243	39	-15	345	81	-128
20	1998	04	04	16:16:52.90	38.100	30.160	15.0	5.2	8.6	16	7.99	0	233	1.18	11	323	-9.16	79	143	313	46	-105	154	46	-75
21	1998	06	27	13:55:59.40	36.870	35.580	29.5	6.3	3.0	18	2.85	17	277	0.22	73	84	-3.07	4	186	321	75	171	53	81	15
22	1998	07	04	02:15:51.10	36.630	35.420	15.0	5.4	1.6	17	1.62	29	289	-0.06	54	149	-1.56	19	30	72	55	8	338	84	145
23	1999	05	25	17:15:29.70	34.560	31.410	15.0	5.5	2.6	17	3.15	35	341	-1.09	51	128	-2.06	16	239	14	53	165	113	78	38
24	1999	08	11	04:28: 0.20	34.420	32.680	20.0	5.6	2.9	17	2.82	67	297	0.22	22	96	-3.04	8	189	303	42	124	80	56	63
25	2000	12	15	16:44:51.70	38.400	31.350	15.0	6.0	1.2	18	1.29	4	202	-0.16	7	292	-1.13	82	81	285	41	-100	118	49	-81
26	2001	06	25	13:28:52.80	37.230	35.710	15.0	5.4	1.7	17	1.64	30	93	0.08	2	2	-1.72	60	269	189	15	-83	1	75	-92
27	2002	02	03	07:11:43.10	38.620	31.210	15.0	6.5	6.0	18	6.77	9	166	-1.53	11	74	-5.23	75	293	269	37	-71	66	55	-104
28	2002	02	03	09:26:49.40	38.230	30.560	15.0	5.8	6.1	17	5.91	4	124	0.40	22	32	-6.31	68	224	236	45	-58	15	53	-118
29	2002	02	03	11:40: 0.40	38.520	31.220	15.0	5.3	1.0	17	0.97	4	332	0.09	14	241	-1.06	76	76	76	43	-70	229	50	-108
30	2003	05	03	11:22:44.80	36.780	31.540	137.5	5.4	1.8	17	1.76	55	350	0.09	28	130	-1.85	19	231	358	36	143	119	69	60
31	2004	10	16	15:28:29.40	34.280	33.090	43.3	4.7	1.3	16	1.14	38	317	0.37	45	100	-1.50	20	211	347	47	164	88	78	44
32	2005	05	14	23:46:48.50	35.630	31.420	27.6	5.1	5.7	16	5.61	44	35	0.08	15	141	-5.69	42	245	46	16	176	141	89	74
33	2006	03	29	22:05:18.30	35.410	35.410	19.6	5.0	3.4	16	3.97	26	79	-1.08	42	323	-2.89	37	190	219	43	-10	317	83	-132
34	2007	03	30	19:24: 3.80	37.920	30.910	13.5	4.9	2.6	16	2.50	6	95	0.23	27	188	-2.73	62	353	158	45	-129	28	57	-57
35	2007	04	10	22:00:41.90	37.960	30.870	14.6	5.1	5.2	16	5.05	0	93	0.18	24	183	-5.24	66	2	161	50	-122	25	50	-58
36	2007	12	13	18:06:24.50	38.910	33.060	12.0	4.9	3.1	16	3.54	24	83	-0.93	55	312	-2.60	23	184	224	55	1	133	89	145
37	2008	02	15	10:36:21.60	33.270	35.320	12.1	5.1	6.6	16	6.38	6	25	0.35	65	129	-6.73	24	292	71	69	-167	336	78	-22
38	2008	11	12	14:03:21.20	38.920	35.460	17.0	5.1	5.4	16	5.62	5	93	-0.51	67	351	-5.11	23	185	227	70	-13	321	78	-160
39	2009	09	10	18:29:56.10	37.760	32.510	21.7	4.9	2.4	16	2.31	3	293	0.11	5	202	-2.42	84	53	28	42	-82	197	49	-97
40	2009	09	11	01:58:33.30	37.720	32.500	18.8	4.9	2.8	16	2.70	7	286	0.23	8	195	-2.94	79	54	26	39	-76	188	52	-101
41	2009	12	22	06:06:24.80	35.500	31.300	57.2	5.3	1.2	17	1.02	72	43	0.27	0	133	-1.29	18	223	313	27	90	133	63	90
42	2010	11	14	23:08:25.00	36.580	36.080	12.0	4.9	2.8	16	2.82	8	117	-0.14	3	27	-2.68	81	273	211	37	-84	24	53	-94
43	2011	07	27	09:58:15.94	38.320	31.820	16.4	4.8	2.2	16	2.03	18	47	0.37	20	311	-2.40	63	175	165	33	-50	301	66	-112

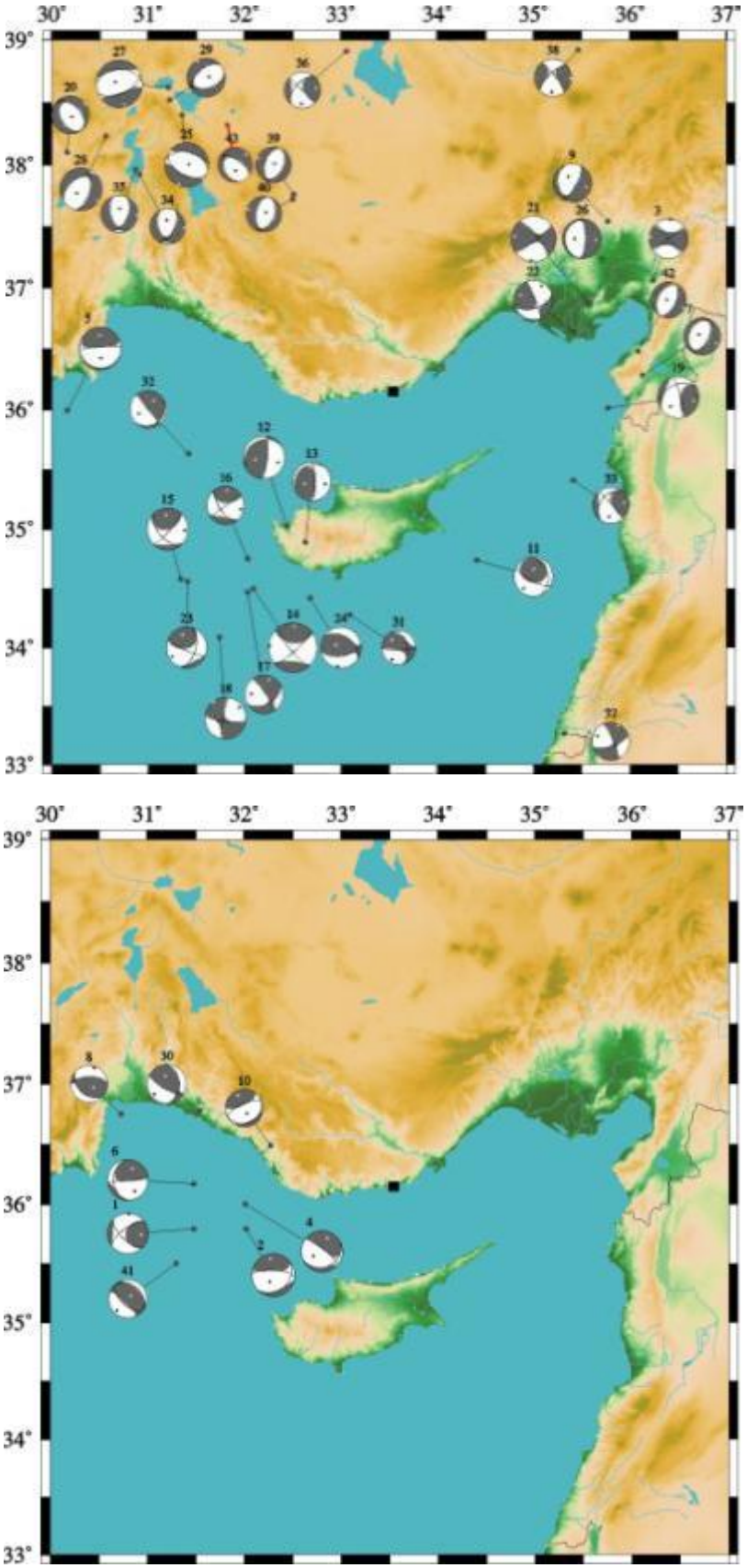

Figure 6/4.27 – Earthquake mechanisms according to the CMT-catalogue [6/106]: above – hypocenter depth h<44 km; below – h≥44 km. The last earthquake occurred in 27.07.2011 is highlighted in red. The black square – NPP site

It was determined that the main type of fault-plane solutions in the western part of the region is normal faulting. The orientation of nodal planes shows great diversity. The majority of earthquakes here are moderate magnitude events. It is usual for such earthquakes to demonstrate large scatter in nodal plane orientations even when they occur within the same area.

In the eastern part the major type of fault-plane solution is also normal faulting, but strike-slip events can also be observed. In the southern part the faulting type is diverse: reverse faulting and strike-slip type together with combination of both types can be seen, but normal faulting is not observed.

There are only 8 deep earthquakes out of 43. Two of them are located close to the north-west coast of Cyprus (normal fault type mechanism); other 3 to the west are reverse faults with some strike-slip component. Three more earthquakes are located along the Turkish coastline (two reverse and one normal faulting).

The instrumental seismicity catalogue compiled by ENVY/BU KOERI covers 111 years period from 1900 to 2010 and is composed of 10059 events as graphically presented in Figure 6/4.28, within the rectangular area bounded by the longitudes 30.55-36.55^{o} E and latitudes 33.15-39.15^{o} N. The earthquake data for the ENVY/BU KOERI catalogue is taken entirely from [6/231, 6/125].

The ENVY/BU KOERI instrumental catalogue in electronic form can be submitted on demand.

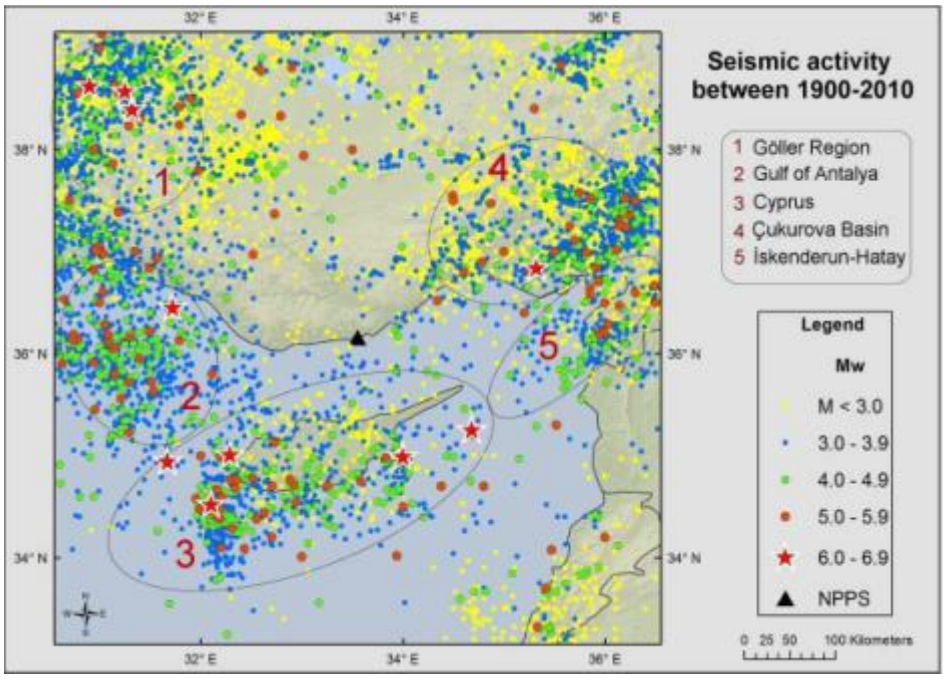

Figure 6/4.28 – Seismicity of Akkuyu NPP Region during the Period from1900 to 2010

The magnitude and depth histograms of the catalogue are given in Figures 6/4.29 and 6/4.30 respectively. Most of the reported earthquake magnitudes lie between Mw=2.9 to Mw=3.4.

Distribution of the earthquake focal depths show that in general earthquakes in the region occurred at shallow depths of about h=0 - 20 km. In general moderate and deep focal depth earthquakes are concentrated in the Mediterranean Sea and the Gulf of Antalya.

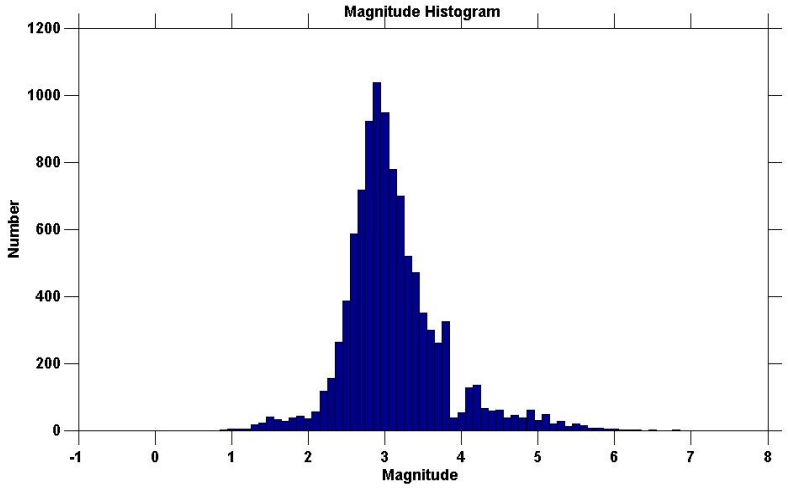

Figure 6/4.29 – Earthquake Magnitude Histogram

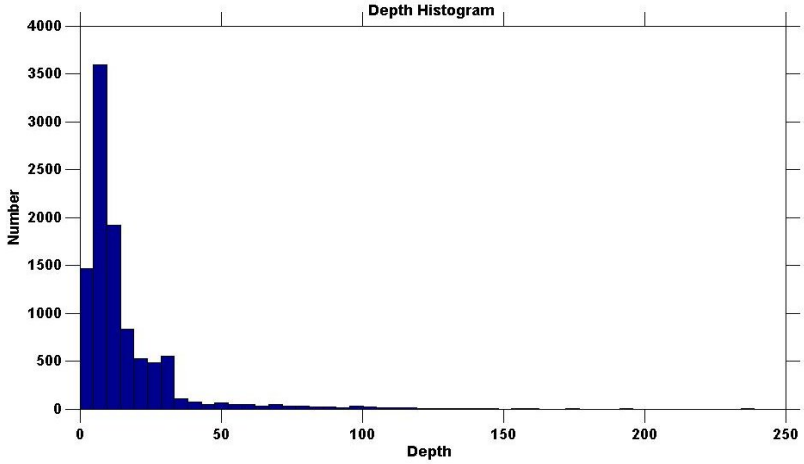

Figure 6/4.30 – Earthquake Depth Histogram

Characteristics of the recorded earthquakes nearest to the site with a magnitude of $M_W \geq 6.0$ are provided in Table 6/4.10 [6/75].

Table 6/4.10 – Strong Earthquakes (Years 1900-2010, $M_W \geq 6.0$), Recorded within 365 km Area from the Akkuyu NPP Site

Distribution of Big Earthquakes for Akkuyu and Surrounding Area 1900-2010; (M ≥ 6.0)

No	Дата			Время			Координаты			Глубина		Магнитуда										Расстояние от площадки
	д	мес	год	ч	мин	с	с.ш.	в.д.	Ref	км	Ref	Ms	Ref	Mb	Ref	Md	Ref	Ml	Ref	Mw	Ref	км (min. 133-max.365)
1	30	4	1911	20	42	3.0	36.00	30.00	M	180	M	6.1	E	5.8	R	5.8	R	5.8	R	6.0	R	310
2	3	10	1914	22	7	2.4	37.70	30.40	8	14	8	6.9	E	6.4	R	6.5	R	6.4	R	6.6	R	325
3	29	9	1916	12	7	5.0	36.20	34.70	9	30	9	6.5	E	6.1	R	6.1	R	6.1	R	6.3	R	146
4	18	3	1926	14	6	14.6	35.84	29.50	1	10	1	6.8	E	6.3	R	6.4	R	6.3	R	6.5	R	355
5	20	1	1941	3	37	7.0	35.00	34.00	G	100	G	6.5	E	6.1	R	6.1	R	6.1	R	6.3	R	133
6	20	3	1945	7	58	56.5	37.11	35.70	1	60	1	6.0	E	5.7	R	5.8	R	5.7	R	6.0	R	217
7	10	9	1953	4	6	3.0	34.80	32.50	9	30	9	6.3	E	5.9	R	6.0	R	6.0	R	6.2	R	175
8	1	10	1995	15	57	12.6	38.06	30.15	4	5	4	6.1	4	5.8	4	6.0	R	6.0	P	6.0	R	365
9	9	10	1996	13	10	50.4	34.53	32.10	4	19	4	6.7	4	6.3	4	6.3	R	6.5	R	6.5	R	219
10	27	6	1998	13	55	53.5	36.85	35.32	4	47	4	6.2	H	5.8	H	6.3	R	6.0	R	6.2	H	174
11	3	2	2002	7	11	28.6	38.58	31.25	R	10	R	6.4	4	5.6	4	6.0	R	6.2	R	6.5	H	337

For the magnitude homogenization, in terms of Mw, the empirical relationships used in ENVY/BU KOERI instrumental catalogue were [6/75]:

$$Md=(1.0377+(0.7863*Ms);$$

$$M_W=0.3247+(0.9870*Mb);$$

$$ML=1.0553+(0.7782*Ms);$$

$$Mb=1.4429+(0.7123*Ms);$$

$$ML=0.2328+(0.9585*Md);$$

$$ML=0.6643+(0.8314*Mb).$$

Declustering process essentially involves the removal of induced seismicity as well as the dependent events: fore- and aftershocks. On the basis of Reasenberg [6/188] method, the original catalog by ENVY/BU KOERI composed of a total of 10059 events has been declustered. A total of 273 clusters have been identified and 1616 events have been removed from the catalogue.

In order to estimate the completeness periods for different magnitude ranges Stepp method was used [6/208]. The results are the following:

- 1902-1965, magnitude of completeness Mc=5.1;
- 1966-2010, magnitude of completeness Mc=2.9.

The summary earthquake catalogue proposed by the Rizzo and Associates is compiled from three sources in its instrumental part:

- The Earthquake Catalogues for Turkey [6/210];
- The University of Athens (UOA) [6/232];
- International Seismological Centre (ISC) On-line Bulletin [6/116].

The catalogues [6/210] and [6/232] are limited by the events that happened until 1964. The period between 1964 and 2009 is represented by the earthquakes from [6/116].

Time intervals covered in catalogues [6/210] and [6/232] were defined by the first record for which more or less confident estimation of magnitude is available. The general time interval in the summary catalogue is, therefore, 2351 years.

Magnitude estimations in the Rizzo catalogue are uniformly transformed in the moment magnitude M_W from conversion relations obtained from the seismological literature [6/197, 6/118 and 6/84]. For some earthquakes, conversion relations are not available; for those the reported magnitude value is assumed to be equivalent to M_W.

The completeness of Rizzo summary catalogue for instrumental period events within 320 km region is provided in Table 6/4.11.

Table 6/4.11 – Year of Completeness of Instrumental Period Earthquakes in the Rizzo Catalogue

Magnitude M_W	Year of catalogue completeness for 320 km region
3.0	1999
4.0	1968
5.0	1918
6.0	1905

The Rizzo instrumental earthquake catalogue may be submitted in electronic form on demand.

The WP Summary Catalogue has been developed on the basis of two sources:

- Yılmaz Bektur, the Seismic Catalogue for Turkey (1996) in which events from 2100 BC to 1994 AD are presented [6/112];
- The catalogue compiled within the scope of works under the Akkuyu project by BU KOERI covering the period between 1900 and 2010 [6/75].

Besides the specified sources of the earthquake data, WP used the data from the IRIS catalogue [6/119]. Earthquake epicenter map (from 1976 to 2010, source is IRIS catalogue) is shown in Figure 6/4.31.

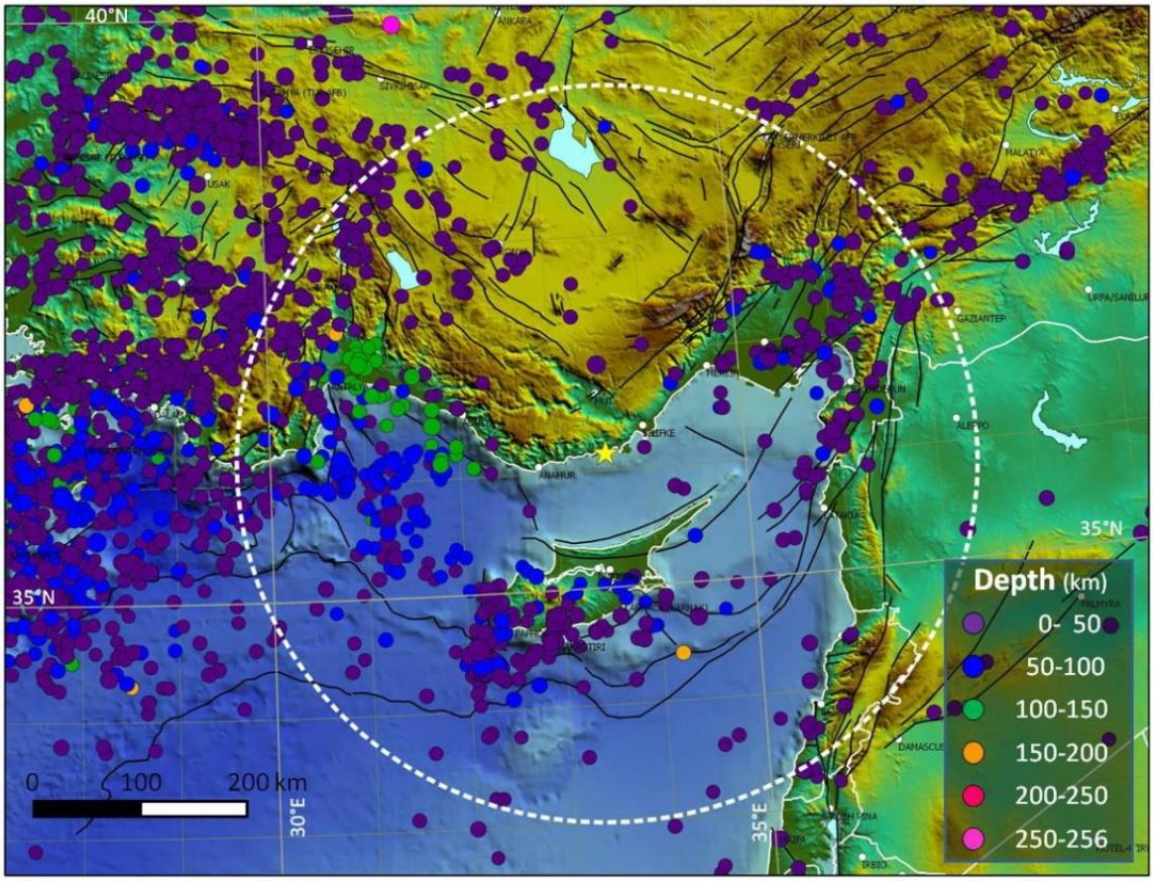

Figure 6/4.31 – Instrumental seismicity (1976-2010) from IRIS database

In the range of magnitudes M_W=3.0 - 8.1 the catalogue includes 4764 events, however in the SHA analysis only events with M_W more than 4.0 have been used.

Completeness of the summary catalogue was assessed.

The completeness periods in the WP summary catalogue for events of different magnitudes are provided in Table 6/4.12.

Table 6/4.12 – Year of Completeness of Instrumental Period Earthquakes in the WP Catalogue

Magnitude M_W	Year of catalogue completeness
3.0	1997
4.0	1964
5.0	1921
6.0	1821

The WP instrumental earthquake catalogue in electronic form may be submitted on demand.

Seismicity maps confirm the absence of epicenters of relatively strong events in the Akkuyu NPP near region. Main events took place in the east (Central Anatolian Fault Zone, East

Anatolian Fault Zone, Dead Sea Fault Zone), in the west (Antalya Region) and in the south (Cyprus) with the strongest event (M=7.1).

The depth distribution of events reveals the thickness of the brittle crust and the geometry of subducting slabs. Figure 6/4.32 shows a north-south cross section providing the distribution with depth of instrumental seismic events: the subducting slab is clearly delineated down to the depth of about 110 km with an angle of 40-45°. No evidence of subcrustal seismicity is present further north to a distance of 50 km from the site. Hence, no seismically active slab is assumed under the site. The thickness of the brittle crust appears to be smaller in the inland sector north of the site, where most of the events appear to occur within 15-20 km depth.

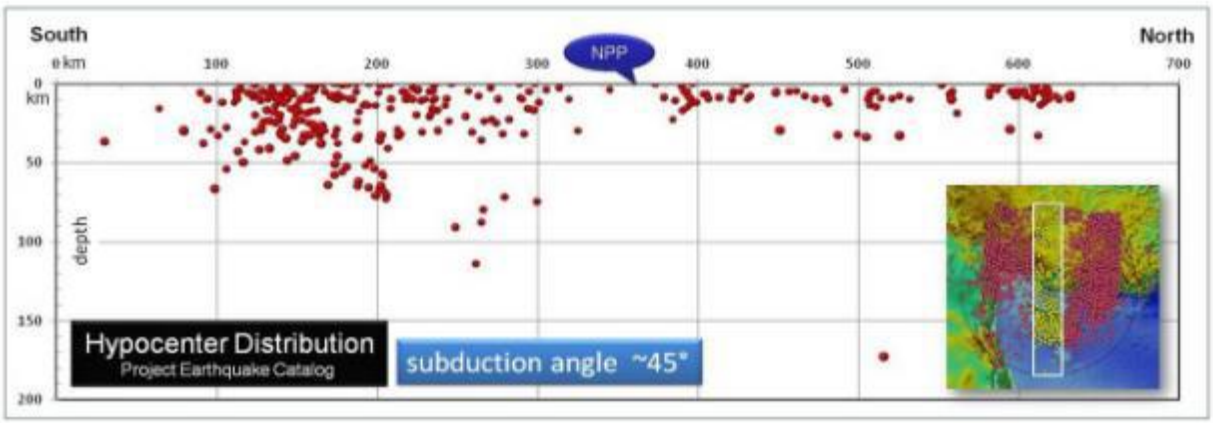

Figure 6/4.32 – Distribution of instrumental seismicity with depth along a north-south cross section extended for the whole regional area (700 km)

Preparation of the compiled catalogues for PSHA has been performed. Rizzo catalogue was declustered using Tibi et al. approach [6/228]; ENVY/BU KOERI catalogue was declustered on the basis of Reasenberg method [6/188]. Completeness of catalogues (events with different magnitude ranges) was estimated by Rizzo, ENVY/BU KOERI and WP using the Stepp procedure [6/208].

The consolidated seismic hazard assessment is utilizing a homogenized project seismological catalogue developed and processed by BU KOERI which is the national seismological institution in Turkey.

6.4.3 INSTRUMENTAL STUDIES OF MICROEARTHQUAKES

The micro-seismicity of the Akkuyu NPP site has been investigated by Istanbul Technical University [6/43, 6/44, 6/215, 6/216, 6/217 and 6/224] in three campaigns during the period of 1977 to 1988.

The first campaign consisted of two phases which took place from June 1977 (about four months) and March-August, 1978. A 10 station network located within a 60 km radius of the

Akkuyu NPP site was utilized. A total number of 122 events were located with magnitudes between 1.2 and 4.3 within the study area bounded by 35.00^{o} N-38.50^{o} N and 30.50^{o} E-36.00^{o} E. During the studies conducted in 1977-1978, no considerable seismic activity has been observed.

A 17 station network located within a radius of about 120km of the NPP site was installed between April, 1985 and May, 1986. A total number of 515 events were located in the study area with magnitudes varying between 1.1 and 4.6. Probably due to the considerable increase in the number of the seismic stations relatively higher seismic activity was observed during this survey period. Two sets of clustering of events constitute NE-SW alignment parallel to the seaside.

During the study for the period of January 1987-1988 a 17 station network was used. The network configuration was similar to the second phase, except that two stations were located further to the east. The major swarms of microearthquakes observed in two previous studies are also observed in this period. There is no strong evidence that the visible part of the Ecemiş fault exhibited microearthquake activity during the course of this study. In the area located between the southern end of Ecemiş fault and the city of Mersin however, there are some microearthquakes with magnitudes M>2.5. Authors assume this activity may not be a sound evidence to propose that the Ecemiş fault zone continues further South of Pozantı town. A total number of 577 events were located in the study area with magnitudes varying between 1.5 and 4.8. A list of the microearthquakes that occurred within an area of radius 60 km centered at the Akkuyu NPP site recorded during the previous three campaigns (1977-1978, 1984-1985, 1986-1988) is given in Appendix L.

The seismic events identified in 1977-1988 by local expeditionary seismic networks were combined with the events recorded by national seismic networks in order to obtain more accurate characteristic of the overall spatial distribution in the near region. As it is shown in Figure 6/4.33, spatial distribution of earthquakes roughly characterizes two blocks: one is affected by internal deformation, the second – practically does not show seismic activity. The line dividing these blocks is extended in the northeast - southwest direction. In spite of the fact that individual geological survey results show presence of some faults extending from northeast to southwest, integration of the results obtained creates a picture of deformation of a fixed block and not a shift along the fault. Whether the northeast-southwest line separating two blocks is a fault – is a subject of a further study, which requires relevant data recorded by the seismic network re-built in 2011 [6/79].

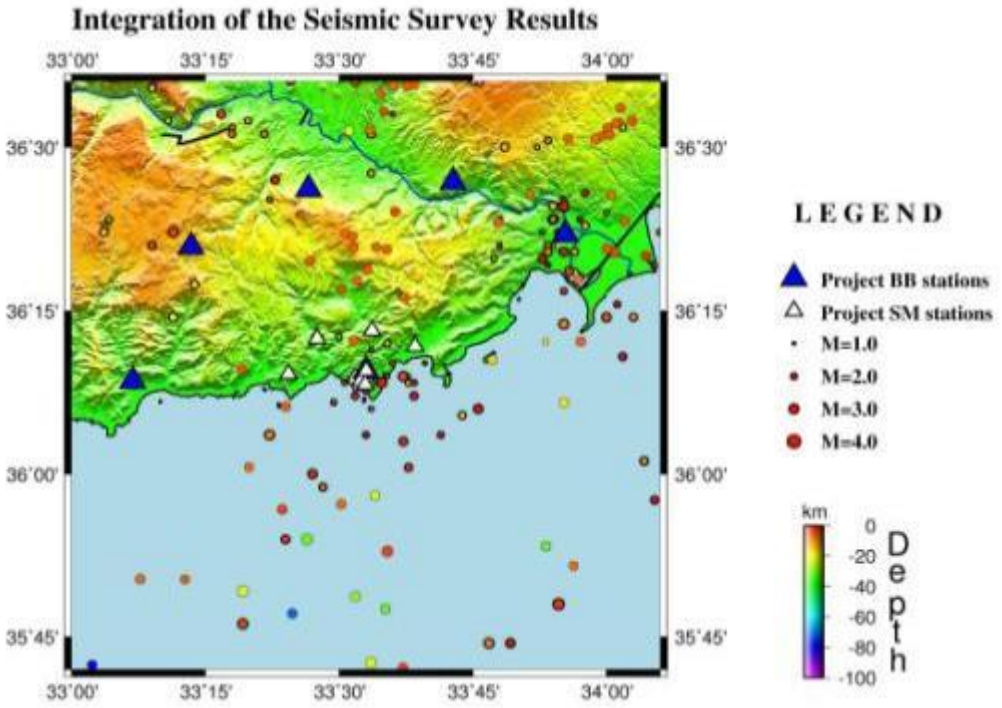

Figure 6/4.33 – Integration of Results of Identification of Epicenters of Earthquakes According to the Expedition Instrumental Survey Data and Data Obtained by National Stationary Seismic Station Networks [6/79]

Thus, the results of instrumental seismic studies demonstrate, firstly, rather low earthquake activity in the vicinity of the site, and secondly – these results, on the whole, are consistent with the the tectonic structure of the area.

The objective of the seismicity survey initiated at the beginning of July, 2011 [6/79, 6/80 and 6/81] is identification of the existing active faults involved in the present day tectonic deformation around Akkuyu NPP site. For this purpose a local seismological network of 13 digital stations were deployed covering an area of approximately 80x40 km^2 with an average spacing of 5 km for the strong motion stations and 20 km for the broadband stations. The local network for monitoring microearthquakes consists of seven strong motion (SM) accelerometers and six weak motion (WM) broad-band seismometers. The network configuration is illustrated in Figure 6/4.34. The SM accelerometers are installed in close distances in an area of 20x10 km^2 and are about 10 – 15 km from the Akkuyu NPP site in places with different surface layer conditions with three of them installed at the Akkuyu NPP site. One of these three accelerometers at the gate of the Akkuyu NPP site is considered as a reference station and consists of both accelerometer and broadband seismometer.

Figure 6/4.34 – Local Seismic Network Configuration; yellow symbols – WM broadband seismometers, triangles – strong motion (SM) accelerometers

Compiled catalogue of instrumental earthquakes for the period from 2nd of July to 31st of October 2011 consists of 135 events with magnitudes $0.7<M_D<2.6$ located within an area of 50 km radius from the Akkuyu NPP site [6/75].

Epicenters of the events shown in Figure 6/4.35 are located within a confidence radius of ± 2 km within the array and relatively larger for events located outside the array. The reliability of the distant events located outside the local network incorporating the first arrivals recorded at several nearby seismic stations which belong to the national seismic networks operated by KOERI and AFAD. The threshold-magnitude of reliable detections for the 2011 study is about 1.4.

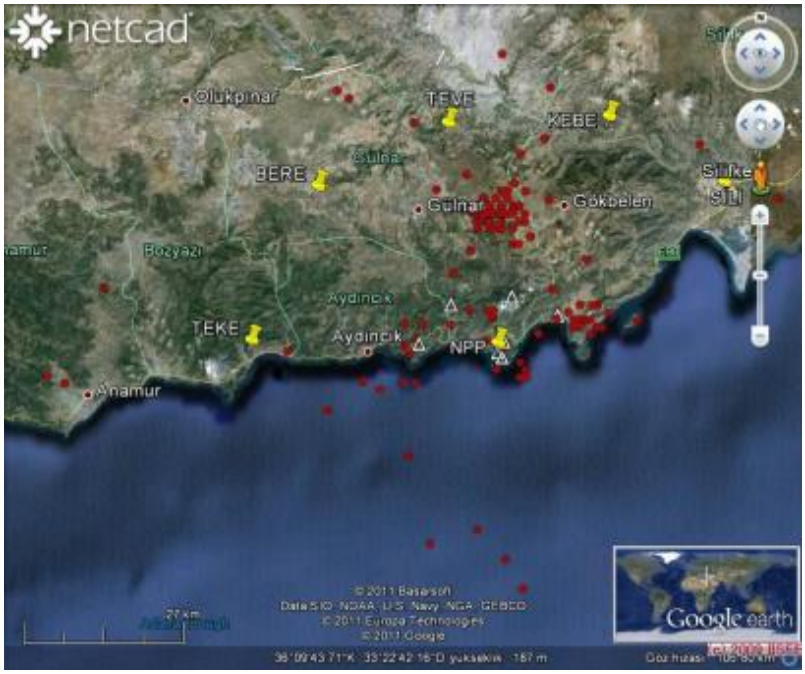

Figure 6/4.35 – The Seismic Events Detected During the Period From 1st of July to 31st of August 2011 Occurred Within an Area 50 km from the Akkuyu NPP Site

Frequency distribution of the epicenter and depth errors in locating the seismic events (according to July-August 2011 observation data) is shown in Figure 6/4.36.

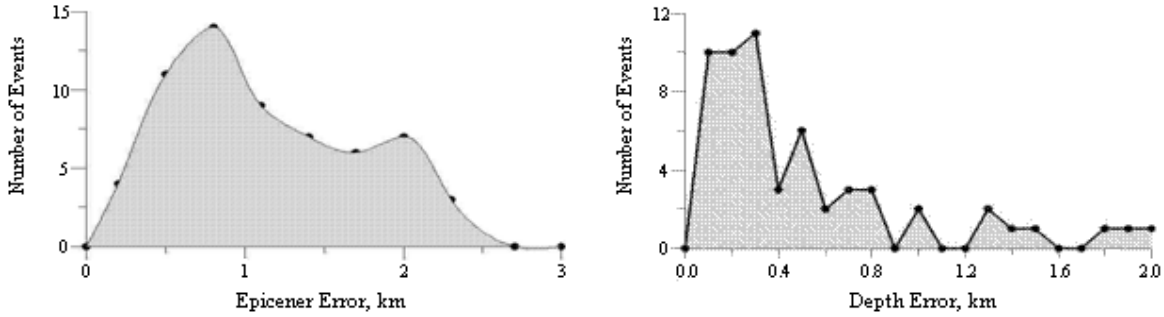

Figure 6/4.36 – Frequency distribution of the epicenter and depth errors in locating the seismic events (July-August 2011)

A considerable part of the recorded events as it was established by a meticulous analysis is caused by industrial or mining explosions. A schematic map showing position of quartzite, building stone and marble quarries within 30 km from the NPP site is provided in Figure 6/4.37. Besides, road works with blasting of small explosive charges are regularly performed in the area. These events are not directly hazardous for the Akkuyu NPP but, they can be erroneously interpreted as natural earthquakes in the instrumental seismicity analysis. Due to this fact, inclusion of an event in the earthquake catalog was preceded by a comprehensive analysis and discrimination of man-induced events (explosions) described in detail in [6/75].

Figure 6/4.37 – Stone Quarries in the Akkuyu NPP site region

As can be seen from Figure 6/4.35, there are two parallel seismic activity traces – offshore along the Mediterranean Sea coast and onshore along the coast west to the Akkuyu NPP site. Seismic activity in these areas was also observed during the previous three campaigns. It is obvious that offshore events are earthquakes. Fourier amplitude spectra for the offshore and onshore events recorded at the AKKU station (Figure 6/4.38) are quite similar, so these events can be referred to have the same origin. Therefore, onshore seismic activity west to the NPP site is caused by natural events – earthquake.

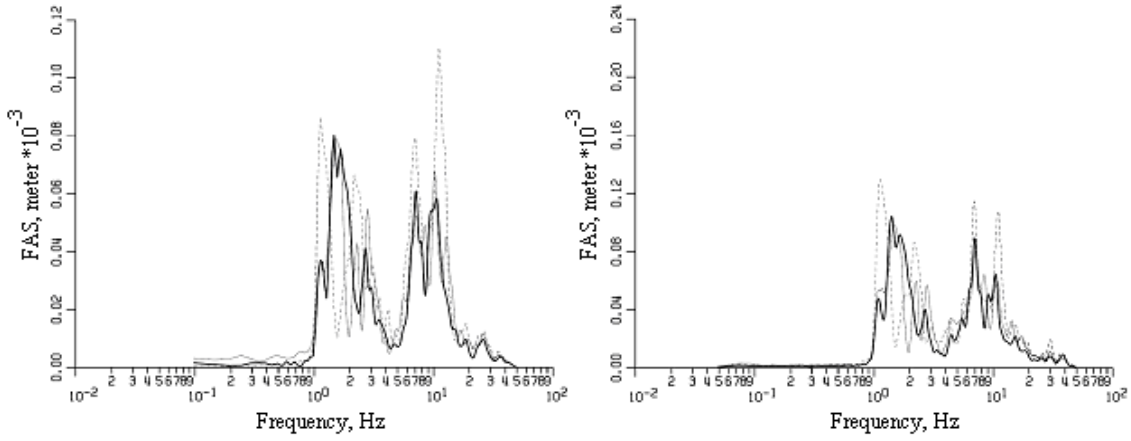

Figure 6/4.38 – Fourier amplitude spectra of September 26, 2011 11:03 offshore event (left) and October 14, 2011 08:54 onshore event (right)

The Centroid Moment Tensor (CMT) solution technique has been applied to further constrain and better understand the depth range of the seismic events. The six broadband seismometers deployed as a semi-circular array with a radius of 40 - 50 km from the Akkuyu site

provide a good coverage to recover the source parameters of the micro-earthquakes taking place in the area of interest using the technique developed by Kuge [6/140].

The method is based on waveform modeling of displacement seismograms at one or more stations at local distances. A centroid location can be searched for in a 3D-grid scheme by achieving the best fit between observed and synthetic displacement seismograms. The synthetics are calculated following Kohketsu [6/136] for a horizontally layered structure.

The CMT depths obtained through the waveform modeling of the broadband records yield shallow depth at the upper crust mostly within 1 - 3 km depth range (Figure 6/4.39). Such a shallow depth range does not rule out the possibility of man-made classification of the daytime events. On the contrary, the shallow depths favour it. The largest depth retrieved is 20 km for an event located 90 km NE from the Akkuyu site showing predominantly normal faulting mechanism. Nine CMT solutions for the events taking place in the proximity of the site lie within 1 - 6 km depth interval. The CMT depth of the event located 10 km to the east of the site is 6 km, showing normal faulting mechanism similar to the one located 90 km away from the site.

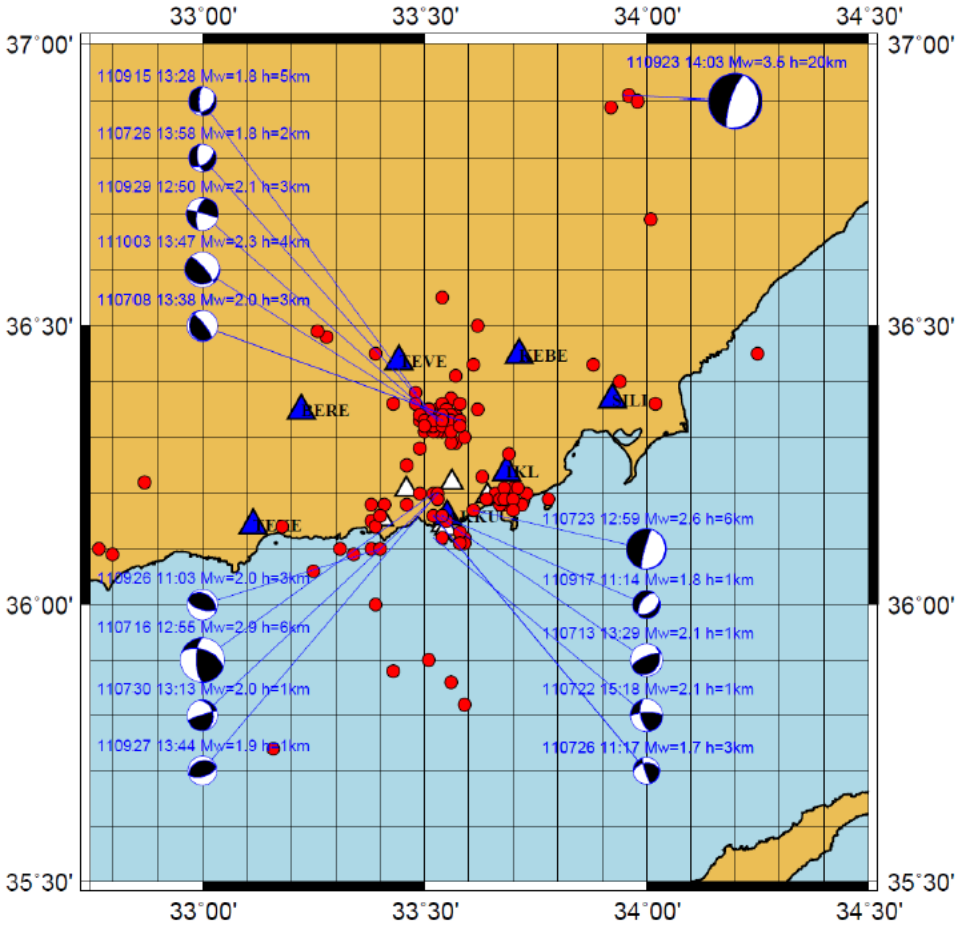

Figure 6/4.39 – The CMT inversion results for some selected events with waveforms of high signal-to-noise ratio, [6/125]

List of microearthquakes recorded during study in 2011 (to October 2011) by local seismic network in the Akkuyu NPP site vicinity is given in Appendix L.

Seismic monitoring at local seismic network stations was continued in 2012 [6/79, 6/80 and 6/81]. For the period from November 15, 2011 to March 31, 2012 three earthquakes were recorded within 50-km area from the site. Sources were located in the sea SW and E to the site (Figure 6/4.40, Table 6/4.13).

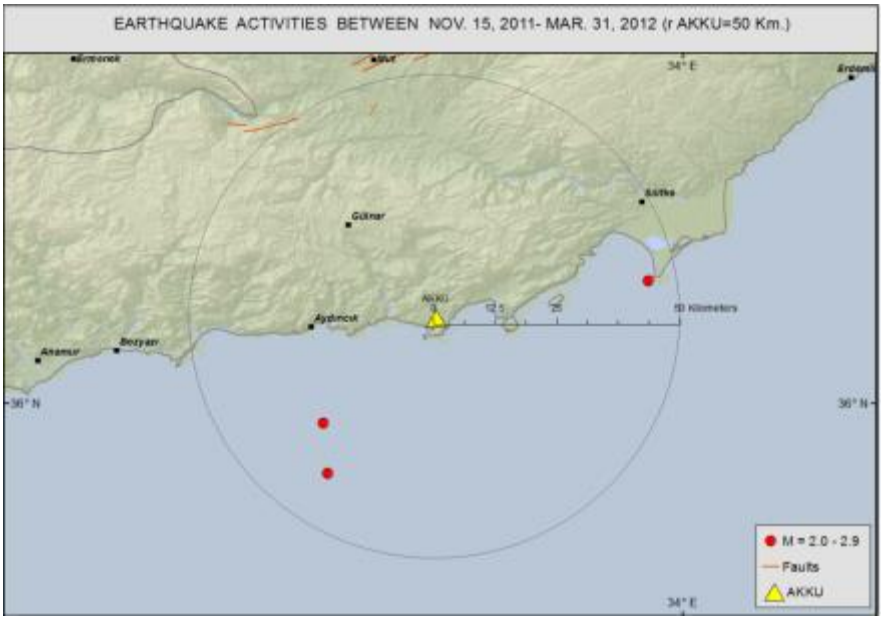

Figure 6/4.40 – Earthquake activity in the proximity (50-km area) of the site recorded during the period from November 15, 2011 to March 31, 2012

Table 6/4.13 – List of earthquakes in the proximity (50-km area) recorded during the period from November 15, 2011 to March 31, 2012

No	Date	Time	Latitude (º N)	Longitude (º E)	Magnitude (Ml)	Depth (km)
1	07.12.2011	11:21:44.00	36.2277	33.9378	2.2	11
2	12.02.2012	11:57:45.09	35.9638	33.3438	2.6	5.3
3	28.02.2012	06:01:03.45	35.8712	33.3523	2.4	24.9

For the period from April 01, 2012 to July 15, 2012 28 earthquakes were recorded within 50-km area from the site. Sources were located in the sea SW and E to the site (Figure 6/4.41, Table 6/4.14).

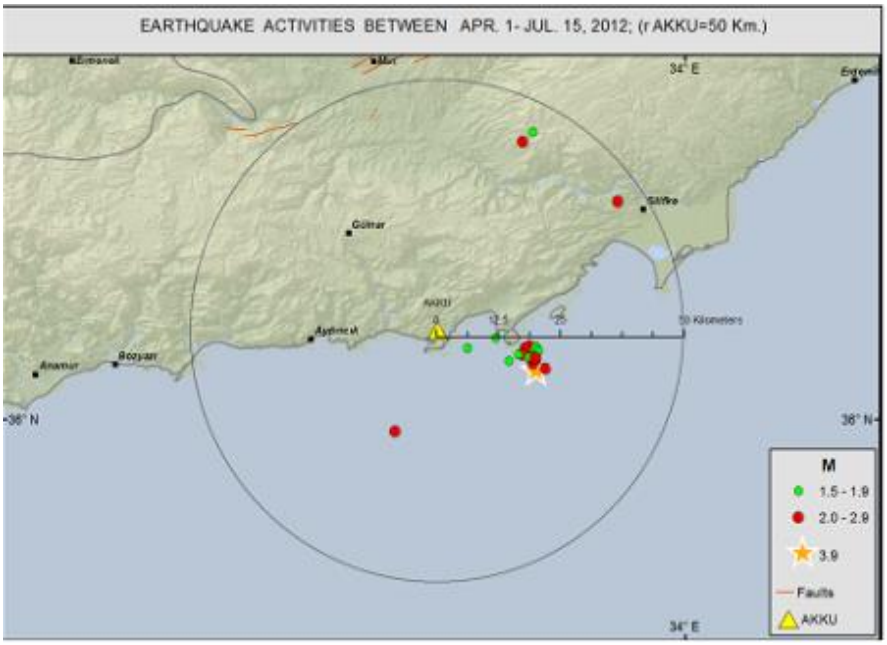

Figure 6/4.41 – Earthquake activity in the in the proximity (50-km area) recorded during the period from April 01, 2012 to July 15, 2012

Table 6/4.14 – List of earthquakes in the proximity (50-km area) during the period from April 01, 2012 to July 15, 2012

No	Date	Time	Latitude (º N)	Longitude (º E)	Magnitude (Ml)	Depth (km)
1	08.04.2012	04:48:26.71	36.4948	33.7055	2.2	13.4
2	03.05.2012	06:24:26.74	36.0887	33.7292	3.9	5.5
3	04.05.2012	10:06:24.03	36.116	33.702	1.8	3.9
4	04.05.2012	16:21:53.94	36.1068	33.7198	1.8	5.2
5	04.05.2012	17:07:07.45	36.1033	33.6805	1.9	3.4
6	06.05.2012	07:47:08.95	36.124	33.7195	1.9	10.3
7	10.05.2012	00:55:11.72	36.1172	33.7255	2.1	9.9
8	10.05.2012	16:52:10.07	36.1302	33.7178	2.1	11.7
9	10.05.2012	21:18:46.76	36.1053	33.7283	2.3	9.3
10	11.05.2012	01:39:53.45	36.1202	33.7253	1.9	9.8
11	13.05.2012	09:05:58.09	36.108	33.7307	1.7	6.1
12	13.05.2012	23:32:55.01	36.1267	33.7095	2.1	11.5
13	14.05.2012	01:12:16.57	36.09	33.7465	2.1	5.2
14	14.05.2012	20:05:23.68	36.104	33.7252	2.3	9.1
15	20.05.2012	08:11:42.93	36.129	33.7292	1.8	9.7
16	22.05.2012	20:22:53.58	36.1157	33.7043	2.1	7.3
17	27.05.2012	21:50:42.59	36.1222	33.7338	1.8	6
18	06.06.2012	17:23:08.48	36.3883	33.8775	2.7	12
19	18.06.2012	15:21:55.23	35.9778	33.4738	2.8	17.8
20	27.06.2012	22:51:36.01	36.0993	33.7233	2.2	5.1
21	30.06.2012	09:40:47.79	36.1093	33.7197	2.0	5.2

No	Date	Time	Latitude (º N)	Longitude (º E)	Magnitude (Ml)	Depth (km)
22	04.07.2012	16:31:20.70	36.1112	33.7173	1.8	3.8
23	06.07.2012	06:49:10.62	36.1265	33.6053	1.5	18.8
24	09.07.2012	00:00:48.94	36.1102	33.7172	1.9	4.8
25	09.07.2012	19:17:55.71	36.511	33.7238	1.9	26.6
26	10.07.2012	08:11:02.53	36.115	33.6975	1.6	3
27	11.07.2012	13:25:51.94	36.1447	33.6563	1.7	9.1
28	15.07.2012	09:03:14.44	36.1098	33.728	2.0	3.4

As it can be seen from Figure 6/4.41, most of the events recorded during the period from April 01, 2012 to July 15, 2012 are located offshore Yeşilovacık composing an obvious cluster. The spatial distribution of this cluster of events points out a NW-SE alignment. The largest event among them is the May 3rd, 2012 Yeşilovacık earthquake (ML=3.9) which is also the most significant earthquake observed since the installation of the network. It was successfully recorded by most of the strong motion and broadband stations of the Akkuyu NPP network. The epicentral distance from the Akkuyu NPP site is approximately 20 km. The event was felt at Akkuyu, Aydıncık, Gülnar and Silifke and the spatial distribution of the predicted intensities is shown in Figure 6/4.42.

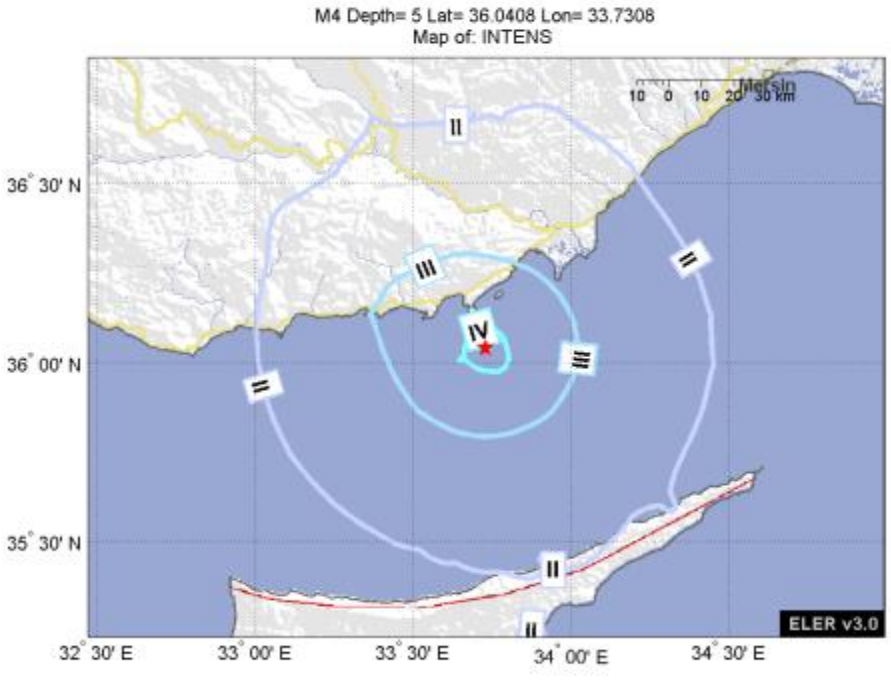

Figure 6/4.42 – Intensity map for May 03,2012 earthquake with epicenter in YeşilOvacık area

Data of the last monitoring cycle was provided for period from July 16 to September 20, 2012. Seven microearthquakes with epicenters in the sea WSW and E to the Akkuyu NPP site were recorded during this period (Figure 6/4.43, Table 6/4.15).

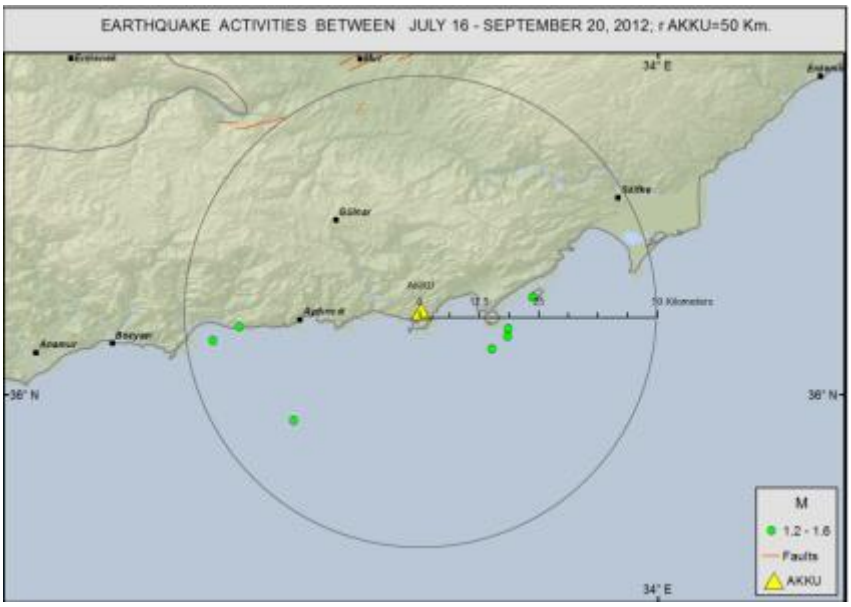

Figure 6/4.43 – Seismic activities in the region between 16, Jul., 2012-20 Sept., 2012 period

Table 6/4.15 – List of earthquakes in the proximity (50-km area) during the period from July 16 to September 20, 2012

No	Date	Time	Latitude (º N)	Longitude (º E)	Magnitude (Ml)	Depth (km)
1	27.07.2012	03:45:20.35	36.0863	33.6853	1.2	4.8
2	01.08.2012	15:39:10.37	36.1027	33.1557	1.5	9.9
3	13.08.2012	13:25:01.88	36.1295	33.2065	1.2	5.2
4	20.08.2012	05:14:13.96	36.1848	33.7638	1.3	12.8
5	27.08.2012	23:48:03.88	35.9508	33.3088	1.5	8.5
6	02.09.2012	00:24:23.95	36.1253	33.7152	1.6	4.7
7	10.09.2012	17:02:58.57	36.1105	33.7142	1.3	12

From November 2011, ENVY/BU KOERI regularly determines response spectra of the strongest events in the region. Examples of recorded response spectra are given in Figures 6/4.44 and 6/4.45. It is planned to use response spectrum for GMPE determination or updating and for verification of seismic parameters included in the Design Basis.

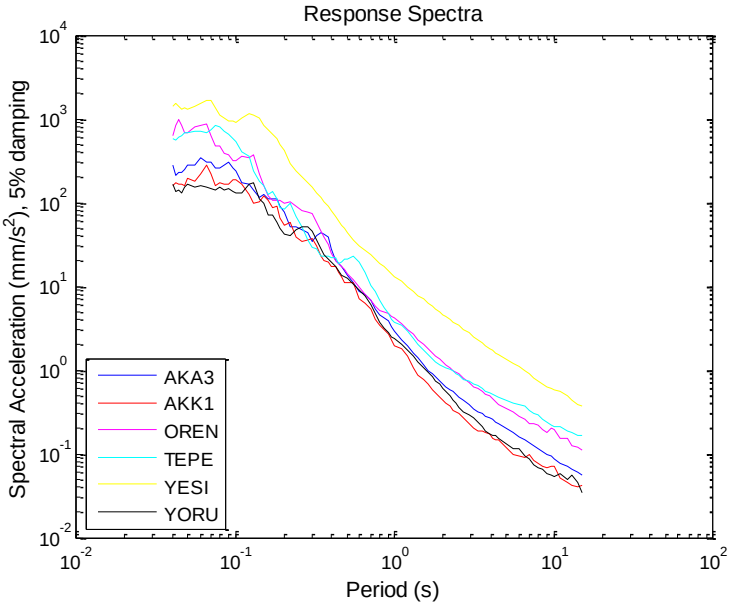

Figure 6/4.44 – 2012.05.03, ML 3.9, Yeşilovacık Offshore-Mersin (Mediterranean Sea), Distance to Akkuyu NPP site: 20.1km

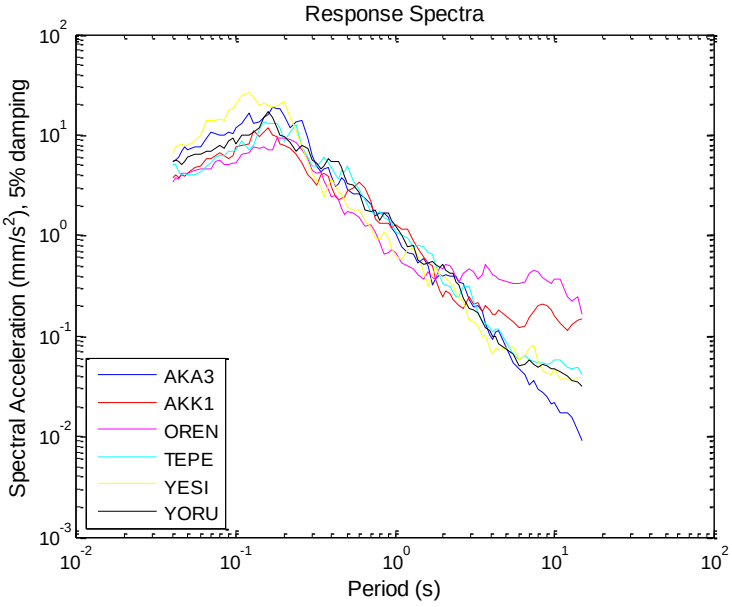

Figure 6/4.45 – 2012.05.11, ML 5.3, Mediterranean Sea, Distance to AKKUYU NPP site: 219.7km

6.5 SEISMIC HAZARD ANALYSES OF AKKUYU NPP SITE

This section will present the previous and current seismic hazard assessment studies for Akkuyu NPP as well as the methodological basis of the study following the national and international standards in the field and the seismotectonic models used in the different analyses. Results of the separate analyses are not provided in this report because they are considered interim studies while the actual design basis parameters are being developed within the framework of the consolidated seismic hazard assessment which is currently ongoing. Hence, the information on the design basis seismic characteristics will be provided in the Site Parameters Report.

6.5.1 CONVENTIONAL EARTHQUAKE ZONING

In accordance with the earthquake zoning map of Turkey (1997) issued after the selection of the NPP site, Akkuyu falls within the least seismic zone of Turkey (Figure 6/5.1).

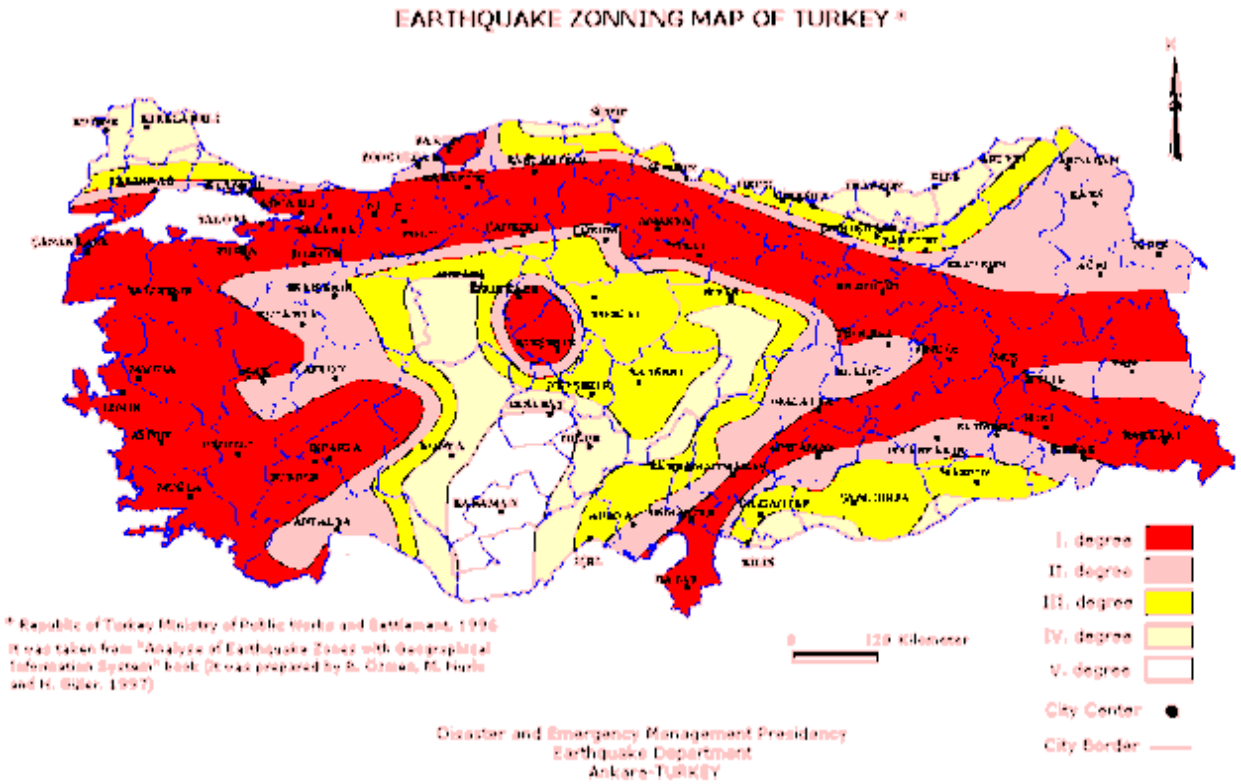

Figure 6/5.1 – Earthquake zoning map of Turkey

It is clear that the Akkuyu NPP site is located in the area with the lowest seismic hazard in Turkey.

The above zoning map is used in civil engineering for conventional design. The map is not applicable for the characterization of seismic hazard of NPP sites. Nevertheless, this provides a comparative indication that from a seismic hazard point of view the site has positive attributes. The national and international nuclear standards [6/113, 6/186 and 6/97] require site specific

investigations for the determination of seismic hazard regardless of the location of the site in the general zonation maps.

6.5.2 HISTORY OF THE SEISMIC HAZARD STUDIES

The early studies were performed under the sponsorship of the Turkish Electricity Authority (TEK). Geological, geophysical and seismological studies were performed by the Geological Department of Mining Research and Exploration Institute (MTA), Earthquake Engineering Research Institute (EERI) of Middle East Technical University (METU), Geophysical Department of Istanbul Technical University (ITU) Mining Department, and also a Swiss consulting group, Engineering-Consulting Consortium ENG (Emch-Berger, Basler und Hofman).

In 1975 TEK issued a report [6/213] with the results of the regional structural-geological studies of the Akkuyu NPP site including a general regional seismotectonic map. It is stated that no significant faults had been identified; however minor vertical faults (fractures) of N10°W direction were observed near the Kuşyuvası upland and Beşparmak islands. Indications of current activity of these faults are not available. Manifestation of faults was considered as indication to hypothetically graben-like structure between the Kuşyuvası upland and Beşparmak islands.

A large NE-SW thrust fault is identified in the northern part of the studied region. This thrust fault had formed in the Alpine orogenesis. Motions stopped in early Paleocene.

When studying seismic hazard in 1975 (METU), the catalogues of earthquakes of Edinburgh data center and Kandilli observatory were used with the events related to the period of 1900-1972. Seismic hazard of the area with radius of 150 km from the site was assessed via a probabilistic method. The deterministic method was used for evaluation of hazard from the specific seismic sources, among which considered were, for the first turn, the areas between Cyprus and South Anatolia shore (M=7.5, Δ=120 km), Ecemiş fault (M=6.2, Δ=60 km), scattered sources immediately near the site (M=6.0, Δ=30 km).

With the purpose of licensing TEK has issued in 1976 the refined report of the Akkuyu NPP site conditions [6/214]. This report presents the tectonic structures analysis made during field seismotectonic studies in the Akkuyu region. The absence of evidence for the existence of a graben-like structure between the Kuşyuvası upland and Beşparmak islands, as it was supposed before, was clearly demonstrated.

At that time all the faults identified in the site near regional area were considered as inactive. The available archaeological and historical information does not provide basis to establish manifestation in the near region of strong earthquakes. The results of the assessment of seismic hazard parameters in the region of 320 km radius acquired via deterministic and probabilistic

methods have been provided (as per Cornell [6/50]). The regionalized (7 regions) seismotectonic zoning was taken as the basis for the analysis. The seismicity parameters (magnitude, recurrence, average depth of earthquake focus) and their uncertainties are determined for each of the seismotectonic provinces. The consolidated compiled earthquake catalogue of the studied region consists of 184 events as of 1976 for the period of 115-1972 years. It is pointed out that the seismotectonic province that includes the site is controlling the hazard. This source is characterized by magnitude M=6.5 (magnitude upper limit).

The report presents a map of the near regional faults in scale 1:25000. It is concluded that local and insignificant (length 0.5 - 4.5 km) faults near the site are inactive since the Miocene period.

The regional seismotectonic features were considered in the ENG report (Emch-Berger, Basler und Hofman) of 1978 and 1980 years [6/64 and 6/65]. Attention was paid to the geological aspects and seismic history of the region (300 km) with the purpose of the areal seismotectonic regionalization. Eight seismotectonic regions (R) and seven seismic source zones (S) were identified. The Akkuyu site is located in region R4. The nearest to the site boundary of the region (R7) is at a distance of about 60 km and seismic source zone (S4.1) is at a distance of about 45 km. The upper and lower magnitude limits were defined for the seismotectonic regions, as well as the maximum observed intensity and magnitude of earthquakes. Three classes of events were considered: earthquakes (R4) immediately at the site ($M \leq 6$); close (S4.1) earthquakes ($M \leq 6.5$) and remote earthquakes (R7) with $M \leq 7$.

In 1979 METU/EERI presented a report of seismic parameters required for the Akkuyu NPP seismic design [6/156]. Each of the three seismotectonic regionalization versions in radius of 320 km from the site was considered as the basis for calculation of the seismic parameters. Regionalization principles, seismicity parameters, parameters of intensity attenuation laws, intensity and acceleration ratios were considered in this report. It was demonstrated that the earthquakes with focuses surrounding Cyprus and earthquakes that occur immediately near the site have the maximum contribution for the ground motion at Akkuyu NPP site. The sensitivity of seismic parameters related with the uncertainty in the input data has been analyzed.

The seismotectonic zoning was refined and summarized again in the METU report of 1989 [6/154]. The essentially refined seismotectonic model proposed for the Akkuyu region consists of 11 seismotectonic regions.

In 1990 the TEK/KOERI summary report of seismicity and the design ground motion parameters of the Akkuyu NPP site was published [6/227].

All seismotectonic and seismological studies performed for the Akkuyu NPP site were compliant with the requirements set forth in the regulatory documents of the USA Nuclear Commission (USNRC) and IAEA applicable at the time of publication of the reports.

The Akkuyu NPP site seismotectonic and seismological conditions were reviewed and evaluated by IAEA experts [6/110 and 6/111].

Following the seismotectonic and seismological criteria, factors prohibiting NPP construction at the Akkuyu site have not been found. Nevertheless, during the past twenty years the seismic hazard practice has significantly evolved. Moreover, a significantly increased number of different seismic stations operating today in the region of Turkey enables to replenish sufficiently, update and actualize the seismological database.

Within the framework of the renewed Akkuyu NPP project in 2011 and 2012 the seismic hazard assessment investigations of the site were restarted. Four different seismic hazard studies have been run in parallel.

ENVY in collaboration with BU KOERI has developed one of the studies [6/75]. This study has been independently reviewed by the Moscow Institute of Physics of the Earth RAS (IPE RAS) [6/117].

Simultaneously with seismological and seismotectonic investigations performed by the Turkish Subcontractor (ENVY Company) in 2011, additional SHA studies were also performed by international consultants – WorleyParsons Nuclear Services JSC and their sub-contractors Paul C. Rizzo Associates (Rizzo) with the main study being the one developed by Rizzo [6/243] while the work of WorleyParsons although including separate analysis [6/246] had the aim of an independent review of the Rizzo study.

Summary on main reports with materials, results and information on target seismotectonic and seismological investigations for Akkuyu NPP site (finalizing the pre-design stage) is given below.

Report title	**Company**	**Month, Year**
Site report. NED-I-14 [6/213]	TEK	November, 1975
Revised site report. NED-I-16 [6/214]	TEK	April, 1976
Akkuyu nuclear power plant. Seismotectonics. Part 1 [6/64]	EERI-METU, EMCH + Berger Ltd., Basler & Hofmann	December, 1978
Akkuyu nuclear power plant. Seismotectonics. Part 2 [6/65]		September, 1980
Earthquake resistant design parameters for the Akkuyu nuclear plant site. Part 1. Report No. 79-4 July, 1979 [6/156]	METU, EERI	July, 1979

Report title	Company	Month, Year
Akkuyu nuclear power plant design basis earthquake ground motion [6/226]	TEK, METU, EERC	May, 1983
Akkuyu nuclear power plant. Detailed site investigation report. Part II. NSD-I-29 [6/222]	TEK	June, 1983
Licensing considerations related to seismic safety for the Akkuyu nuclear power plant by Aybars Gurpinar, IAEA Expert. Report to the Government of Turkey [6/110]	IAEA	January, 1985
Review of geological and seismological aspects of Akkuyu site. Report to the Government of Turkey. IAEA-TA-2366 [6/111]	IAEA	May, 1986
Seismotectonic evaluation of the Akkuyu Nuclear Power Plant site. METU/GGRC [6/154]	METU	August, 1989.
Akkuyu nuclear power plant design basis ground motion. Report No. 90-2 [6/227]	TEK,BU KOERI	May, 1990
Seismological and seismotectonic investigations of the territory with the implementations of stage II comments. Stage III. [6/75]	ENVY, BU KOERI	November, 2011
Elaboration of seismic hazard assessment alternative model for the NPP "Akkuyu" installation site in Turkey based on seismological and seismotectonic conditions [6/117]	IPE RAS	November, 2011
Initial Seismic Input to be provided to the General Designer [6/243]	WP/Rizzo	December, 2011
Independent Review of the Seismic Hazard Assessment of Akkuyu NPP Site. Final Report. [6/246]	WP	June, 2012

TEK – Turkish Electricity Authority (Ankara)
ITU – Istanbul Technical University (Istanbul)
METU – Middle East Technical University (Ankara)
EERI –Earthquake Engineering Research Institute, METU (Ankara)
EERC – Engineering Earthquake Research Center, METU (Ankara)
IAEA – International Atomic Energy Agency (Vienna)
BU KOERI – Boğaziçi University, Kandilli Observatory and Earthquake Research Institute (Istanbul)
ENVY – ENVY Energy and Environmental Investments Inc. (Ankara) – Turkish Subcontractor
IPE RAS – Foundation of the Russian Academy of Sciences Schmidt Institute of Physics of the Earth
WP – WorleyParsons Nuclear Services JSC (Sofia)

6.5.3 SEISMIC HAZARD METHODOLOGICAL BASIS

Following the IAEA guidance [6/113] the main elements of a seismic hazard study are: development of a project specific geological, geophysical and geotechnical database in four areal scales – regional, near regional, site vicinity and site area; development of project specific seismological catalogue; development of coherent seismotectonic models; selection of the ground

motion prediction equations (GMPE) applicable for the area and hazard determination using both probabilistic (PSHA) and deterministic applications (DSHA).

The seismicity of the territory is usually considered on the basis of seismic events that can be divided into three groups (see Section 6.4). Different methods are used for analysis of these groups:

- Historical seismicity (earthquake and effect described in written sources) including events prior to 1900 year;
- Instrumental seismicity (time, source coordinates, magnitude and other parameters recorded by seismometers) after 1900 year.
- Microseismicity in the site near region

Other types of study evaluating previous strong events in seismicity analysis involve archeoseismology and paleoseismology.

Once the database and the seismological catalogues are in place in the next stage of the analysis are developed seismotectonic models aiming to represent the geotectonic structure in the area of interest. Several seismotectonic models are normally developed in order to account for the epistemic uncertainty in the characterization and the areal boundaries of the potential sources. Fault modeling could be performed if there is very strong and unambiguous dataset related with the fault orientation and its kinematic parameters.

When areal modeling is performed the boundaries of the seismotectonic provinces are normally defined on the basis of common geotectonic features in particular area. Empirical regressions between the magnitude versus fault rupture length and/or fault displacement such as widely used Wells & Coppersmith relationship [6/238] are also applied in the process for constraining the areal extent of the zone based on the geological potential of the faults in the area. Wells and Coppersmith empirical relationship of rupture length and moment magnitude (M) is:

$$M_W = a + b \lg(SRL),$$

where:

- a and b – coefficients;
- SRL – rupture length, km.

Summary on a- and b- values for different kinematic fault types is given below:

Slip type	*a*		*b*	
	mean	Standard deviation	mean	Standard deviation
SS	5.16	0.13	1.12	0.08
R	5.00	0.22	1.22	0.16

N	4.86	0.34	1.32	0.26
All	5.08	0.10	1.16	0.07

The segmentation method involves the identification of individual fault segments that have a continuity, character, and orientation that suggests the segment will rupture as a unit. The use of 100% rupture length for a fault segment is found to lead realistic values for maximum magnitude estimates [6/205]. However, if the segment separation (step over) between the fault segments is less than 5 km the overall fault length should be considered. On the contrary, if the segment separation is more than 5 km the continuous segment lengths should be taken into consideration in the calculation of Mmax values. It is known that earthquakes can rupture more than one fault segment, if the separation between the segments is less than 5 km.

Determination of Ground Motion

Probabilistically, seismic hazard may be described as the mean annual frequency of exceedance (or non-exceedance) of the assigned levels of ground motion at “free field” conditions in a specific point (site).

Typically, two levels of ground motion hazard, named SL-1 and SL-2, are defined as the ground motion design basis in IAEA SSG-9 [6/113] (in Russia and in the US these levels correspond to OBE (Operating Basis Earthquake) and SSE (Safe Shutdown Earthquake). The SL-1 and SL-2 (S1 and S2 in Turkish regulations) will be developed following the requirements of the Turkish regulations and the recommendations of the IAEA.

In compliance with the IAEA guidance [6/113] the seismic hazard studies performed after 2010 include both deterministic (DSHA) and probabilistic (PSHA) methods. In PSHA and DSHA the following key hazard components are used: model (several models) of seismic sources (ESO zones) and model (several models) of ground motion prediction (attenuation relationship). In Akkuyu NPP site studies, the standard PSHA model was used which postulates that earthquake occurrence in time and space can be modeled as a Poisson process [6/50].

Following IAEA SSG-9 [6/113], the uncertainties in ground motion prediction, earthquake source location and seismicity parameters in ESO zones are taken into account in the analyses.

A typical model for analyzing seismic hazard includes several stages as follows:

- Determination of probabilistic distribution of earthquakes magnitudes on basis of Gutenberg-Richter recurrence law;

$\log N = a - bm$, where N — number of shocks with magnitude higher or equal to m per time unit and territory unit (or extension unit), a and b — seismic constants for any assigned region. Value N is as usual found, if it is supposed that m has the top and bottom boundary m_{max} and m_o.

- Determination of probabilistic distribution of earthquakes in time;
- Determination of ground motion parameters at the site on the basis of magnitude, distance, focal depth, fault type, soil/rock profile representation of the site, etc.;
- Calculation of exceedance probability of the ground motion parameter within the assigned timeframe.

Mathematically, it can be described by the following equation:

$$\lambda[Y \geq y] = \sum_{i=1}^{N} v_i \int_{m_0}^{m_{\max}} \iint_{R\ \varepsilon} P[Y \geq y \mid m, r, \varepsilon] \cdot f_{M_i}(m) \cdot f_{R_i}(r) \cdot f_{\varepsilon}(\varepsilon) \cdot d\varepsilon \cdot dr \cdot dm,$$

where *Vi* is the annual rate of earthquakes with magnitudes m0 ≤ m ≤ mmax in i-th ESO zone, P[Y > y | m, r, ε] conditional probability that the earthquake with magnitude *m* will produce at distance *r* ground motion level *y*; ε is standard deviation (in logarithmic units) from median value predicted by the attenuation relationship fM(m), fR(R) fε(ε) are distribution of probability densities of magnitude, distance and ε, correspondingly.

The functional from of the hazard integral postulates that probabilistic analysis considers effects at the site from all possible magnitudes and distances.

IAEA SSG-9 [6/113] emphasizes the explicit treatment of both epistemic and aleatory uncertainties inherent to the parameters and the modeling process.

Account of the epistemic uncertainties connected with the incompleteness of knowledge about the spatial and temporal distribution of future earthquakes is taken as per the “logic tree” concept. The epistemic uncertainty may be incorporated by means of inclusion of alternative datasets or models with particular “weight” practically at each SHA stage. A “logic tree” technique enables, taking into account expertly assigned weights, to reduce an arbitrary rule of selection of specific alternatives.

The second group of uncertainties (aleatory) is connected with the random character of the physical processes of earthquake generation, it characterizes the dispersion of the ground motion from one earthquake to another and may be reduced only to the certain limit depending on the general peculiarities of the region. The aleatory uncertainty is taken into account mainly by the GMPEs standard deviation.

In order to provide for the applicability of the Poisson model the initial earthquake catalogues were subject to declustering [6/188 and 6/208].

Sections 6.1 to 6.3 of this report provide the main elements of the geological, geophysical and geotechnical database of the site. Section 6.4 provides the seismological data and sources used for compilation of the seismological catalogue. The next section will describe the different seismotectonic models developed for the site.

6.5.4 SEISMOTECTONIC MODELLING

IAEA SSG-9 [6/113] provides the following recommendations with respect to seismotectonic modeling:

Paragraph 4.1:

"The link between the geological, geophysical, geotechnical and seismological databases and the calculation of the seismic hazard is a regional seismotectonic model, which is based on a coherent merging of the databases. In the construction of such a model, all relevant interpretations of the seismotectonics of the region that may be found in the available literature are taken into account. Above all, a sound database is essential in the construction of a reliable seismotectonic model. It should be noted that the most sophisticated methods will not yield good models if the database is poor or insufficient."

Paragraph 4.2:

"The standard procedure is to integrate the elements of the seismological, geophysical and geological databases in order to construct a coherent seismotectonic model (and alternative models) consisting of a discrete set of seismogenic structures."

Paragraph 4.3:

"The seismogenic structures identified may not explain all the observed earthquake activity. This is because seismogenic structures may exist without recognized surface or subsurface manifestations, and because of the timescales involved; for example, fault displacements may have long recurrence intervals with respect to seismological observation periods."

Paragraph 4.4:

"Consequently, any seismotectonic model should consist, to a greater or lesser extent, of two types of seismic source:

(1) Those seismogenic structures that can be identified by using the available database;

(2) Diffuse seismicity (consisting usually, but not always, of small to moderate earthquakes) that is not attributable to specific structures identified by using the available database."

Paragraph 4.7:

"When it is possible to construct alternative models that can explain the observed geological, geophysical and seismological data, and the differences in these models cannot be resolved by means of additional investigations within a reasonable time frame, all such models should be taken into consideration in the final hazard evaluation, with due weight given to each model. The epistemic uncertainty (i.e. the uncertainty associated with the modelling process) should be adequately assessed, to capture the full range of hypotheses regarding the characterization of the seismic sources and the frequencies of the earthquakes."

As mentioned earlier within the framework of the Akkuyu studies that started in 2011, four different seismic hazard studies have been performed - ENVY/BU KOERI, AEP/IPE RAS, Rizzo and WorleyParsons. The four studies account for a multitude of seismotectonic models since all of them considered more than one model. For example two models developed during an earlier stage of investigations were utilized. WorleyParsons utilized METU model from 1980 in its original form and ENVY/BU KOERI used modified METU model from 1989 also in original form.The following subsections provide a summary of the seismotectonic investigations performed for Akkuyu site including the original studies from the 1980s. In addition, the technical rationale used in the development of the seismotectonic models for the site closely following the IAEA recommendations is described.

6.5.4.1 EARLY AKKUYU NPP STUDIES

Seismotectonic zonation models (ESO zone models) were developed at the earliest investigation stage in 1970-1980s for the seismic hazard assessment of the Akkuyu NPP site

The first zonation model (further on TEK Model) was presented in the TEK Site Revised report in 1976 [6/214]. Map of TEK model is given in Figure 6/5.2.

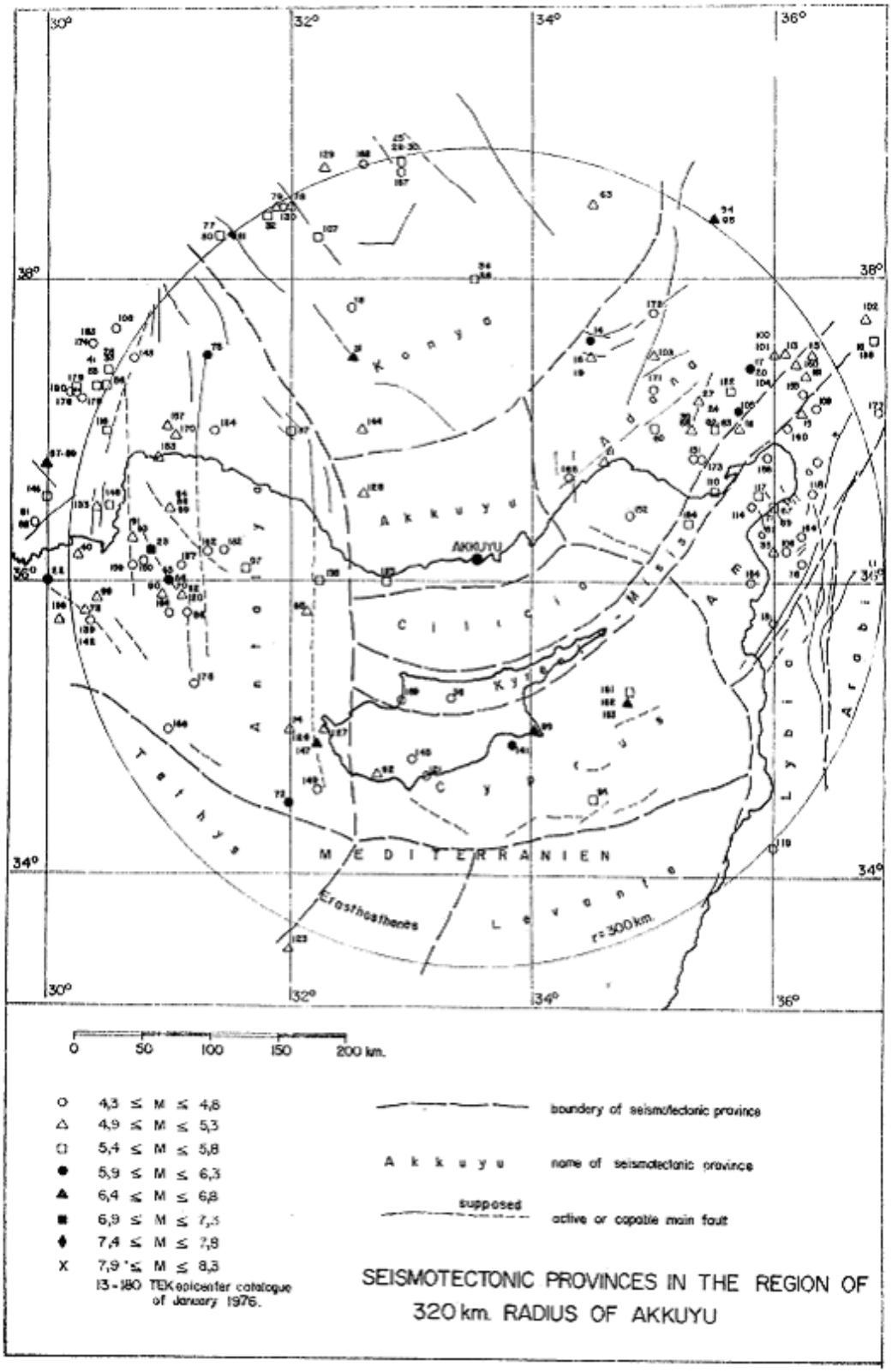

Figure 6/5.2 – Map of TEK seismotectonic zonation model of the Akkuyu NPP site 320-km region [6/214]

Parameters of seismotectonic provinces in TEK Model are given in Table 6/5.1.

Table 6/5.1 – Parameters of seismotectonic provinces in TEK Model

Province No	Name	Lower Limit m_o	Upper Limit m_1	Events/Yr	Average Depth, km	B
1	Adana	4.3	7.4	0.400	50.0	1.514
2	Kyrenia-Misis	"	6.7	0.157	45.0	1.354
3	Amanos	"	8.0	0.305	60.0	1.379
4	Konya	"	7.2	0.314	30.0	1.687
5	Antalya	"	7.5	1.100	60.0	1.745
6	Cyprus	"	7.5	0.129	75.0	0.779
7	Akkuyu	3.3	6.5	0.129	15.0	1.02[illegible]

Map of South Anatolia ESO zones is given in Figure 6/5.3. This Model was presented by ENG Consortium in 1978 [6/64] (further on ENG-1978 Model).

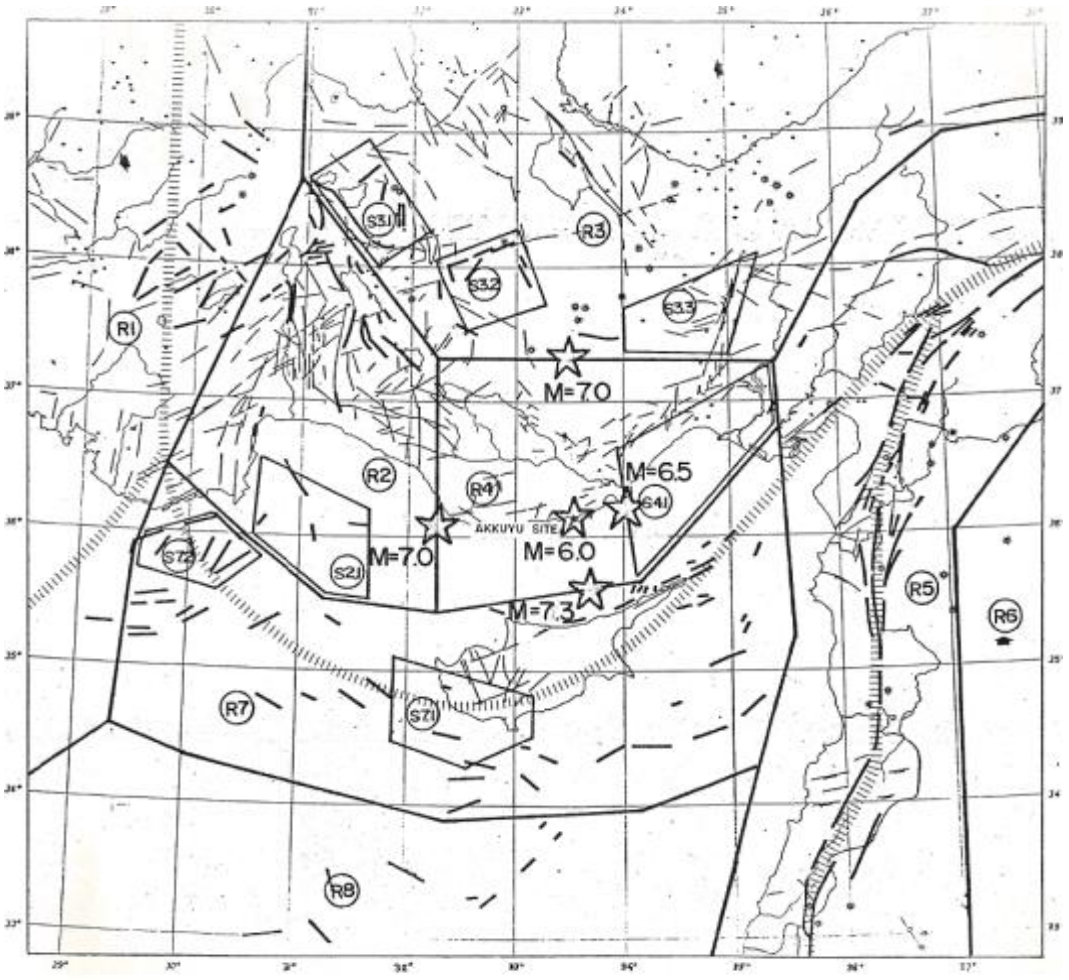

Figure 6/5.3 – Map of South Anatolia ESO zones (ENG-1978), [6/64]

ENG-1978 Model was updated in 1980 in collaboration with METU/EERC [6/65] (further on ENG/METU-1980 Model, Figure 6/5.4).

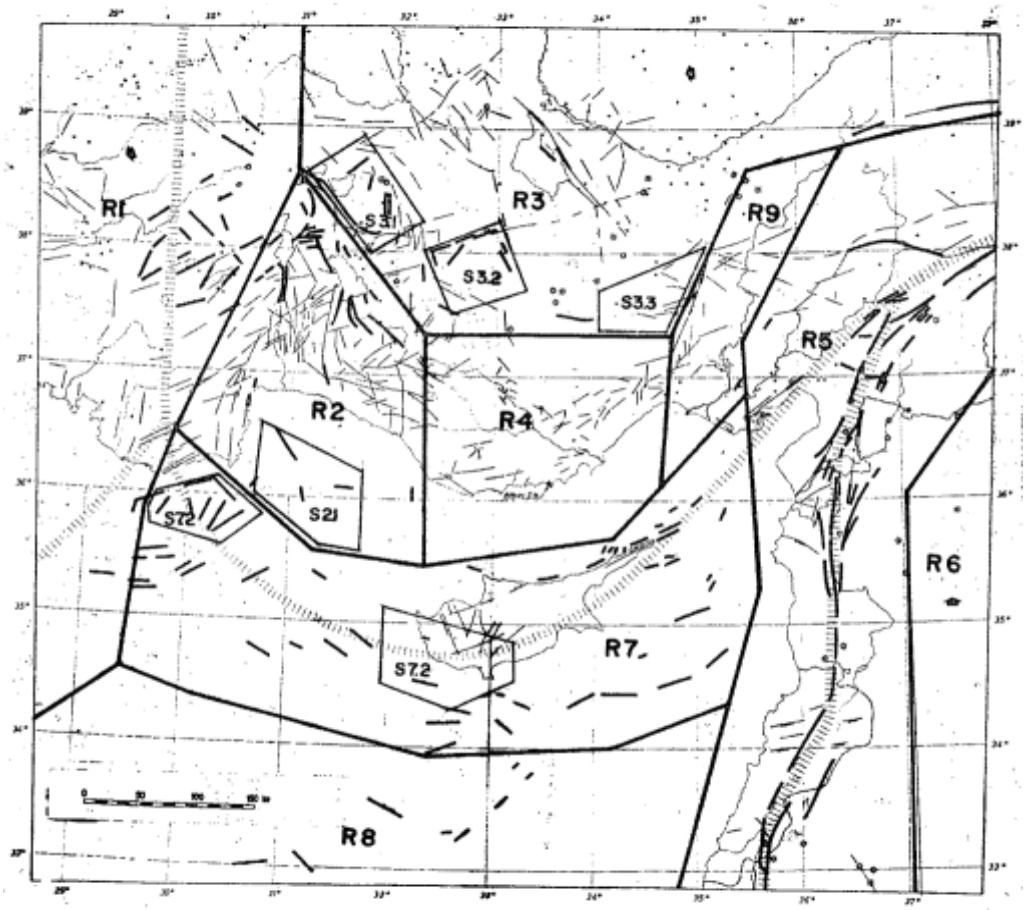

Figure 6/5.4 – Map of ENG/METU-1980 Model, [6/65]

Seismicity characteristics (per Gutenberg-Richter lgN(M)=a-bM) of ESO zones in ENG-1978 and ENG/METU-1980 models are given in Table 6/5.2.

Table 6/5.2 – Seismicity characteristics (per Gutenberg-Richter lgN(M)=a-bM) of ESO zones in ENG-1978 and ENG/METU-1980 models

Model	Code of zone	M_{max}	a (N_4)	υ_4	b	$R_{min,}$ km
ENC-1978	R1	7.8	3.1	1.29	0.9	320
	R2	7.0	2.1	0.50	1.2	110
	S2.1	7.0	2.1	2.80	1.2	170
	R3	7.0	2.4	0.42	1.0	130
	S3.1	7.0	1.0	1.66	0.8	260
	S3.2	7.0	0.25	0.56	1.1	170
	S3.3	7.0	1.0	1.54	1.1	140
	R4	6.0	0.08	0.03	1.1	0
	S4.1	6.5	0.46	0.38	0.8	45
	R5	8.0	2.5	0.55	0.8	180
	R6	6.0	0.07	0.02	0.8	320
	R7	7.3	4.0	0.43	0.9	60
	S7.1	7.3	1.35	1.80	1.0	150
	S7.2	7.3	0.75	1.67	0.9	255
	R8	6.5	0.06	0.01	0.9	245
ENG/METU-1980	R3	7.0	2.4	0.42	1.1	130
	S3.3	7.0	0.25	0.77	1.1	140
	R4	6.0	0.14	0.04	1.2	0
	R9	7.3	0.95	0.41	0.7	95

M_{max} – maximum magnitude (M_S);
N_4 – number of earthquakes M≥4.0 in zone per one year (à-coefficient);
υ_4 – à-coefficient normalized for one square unit 10^4 km^2

ENG/METU-1980 model differs from ENG-1978 model due to the presence of R9 zone (related to Ecemiş regional fault) and the absence of S4 subzone in R4 zone. They are located together east to the Akkuyu NPP site (Figure 6/5.4). Therefore, configuration of zones and seismicity parameters in R3, S3.3, R4 zones were updated. R1, R2, S2.1, S3.1, S3.2, R5, R6, R7, S7.1, S7.2 and R8 zones in METU-1980 and ENG-1978 are identical.

In 1983 METU/EERC [6/226] developed modification of the previous model provided in Figure 6.5.5.

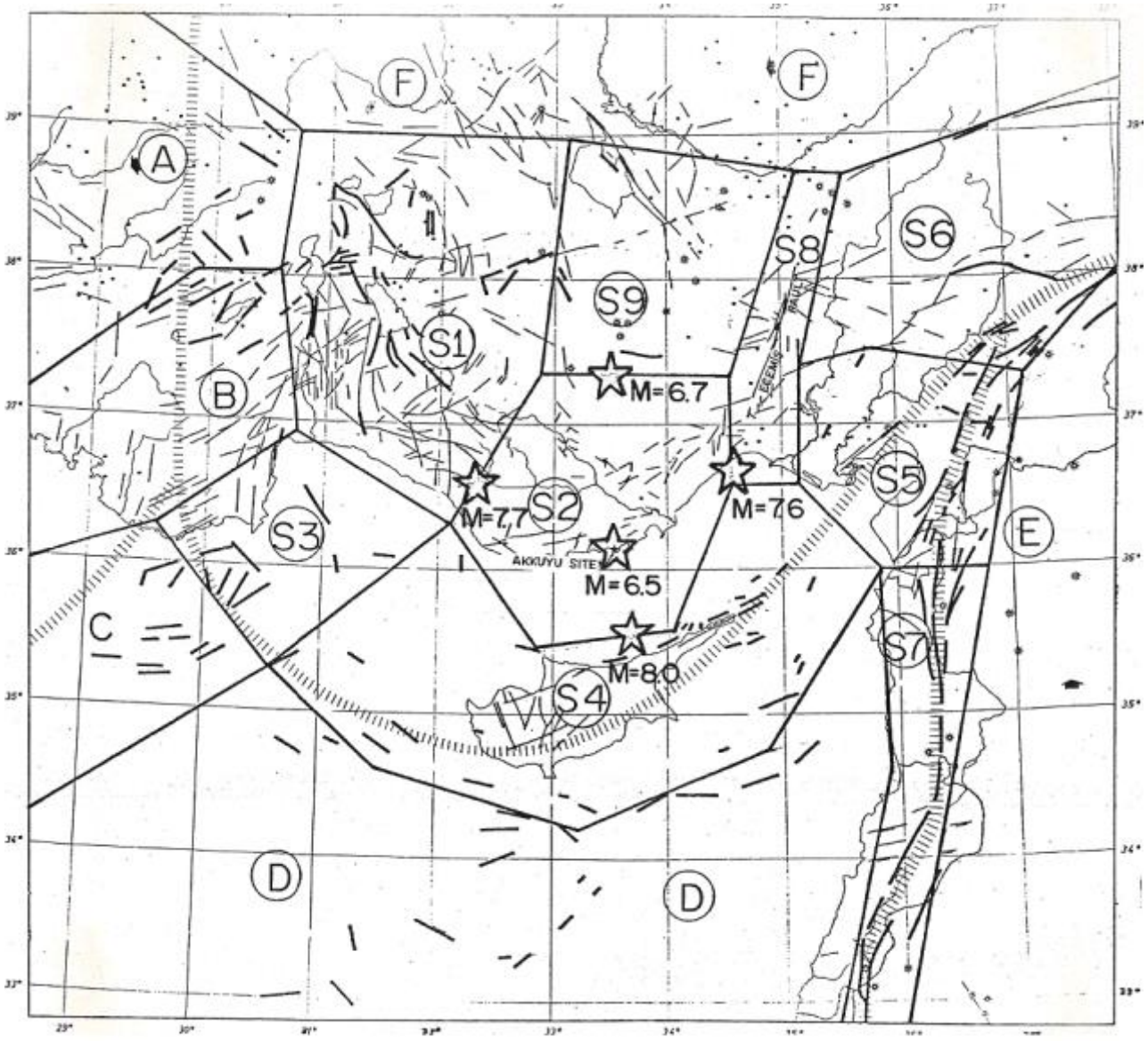

Figure 6/5.5 – Map of METU/EERC-1983 model (stars indicate reference location of earthquake sources with Mmax in SES zones that are adjacent to the site zone, at the boundaries of these zones within the nearest distance from the site) [6/226]

Seismicity parameters (per Gutenberg-Richer lgN(M)=a-bM) of ESO zones in METU/EERC-1983 model are given in Table 6/5.3

Table 6/5.3 – Seismicity parameters of ESO zones in METU/EERC-1983 model

Code of zone	N_4 (number of earthquakes with M≥4.0 in zone per one year)	a	b	M_{max} (M_S)
S1	4.2	4.51	0.97	7.7
S2	0.32	4.5	1.25	6.5
S3	2	6.11	1.2	7.6
S4	4	4.08	0.87	8
S5	10	5.44	1.11	7.6

Code of zone	N_4 (number of earthquakes with M≥4.0 in zone per one year)	a	b	M_{max} (M_S)
S6	6.61	4.3	0.87	8
S7	6.61	4.3	0.87	8
S8	0.85	3.95	0.92	7.6
S9	0.6	3.76	0.99	6.7
B	11.48	4.7	0.91	8
C	14.45	4.2	0.76	8
D	20.89	2.28	0.9	6.5

Finally METU/EERC-1983 model was modified in 1989 and is known as METU/GGRC-1989 model [6/154] (Figure 6/5.6). Structural and seismological data of the Akkuyu NPP region was considered in this model. Therefore, METU/GGRC-1989 model can be considered as significantly improved version of the previous models.

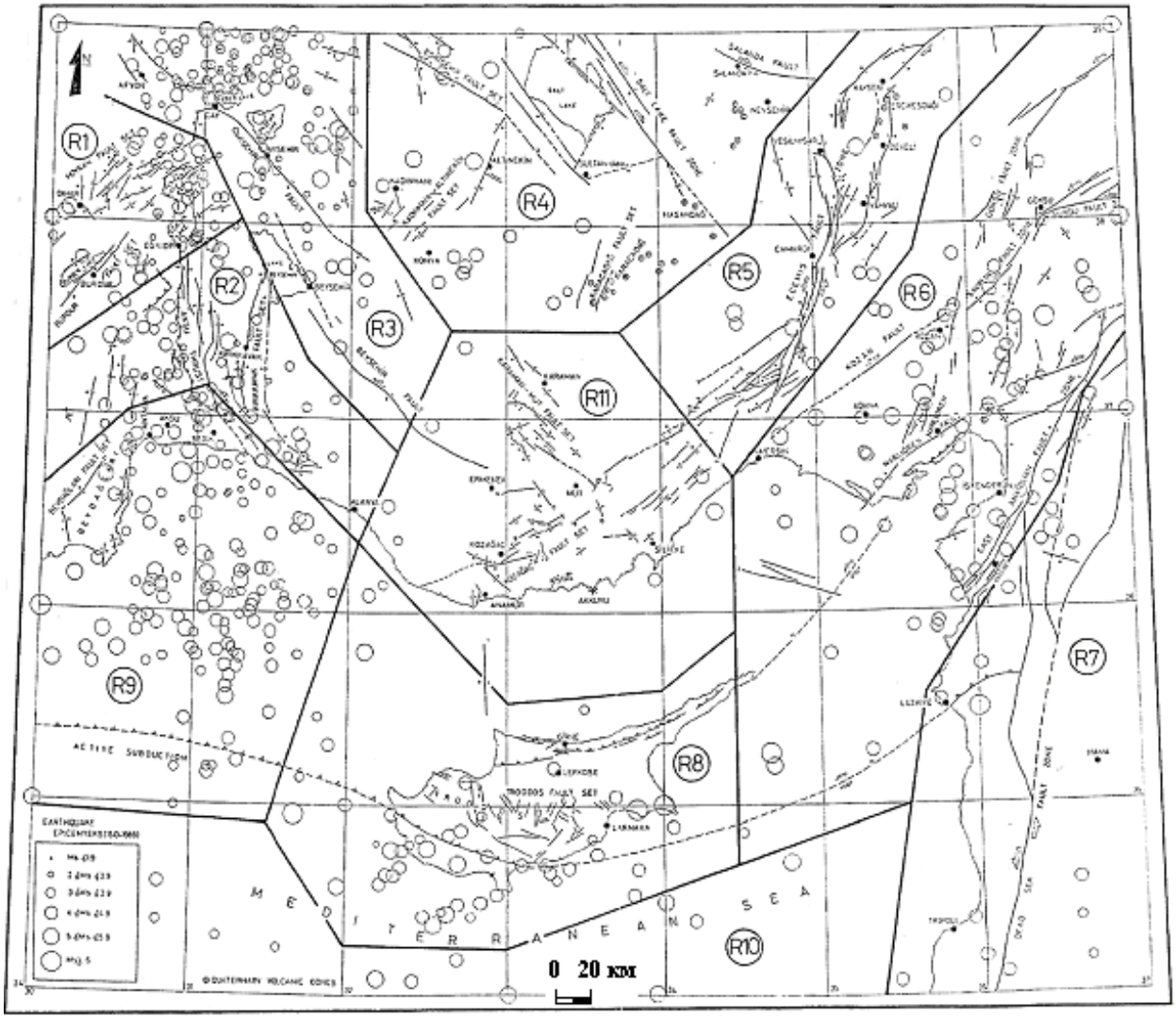

Figure 6/5.6 – Map of Modified METU/GGRC-1989 model [6/154]

Maximum earthquake potential in ESO zones of METU/GGRC-1989 model (in terms of magnitude) is given in Table 6/5.4.

Table 6/5.4 – Maximum earthquake magnitude in ESO zones of METU/GGRC-1989 model

Code of zone	R1	R2	R3	R4	R5	R6	R7	R8	R9	R10	R11
M_{max}	7.6	7.6	7.4	6.4	7.6	8.0	8.0	8.0	7.8	6.4	6.4

ENG-1978 and METU/EERC-1983 regionalizations were utilized for the approval of site parameters [6/222]. In the ENG regionalization there were 8 main source zones with sub-zones in some of these zones, whereas in METU/EERC regionalization there were 7 source zones with no internal sub-zones. The source zones encompassing the site (R4 in ENG and S2 in METU/EERC regionalization) are similar, and specifically, the critical boundaries with the Ecemiş Fault Zone to the East and the Cyprus Zone to the South were almost identical.

As seismological basis for development of the model the authors of METU/GGRC-1989 model [6/154] used the updated earthquake catalogue of the region with uniform and agreed data on earthquake hypocenters and magnitude [6/231].

6.5.4.2 RECENT SEISMOTECTONIC MODELS

In order to understand the subjective variability and include it in alternative models representing the available seismotectonic data, it is recommended by IAEA SSG-9 [6/113] to consider and use several seismotectonic models accounting for the epistemic uncertainty related with the level of knowledge on the seismotectonics in the area.

Within the restarted Akkuyu studies in 2011, four different seismic hazard studies have been performed - ENVY/BU KOERI [6/75], AEP/IFE RAS [6/117], Rizzo [6/243] and WorleyParsons [6/246]. The four studies account for several seismotectonic models since all of them took into account more than one model. For example two models developed during earlier stage of investigations were utilized. WorleyParsons utilized METU model (1980) in its original form and ENVY/BU KOERI – modified METU model (1989) (also in original form).

ENVY/BU KOERI Models

For standard seismic hazard analysis three seismotectonic models (ESO zone models) have been used. Seismotectonic regions were allocated according to the principles of [6/187]. Detailed information on elements of these models is given in [6/75].

The first model (ENVY/BU KOERI-1 model) was developed within the context of SHARE ”Seismic Hazard Harmonization in Europe“ (www.share-eu.org) and EMME ”Earthquake Model of Middle East“ (www.emme-gem.org) projects. This model describes ESO zones for the whole territory of Turkey.

Map of ENVY/BU KOERI-1 model is given in Figure 6/5.7, whereas a closer view of the region surrounding the Akkuyu NPP site is given in Figure 6/5.8. Seismotectonic features in ESO zones of ENVY/BU KOERI-1 model are given in Table 6/5.5 and Table 6/5.6.

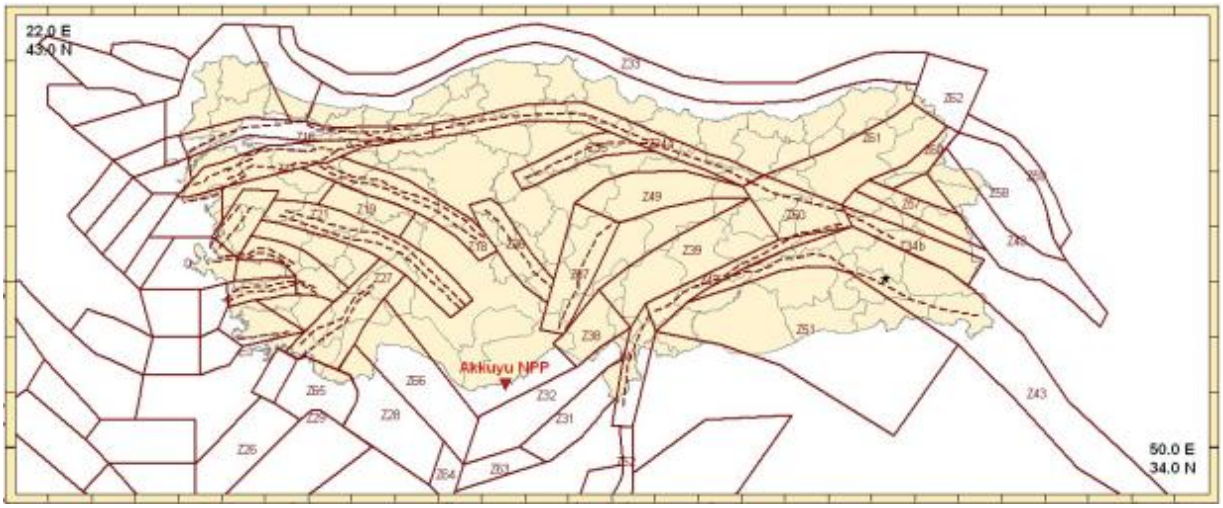

Figure 6/5.7 – Map of ESO zones of ENVY/BU KOERI-1 model [6/75]

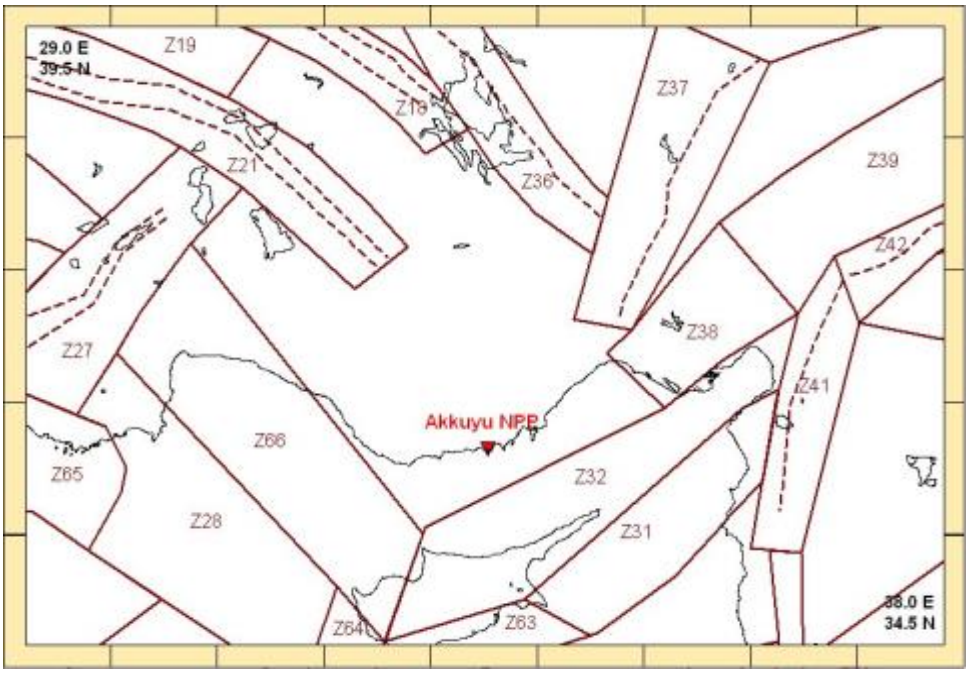

Figure 6/5.8 – Close up view of map of ESO zones of ENVY/BU KOERI-1 model [6/75]

Table 6/5.5 – Seismotectonic features in areal ESO zones in ENVY/BU KOERI-1 model [6/75]

Zone	Name	a	b	Mmax	Mmin	β	λ(Mmin)
Z18	Eskişehir Zone	4.3	1	6.6	5	2.3026	0.1995
Z19	Kütahya Zone	3.8	1	5.8	5	2.3026	0.0631
Z21	Simav-Sultandağ Zone	5.4	1.1	6.9	5	2.4985	0.9748
Z27	Fethiye-Burdur graben	7.7	1.5	6.8	5	3.4909	1.2847

Zone	Name	a	b	Mmax	Mmin	β	λ(Mmin)
Z28	Cyprian Trench-Florence Rise	4.9	1.1	7	5	2.4599	0.3726
Z31	Cyprian Trench	4.7	1	7	5	2.4025	0.3178
Z32	Cyprus Trough Misis Nikeryan	4.4	1	6.8	5	2.2913	0.2854
Z36	Tuz Gölü Zone	2.9	0.8	6.7	5	1.8421	0.0794
Z37	Ecemiş Zone	3.7	0.9	6.7	5	2.1617	0.1123
Z38	Adana Zone	4.2	0.9	7	5	2.1428	0.3455
Z39	Göksun Fault Zone	3.6	0.8	6.9	5	1.8978	0.2777
Z41	Hatay Zone	2.8	0.8	6.7	5	1.7914	0.0843
Z42	East Anatolian Fault Zone	4.5	1	6.7	5	2.2816	0.341
Z63	Cyprian Trench	6.2	1.4	7	5	3.1094	0.2941
Z64	Cyprian Trench	6.3	1.3	7	5	2.9717	0.6349
Z65	Cyprian Trench	4.6	1	7.8	5	2.2347	0.5757
Z66	Aksu thrust	5.5	1.1	6.7	5	2.5356	0.8956
ZBK1	Cyprian Trench	5.1	1	6.5	5	2.2929	1.4217

Table 6/5.6 – Seismotectonic features in linear ESO zones in ENVY/BU KOERI-1 model [6/75]

Fault	Name	a	b	Mmax	Mmin	β	λ(Mmin)
FT18_1	Eskişehir Zone	3.98	1.01	7	6.7	2.3256	0.0016
FT18_2	Eskişehir Zone	3.98	1.01	7	6.7	2.3256	0.0016
FT21_1	Simav-Sultandağ Zone	5.11	1.09	7.3	7	2.4985	0.0033
FT21_2	Simav-Sultandağ Zone	5.11	1.09	7.3	7	2.4985	0.0033
FT27_1	Fethiye-Burdur graben	7.38	1.52	7.4	6.9	3.4909	0.0008
FT27_2	Fethiye-Burdur graben	7.4	1.52	7.4	6.9	3.4909	0.0009
FT36	Tuz Gölü Zone	2.92	0.8	7.9	6.8	1.8421	0.003
FT37	Ecemiş Zone	3.74	0.94	7.9	6.8	2.1617	0.0023
FT39	Göksun Fault Zone	2.69	0.75	7.5	7	1.72	0.0029
FT41	Hatay Zone	2.82	0.78	7.9	6.8	1.7914	0.0034
FT42	East Anatolian Fault Zone	4.49	0.99	7.9	6.8	2.2816	0.0056

The second (ENVY/BU KOERI-2 Model) was developed within the scope of target investigations for Akkuyu NPP carried out by METU/EERC in 1983 for TEK [6/222] and modified and updated in 1989 [6/154]. Inherently the ENVY/BU KOERI-2 model is identical to METU/GGRC-1989 model. Map of ENVY/BU KOERI-2 model is given in Figure 6/5.9. Seismotectonic features in ESO zones of ENVY/BU KOERI-2 model are given in Table 6/5.7.

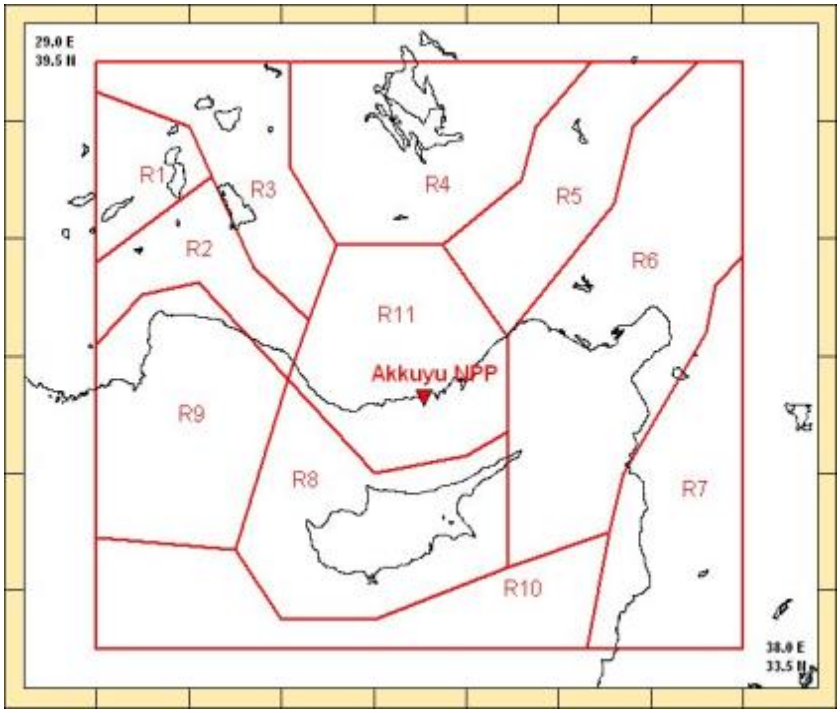

Figure 6/5.9 – Map of ESO zones of ENVY/BU KOERI-2 model [6/75]

Table 6/5.7 – Seismotectonic features in ESO zones of ENVY/BU KOERI-2 model [6/75]

ESO zone code BO3	a	b	Mmax	Mmin	β	λ(Mmin)
R1	5.3	1.24	7.6	3.5	2.7631	7.9305
R2	4.3	1.02	7.6	3.5	2.6019	5.2048
R3	5	1.07	7.4	3.5	2.8092	15.5078
R4	4.5	1.1	6.4	3.5	2.5559	4.3772
R5	5.1	1.25	7.6	3.5	3.1315	4.9848
R6	5.1	1.06	8	3.5	2.6019	22.1769
R7	4.5	1.17	8	3.5	2.8782	2.5787
R8	4.9	1.02	8	3.5	2.3026	23.4099
R9	4.7	1	7.8	3.5	2.2335	16.263
R10	3.1	0.82	6.4	3.5	1.9572	1.6562
R11	5.2	1.33	6.4	3.5	3.2466	3.7265

The third model (ENVY/BU KOERI-3 model) is modification of Model 2 where the Ecemiş fault trace is represented as a separate narrow zone and its hypothetical continuation in the SW direction.

Map of ENVY/BU KOERI-3 model is given in Figure 6/5.10. Seismotectonic features in ESO zones of ENVY/BU KOERI-3 model are given in Table 6/5.8.

In Model ENVY/BU KOERI-3 when compared to Model 2 maximum magnitude of ESO zone R11 was revised. Mmax=6.0 is designated to R11 zone in Model 3, and Mmax=8.0 to Ecemiş fault zone.

Model ENVY/BU KOERI-3, according to [6/75], has a "trial" purpose. The narrow Eñemiş fault zone "introduced" in zone R11 of Model ENVY/BU KOERI-2 and located at a distance of about 25 km from the NPP site, is considered as a conservative assumption.

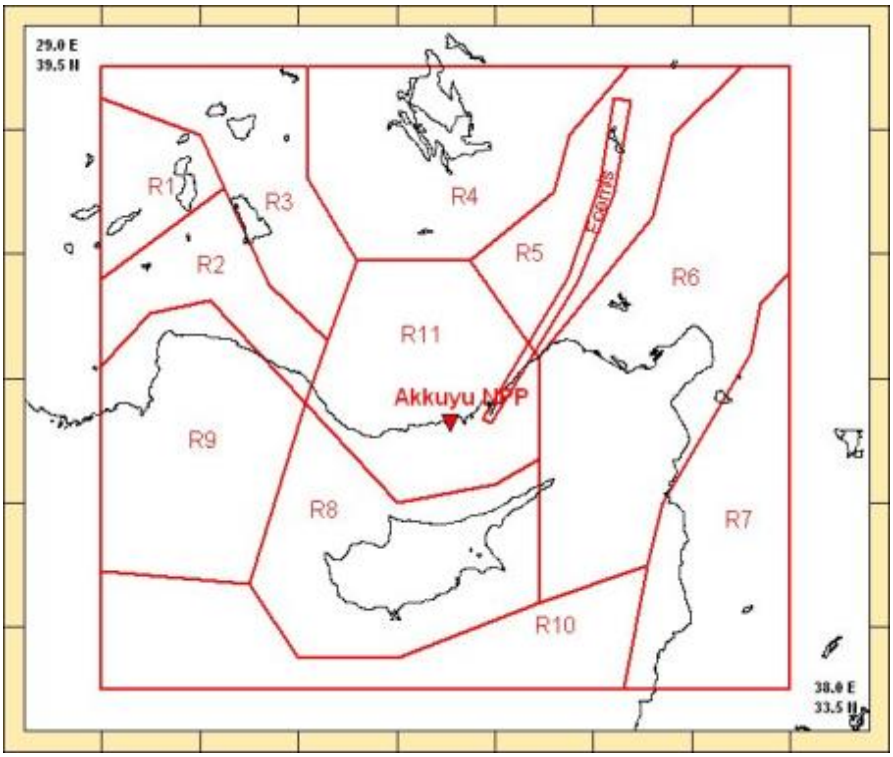

Figure 6/5.10 – Map of ESO zones of ENVY/BU KOERI-3 model [6/75]

Table 6/5.8 – Seismotectonic features in ESO zones of ENVY/BU KOERI-3 model [6/75]

ESO zone code	a	b	Mmax	Mmin	β	λ(Mmin)
R1	5.3	1.24	7.6	3.5	2.7631	7.9305
R2	4.3	1.02	7.6	3.5	2.6019	5.2048
R3	5	1.07	7.4	3.5	2.8092	15.5078
R4	4.5	1.1	6.4	3.5	2.5559	4.3772
R5	5.1	1.25	7.6	3.5	3.1315	4.9848
R6	5.1	1.06	8	3.5	2.6019	22.1769
R7	4.5	1.17	8	3.5	2.8782	2.5787
R8	4.9	1.02	8	3.5	2.3026	23.4099
R9	4.7	1	7.8	3.5	2.2335	16.263
R10	3.1	0.82	6.4	3.5	1.9572	1.6562
R11	5.2	1.3314	6.0	3.5	3.2466	3.7265
Ecemiş	1.8	0.6482	8.0	3.5	1.4925	0.3751

Earthquake recurrence parameters of zones in ENVY/BU KOERI models (Guttenberg-Richter) were determined using maximum-likelihood method.

IPE RAS Model

IPE RAS model was developed by the O.Yu. Schmidt Institute of Physics of Earth of the Russian Academy of Sciences (IPE RAS) [6/117].

When selecting width and configuration of the zones priority was given to more conservative solutions. When a large region is studied, moving away from the site, the precision decreases and the generalization increases. Such approach is justified from the point of view of optimal strategy and does not affect the final results adversely. In fact, the IAEA SSG-9 [6/113] recommends a graded modeling in which the scale of investigation gets coarser as the distance to the site increases.

Resulting from seismotectonic studies, seismological observations and interpretation of archive and published materials, the following ESO zones can be specified in IPE RAS Model in the NPP site region (300 km circle):

(1) Ecemiş ESO zone is traced in geodynamic zones of Central Taurus and eastern part of Cilician Taurus. The general orientation of the ESO zone is south-south-west. Its length is about 100 km. The zone is characterized by expected earthquake maximum magnitude 7.5. The zone is traced locally in the sedimentary cover as a system of sub-parallel active faults by geological methods and space images. Pre-Alpine basement within the Ecemiş fault zone is located at 10-12 km depth.

(2) Tuz Gölü ESO zone strikes south-east. It is 200 km long and 60 km wide. Maximum expected magnitude for this ESO zone is 7.0. Several active faults reaching the surface are located there: Bezirji, Tuz and others forming en-echelon system characteristic for right-lateral displacement. Fault kinematics is right-lateral strike-slip. Small earthquakes (M= 2 – 4) are recorded at 10 km depth. Therefore, the zone passes through the sedimentary cover and reaches upper horizons of the basement. The shortest distance from the site is 100 km.

(3) Beyşehir ESO zone belongs to the northern part of diagonally striking western Taurus geodynamic province and is associated to Beyşehir active fault zone and its accompanying folds. The ESO length is 250 km and its width is 60 km. Maximum expected earthquake magnitude for the zone is 6.5. Kinematics of displacements is right-lateral strike-slip with normal faulting. The zone is expressed on the surface as en-echelon system of south-east and south-south-east faults. In the northern part of the zone earthquakes with magnitudes 5 to 6 are recorded. Minimum distance from the NPP site is 80 km.

(4) Kadınhan-Altınekin ESO zone total length is 100 km; its width is 50 km. The zone strikes north-east. Maximum expected earthquake magnitude is 6.5. On the surface, the zone coincides with the system of faults expressed by the set of closely located faults demonstrating small amplitudes of left-lateral normal faults forming en-echelon system of faults characteristic to left-lateral displacements. Normal faults with strike-slip component is accumulated in micro-grabens disturbing Miocene, Pliocene, Pleistocene and even Holocene layers. The earthquake sources are located within all 10 km of the sedimentary cover. There are no evidences that tectonic disturbances of this ESO zone reach the basement. The shortest distance from the NPP site is 100 km.

(5) Kozan ESO zone belongs to the southern part of diagonally stretching central Taurus geodynamic province and is associated with Kozan-Savrun zone of active faults and accompanying folds of central and eastern Taurus. The zone length is 150 km; its width is 50 – 80 km. Maximum expected earthquake magnitude is 7.0. Displacement kinematics along faults is left-lateral strike-slips. On the surface the zone is expressed as linear system of south west and south-south-west ruptures. There are earthquakes with magnitudes from 3 to 6.5 recorded within the zone. Minimum distance from the NPP site is 110 km.

(6) North Cyprian ESO zone has total length of 600 km and 50 – 100 km width. It has arc-wise shape. Maximum expected earthquake magnitude is 7.5. On the surface the zone coincides with faults of the same orientation and is expressed by close system of overlapping trusts. Actually, these faults can be seen only in northern part of Cyprus. In other parts the ruptures are hidden by the sea and recognized by geophysical methods. In western part the zone coincides with geodynamic zone of Antalian sigmoid presented by system of tectonic nappes and modern meridianal ruptures located in the sea-shore part of the Antalian Gulf. The zone demonstrates seismic activity. Several earthquakes up to magnitude 6.5 were recorded within the ESO zone. The hypocenters are located within the sedimentary cover up to 20 km depth. The nearest distance from the NPP site is 100 km.

(7) Marine Cyprian ESO zone extends up to 800 km and has 50 – 150 km width. It has arc-wise shape. Maximum expected earthquake magnitude is 8.0. On the bottom of the Mediterranean Sea the one coincides with fault system on the continental shelf of southern Cyprus and Levant trench. The system of seismogenic ruptures is expressed by the set of listric overlapping trusts. These faults can be found only on the seismic prospecting profiles crossing the island arc [6/194]. In general the whole zone is covered by the sea water. The zone is seismically active. Several earthquakes with magnitudes up to 7.5 are recorded within this zone. The hypocenters are located within 70 km of the sedimentary cover. The nearest distance from the NPP site is 200 km.

(8) Antioch ESO zone is traced through geodynamic zone of eastern Syria and Dead Sea rifts, starting from the place of their coupling with East-Anatolian system of left-lateral seismic active faults. The general trend of the zone is south-south-west. Its length is 300 km; width is 30-40 km. The zone is characterized by maximum expected earthquake magnitude 8.0 and left-lateral kinematics of displacements. The zone is traced in the sedimentary cover in form of sub-parallel active faults by geological methods and by remote sensing methods. The zone is very clearly expressed in the modern seismic activity. The nearest distance from the NPP site is 180 km.

Map of IPE RAS Model is given in Figure 6/5.11. Information on the ESO zones is summarized in the Table 6/5.9. The zone numbers in the table correspond to the numbers on the ESO zone map.

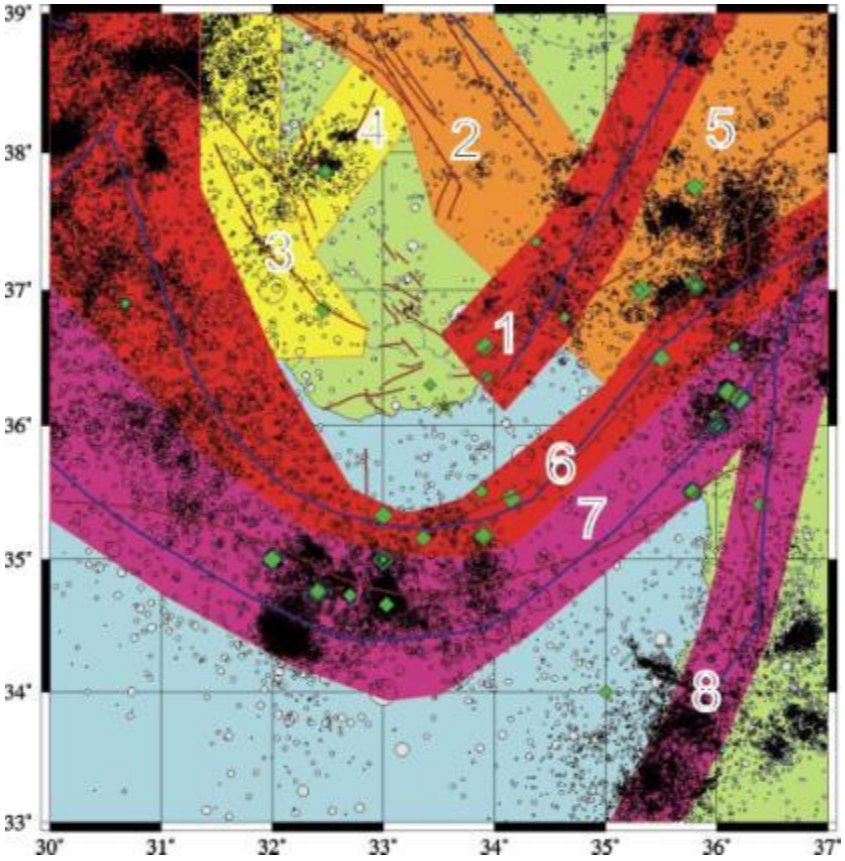

Figure 6/5.11 – The ESO zones of the IPE RAS model [6/117]. Earthquake epicenters of instrumental (circles) and historical (rhombs) time-periods are shown. Faults (brown lines) are shown according to the ENVY/BU KOERI materials [6/75]; blue lines – main tectonic elements according to [6/102]

Table 6/5.9 – Maximum Magnitudes of Earthquakes for ESO zones in IPE RAS Model [6/117]

Zone	Name of zone	Mmax	Displacement type
1	Ecemiş	7.5	Left-lateral S
2	Tuz	7.0	TS
3	Bevsehir	6.5	Right-lateral SN

Zone	Name of zone	Mmax	Displacement type
4	Kadınhan-Altınekin	6.5	Left-lateral NS
5	Kozan	7.0	TS
6	North Cyprian	7.5	TS
7	Marine Cyprian	8.0	Subduction
8	Antioch (Levant)	8.0	Left-lateral S

The magnitude-frequency relationship of Gutenberg-Richter is one of the universal seismological laws. Significant departure of lg N(M) graph from straight line usually reflect low data quality or other deficiencies in the catalogue. A magnitude-frequency graph for the earthquake catalogue within the selected region is presented in Figure 6/5.12.

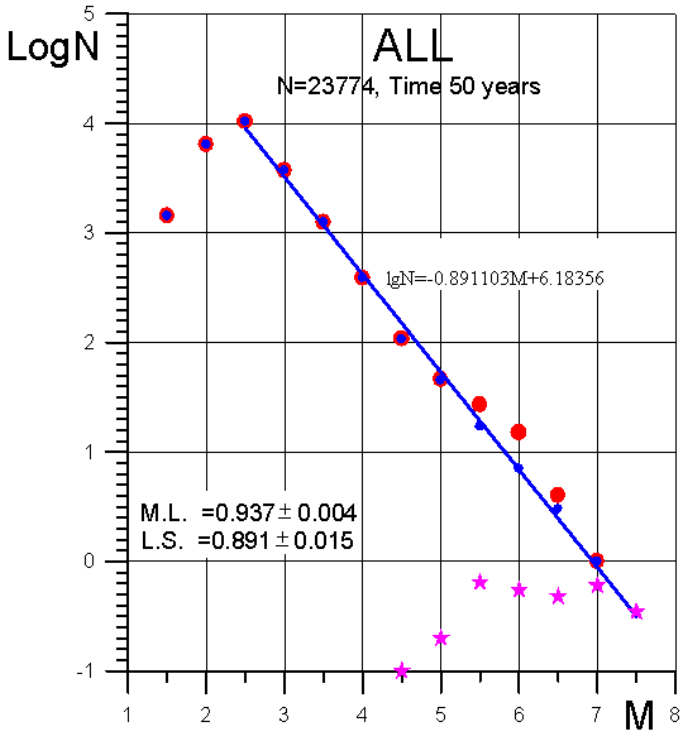

Figure 6/5.12 – Frequency Graph for the Studied Region [6/117]

This graph presents earthquakes in the last 50 year. Earthquakes since 1900 are indicated with red dots as well. It is clear that before 1960 the catalogue is not complete. Historical earthquakes are presented in the graph with stars. Data is normalized only in the time domain. It is clear that historical catalogue is far from being complete. Only the earthquakes M≥7.5 are considered completely reported throughout the catalogue. On all graphs the following notation is used: M.L. – maximum likelihood method, L.S. – least square method (truncated principal axes). The regression line is in blue colour. It's mathematical expression is given on the graph.

Magnitude-frequency graphs for selected ESO zones are provided in Figure 6/5.13 and for the diffuse seismicity in Figure 6/5.14. Data is normalized to 50 year interval (blue circles) but not

on the area. On all graphs the green line corresponds to data since 2000. These data is not used for further calculations, but is useful as quality (completeness) control.

For PSHA the magnitude frequency is obtained by the maximum-likelihood method (L.S.).

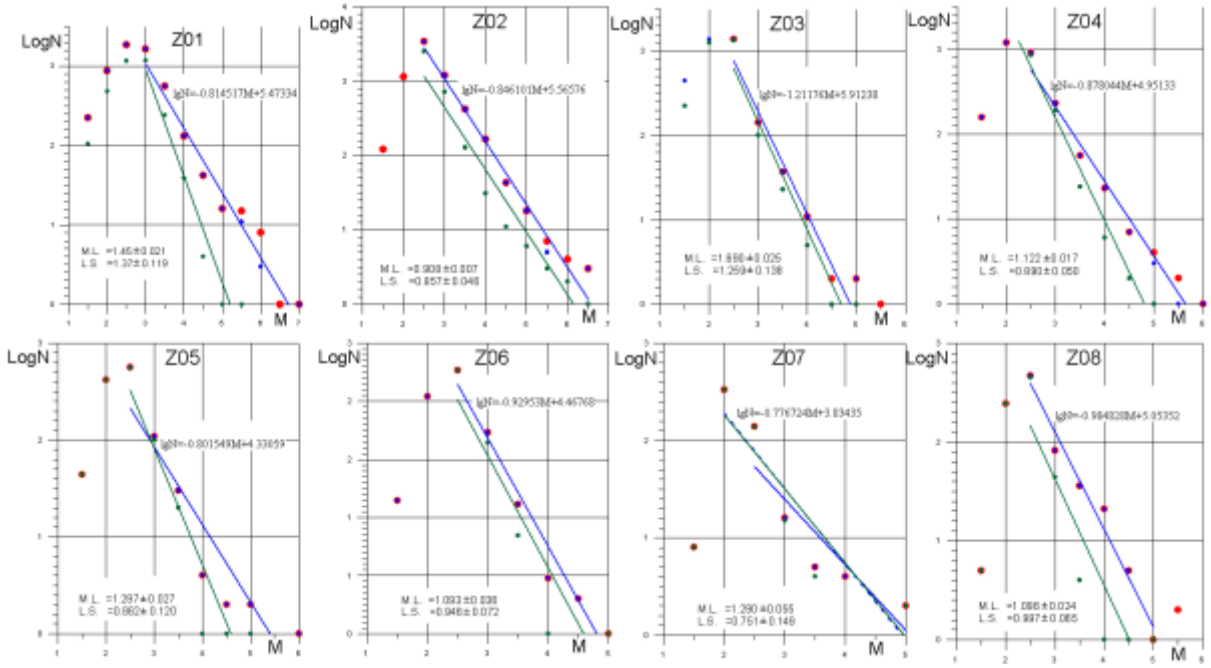

Figure 6/5.13 – Magnitude-Frequency Graphs for Selected ESO Zones [6/117]

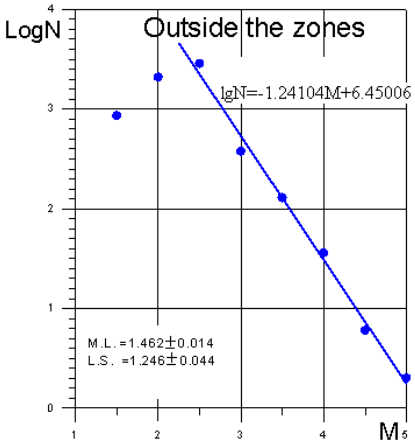

Figure 6/5.14 – Frequency Graph for Diffuse Seismicity (Outside of the ESO Zones) [6/117]

Evaluation of background earthquake potential

Seismicity at global scale is associated with plate boundaries. But as the experience shows not always an earthquake can be spatially linked to known faults. Of course, after the earthquake occurred it always can be related to some geological structure. It follows from the fact that the earth crust structure is very complicated at different spatial scales. Practically in any seismoactive region one can find some faults (active or not, recognized based on that or the other features, etc.).

Therefore it is very useful at earlier stages to study the inherent structure of seismicity without preliminary geological and tectonic assumptions, based only on spatial distribution of earthquakes [6/165]. Further comparison of the inherent seismicity structure with geological and geophysical data can bring new information on the regional seismotectonic features.

Developing the methods of cluster analysis to the seismicity studies the concept of concentrated and dispersed spatial components of seismicity was suggested in [6/165 and 6/193] (see Figure 6/5.16). Even without strict formal definitions, dividing seismicity into spatial components can help to reveal inherent regularities of the seismicity. It is assumed that the earthquake epicenters close to each other compose concentrated component of the seismicity; while the ones located far from each other form the dispersed component.

Division of seismicity into components is done in two stages. At the first stage based on cluster analysis the epicenter groups are recognized. Clusters composed by number of earthquakes less than the given threshold are considered as part of the dispersed component, while the ones including number of earthquakes above the threshold are classified as concentrated component. To define the threshold value, distribution of clusters versus the number of earthquakes composing them is studied. Usually the distribution is not homogeneous and its peculiarities are used to define the threshold.

To control the quality of subdivision, Morishita index is used [6/158] (Figure 6/5.15). Such independent control is useful because the algorithm of partitioning has several free parameters that have to be adjusted. From the graph it is clear that different spatial components significantly differ according to the index.

According to this solution, the maximum observed earthquake within the dispersed component has magnitude 5.0. This magnitude is representative for time period since 1960. To evaluate the maximum expected background earthquake magnitude a 0.5 increment to the maximum observed value is added. This approach is quite usual in the seismological practice. Finally, it is assumed that in any place within the study region can occur earthquake with Mmax=5.5.

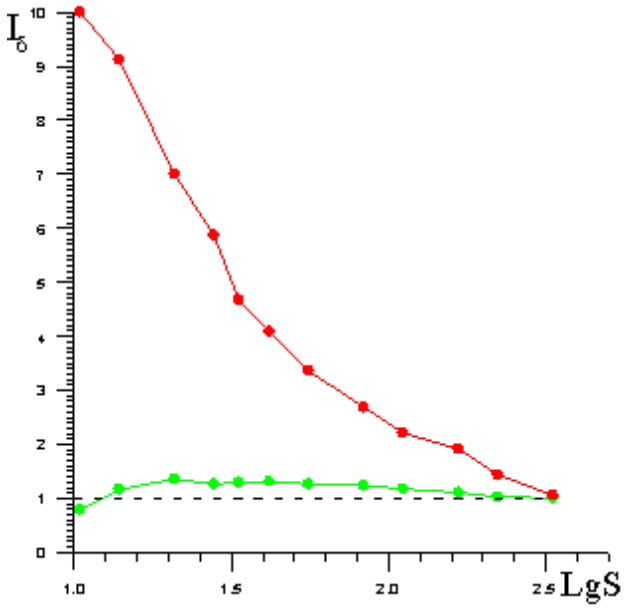

Figure 6/5.15 – Morishita Index Graph for Seismicity of Territory [6/117]

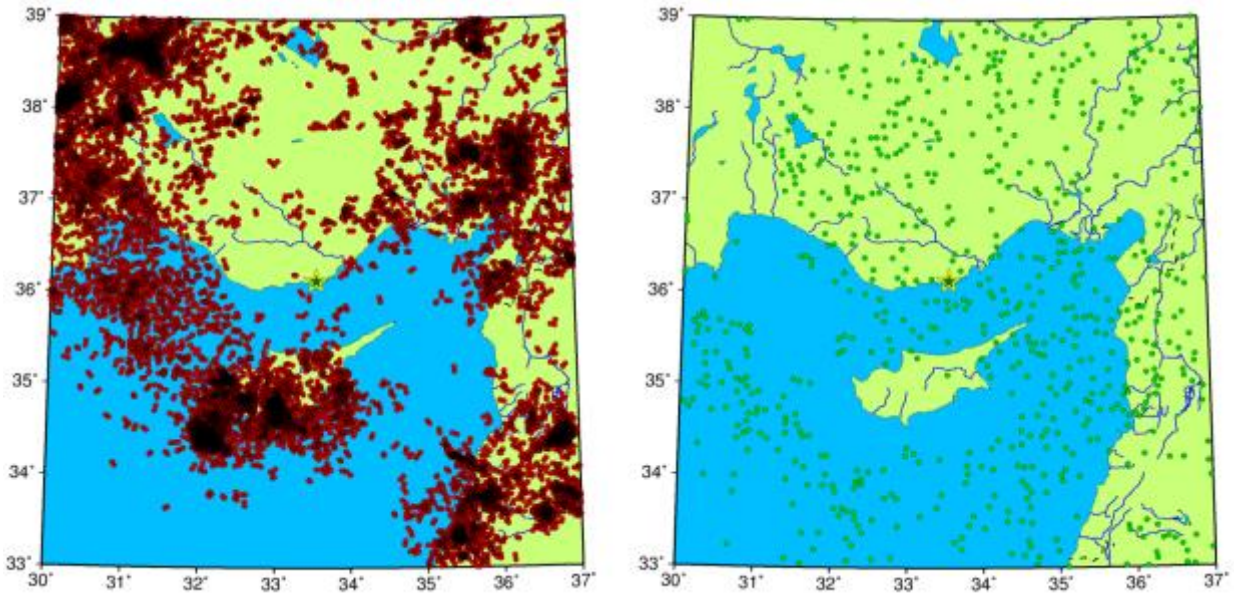

Figure 6/5.16 – Seismicity of the Region (Left – Concentrated Component; Right – Dispersed Component) [6/117]

WP Models

Model B

WP Model (Model B) was developed by WorleyParsons in 2011-2012 [6/246]. A thorough evaluation of the most prominent tectonic elements in the area (extending more than 350 km radius from the site) is performed: in the western part of Turkey – Fethiye-Burdur fault zone, Antalya Gulf fault zone, Akshehir, Beysehri, Karaman faults; in the eastern part of Turkey – east part of the Anatolian fault and its branching, Sivas fault, Tuz Gölü fault; in the south the tectonic structures

belong to the Hellenic and the Cyprian trenches. Most of these faults are significant seismic sources.

The WP Model (presented in Figure 6/5.17) has been developed on the basis of the available geological evidence of active tectonic movements in the regional area. Thus, each zone corresponds to a specific active fault system delineated in published scientific papers and reports. The description of each zone has been focused on available quantitative estimates of fault parameters (e.g. length of single fault segments, long term and short term slip rates) that allow to constrain the degree of active tectonics and to estimate the Mmax value based on [6/204] and [6/238].

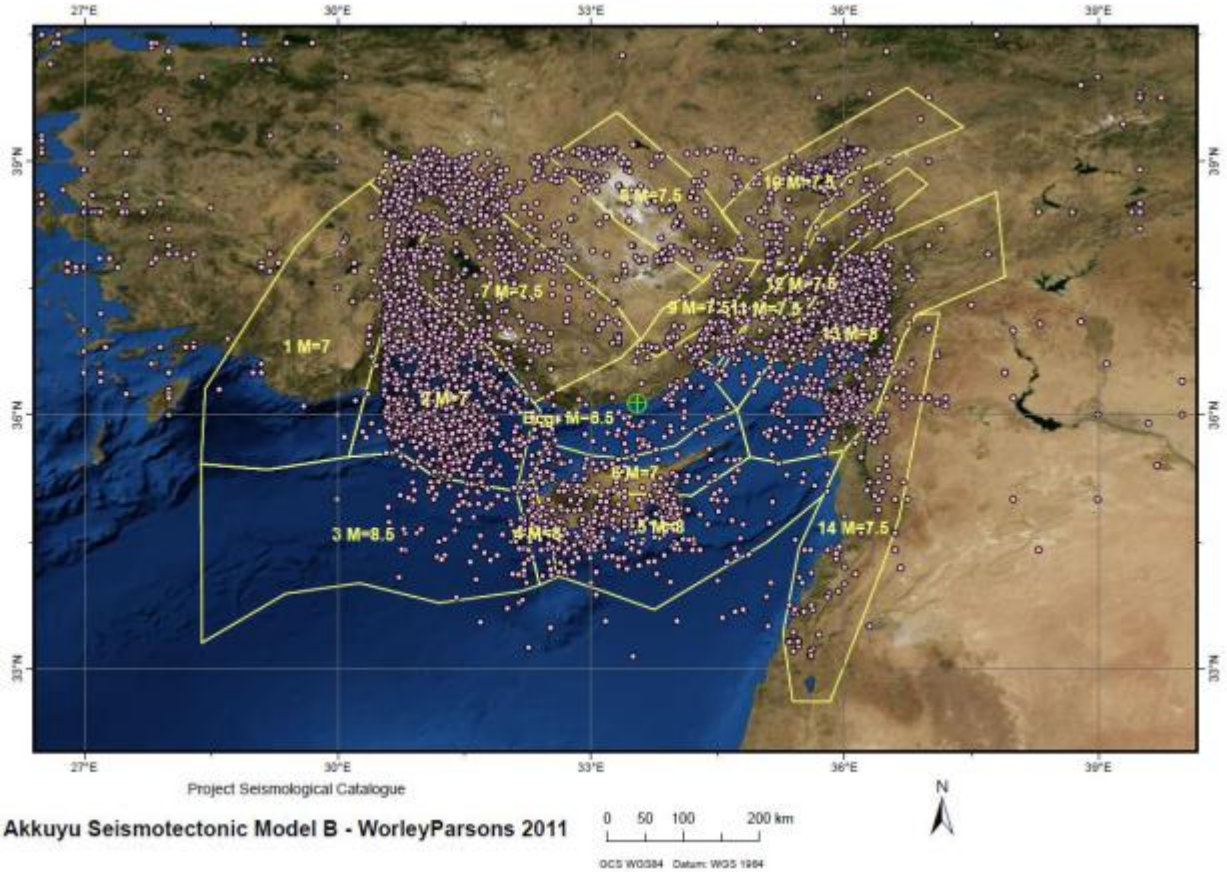

Figure 6/5.17 – Map of Model B ESO zones [6/246]

Model B includes the following zones:

<u>Zone 1 – Fethiye-Burdur fault zone</u>

The FBFZ is defined by NE–SW trending major faults with numerous NW–SE trending shorter faults representing extensional features in a 50 km wide shear zone [6/126 and 6/103]. Several medium to large earthquakes, with different fault plane solutions, occurred in this zone. The 1957(M = 7.1) Fethiye earthquake and other historical earthquakes (417 and 7th century AD, along Cybra Fault) show evidence of left lateral motion [6/126] and, according to [6/24], this left-lateral

motion is corroborated by GPS measurements showing a movement of at least 15 mm/yr. The 1914 (M=7) and 1971 (M=6.2) Burdur earthquakes indicate normal motion predominantly. The October 3, 1914, Burdur earthquake is associated to a 23 km fault rupture along the southeast coast of the Burdur Lake [6/85]. Oblique slip normal faulting controlled the margins of several extensional basins. Geological and archeological data, in agreement with historical and modern seismicity, consistently provide a Mmax value equal to 7.5.

Zone 2 – Antalya Gulf

This zone is characterized by deep seismicity. The distribution of deep earthquakes suggests that subduction takes place west of Cyprus in the Antalya basin and underneath southern Turkey [6/120, 6/30, 6/11 and 6/235]. This region is also characterized by compressional deformation of shallow young sediments [6/16]. North-south trending reverse faults are locally reactivated as normal faults. The largest recent earthquake occurred on May 28, 1979(M= 6.0). The Mmax is estimated equal to 7.0.

Zone 3 – Eastern Mediterranean subduction zone – Florence Rise

The zone 3 encloses the northeastern sector of the Mediterranean Ridge. According to [6/138] and [6/235], the Mediterranean Ridge is affected by reverse faulting and associated earthquakes, under the influence of the active compression to the north (along the Aegean–Cyprus Trench). In fact, seismic profiles show clear thrust structures (reverse faults) in the deformation front of the accretionary wedge. The seismicity record is characterized by reverse faulting focal mechanisms as well as NW-SE and NE-SW trending strike-slip faults. The convergence rate increases northwestward from Cyprus to the Anaximander Seamount and is in the range of 9 – 14 mm/yr [6/235]. The largest earthquake recorded in IRIS catalogue is M=6.7 (9 October 1996) but, on the basis of geological constrains Mmax=8.5 is assigned.

Zone 4 – Western Cyprus (Paphos fault zone)

The major structural element of this zone is the NE-SW trending dextral transform fault (Paphos transform fault), associated with intermediate depth seismicity. Associated with this fault is the October 9, 1996, (M= 6.8) earthquake. According to [6/178], this earthquake has produced a fault rupture 30 km long and 15 km wide. The 1996 epicenters occurred at a depth of 76 – 85 km [6/181]. The convergence rate is 7 – 8 mm/yr [6/235]. Mmax in this zone is equal to 8.0.

Zone 5 – Southern Cyprus

The zone 5 corresponds to the central sector of the southern Cyprian Trench which has a similar geometry to the Hellenic Trench. However, the convergence across the Hellenic Trench is about two-three times faster than across the Cyprian Trench. Subduction of the African plate under

the Hellenic Trench is continuous. However, diffuse seismicity and distributed contraction suggest that the Cyprus Trench is in transition form subduction to collision. Eratosthenes Seamount, a continental fragment of the African Plate, is drifting northward towards Cyprus. Its impinging on the Cyprus Trench is partly responsible for the uplift of Cyprus [6/147 and 6/104]. The subducted Slab is detached [6/89] or steep and segmented, perhaps in Early detachment phase [6/32]. The depth of earthquakes increases northward from shallow to intermediate. The most recent significant earthquakes are related to Lemessos and Larnaka oblique thrust faults with max rupture length of 24 km and displacement of 72 cm max (24 June 1896 earthquake, M=6.5) [6/178]. The maximum historical earthquake is that occurred on 342 AD (Mw=7.4).The maximum estimated earthquake magnitude is 8.0.

Zone 6 – Northern Cyprus

The northern part of the island is characterized by the Kyrenia fold/thrust belt that preserves evidence of passive and active margin phases, the latter involving both strike-slip and thrust faulting. The uplift of the Kyrenia range occurred in the mid-late Pliocene, but is continuing to the present [6/8]. North of the range, east-west trending north- dipping normal faulting took place. Historical and recent seismicity of Cyprus is concentrated in the southern and western sector which is why the maximum estimated magnitude for the northern part is 7.0.

Zone 7 – Aksehir, Beysehri, Karaman fault

This zone is characterized by prevalent NW-SE trending normal faulting, locally with strike-slip component, in some cases along older thrusts, as evidenced by the recent Sultandağı earthquakes (2000, 2002) with Mw=6.3. The latter showed predominantly normal faulting mechanisms and took place on the “well-known Sultandağ thrust fault” [6/10]. Some paleoseismic events have been identified along the Konya fault zone but not yet dated [6/6]. This fault zone, with prevalently NE-SW trending east-dipping normal slip faults, extends in length for about 65 km. The Aksehir Master Fault borders the Aksehir-Afyon graben (130 km long, 4 – 20 km wide) and shows oblique-slip motion with a minor right-lateral strike-slip component. The maximum rate of motion is about 0.3 mm/yr [6/134]. Mmax is 7.5.

Zone 8 – Salt Lake – Tugzolu faults

Prevalent tectonic movements in this zone occur along NNW-SSE trending right lateral strike-slip faults. Locally normal or reverse components may become relevant. Several moderate events, with magnitudes slightly larger than 5 have been instrumentally recorded. The active structures located in this zone are part of an about 15 – 25 km wide, 400 km long active fault system consisting of three main fault zones. So, the average length of each individual fault zone

should be larger than 100 km. Mmax value of 7.5 has been estimated based on this assumption in a conservative way, considering the Mmax – SRL relationships provided in [6/238].

Zone 9 – Central Anatolian fault zone (CAFZ)

In this zone prevalent tectonic movements occur along NE-SW trending left lateral strike-slip faults, locally with normal or reverse component. Modern seismicity records reveal a M = 6.2 earthquake (at about 180 km from the NPP site) and several other events with magnitude ranging between 5 and 6. Length of fault segments is in the order of 100 km (e.g. the Sulucaova-Pozanti segment, [6/133]). Long term slip rates could be larger than 1 mm/yr: this value has been evaluated along the Kizihirmak fault segment, based on the amount of left lateral offset of Oligo Miocene deposits [6/115 and 6/174]. Quaternary slip rates could be larger than 2 mm/yr: in fact, different fault segments located in this zone have systematically displaced stream beds with values in the order of several kilometers [6/133]. This geological evidence is in good agreement and consistent with a Mmax value equal to 7.5.

Zone 10 – Sivas faults

In this zone tectonic movements prevail along ENE-WSW trending left lateral strike-slip faults. A historical event (1205, M=6.5) occurred in this zone. Fault segments located in this zone constitute the NE prosecution of the CAFZ, forming a series of pull-apart basins. The longest among them (Erciyes basin) is about 120 km long. Quaternary activity is pointed out by Plio-Quaternary terrace conglomerates that have been elevated and dissected and Plio-Quaternary fissure eruption-induced basaltic plateaus [6/133].

Zone 11 – Ecemiş fault zone

This zone comprises the SE portion of the CAFZ, including the so-called Ecemiş corridor. NNESSW trending left lateral strike-slip tectonic movements typically occur along this fault zone. Instrumental seismicity reveals only moderate events in this zone (magnitudes between 5.0 and 5.5). Considering the total offset constrained between 60 and 90 km [6/122, 6/196 and 6/247] since the Oligocene – Miocene time, long term slip rates are in the order of 3 mm/yr. Quaternary slip rates are also in the order of 3 mm/yr [6/133, 6/27 and 6/28]. This estimate is based on the amount of displacement of active stream courses. Other geomorphic features showing the recent activity of these faults are shutter ridges, pressure ridges and warped terraces. This geological evidence is consistent and allows t a conservative estimate of the Mmax value equal to 7.5.

Zone 12 – Kozan Göksu fault zone

This zone comprises two fault zones (Kozan and Göksu) mainly characterized by NNE-SSW trending left lateral tectonic movements. A historical earthquake (1268) with M = 6.2 is

located in this zone. Long term slip rates have been provided by [6/241] along the Göksu fault as equal to 2 mm/yr. Moreover, since these active faults are located between the Ecemiş fault and the EAFZ, the length of fault segments is expected to be comparable to those located in the adjacent zone, i.e. at least 100 km. This evidence allows constraining the Mmax in this zone to 7.5.

Zone 13 – Eastern Anatolian fault zone and Adana Basin

The Eastern Anatolian fault zone is characterized by mainly NE-SW trending left lateral strike-slip tectonic movements. A strong historical earthquake (526 AD; M = 7.9) along the EAFZ took place within this zone. Instrumental seismicity has never registered here events larger than M=6. Long term slip rates have been estimated in the order of 10-11 mm/yr [6/47 and 6/189] or 9 mm/yr [6/248]. These values have been based on the total offset along the EAFZ (up to 30 km) in the last 3 – 4 Ma. Space geodesy data have provided quite consistent values. Based on the abovementioned geological constraints and in agreement with the documented historical event, it is possible to estimate Mmax in this zone equal to 8.0.

Zone 14 – Dead Sea Fault

The Dead Sea Fault is a north-south trending left lateral transform fault, extending for about 1000 km. A strong earthquake (M = 7.4) occurred in 1992 along the southern portion of this fault. Total offset since Middle Miocene has been slightly larger than 100 km [6/26, 6/91 and 6/241]. Thus, long term slip rates are in the order of 7 mm/yr. The offset of Late Pleistocene to Holocene geomorphic features in the southern portion (Araba Valley) has allowed to constrain the short term slip rates between 2 and 6 mm/yr [6/132]. According to [6/96], Holocene slip rates along the Serghaya fault segment (Lebanon) are in the order of 1 – 2 mm/yr. The occurrence of M>7 earthquakes has been demonstrated also by archeological and paleoseismological studies, that pointed out the coseismic reactivation of an about 100 km-long segment of the DSF in historical time (749 AD, [6/145]) and coseismic fault displacement of 2.2 m (1458 AD earthquake, [6/96]). So, geological, archeological and paleoseismic data, in agreement with historical and modern seismicity, consistently provide a Mmax value equal to 7.5.

All the sectors of the regional area out of these zones, including the near regional area, are characterized by diffuse seismicity. To these areas in WorleyParsons investigations "…a background value of Mmax equal to 6.5 has been conservatively assigned".

WP METU 1980 Model (Model C)

This model was developed by METU and ENG in 1980 [6/65] and accepted in its original form as one of two alternative models in the probabilistic seismic hazard analysis performed in 2011 by WorleyParsons group in order to represent epistemic uncertainty in modeling. Map of

METU 1980 Model is shown in Figure 6/5.18. This model includes nine ESO zones. Zone R4 in which the NPP site is placed has Mmax=6.0.

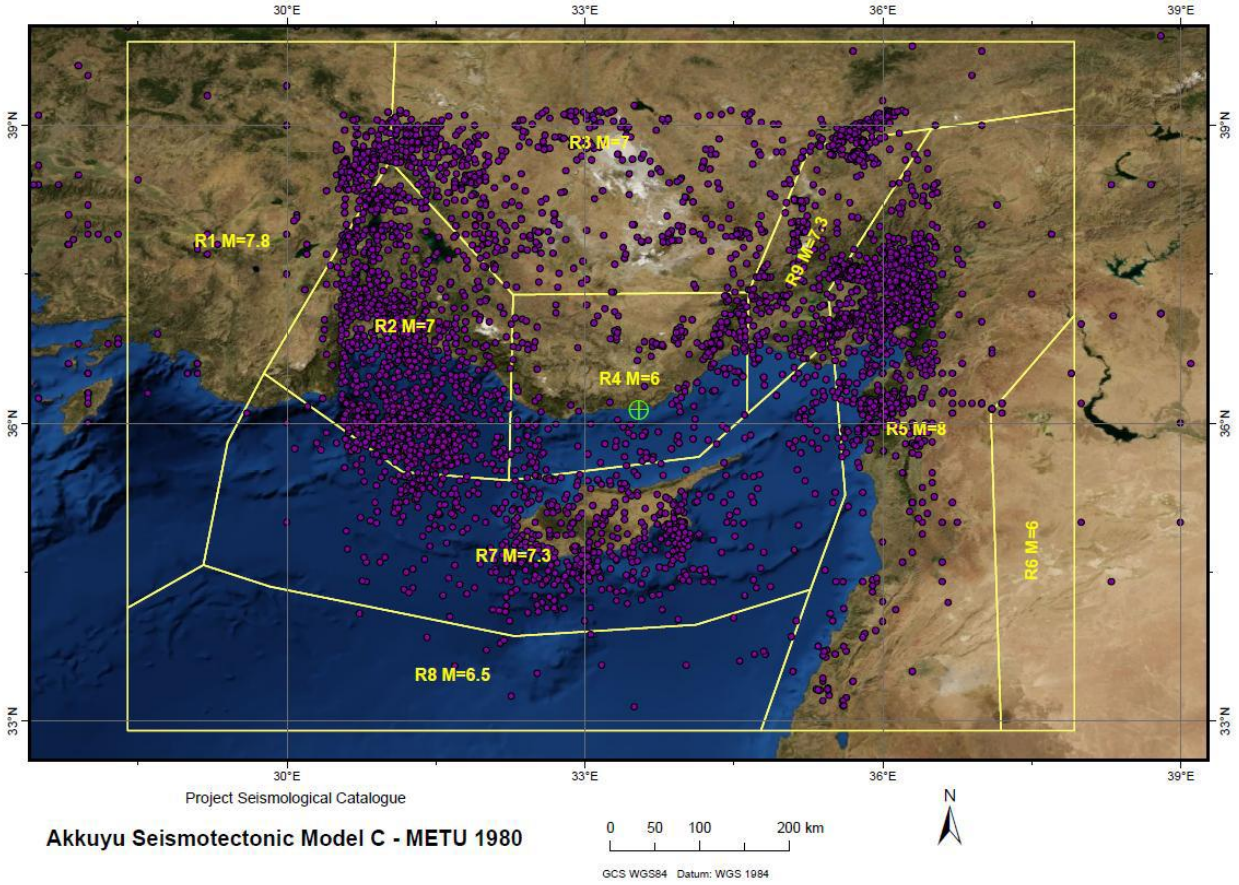

Figure 6/5.18 – Map of METU-1980 Model (Model C)

Detailed characteristics of Models B and C prepared by WorleyParsons and other SHA input data are given in Appendix N.

Rizzo 2011 Model

Rizzo 2011 Model consists of 16 ESO zones, however the overal configuration has several alternatives. A special feature of Rizzo zoning pattern [6/243] is breaking the Cyprian Trench zone into a number of smaller subzones (zones 4, 5, 6, 7, 8). Exactly the same, the Dead Sea fault zone is split into two (zones 9 and 10). The Ecemiş fault zone (zone 13) is presented by two alternatives, close to ENVY/BU KOERI-2 and ENVY/BU KOERI-3 model zones. Two alternatives have been evaluated for the configuration of zone 16 (Namrun).

Source Zone 1 – Eskişehir Fault Zone

The source zone lies north-northwest of the site, primarily beyond the 320-km Site region. Scattered seismicity is documented in the vicinity of the fault zone. A Mw=6.2 earthquake that occurred in 1956 has been attributed to a segment of the fault. The largest earthquake within the zone occurred in 1400 with Mw=6.5.

Source Zone 2 – Simav-Sultandağ Fault System

The Zone is located 200 – 400 km northwest of the Site (Figure 6/5.19). Diffuse seismicity is located within the source zone. The largest earthquake located within the Zone occurred in 1931 with Mw=6.8.

Source Zone 3 – Fethiye-Burdur Fault

This 300-km long Fault Zone is located mostly outside of the Akkuyu NPP site region to the west-northwest of the site. The zone is characterized by diffuse seismicity. Authors of [6/86] associate a number of surface wave magnitude (MS) greater than 5.0 earthquakes with this fault zone. The largest earthquake located within the zone occurred in 1914 with Mw=7.2.

Source Zone 4 – Overriding Plate

Source zone 4 represents the portion of the Anatolian microplate that overrides the Cyprian Trench subduction zone. It includes a portion of the Antalya Offshore Basin. The Zone is located about 150 – 300 km west of the site. Seismicity in the zone is diffuse. A Mw=6.1 earthquake occurred in 1930 is the largest documented in this zone.

Source Zone 5 – Cyprian Trench Interface

Source zone 5 is based on the interface portion of the Cyprian subduction zone [6/235 and 6/179]. West and southwest of the site, a zone of seismicity dips beneath the Anatolian microplate associated with subduction of the Nubian portion of the African plate beneath the Anatolian microplate. Based on [6/179], the interface zone is modeled with a dip of 25 degrees to the northeast. The interface is taken to extend from the surface at the southwestern edge of the zone to a depth of 60 km at the northeastern edge. The surface projection of the deeper seismically active part of the subduction zone is located about 150 km from the Site. While seismicity indicates a subducting slab, no large interface earthquakes are documented in the historical and instrumental record. The largest earthquake with a depth less than 60 km occurred in 530 with an Mw=6.3. However, uncertainty in focal depths leads to uncertainty with respect to whether this earthquake is associated with the interface zone or with shallow seismicity in the overriding plate.

Source Zone 6 – Cyprian Trench Intraslab

Source zone 6 represents intraslab earthquakes at depths greater than 60 km. These earthquakes represent deformation within the subducted slab below the interface zone rather than movement between the subducting slab and the overriding plate. The largest earthquake observed from this zone occurred in 1979 with Mw=6.0.

Source Zone 7 – Cyprus Trodos Mountains

Source zone 7 represents a collision zone on the island of Cyprus. In the vicinity of Cyprus earthquakes at depths below 80 km are no longer observed. Authors of [6/179] interpret a transform fault to the west of Cyprus that offsets the Cyprian subduction zone to the west from the collision zone. Authors of [6/235] interpret the seismicity as supporting a tear in the subducting plate, separating the subduction zone from the collision zone. The zone is located about 150 km south-southwest of the site. The transition from subduction to collision may be related to the Eratosthenes Seamount, a continental fragment located south of Cyprus on the Sinai portion of the African plate [6/235]. The largest earthquake documented from Source zone 7 occurred in 337 with Mw=7.1.

Source Zone 8 – Cyprian Trench-Transform

Source zone 8 encompasses the interpreted zone of shearing that connects the Cyprian subduction and collision zone to the Dead Sea Transform System. The zone is located about 150 – 250 km to the southeast of the site.

Source Zone 9 – Dead Sea Fault

Source zone 9 is based on the Dead Sea Transform Fault that connects the spreading center in the Red Sea with the continental collision zone in Iran and westward squeezing of the Anatolian microplate in Turkey. The fault separates the Arabian plate to the east from the African plate to the west and is characterized by left-lateral motion. Authors of [6/145] estimate a slip rate of 2 – 6 millimeters per year (mm/yr) based on investigations in Jordan. The Fault System has experienced significant seismic activity, including large earthquakes [6/130 and 6/129]. The source zone is located 200 to over 300 km from the Site.

Source Zone 10 – Hatay-Northern Dead Sea Fault

Source zone 10 discriminates the northern portion of the Dead Sea Transform System from the transform to the south. This source zone lies about 250 to 300 km to the east-northeast of the site. Seismic activity characterizes the zone with the largest recorded earthquake occurring in 521 with Mw=7.5.

Source Zone 11 – Kozan-Savran-Sürgü Fault Zone

Source zone 11 encompasses the Kozan-Savrun-Sürgü Fault System. The zone lies to the northeast about 150 km from the site at its closest point. Seismicity in the southwestern portion of the zone shows a relatively high rate. The largest earthquake recorded in the zone occurred in 242 with Mw=7.6.

Source Zone 12 – Beyşehir Fault

Source zone 12 is based on the Beyşehir Fault. The zone is located about 100 – 200 km northwest of the site. The zone is characterized by a low level of diffuse seismicity. The largest earthquake observed in the zone occurred in 1977 with Mw=4.5.

Source Zone 13 – Ecemiş Fault

Source zone 13 represents the Ecemiş fault. Because the southern extent of this fault is not well resolved and it potentially is located relatively close to the Site, alternative interpretations of the source zone configuration are included in Model 7 of the study.

Source zone 13A represents the interpretation in which the fault ends near Gülek [6/24], about 150 km northwest of the site. This is the southern extent of the more well-established portion of the fault with clear evidence of left-lateral strike-slip offset and development of pull-apart basins.

Source zone 13B represents an alternative interpretation in which the fault zone extends to the south-southwest following a tectonic lineament along the western portion of the Adana Basin, ending just offshore near Silifke. In this interpretation the southern extent of the fault reaches to about 25 km of the Site. Given the less clear definition of the fault along its potential southern extension, Source Zone 13B, which includes both the northern and southern portions, is given a probability of 0.5 in the logic tree for PSHA. As activity of the northern portion of the fault is more certain, Source Zone 13A is also given a weight of 0.5. Thus in the model, the northern portion of the Ecemiş fault source zone is always active, while there is an 0.5 probability that the southern portion is also active.

Source Zone 14 – Tuz Gölü Fault

The Zone is located about 200 km north of the site. Diffuse seismicity characterizes the zone. The largest observed earthquake occurred in 1924 with Mw=6.0.

Source Zone 15 – 5-km Site Vicinity

Source zone 15 represents the site vicinity within 5 km of the Akkuyu NPP site. This area has been well studied and no evidence of Quaternary surface faulting has been uncovered. A lack of surface faulting during the Quaternary is considered in evaluating the maximum magnitude for the zone. The earthquake catalogue includes no earthquakes within Source zone 15.

Source Zone 16 – Namrun Fault Zone

Source zone 16 is confined to the Namrun fault zone. This fault zone is located to the north and northeast of the site. In [6/133] authors interpret the fault zone as the southwestern portion of the Central Anatolian fault zone. However its current activity is not well established and its

orientation differs slightly from the Ecemiş fault zone that truncates it to the northeast. Based on the available data, the fault zone is identified as a source zone separate from the Ecemiş fault (Source Zone 13). Its probability of activity is assessed to be 0.5. Two source zone configurations are included in the PSHA to represent epistemic uncertainty in the extent of the zone. It is believed that source zone 16A configuration extends to within 25 km of the site. It is believed that source zone 16B configuration extends to within 5 km of the site. Given the increased level of detail in geologic investigations in the site vicinity (within 5 km) versus the site near-region (within 25 km), Alternative 16A is given a logic tree probability of 0.9 and Alternative 16B a probability of 0.1. Combined with the overall probability of activity of 0.5 for the source zone, this results in logic tree weights of 0.45 for the configuration of source zone 16A, 0.05 for the configuration of source zone 16B, and 0.50 for the source zone area being part of the background source zone and not active as a separate zone.

Background Source Zone

To represent seismicity within the site region that is not associated with the source zones described above, a background source zone is used. This source zone represents the interpretation that even in areas where active faults or distinctive zones of seismicity are not observed, earthquakes can still occur. The spatial configuration of the Background source zone depends on the combined configuration of the other source zones because it encompasses area that is not included in the other source zones. Because of the alternative configurations for source zone 13 and source zone 16, there are six alternative configurations of the Background source zone. The configurations resulting from the various source zone combinations and their weights are:

1) – Source Zone 13A active and Source Zone 16 not active (Figure 6/5.19), weight=0.250;
2) – Source Zone 13B active and Source Zone 16 not active (Figure 6/5.20), weight=0.250;
3) – Source Zone 13A active and Source Zone 16A active (Figure 6/5.21), weight=0.225;
4) – Source Zone 13A active and Source Zone 16B active (Figure 6/5.22), weight=0.025;
5) – Source Zone 13B active and Source Zone 16A active (Figure 6/5.23), weight=0.225;
6) – Source Zone 13B active and Source Zone 16B active (Figure 6/5.24), weight=0.025.

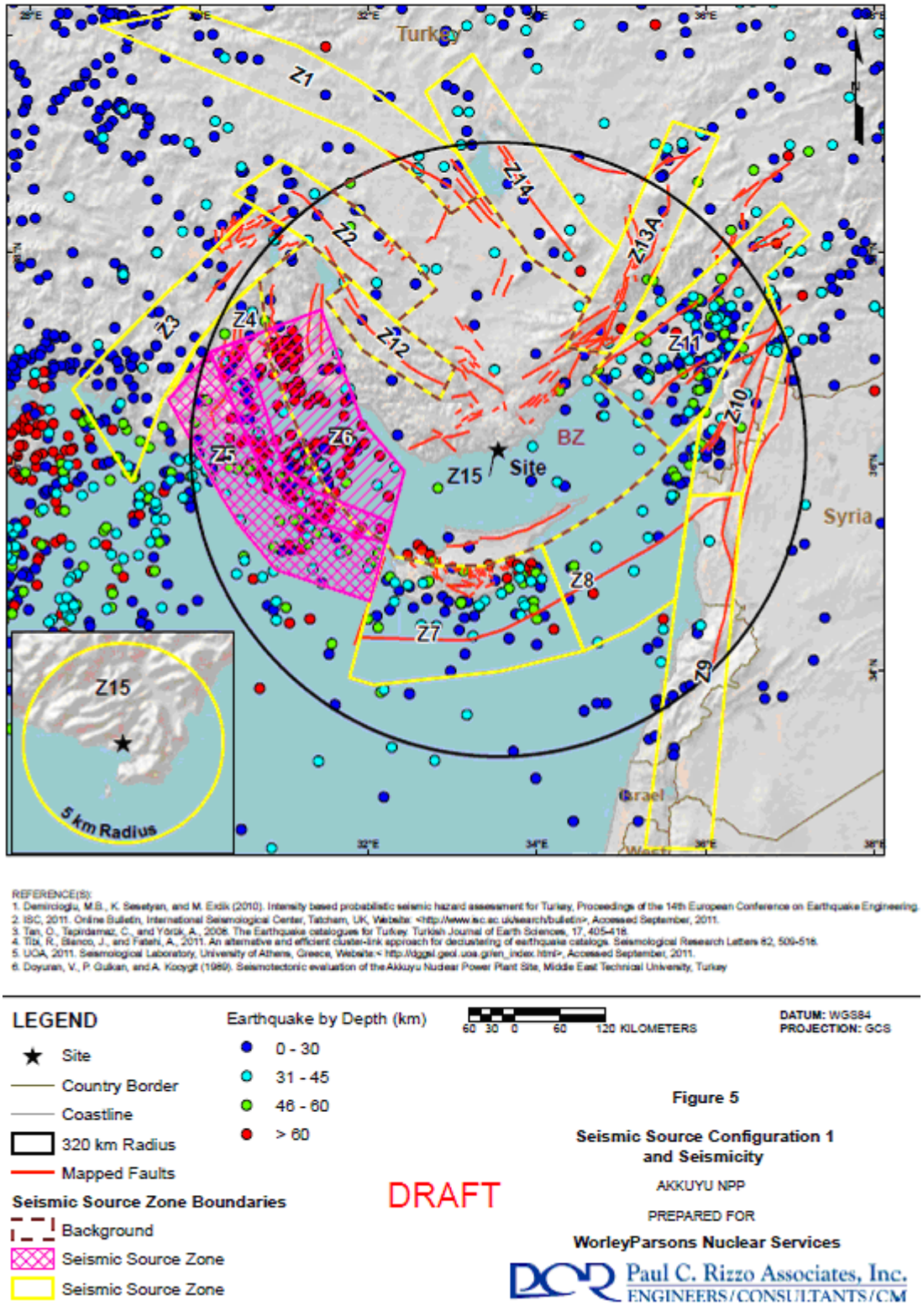

Figure 6/5.19 – Rizzo 2011 Model. Seismic Source Configuration 1 and Seismicity [6/243]

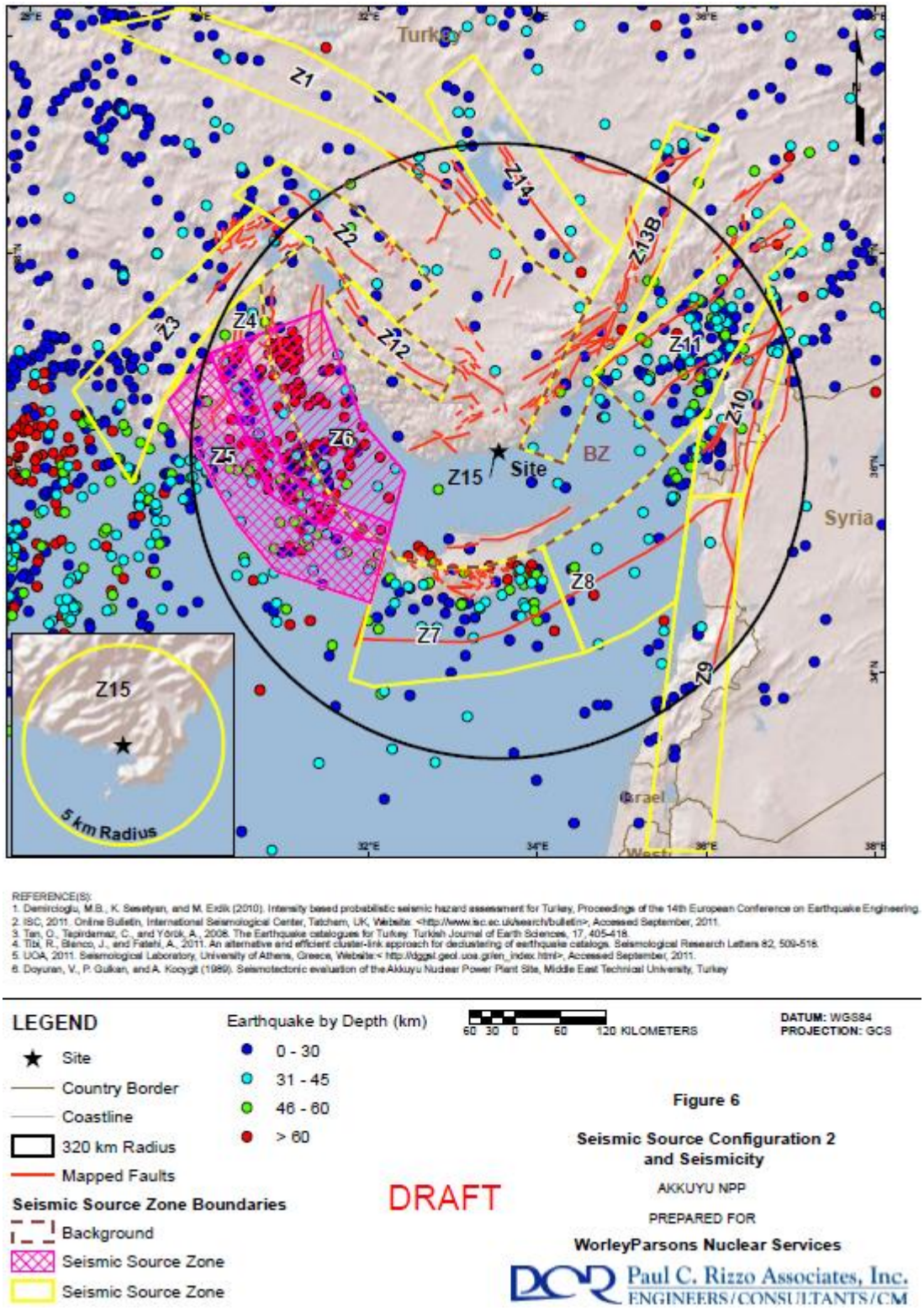

Figure 6/5.20 – Rizzo 2011 Model. Seismic Source Configuration 2 and Seismicity [6/243]

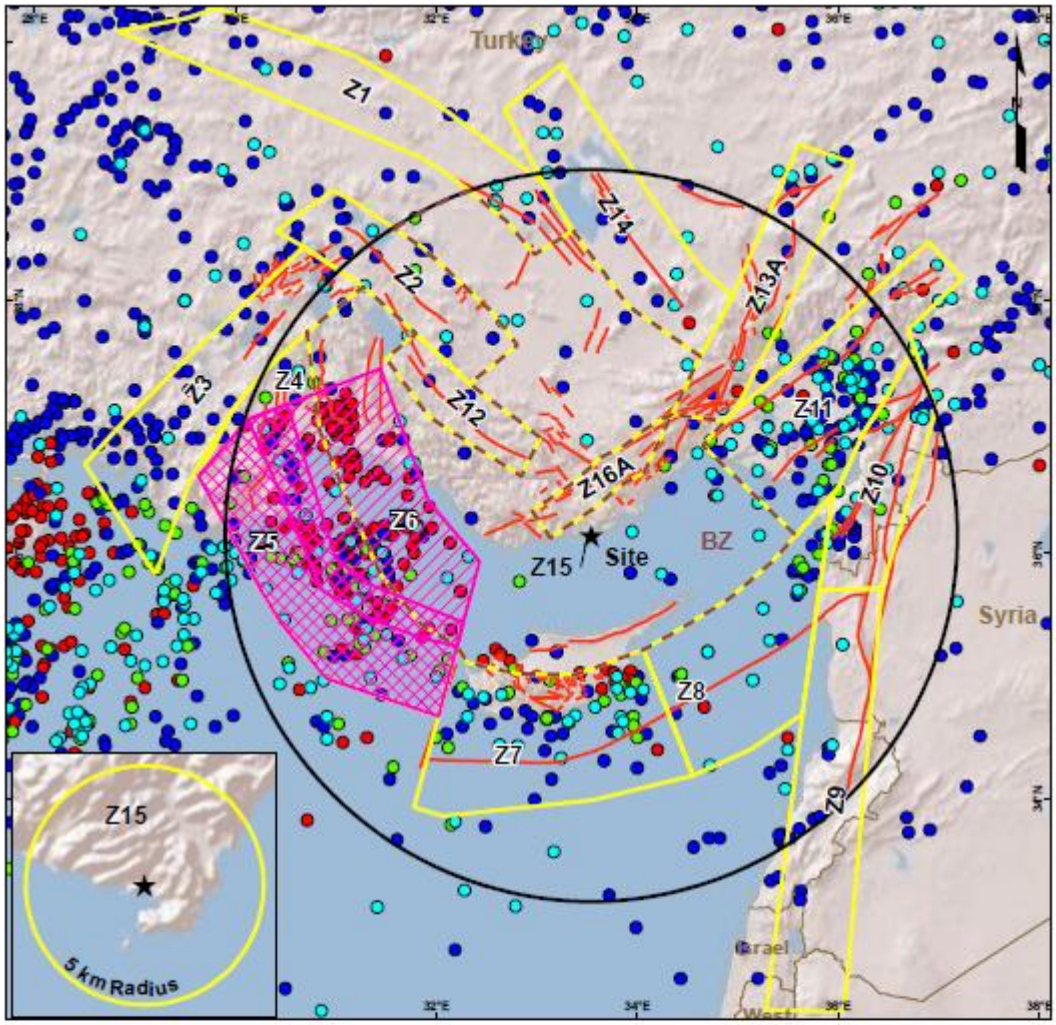

REFERENCE(S):
1. Demircioglu, M.B., K. Sesetyan, and M. Erdik (2010). Intensity based probabilistic seismic hazard assessment for Turkey, Proceedings of the 14th European Conference on Earthquake Engineering.
2. ISC, 2011. Online Bulletin, International Seismological Center, Tatcham, UK, Website: <http://www.isc.ac.uk/search/bulletin>, Accessed September, 2011.
3. Tan, O., Tapirdamaz, C., and Yörük, A., 2008. The Earthquake catalogues for Turkey. Turkish Journal of Earth Sciences, 17, 405-418.
4. Tibi, R., Bianco, J., and Fatehi, A., 2011. An alternative and efficient cluster-link approach for declustering of earthquake catalogs. Seismological Research Letters 82, 509-518.
5. UOA, 2011. Seismological Laboratory, University of Athens, Greece, Website:< http://dggal.geol.uoa.gr/en_index.html>, Accessed September, 2011.
6. Doyuran, V., P. Gulkan, and A. Kocygit (1989). Seismotectonic evaluation of the Akkuyu Nuclear Power Plant Site, Middle East Technical University, Turkey

LEGEND

- Site
- Country Border
- Coastline
- 320 km Radius
- Mapped Faults

Seismic Source Zone Boundaries

- Background
- Seismic Source Zone
- Seismic Source Zone

Earthquake by Depth (km)

- 0 - 30
- 31 - 45
- 46 - 60
- > 60

60 30 0 60 120 KILOMETERS

DATUM: WGS84
PROJECTION: GCS

DRAFT

Figure 7

Seismic Source Configuration 3 and Seismicity

AKKUYU NPP

PREPARED FOR

WorleyParsons Nuclear Services

Paul C. Rizzo Associates, Inc.
ENGINEERS/CONSULTANTS/CM

Figure 6/5.21 – Rizzo 2011 Model. Seismic Source Configuration 3 and Seismicity [6/243]

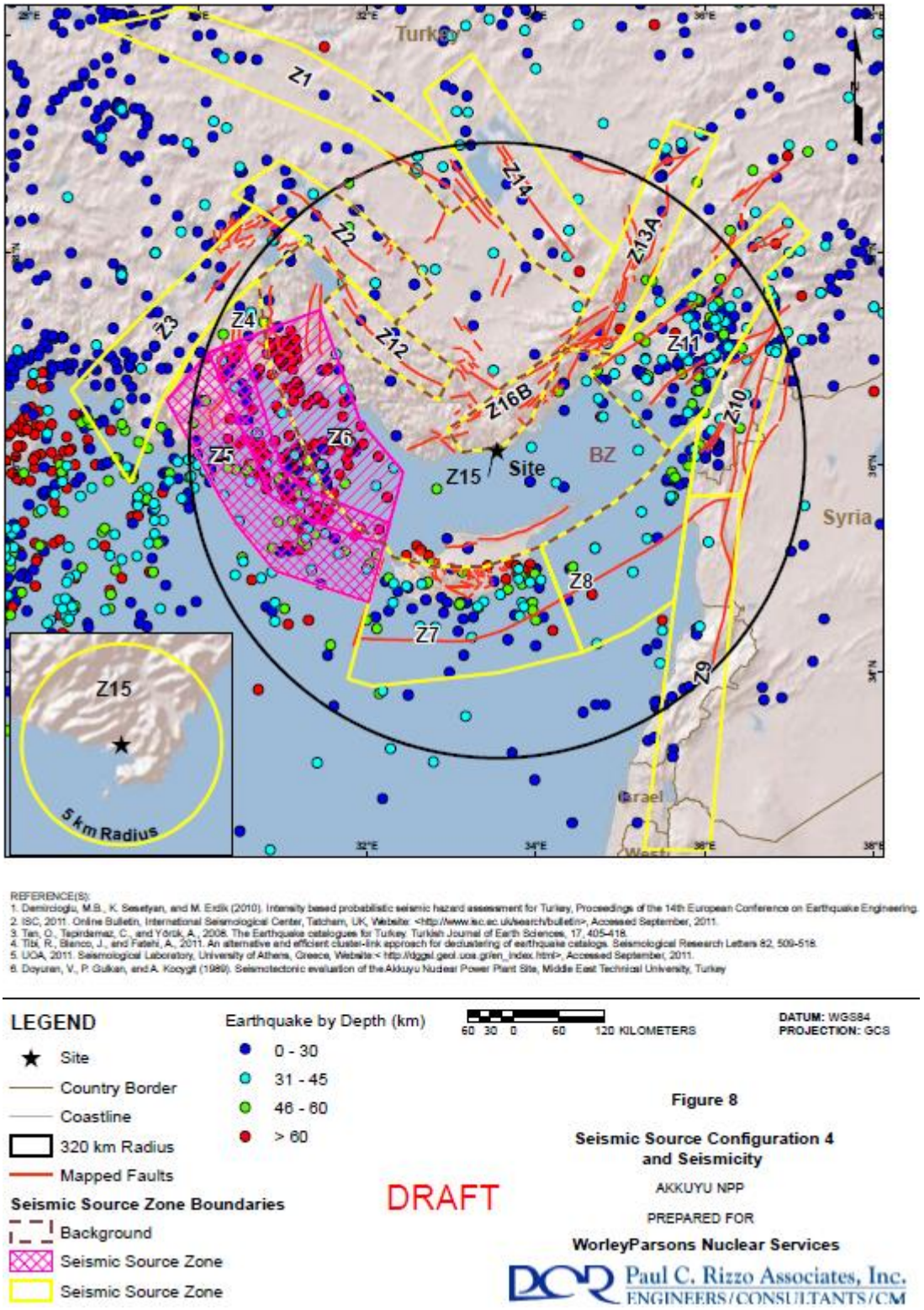

Figure 6/5.22 – Rizzo 2011 Model. Seismic Source Configuration 4 and Seismicity [6/243]

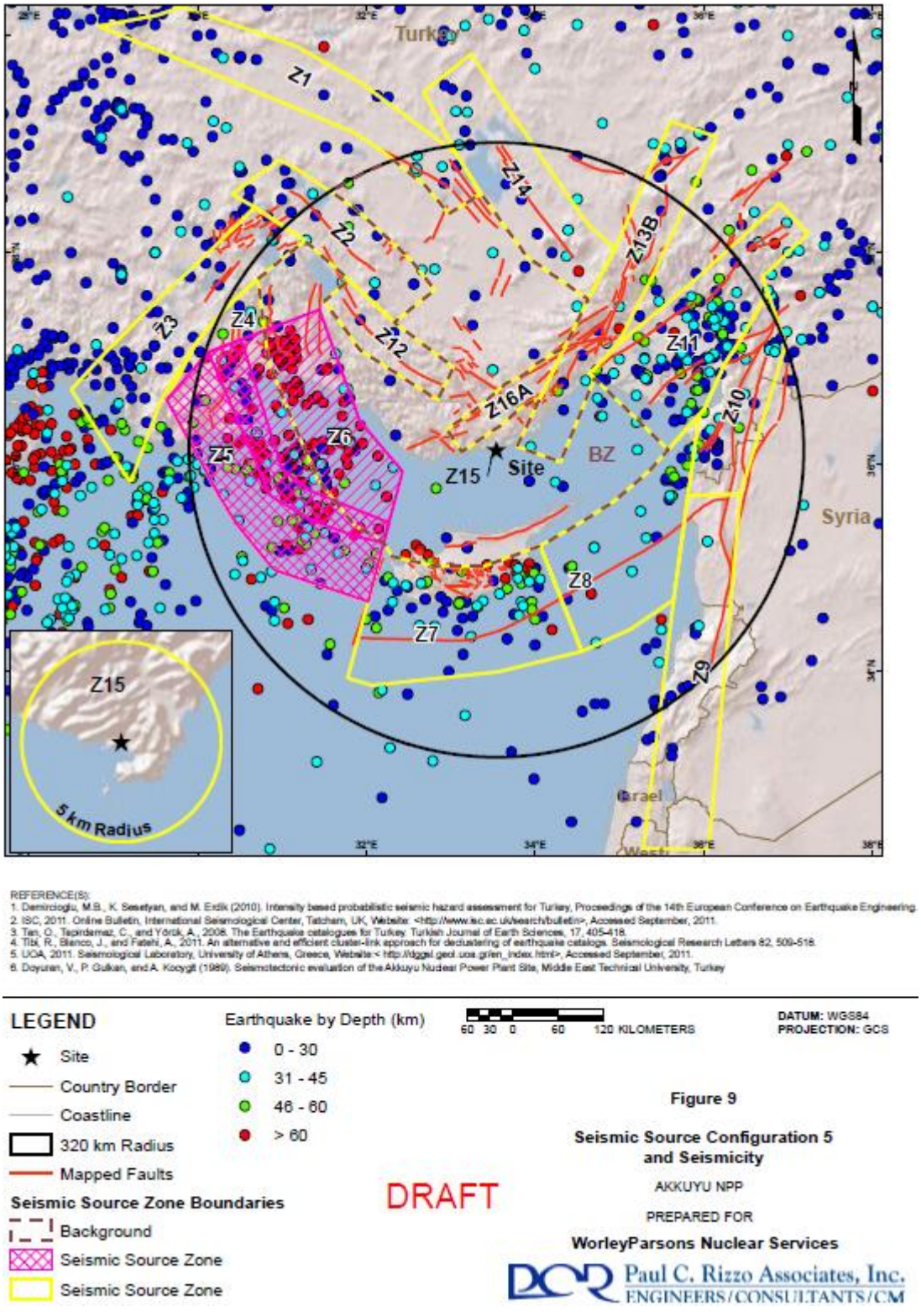

REFERENCE(S):
1. Demircioglu, M.B., K. Sesetyan, and M. Erdik (2010). Intensity based probabilistic seismic hazard assessment for Turkey, Proceedings of the 14th European Conference on Earthquake Engineering.
2. ISC, 2011. Online Bulletin, International Seismological Center, Tatcham, UK, Website: <http://www.isc.ac.uk/search/bulletin>, Accessed September, 2011.
3. Tan, O., Tapirdamaz, C., and Yörük, A., 2008. The Earthquake catalogues for Turkey. Turkish Journal of Earth Sciences, 17, 405-418.
4. Tibi, R., Bianco, J., and Fatehi, A., 2011. An alternative and efficient cluster-link approach for declustering of earthquake catalogs. Seismological Research Letters 82, 509-518.
5. UOA, 2011. Seismological Laboratory, University of Athens, Greece, Website:< http://dggal.geol.uoa.gr/en_index.html>, Accessed September, 2011.
6. Doyuran, V., P. Gulkan, and A. Kocygit (1989). Seismotectonic evaluation of the Akkuyu Nuclear Power Plant Site, Middle East Technical University, Turkey

LEGEND

- Site
- Country Border
- Coastline
- 320 km Radius
- Mapped Faults

Seismic Source Zone Boundaries

- Background
- Seismic Source Zone
- Seismic Source Zone

Earthquake by Depth (km)

- 0 - 30
- 31 - 45
- 46 - 60
- > 60

60 30 0 60 120 KILOMETERS

DATUM: WGS84
PROJECTION: GCS

DRAFT

Figure 9

Seismic Source Configuration 5 and Seismicity

AKKUYU NPP

PREPARED FOR

WorleyParsons Nuclear Services

Paul C. Rizzo Associates, Inc.
ENGINEERS/CONSULTANTS/CM

Figure 6/5.23 – Rizzo 2011 Model. Seismic Source Configuration 5 and Seismicity [6/243]

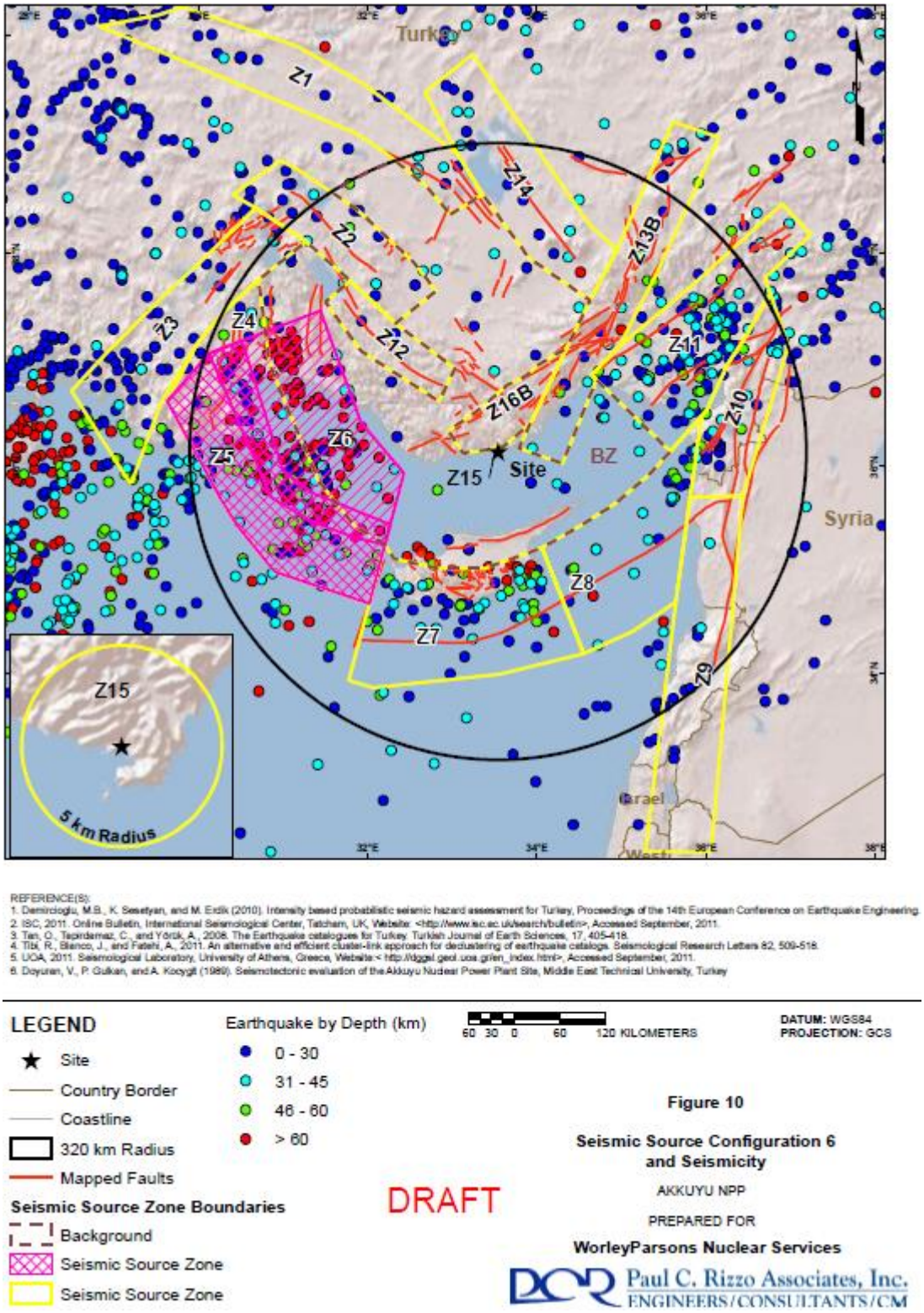

Figure 6/5.24 – Rizzo 2011 Model. Seismic Source Configuration 6 and Seismicity [6/243]

Maximum magnitude, fault type, source depth, recurrence of earthquakes are defined in the Rizzo Model in the form of logic tree and assigned weights of logic tree branches. There are six types of logic trees used to account for the epistemic uncertainty:

- For treatment of uncertainty in ESO zone configuration;
- For treatment of uncertainty in Mmax evaluation;
- For uncertainty treatment in fault type;
- For treatment of uncertainty in source depth evaluation;
- For treatment of uncertainty in earthquake catalogue completeness;
- For treatment of uncertainty in recurrence curve parameters of earthquakes in ESO zones.

One of two approaches is used in Rizzo 2011 Model to evaluate Mmax depending on the data available for each source zone. For source zones for which information is available on the length of faults expected to be the source of future earthquakes, an empirical relation between rupture length and MW is used. For other source zones, an increment to the largest observed earthquake is used as the basis for the Mmax distribution.

The rupture length approach is applied for Source Zones 1, 2, 3, 5, 9, 10, 11, 12, 13, 14, and 16. For each source zone, the length of the associated fault is determined from available data. Rupture length for the maximum magnitude earthquake is then taken as one-third of the total fault length. Next the maximum magnitude is estimated from the empirical relations of [6/238], except for Source Zone 5. For Source Zone 5, which represents subduction along the Cyprus Trench, the empirical relation of Strasser et al. [6/209] for interface subduction earthquakes is used.

For Source Zone 15 (5 km site vicinity), the Mmax distribution is developed taking into account the lack of evidence for surface faulting in the site vicinity. As investigations have uncovered no evidence of surface faulting during the Quaternary period, the Mmax distribution is defined such that there is reasonable likelihood that the Mmax earthquake will not produce surface faulting.

The logic trees representing uncertainty in Mmax based on rupture length generally consist of three values: the mean Mw and the plus and minus one standard deviation values based on the assessed rupture length. The branch for the mean value is given a probability of 0.6 and the other two branches are each given a probability of 0.2. For Source Zone 5, multiple values of rupture length were considered in determining the Mmax distribution.

For source zones that are not associated with a fault zone, the Mmax distribution is determined by incrementing the magnitude of the largest earthquake that has been observed in the source zone. The limited duration of the historic record relative to the recurrence time of large earthquakes and the incompleteness of the record result in a significant likelihood that the Mmax earthquake has not been observed. A Mmax distribution is developed by using increments of 0.3,

0.6, and 0.9 with weights of 0.2, 0.6, and 0.2, respectively. Uncertainty in the MW estimate for the largest observed earthquake is not taken into account explicitly, but is considered in defining the range of increments used.

The Mmax distributions for Rizzo 2011 Model are summarized in Table 6/5.10.

Table 6/5.10 – Logic tree representing epistemic uncertainty in Mmax evaluation of ESO zone [6/243]

ESO zone	Mmax distribution		Largest observed earthquake	
	Mw	Weight	Mw	Year
1 – Eskişehir Fault Zone	6.9 7.2 7.5	0.2 0.6 0.2	6.5	1400
2 – Simav-Sultandagh Fault System	6.8 7.1 7.4	0.2 0.6 0.2	6.8	1931
3 – Fethiye-Burdur Fault	7.2 7.5 7.8	0.2 0.6 0.2	7.2	1914
4 – Overriding Plate	6.4 6.7 7.0	0.2 0.6 0.2	6.1	1930
5 – Cyprus Trench Interface	7.4 7.7 8.0 8.3 8.6	0.08 0.32 0.36 0.20 0.04	6.3	1911
6 – Cyprus Trench Intraslab	6.3 6.6 6.9	0.2 0.6 0.2	6.0	1979
7 – Cyprian Trench-Trodos Mountain	7.4 7.7 8.0	0.2 0.6 0.2	7.1	331
8 – Cyprus Trench Transform	7.2 7.5 7.8	0.2 0.6 0.2	6.9	76
9 – Dead Sea Fault	7.7 8.0 8.3	0.2 0.6 0.2	4.9	1983
10 – Hatay-Northern Dead Sea Fault	7.5 7.8 8.1	0.2 0.6 0.2	7.5	521
11 – Kozan-Savran-Surgu Fault Zone	7.6	0.2	7.6	242

ESO zone	Mmax distribution		Largest observed earthquake	
	Mw	Weight	Mw	Year
	7.9 8.2	0.6 0.2		
12 – Beysehir Fault	7.2 7.5 7.8	0.2 0.6 0.2	7.2	1213
13A – Ecemiş Fault I	7.0 7.3 7.6	0.2 0.6 0.2	6.8	1940
13B - Ecemiş Fault II	7.2 7.5 7.8	0.2 0.6 0.2	6.8	1940
14 – Tuz Gölü Fault	6.9 7.2 7.5	0.2 0.6 0.2	6.0	1924
15 –5-km Site Vicinity	5.9 6.2 6.5	0.2 0.6 0.2	None in Catalogue	
16 – Namrun Fault	6.9 7.2 7.5	0.2 0.6 0.2	None in Catalogue	
Background	6.5 6.8 7.1	0.2 0.6 0.2	6.2	1718

In the case for which sufficient data are available, the constants *a* and *b* are fit from the seismicity observed within a source zone using the maximum likelihood approach of Weichert [6/237]. The formulation of Weichert incorporates estimates of earthquake catalogue completeness that vary with magnitude.

For the Akkuyu NPP site PSHA, two cases are considered for recurrence characterization.

In the first case, adequate past seismicity is located within a source zone such that the *a*- and *b* value can both be determined from the data. This approach is used for all source zones except Source Zones 15 and 16.

In the second case, seismicity data are too limited to determine the a-value and b-value. In this case, both the *a*- and *b*-value are adopted from a nearby source zone. This approach is used for Source Zone 15 (5 km site vicinity) and Source Zone 16 (Namrun Fault Zone). The same seismicity

parameters as determined for the Background source zone are used, adjusting the *a*-value proportionally according to the relative areas of the source zones.

In calculating the recurrence parameters for the different source zones, the observed rates are determined for magnitude bins for which completeness may vary [6/237]. The minimum magnitude included in the calculation for each source zone is based on a visual inspection of the determined observed rates, taking into account the expectation that rates should increase as magnitude decreases.

Uncertainty in the recurrence of future seismicity is incorporated in the PSHA. For source zones for which both the *a*- and *b*-value are determined from the data, the approach used is based on Bollinger et al. [6/35] and Weichert [6/237].

Recurrence parameters (per Guttenberg-Richter) in form of logic tree for uncertainty treatment are given in Table 6/5.11.

Table 6/5.11 – Logic tree for recurrence parameters [6/243]

ESO zone	Mmin	A-VALUE (LOG(N(M=0))		B-VALUE		Weight
		Set 1	Set 2	Set 1	Set 2	
1 – Eskişehir Fault Zone	4.25	2.235	2.044	0.657	0.617	0.6
		2.500	2.024	0.772	0.662	0.2
		1.920	1.949	0.532	0.547	0.2
2 – Simav-Sultandagh Fault System	3.5	0.817	0.395	0.447	0.330	0.6
		0.661	0.161	0.481	0.336	0.2
		0.941	0.567	0.410	0.312	0.2
3 – Fethiye-Burdur Fault	3.5	2.243	2.132	0.657	0.641	0.6
		2.300	2.218	0.703	0.695	0.2
		2.143	1.994	0.598	0.573	0.2
4 – Overriding Plate	3.5	1.685	1.884	0.501	0.574	0.6
		1.661	1.858	0.524	0.596	0.2
		1.665	1.867	0.466	0.540	0.2
5 – Cyprus Trench Interface	3.5	2.033	2.218	0.637	0.704	0.6
		2.180	2.357	0.714	0.778	0.2
		1.867	2.060	0.556	0.626	0.2
6 – Cyprus Trench Intraslab	3.5	2.499	2.685	0.620	0.688	0.6
		2.552	2.735	0.653	0.720	0.2
		2.434	2.624	0.584	0.653	0.2
7 – Cyprian Trench-Trodos Mountain	3.5	2.049	1.894	0.591	0.561	0.6
		2.055	1.917	0.621	0.596	0.2
		2.014	1.836	0.552	0.517	0.2
8 – Cyprus Trench Transform	4.25	3.399	3.687	0.894	0.975	0.6
		4.217	4.488	1.125	1.201	0.2
		2.517	2.822	0.645	0.732	0.2

ESO zone	Mmin	A-VALUE (LOG(N(M=0))		B-VALUE		Weight
		Set 1	Set 2	Set 1	Set 2	
9 – Dead Sea Fault	3.5	1.779	1.867	0.709	0.747	0.6
		2.054	2.144	0.850	0.888	0.2
		1.608	1.695	0.601	0.639	0.2
10 – Hatay-Northern Dead Sea Fault	3.5	0.232	0.453	0.199	0.284	0.6
		0.061	0.283	0.199	0.284	0.2
		0.401	0.622	0.199	0.284	0.2
11 – Kozan-Savran-Surgu Fault Zone	3.5	2.587	2.463	0.666	0.645	0.6
		2.592	2.474	0.688	0.668	0.2
		2.508	2.374	0.623	0.600	0.2
12 – Beysehir Fault	3.5	0.570	0.517	0.651	0.651	0.6
		-0.193	-0.245	0.651	0.651	0.2
		-0.794	1.228	0.087	0.651	0.2
13A – Ecemiş Fault I	4.25	2.820	2.803	0.826	0.837	0.6
		3.388	3.479	1.021	1.056	0.2
		2.069	1.871	0.587	0.557	0.2
13B - Ecemiş Fault II	4.25	3.320	3.210	0.901	0.886	0.6
		3.864	3.685	1.076	1.044	0.2
		2.488	2.325	0.656	0.632	0.2
14 – Tuz Gölü Fault	3.5	1.279	1.473	0.538	0.609	0.6
		1.543	1.725	0.674	0.740	0.2
		1.115	1.320	0.434	0.509	0.2
15 –5-km Site Vicinity	The same values are used as for the Background Zones, except the a-values are scaled according to the relative area of Source Zone15					
16 A – Namrun	The same values are used as for the Background Zones, except the a-values are scaled according to the relative area of Source Zone					
16 B – Namrun	The same values are used as for the Background Zones, except the a-values are scaled according to the relative area of Source Zone					
Background 1	4.25	4.569	4.498	1.100	1.094	0.6
		5.111	4.929	1.254	1.221	0.2
		3.927	3.982	0.922	0.946	0.2
Background 2	4.25	4.558	4.617	1.112	1.137	0.6
		5.184	5.170	1.288	1.295	0.2
		3.839	3.987	0.914	0.960	0.2
Background 3	4.25	4.569	4.498	1.100	1.094	0.6
		5.111	4.929	1.254	1.221	0.2
		3.927	3.982	0.922	0.946	0.2
Background 4	4.25	4.390	4.351	1.057	1.058	0.6

ESO zone	Mmin	A-VALUE (LOG(N(M=0))		B-VALUE		Weight
		Set 1	Set 2	Set 1	Set 2	
		4.880	4.734	1.199	1.174	0.2
		3.808	3.883	0.893	0.922	0.2
Background 5	4.25	4.558	4.617	1.112	1.137	0.6
		5.184	5.170	1.288	1.295	0.2
		3.839	3.987	0.914	0.960	0.2
Background 6	4.25	4.558	4.617	1.112	1.137	0.6
		5.184	5.170	1.288	1.295	0.2
		3.839	3.987	0.914	0.960	0.2

Characteristics of the examined source zones and other PSHA input data is given in Appendix N.

Geographical coordinates of the polygons limiting ESO zones in Rizzo models and also parameters of seismicity in the zones are provided in Appendix N.

6.5.5 GROUND MOTION PREDICTION EQUATIONS AND LOGIC TREES

This section will present only the new studies since GMPEs were very simplistic at the time of the previous SHA studies and logic trees were not used.

ENVY/BU KOERI Study

Four ground motion prediction equations (GMPE) from the family of NGA equations [6/184] are discussed and utilized in calculations:

- Abrahamson and Silva (2008) [6/1] – AS2008;
- Boore and Atkinson (2008) [6/37] – BA2008;
- Campbell and Bozorgnia (2008) [6/42] – CB2008;
- Chiou and Youngs (2008) [6/48] – CY2008.

The listed above equations are suitable for utilization in regions with high activity of shallow crust earthquakes (“active shallow region”).

The authors of the report did not give a preference to any one of four equations, at probabilistic hazard analysis having them built into the structure of logic tree with equal weights.

The source zonation models and the GMPEs form the two levels of the PSHA logic tree structure developed for the Akkuyu NPP site.

To consider the epistemic uncertainty ENVY/BU KOERI have conducted PSHA analysis with three distinct source models each having thoroughly rationalized recurrence relationships, maximum and minimum magnitudes.

The final weights assigned to different branches of the logic tree are summarized in Table 6/5.12.

Three intensity prediction models were utilized for the computation of the probabilistic intensity distributions (Table 6/5.13).

Table 6/5.12 – The Logic Tree Structure for the Computation of Ground Motion Acceleration [6/75]

Source Model		GMPE	Branch No	Model Weight	Parameters
Model 1	Turkey-Wide Source Zonation (KOERI-SHARE - EMME)	BA, 2008	GM1	1/3	PGA Sa (T=0.2s) Sa(T=1.0s)
		CB, 2008	GM2		
		CY, 2008	GM3		
		AS, 2008	GM4		
Model 2	Updated METU-EERC (1990) Source Zonation	BA, 2008	GM5	1/3	PGA Sa (T=0.2s) Sa(T=1.0s)
		CB, 2008	GM6		
		CY, 2008	GM7		
		AS, 2008	GM8		
Model 3	Updated and Modified METU-EERC (1990) Source Zonation	BA, 2008	GM9	1/3	PGA Sa (T=0.2s) Sa(T=1.0s)
		CB, 2008	GM10		
		CY, 2008	GM11		
		AS, 2008	GM12		

Table 6/5.13 – The Logic Tree Structure for the Computation of Intensity [6/75]

Source Model		Intensity model	Branch No	Model Weight	Parameter
Model 1	Turkey-Wide Source Zonation (KOERI-SHARE - EMME)	Erdik&Eren 1983, [6/83]	Int1	0.1111	Intensity
		Musson 2000, [6/163]	Int2	0.1111	
		Sesetyan et al 2005, [6/202]	Int3	0.1111	
Model 2	Updated METU-EERC (1990) Source Zonation	Erdik&Eren 1983	Int4	0.1111	Intensity
		Musson 2000	Int5	0.1111	
		Sesetyan et al 2005	Int6	0.1111	
Model 3	Updated and Modified METU-EERC (1990) Source Zonation	Erdik&Eren 1983	Int7	0.1111	Intensity
		Musson 2000	Int8	0.1111	
		Sesetyan et al 2005	Int9	0.1111	

IPE RAS Study

In the SHA performed by IPE RAS [6/117], six GMPEs are discussed and utilized in the analysis:

- Abrahamson, Silva (2008) – AS2008 [6/1];
- Campbell, Bozorgnia (2008) – CB2008 [6/42];
- Graizer, Kalkan (2009) – GK2009 [6/98];
- Akkar, Bommer (2007) – AB2007 [6/4];
- Akkar, Bommer (2010) – AB2010 [6/5];
- Aptikaev (2004) – Apt2004 [6/17].

CY2008 [6/48] equation was not used, because it takes into account non-linear behavior of grounds, which is described by the coefficients determined only for California.

To take into account regional peculiarities, AB2007 and AB2010 [6/4 and 6/5] were used, because they were developed especially for Europe, Middle East and Mediterranean. The database contains 532 accelerograms from the region, recorded up to 100 km distance from 131 earthquakes in the magnitude range from 5 to 7.6.

In probabilistic analysis of seismic hazard the following GMPE weights were used:

- AS2008 – 0.15;
- CB2008 – 0.15;
- GK2009 – 0.15;
- AB2007 – 0.15;
- AB2010 – 0.20;
- Apt2004 – 0.20.

A macroseismic equation was used for probabilistic analysis in terms of seismic intensity:

$$I_i = bM - \nu \lg \sqrt{\Delta_i^2 + h^2} + c;$$

where:

- Δ_i – distance from epicenter;
- h – focus depth;
- b, ν and c – constants (in average, b=1.5, ν=4.0 and c=3.8).

In models of earthquakes recurrence (according to Gutenberg-Richter) recurrence parameters were utilized in three variants of calculations:

7) 1. According to the actual graph for the given ESO zone. This variant is preferable and has the highest weight.
8) 2. The graph is reconstructed according to the maximum observed magnitude in the zone.
9) 3. The graph is reconstructed according to maximum expected earthquake magnitude Mmax. Reconstruction is done assuming that such magnitude can occur once in 10000 years.

Less weight is assigned to the last two alternatives compared with the first one.

The logic tree used by IPE RAS in PSHA is demonstrated in Figure 6/5.25.

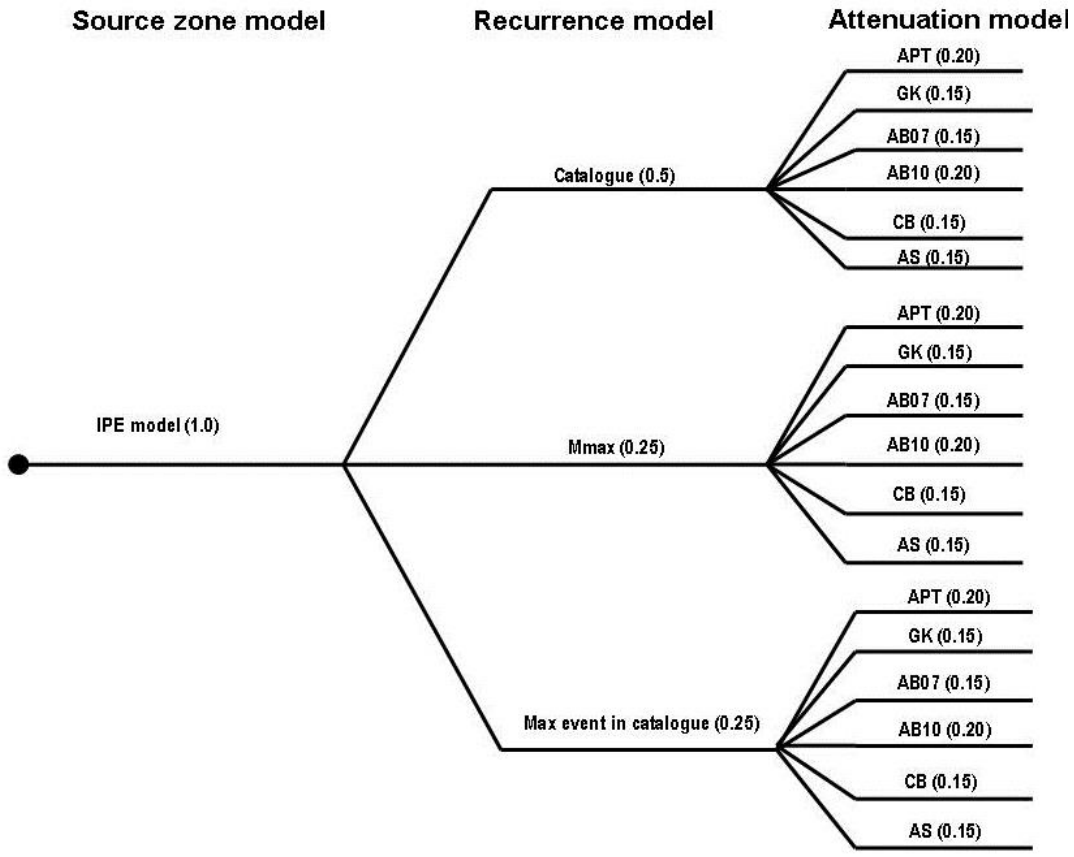

Figure 6/5.25 – Logic-Tree for Analysis and Taking into Account of Epistemic Uncertainty in PSHA in terms of acceleration (IPE RAS) [6/117]

Rizzo Study

In the SHA performed by Rizzo group [6/243], seven equations are discussed and utilized in calculations:

o) For shallow crust earthquakes:

- Akkar, Bommer (2010) – AB2010 [6/5];
- Boore and Atkinson (2008) – BA2008 [6/37];

- Campbell, Bozorgnia (2008) – CB2008 [6/42];
- Zhao et al. (2006) – Z2006 [6/251];

p) For earthquakes with focuses in subduction zones:

- Atkinson and Boore (2003) – AB2003 [6/19];
- Youngs et. al. (1997) – Y1997 [6/250];
- Zhao et al. (2006) – Z2006 [6/251].

All the GMPEs have equal weight in the Rizzo logic tree.

The maximal magnitudes, motion type in ESO zones focuses, depth of focuses, recurrence of earthquakes in zones are also assigned in the Rizzo model in alternative variants (in a form of logic trees with assigned weights of their branches).

Number of alternative branches of logic trees is considerably higher in Rizzo probabilistic analysis than in ENVY/BU KOERI, IPE RAS and WP analysis. Each procedure step of calculations and almost every group of input data and variables have alternatives. Logic tree branches were reviewed in Section 6.5.4 and are available in Appendix N.

WorleyParsons Study

In the SHA performed by WorleyParsons [6/246], four equations are discussed and utilized in calculations:

q) for shallow crust earthquakes:

- Campbell, Bozorgnia (2008) – CB2008 [6/42];
- Atkinson and Boore (2006) – AB2006 [6/18];

r) for earthquakes with focuses in subduction zones:

- Zhao et al. (2006) – Z2006 [6/251];
- Youngs et. al. (1997) – Y1997 [6/250].

Equations Z2006 and Y1997 are used with equal weight (0.5).

The CB2008 equation is used in pair with AB2006 with weight 0,9 (accordingly, AB2006 – with weight 0.1).

The logic tree used in PSHA (and DSHA), implemented by WP, has 72 alternative calculation branches (Figure 6/5.26).

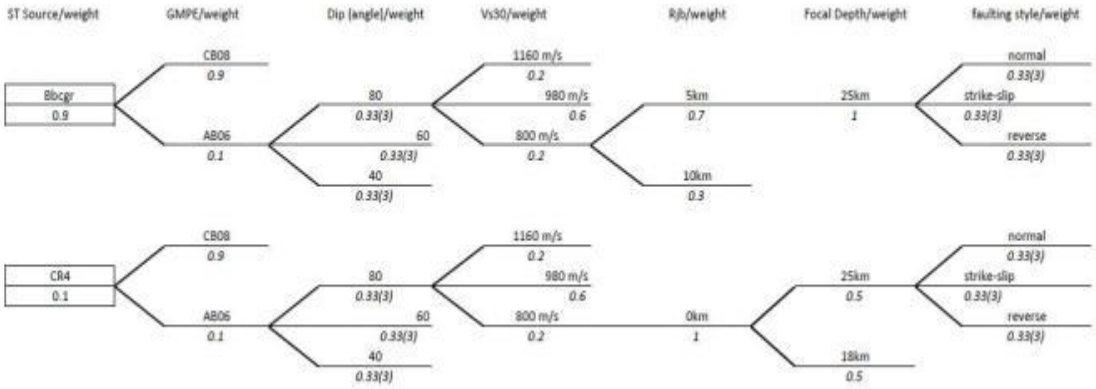

Figure 6/5.26 – Logic Tree for Analysis and Account of Epistemic Uncertainty in DSHA and PSHA in the WP study [6/246]

The authors of four studies use GMPE in different combinations, assigning different weights in analysis of epistemic uncertainty as per logic tree technology, in compliance with their own experience and intuition. As at present time verification with ground motions recorded at the site and predicted via selected GMPE is not done yet because of the lack of site specific ground motion data, so it is difficult to give a preference to any of the GMPEs.

6.5.6 DETERMINISTIC SEISMIC HAZARD ANALYSIS

IAEA Safety Guide SSG-9 [6/113] recommends the consideration of both a PSHA and a DSHA.

In the deterministic approach, individual earthquake scenarios are developed for each seismic source and these scenarios are evaluated separately. For each source, a scenario earthquake is defined (magnitude, distance and style-of-faulting). The ground motion for the scenario earthquake is usually estimated using GMPEs with a selected ground motion confidence level (i.e. amount of standard deviation). For fault ruptures, the closest point on the fault to the site is taken as the distance. For areal source zones, commonly the shortest distance to the source boundary is selected as the distance. For the zone that contains the site or for the background source, the worst case would be to have the earthquake occur right under the site. The geological and seismological information, associated with distinct seismic source zones forms the basis to predict the appropriate scenario earthquakes to be used for deterministic assessment of the hazard at the site.

On the basis of the IAEA SSG-9, the assessment of seismic hazard by deterministic methods specifically includes (paragraph 7.1):

"(1) Evaluation of the seismotectonic model for the site region in terms of the defined seismic sources identified on the basis of tectonic characteristics, the rate of earthquake occurrence and the type of magnitude–frequency relationship;

(2) For each seismic source, evaluation of the maximum potential magnitude;

(3) Selection of the attenuation relationships for the site region and assessment of the mean and variability of the ground motion as a function of earthquake magnitude and seismic source to site distance;

(4) Performing the hazard calculation as follows:

(i) For each seismogenic structure, the maximum potential magnitude should be assumed to occur at the point of the structure closest to the site area of the nuclear power plant, with account taken of the physical dimensions of the seismic source. When the site is within the boundaries of a seismogenic structure, the maximum potential magnitude should be assumed to occur beneath the site. In this case, special care should be taken to demonstrate that the seismogenic structure is not capable.

(ii) The maximum potential magnitude in a zone of diffuse seismicity that includes the site of the nuclear power plant should be assumed to occur at some identified specific horizontal distance from the site. This distance should be determined on the basis of detailed seismological, geological and geophysical investigations (both onshore and offshore) with the goal of showing the absence of faulting at or near the site, or, if faults are present, of describing the direction, extent, history and rate of movements on these faults as well as the age of the most recent movement. If the absence of faulting in the area is confirmed, it can be assumed that the probability of earthquake occurrence in this area is negligibly low. This investigation is typically for the range of a few kilometers to a maximum of about ten kilometers. The actual distance used in the attenuation relationships will depend on the best estimate of the focal depths and on the physical dimensions of the potential earthquake ruptures for earthquakes expected to occur in the seismotectonic province.

(iii) The maximum potential magnitude associated with zones of diffuse seismicity in each adjoining seismotectonic province should be assumed to occur at the point of the province boundary closest to the site."

Taking into account the SSG-9 procedure the following approach will be used in the consolidated DSHA of Akkuyu NPP site:

10) The maximum magnitudes and the corresponding distances associated for seismic source zones that would create the largest ground motion amplitudes at the site will be determined for each source zonation model;
11) The average of results from the selected ground motion prediction models will be calculated for each scenario;

12) For each zonation model, the maximum values corresponding to each ground motion parameter (PGA and SA at various periods) will be selected among the calculated amplitudes. This step will yield the maximum values for each zonation model;

13) Following the logic tree approach used in the probabilistic hazard assessment study, the equally weighted average of the maximum values obtained from the four source zonation models will be computed.

The procedure will be applied based on the same input database used in the PSHA in terms of seismotectonic models, maximal magnitudes, GMPEs etc. The median and median +1 standard deviation ground motion will represent the DSHA results of the site.

In particular, for the source zone in which the Akkuyu NPP site is located, several assumptions are made regarding the postulated faults including their geometry and style. In this evaluation, the rupture surface is postulated such that its propagation to the surface is not possible. This is because it has been demonstrated through a fault displacement hazard analysis that such a scenario is not applicable in the site vicinity.

6.5.7 PSHA SOFTWARE

In the ENVY/BU KOERI and IPE RAS study the widely known SeisRisk III software [6/31] was used. ENVY/BU KOERI used this software only for hazard calculation in terms of intensity, while IPE RAS – as in terms of intensity, as in terms of accelerations. For seismic hazard calculation in terms of accelerations, ENVY/BU KOERI has utilized another conventional seismic hazard software EZ-FRISK (Risk Inc), enabling to carry out both PSHA and DSHA, and moreover enabling to deaggregate hazard.

General principles of SeisRisk III software

Earthquakes occurred in the source zones and on the faults are limited by the certain magnitude interval, i.e. for any zone it is assumed that maximum and minimum magnitude values m_{max}, m_0 and Δm interval are known. The calculations are done for finite set n of magnitudes m_j:

$$m_j=m_0+(j+1/2)\Delta m,\ \ j=\overline{0,n-1},$$

$$\Delta m=(m_{max}-m_0)/n.$$

The number of earthquakes occurred in the time-unit is given by the user based on the magnitude-frequency graphs. If $N_{m(j)}$ is the number of earthquakes within magnitude interval j in the homogeneous zone of area A, then the number of earthquakes expected in its sub-area ΔA, will be equal to $N_{m(j)}A/\Delta A$.

To predict the ground motion, attenuation functions are used relating displacement (velocity, acceleration) at the site to an earthquake of certain magnitude occurred at certain distance. Only ground motion acceleration has been considered in the analysis. It is supposed that as the magnitude increases, so does the ground motion acceleration and the acceleration decreases with the increased distance. Based on given source zones or faults, seismic activity and attenuation function, the probability to observe in any given point acceleration a within the interval $a_{j-1}<a \le a_j$ is assessed.

For the given attenuation relationship $d_m(i)$ is the distance at which earthquake with magnitude m will produce average acceleration a_i at given point. The probability that the acceleration at given point will be within the interval $a_{i-1}< a \le a_i$ is equal to the probability of the occurrence of earthquake with given magnitude m at distances $d_m(i) \le d < d_m(i\text{-}1)$, which define the sub-area of the source zone:

$$A\big(m(i)\big) = f\left(\bar{d}_m(i), \Delta d_m(i)\right)$$

As function

$$\bar{d}_m(i) = \big(d_m(i-1) + d_m(i)\big)/2 \text{ and } \Delta d(i) = d_m(i\text{-}1) - d_m(i)$$

The number of such earthquakes is, correspondingly:

$$\rho_m(i) = \frac{A\big(m(i)\big)}{A} N_m .$$

The program calculates $A\big(m(i)\big)$ for each magnitude and accumulates $\rho_m(i)$ as i-th element in a special routine. The overall seismic activity level, generating accelerations within the interval $a_{i-1}< a \le a_i$ is

$$\rho(i) = \sum_{j=1}^{n} \rho_{m_j}(i),$$

where n is number of magnitude intervals.

These calculations do not consider the attenuation scatter. The scatter is usually modeled using the assumption that accelerations produced by the earthquakes within the given magnitude interval at given distance are log-normally distributed with standard deviation σ_a. It has to be noted that the assumption increases expected acceleration levels in all points. The Probability that there will be recorded acceleration within the interval $a_1 < a \le a_2$, is:

$$p(a_1, a_2) = \frac{1}{\sqrt{2\pi}\sigma_a} \int_{\ln a_1}^{\ln a_2} \exp\left(-\frac{(\ln a_1 - \ln \bar{a})^2}{2\sigma_a^2}\right) d(\ln a_1),$$

where $\ln(\bar{a}) = 1/2\left(\ln(a_{j-1}) + \ln(a_j)\right)$.

Seismicity level $\rho(j)$ of the j-th interval will be partially transferred into the k-th interval according to the following expression:

$$f(k) = p(a_{k-1},a_k)\rho(i).$$

The scatter of accelerations is taken into account after calculation of mean accelerations, which accelerates significantly the calculations. It is assumed that σ_a does not depend on magnitude and distance.

After calculation of mean annual seismicity level producing accelerations in the interval $a_{j-1} < a \le a_j$, $1 \le j \le 55$, the annual level of accelerations $a > a_j$ can be defined as

$$Ex(a_j) = \sum_{i=j+1}^{55} \rho(i).$$

For Poisson distribution characterized by mean value μ, the probability that within the time-interval t will occur k events is equal to:

$$P(k,t) = \frac{(\mu t)^k \exp(-\mu t)}{k!}$$

and correspondingly, the probability that no one earthquake will not occur in the same time-period is:

$$P(0, t) = \exp(-\mu t).$$

Setting $\mu = Ex(a)$,

$$P(0, t) = \exp(-Ex(a)t) \text{ or } Ex(a) = -\ln(P(0, t))/t.$$

Therefore, the acceleration fitting to the last equation will not be exceeded with probability $p = P(0, t)$ in the time interval t. In the same manner $q = 1 - P(0, t)$ is the probability that the acceleration a will be exceeded in the same time interval. The program calculates accelerations for given probabilities and time intervals.

Source zone modeling

Assumption that seismicity is homogeneously distributed within the source zone leads to the unrealistic consequence; the seismicity will sharply change at the zone boundaries, which will produce very different expected accelerations in neighbouring points. To compensate this, it is assumed that expected earthquake epicenters are normally distributed, i.e. epicenters are evenly distributed with respect to some average points with scatter defined by two-dimensional normal

distribution. Strictly formulated, if standard deviation in epicenter location is σ and if expected (mean) epicenter coordinates are (*X*, *Y*), then the probability that the earthquake will occur in small vicinity *A* of this point (*X*+Δ*x*, *Y*+Δ*y*) is:

$$p_A(\Delta x, \Delta y) = \frac{A}{2\pi\sigma^2}\exp\left(-\frac{\Delta x^2 + \Delta y^2}{2\sigma^2}\right).$$

In this manner it is possible to smooth variation of seismicity close to the zone boundaries, without affecting the seismicity level in the central part. Increasing of σ increases the number of earthquakes occurred out of the source zone; therefore larger area is included in calculations. For such model the calculations are done in two steps. At first, accelerations corresponding to the homogeneous source zone are calculated. Then, it is taken into account that the acceleration in the given (*X*, *Y*) point is equal to the weighted sum of accelerations calculated in each node of the given grid for homogeneous zone. Weight assigned to acceleration $a_{j-1} < a \le a_j$ in point (X_i+k_1dx,Y_i+k_2dy) is equal to:

$$w(k_1, k_2) = \frac{dxdy}{2\pi\sigma^2}\exp\left(-\frac{k_1^2dx^2 + k_2^2dy^2}{2\sigma^2}\right),$$

and the probability to record the acceleration $a_{j-1} < a \le a_j$ will be:

$$D = \frac{\sum_{k_1}\sum_{k_2} w(k_1, k_2)\rho\left((X_i + k_1dx, Y_i + k_2dy), j\right)}{\sum_{k_1}\sum_{k_2} w(k_1, k_2)},$$

where ρ((*X*$_i$+k_1dx,*Y*$_i$+k_2dy), *j*) is the probability of $a_{j-1} < a \le a_j$ in point (X_i+k_1dx,Y_i+k_2dy) for homogeneous seismic zone.

WorleyParsons used in-house developed Seismic Hazard Analysis Program (SHAP) which is based on the widely known EQRISK Seismic Risk Evaluation program [6/151]. SHAP provides a user interface to prepare the problem data for EQRISK and to post-process the results. The development of SHAP includes a small modification in the EQRISK software to introduce possibility for additional GMPEs and to enable varying seismic hazard parameters thus developing a logic tree.

EQRISK evaluates the hazard for each site-source combination and acceleration level and calculates the total annual expected number of occurrences of acceleration greater than preliminary defined levels of interest at the site by summing the expected numbers from all sources. The total annual hazard is calculated assuming that earthquakes occur as Poisson arrivals.

SHAP is designed to model a seismic hazard problem and prepare input data to EQRISK. In order to enhance the functionality of the EQRISK code, FORTRAN source code has been modified to have user defined GMPES in addition to the default one which is available in the EQRISK original code which is calculating only PGA (at that time GMPEs were not accounting for other spectral ordinates).

The SHAP is structured to enable building a logic tree by taking into account the variations in the selected problem parameters for each seismic source. A logic tree can be built by entering different values for different problem parameters and their associated weights to the problem. A number of SubProblems are built and their weights to the total hazard are calculated by SHAP. Each SubProblem represents one end branch in the logic tree.

SHAP prepares input file and runs the EQRISK separately for each of the SubProblems. After each run, the output file of EQRISK is read by SHAP and the results are transferred to the SHAP database. At the end of running all of the SubProblems, the total hazard is calculated by summing the risks for each SubProblem using the corresponding weight of each SubProblem.

Rizzo used in-house developed software RIZZO-HAZARD . Detailed information about this software is available in the original report [6/243].

6.5.8 SEISMIC HAZARD SOURCE CONTRIBUTION

At the final stage of PSHA, de-aggregation of seismic hazard was carried out, enabling to define earthquakes (magnitude and distance), which represent maximal contribution to the ground motion at the site. The methodology proposed by McGuire (1995) [6/150] has been followed. Modal (or scenario) earthquakes are defined by accumulation of annual levels of exceedance over given acceleration level at given spectral periods in certain magnitude intervals, distances and ε (number of standard deviations (in logarithmic units) from median level predicted by attenuation relationship). The probability that the given combination of magnitude, distance and ε will exceed the given level of ground motion can be calculated by dividing the frequency of exceedance in each parameter interval to the total frequency of exceedance of the given ground motion level.

Impact of each combination of magnitude, distance and ε is calculated by replacing the probability in the equation by Dirac's delta-function:

$$P\,[Y > y \mid m, r, \varepsilon] = \delta[\ln Y(m, r, \varepsilon) - \ln y]$$

Therefore, the method accumulates only those frequencies of exceedance, when

$\ln Y\,(m, r, \varepsilon) = \ln y.$

The main goal of such problem formulation is to find the combination of magnitude, distance and ε, which when substituted into the attenuation relationship will give the same ground

motion as the target one. This procedure finds the earthquake, which corresponds to the given level of ground motion, but does not guarantee that such an earthquake will exceed it with maximum probability (Bazzurro and Cornell, 1999) [6/29].

The results of deaggregation usually are shown in histograms demonstrating impact of each magnitude, distance and ε into the total hazard level. Histograms are usually presented in terms of probability distribution function. Different scenario earthquakes can be deaggregated for different periods and different exceedance levels.

In the IPE RAS study [6/117] deaggregation was done in the following intervals:

Magnitude interval M=3.5 – 7.5 with step 0.1 unit;

Distance R = 0 – 200 km with step 2 km;

ε = from -2 to 2 with step ε =1.0.

The deaggregation was done for periods 0.1 and 1 sec. From results of deaggregation the following scenario earthquakes are selected:

SSE level: M = 5.5, R = 4 km;

M = 7.5, R = 36 km;

OBE level: M = 4.5, R = 2 km;

M = 6.5, R = 38 km.

In ENVY/BU KOERI study [6/75], de-aggregation of hazard was performed in terms of accelerations (including spectral at periods 0.2 s and 1.0 s). As a result of the deaggregation, two groups of earthquakes focuses were distinguished introducing the major contribution in SHA for the Akkuyu NPP site:

- local focuses with M<6.0 at a distance to 20 km from the site (prevailing contribution);
- focuses with M=6.0 – 8.0 in a range of distances 30 - 100 km from the site (relatively lower contribution, in its turn – at SSE lower than at OBE).

For the short-period spectral accelerations (including PGA) seismic hazard at SSE and OBE is determined by local sources. For the long-period (1.0 s) spectral accelerations hazard is originated from remote earthquakes with M>6.0.

As appeared, focuses of earthquakes connected with the Ecemiş fault, do not present a main source of seismic hazard for the site in any of three models of ESO zones.

In WP study [6/246], the analysis of the source contribution to probability of occurrence show that in the region there are two sources, controlling hazard:

- Background seismic activity source;
- Source 5 Cyprian Trench.

The reason why the Cyprian Trench has high contribution to the ground motion is the relatively high annual recurrence rate in that source, its relatively close proximity to the site i.e. 115km and high magnitude Mw=8.

The following controlling earthquakes were determined in the study of Rizzo [6/243] using deagreggation method (Table 6/5.14).

Table 6/5.14 – Parameters of Controlling Earthquakes by Rizzo

Response frequency (hz)	Description	Magnitude (Mw)	Epicentral distance (km)	Fractional contribution to hazard
1.75	Near	6.05	11	0.64
	Far	7.37	180	0.36
7.5	Near	5.72	9	0.96
	Far	7.20	160	0.04

6.5.9 CONCLUSION

The four above mentioned seismic hazard studies have been performed in 2011 – 2012. The works were carried out by the groups representing different countries as follows: ENVY/BU KOERI (Turkey), IPE RAS (Russia), WorleyParsons (Europe) and Rizzo (USA).

As a result of these investigations each of the groups has compiled databases (catalogues) for the historical and instrumental earthquakes, different models were developed for seismotectonic zoning (ESO zones), different attenuation models (GMPE) were selected, methodologies of probabilistic and deterministic analysis of seismic hazard were applied using different V_{S30} values.

For that reason the consolidation SHA study has been initiated in 2012 integrating the efforts of all participants (ENVY, WP, RIZZO, and IPE RAS), which will serve as basis for the PSHA and DSHA defining the design ground motion parameters at the site. Epistemic uncertainties have been considered and included in the analysis for the following aspects:

- Seismic source models;
- Maximum magnitude (M_{max}) of the event in diffuse seismicity zone, where the NPP site is located;
- Attenuation relationships to be used in the analysis (GMPE);

– Reference shear wave velocity representation V_{S30} for the site.

The consolidation study is underway utilizing the consensus database and different interpretations of the database by the four groups. The consolidated SHA takes into account the conclusions reached during the several meetings held between the participants on how to incorporate a commonly agreed database and the different seismotectonic models in the form of a single logic tree.

The results of the consolidated study will provide the final design basis ground motion parameters at the Akkuyu NPP site in the form of free field design response spectra and associated acceleration time histories. The design basis ground motion parameters will be provided in the Site Parameters Report.

6.6 SURFACE FAULTING

6.6.1 NEAR REGIONAL ANALYSIS

A wider area than that recommended in IAEA SSG-9 [6/113] for near regional investigations (25km radius) has been studied in order to clarify the relationships of the near regional geological and morphological features with other more distant regional structures and lineaments.

The near regional area, located at the southern margin of the Taurus mountain range, is characterized by a mountainous landscape with a plateau at an elevation around 1200 – 1300 meters a.s.l. in its northernmost edge, sloping down toward south, deeply incised by narrow valleys. The sea margin is marked by a high coast, interrupted by minor bays and low coastal areas, the largest ones being that of Yeşilovacık, near the eastern edge of the Near Region and Aydıncık to the west. Valleys and lineaments predominantly strike northeast-southwest and secondarily north-south and northwest-southeast, being the first trend clearly controlled by the dominant tectonic-structural frame of the region.

The tectono-stratigraphy of the near region area includes various nappes of autochthonous and allochthonous units (Figure 6/6.1),

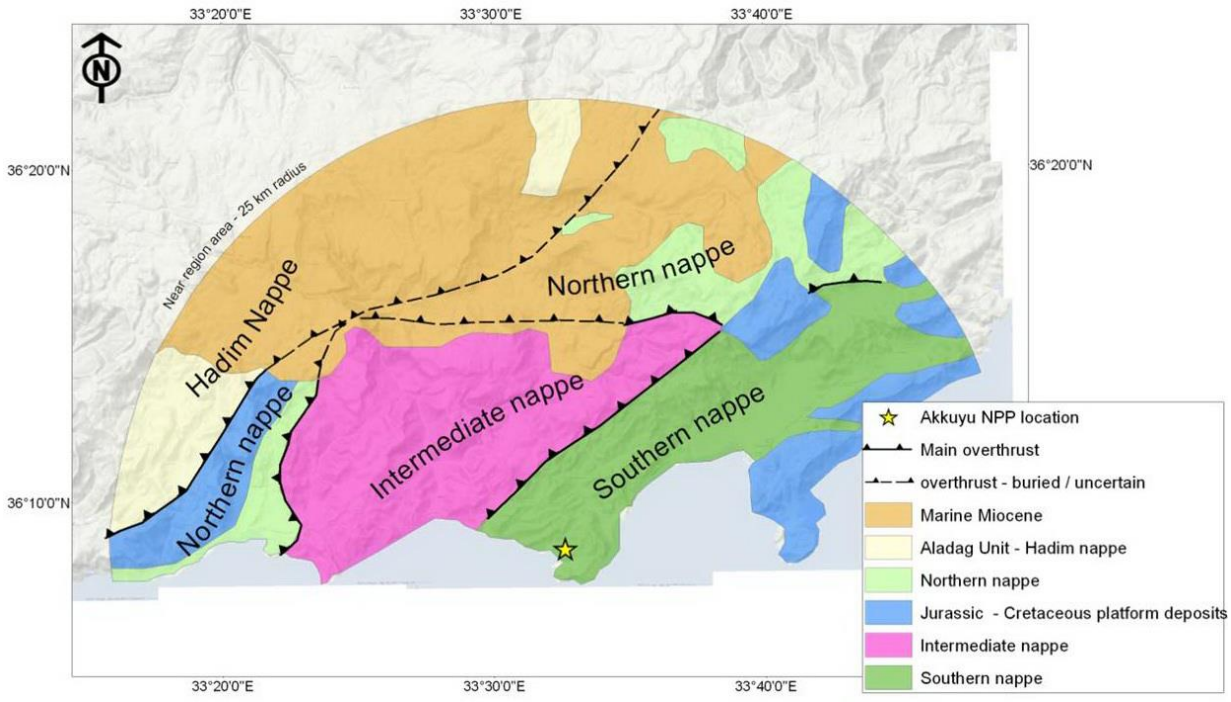

Figure 6/6.1 – Basic morphology of the near regional area (25 km radius) and surroundings, based on GMRT digital elevation model (resolution inland 99 m)

These units can be summarized as follows [6/57]:

14) The Southern Zone, including platform and marine Paleozoic sedimentary units strongly folded and faulted;
15) The Intermediate Zone: also this nappe is made of a deeply deformed Paleozoic sedimentary sequence, thrust onto the Southern zone along a NE-SW overthrust (Büyükeceli Overthrust) since Jurassic. The Paleozoic units are unconformably overlain by a Late Triassic to Upper Jurassic-Cretaceous sedimentary sequence;
16) The Northern Zone, mainly composed by the same Paleozoic units of the two former zones, was probably thrust onto the Intermediate zone prior to Late Permian. The Late Permian units are unconformably overlain by Jurassic limestones. In general Triassic units are lacking.

The Aladağ Unit of the Hadım Nappe: this unit comprises Paleozoic (Late Devonian) limestones and sandstones overlain by a Carboniferous sequence, and Mesozoic clastics and carbonates. Aladağ Unit is an allochthonous sequence transported to the south along the Hadım Nappe after the Late Eocene [6/55].

To the north of the near region, Miocene marine sediments capping the southern margin of the Taurides, point to a post collisional phase of surface uplift. The post-late Miocene uplift field (post 8 Ma [6/51]) can be well constrained by the elevation distribution of the Miocene marine sediments which rise up to about 2 km in elevation along the crest of the Central Taurides, before dropping to about 1 km at the northern margin of the range and thus depicting a wide drape fold consistent with present-day topography (Figure 6/6.2).

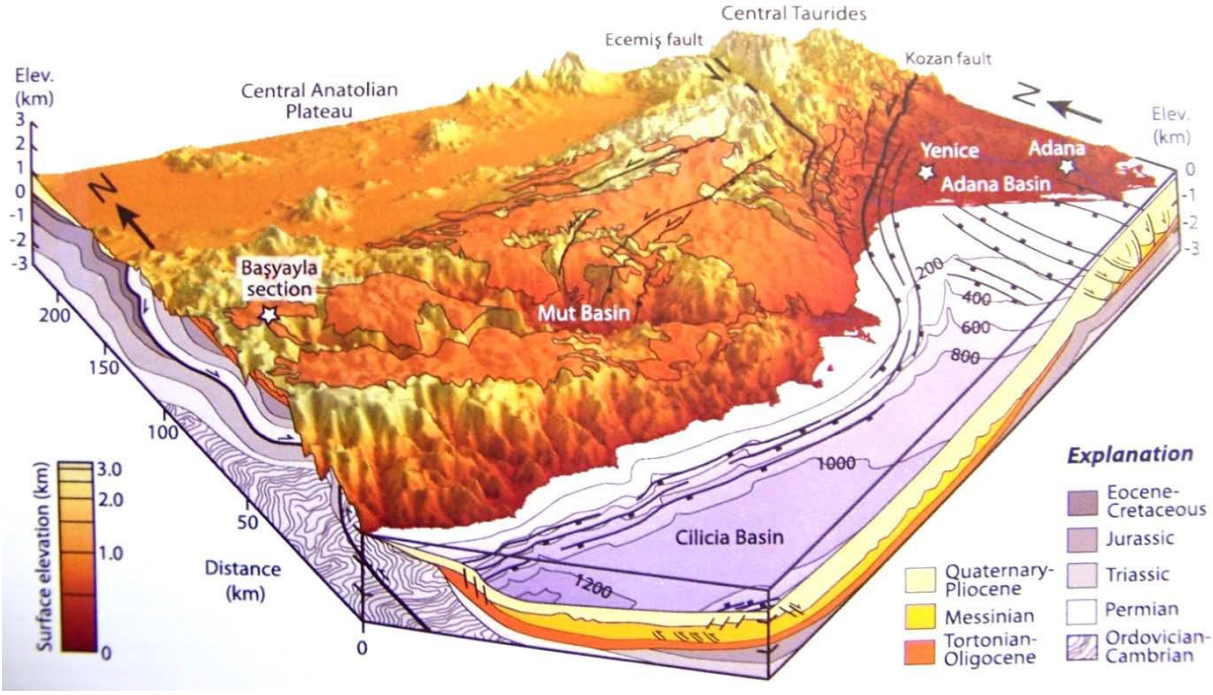

Figure 6/6.2 – Pattern of Miocene marine sediments uplifted over the southern margin of the Central Taurides [6/51]. The orange polygon overlay indicates the surface outcrop pattern of late Miocene marine sediments. Vertical exaggeration is 7:1

Surface folding over approximately 100 km around the site yet produces no observable deformation (in the order of tens of kilometers). No post-Miocene contractional structures or positive flower structures have been identified along the major fault zones nor are there any reported deep seated thrusts in this region. Instead post-Miocene deformation is dominated by normal or strike-slip faulting [6/122 and 6/121].

Such deformation pattern is associated with processes either deep within the crust or in the mantle. In 2011 Cosentino [6/51] recently proposed an astenospheric mantle upwelling, following the westward propagation of slab break-off from the Eastern Anatolia Plateau region.

The near regional area does not include relevant capable faults, based on the knowledge acquired so far, either from literature data, previous studies or field reconnaissance. However, according to the literature, some faults may extend relatively close to the site, although outside the Near Region. These faults were specifically analyzed in respect of their ground motion and fault displacement hazard potential. They are (Figure 6/6.3):

- Ecemiş Fault Zone;
- Namrun Fault Zone;
- Kozağaç Fault Zone;
- Kozan Fault Zone.

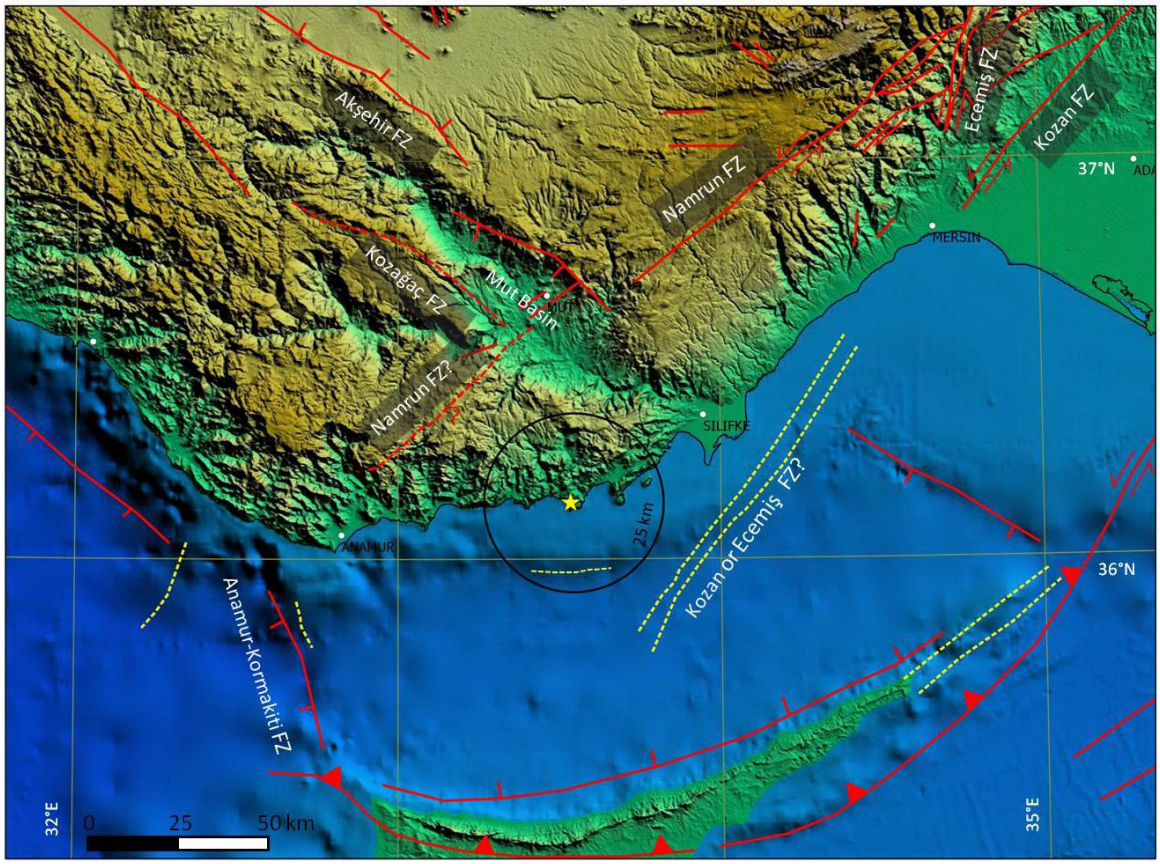

Figure 6/6.3 – Fault zones from literature data of potential interest for the site, either inland or offshore. The yellow star indicates the Akkuyu NPP site

6.6.2 MORPHOTECTONIC INVESTIGATIONS

An air-photo interpretation has been performed in the near regional area of the Akkuyu NPP site in 2011 [6/245] in order to verify the absence of potential capable tectonic structures. A multi-scalar approach has been adopted for this purpose, investigating both morphostructural features on small scale and evidence for surface faulting and deformation on a larger scale.

Added to the near regional area, a wider region, corresponding to a circular area of 50 km in radius, has been considered in a conservative perspective, since additional sets of aerial photography coverage were made available.

Two different sets of aerial photography coverage have been analyzed.

Near Regional analysis made use of 1:60 000 scale black-and-white aerial photographs. This is composed by 5 different flight paths, acquired in the E-W direction, covering approximately 78% of the near region area (Figure 6/6.4).

Average lateral overlapping is approximately 65% in the east-west direction and 40 % in the north-south direction, ensuring an optimal 3D coverage of the investigated area.

The SE sector of the near region area has been also analyzed through 1:30,000 scale black-and white aerial photographs, used to investigate in greater detail some selected areas.

The total area covered by the photos is 2 313 km^2, being equivalent to the 78% of the inland near region area (25 km in radius) and to the 64% of the inland extended area (50 km in radius).

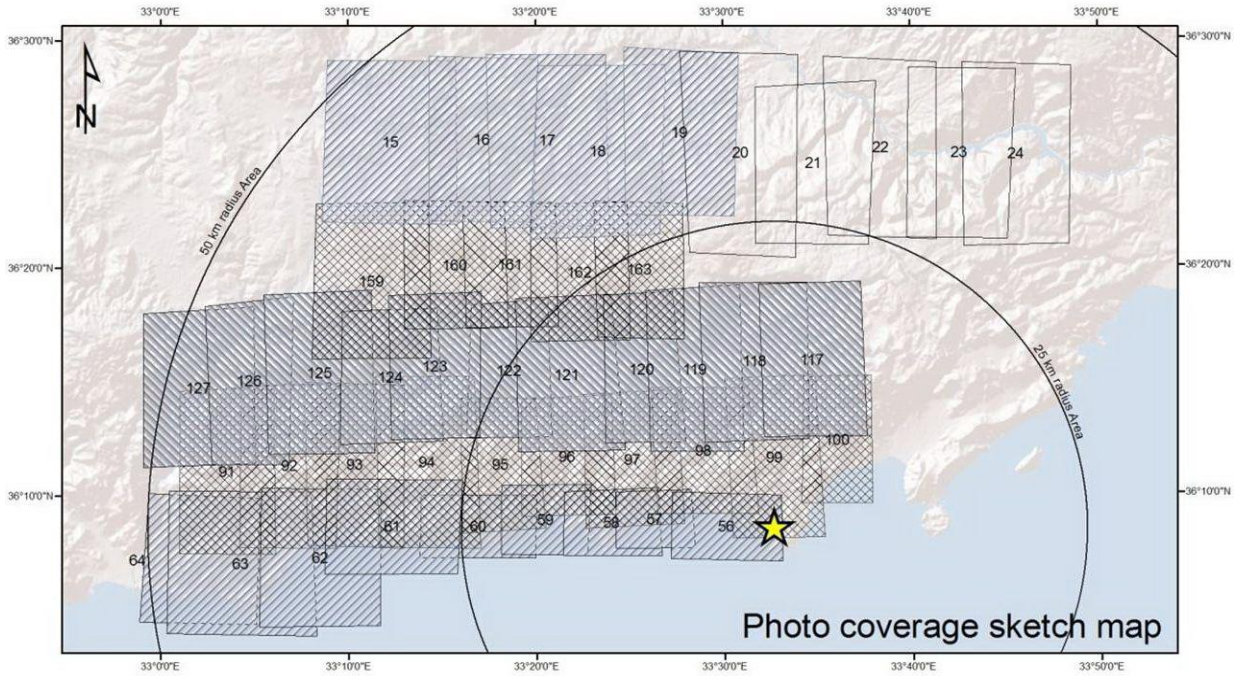

Figure 6/6.4 – Air-photo coverage for Near Region Area [6/245]. Original photo scale 1:60,000. The yellow star indicates the Akkuyu site

Aerial photographs have been analyzed through a SOKKIA stereoscope in real scale and through a 3X optical magnifier device.

Interpreted features have been then georeferenced through a GIS based platform on a free topographic base map at 1:20 000 scale.

Photo-interpretation mapping highlighted all morphostructural features though a detailed comparison with published and un-published geological maps of the area [6/56, 6/57, 6/55 and 6/87]. In order to distinguish between inherited morphostructural features, passively highlighted by morphoselection and tectonic features actively sculpting the landscape, particular attention has been paid to areas covered by quaternary deposits or interested by recent geomorphological features/processes.

A brief description of each mapped feature follows, according to the map legend:

Bedding attitude: where easily recognizable, bedding strand has been followed in small sectors, in order to highlight bedding vs. topography relationship. A symbol indicating bedding attitude (inclined, horizontal or vertical strata) has been added to summarize strike and dip

direction. High dipping strata (more than 60 degrees) can show an uncertain dip direction from 3D air-photo imaging, while strike is always well expressed.

Flatiron: these are triangular-shaped morphostructural feature caused by morphoselection; they result from the long term erosion of homoclinic slopes (Hogback or Cuesta) characterized by alternating more and less erodible strata.

"Fluvial elbow" is a right-angle or a series of right-angle turns of thalweg.

"Saddle" indicates a depression in the water divide.

Scarps: features marking a linear detectable break in the slope. Scarps mapped as "morphological scarps" include features traceable to diverse erosive processes (i.e., coastal cliffs, landslide niches, fluvial erosion). "Counterslope scarps" indicate trenches-like linear features, locally inverting the main slope direction. "Plateau Margin" indicates major scarps, ten to hundreds of meters high, usually sinuous in map view, bordering geomorphologic plateau, mesa or butte and thus separating areas of different relative base level.

"Intramountain basin depression" indicates a morphologic depression closed on almost all its sides by elevations and located inside an area of elevated relief. Sometimes these are endoreic basins, filled with recent sediments. These depressions are usually located on the top of plateau or mesa.

"Photo-interpreted faults and lineaments" indicates a structural feature highlighted by

s) angular unconformities in bedding attitude,

t) aligned point features as "saddles";

u) "fluvial elbows", aligned valleys/water divide and/or counterslope scarps.

This term does not indicate any inference on fault activity since also a well expressed structural feature could have been highlighted through time by morpho-selection without any movement on the fault itself.

"Terraces" are of fluvial origin. These include both fill&cut and strath terraces, whose genesis has to be ascribed to the concurrent action of cyclically climate-driven sea-level changes and tectonic uplift.

Map plotted by results of morphotectonic analysis [6/245] is shown in Figure 6/6.5.

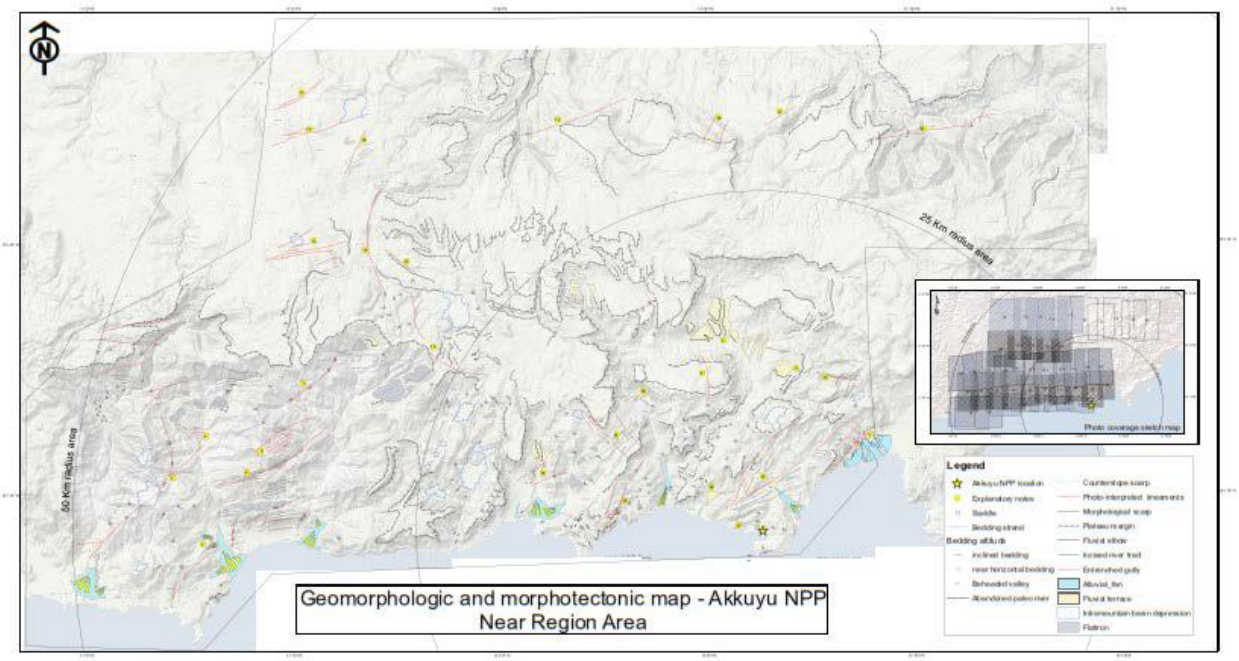

Figure 6/6.5 – Map summarixzing results of morphotectonic analysis [6/245]

Morphotectonic framework

The near regional area is occupied by a ENE-WSW emergent coastline, characterized by northsouth elongated peninsulas (Ovacık, Akkuyu and Sancak) and alternating bays. Coastlines are typically concordant in the NE-SW directed sectors and discordant in the NW-SE directed sectors, featuring distinctive landforms such as bays and headlands.

From a morphologic point of view the area can be divided into two main sectors:

v) Southeastern, draining to the south across a landscape characterized by deep and wide valleys excavated into the mainly Paleozoic folded and thrust bedrock. Three main valleys drain this sector toward the south, closed between the aforementioned peninsulas. Headwater basins are typically located just northward of the southern margin of the plateau. Inside this area some mesa are present, typically associated with Mesozoic sedimentary covers, unconformably overlying the older Paleozoic rocks;

w) Northwestern, draining to the north and occupied by a large gently N-dipping plateau, capped by the Miocene marine units. Some mesas are recognizable to the SE, just north of the Ulupinar village.

SE Sector

Thrusting and folding drive the structural forms of the landscape in this sector.

Bedding is often easily recognizable at medium scale through photo-interpretation and alternating different textures and colors on the analyzed images highlight different types of rocks.

Along folds flanks, where competent strata are alternating with more erodible ones, aligned flatirons, derived from eroded hogback or cuesta, are recognizable. These features are often underlined also by counterslope scarps in the upslope sector and subsequent thalweg, following the bedding plane, along their sides. Parallel or trellis drainage pattern is dominant, driven by subparallel folding and high angle homoclinalic slopes.

Near Aydıncık village and north of Beydili village, respectively 20 km and 12 km north from the site, Triassic to Jurassic units unconformably overlay the Paleozoic succession. The outcropping Mesozoic sequence is morphologically underlined by an elevated, flat lying and faintly corrugated area, constituting a plateau between 500 and 800 meters in elevation. A high cliff marks the borders of these plateaus.

The passage of the main overthrust is underlined by sub-parallel valley, and by the alignment of fluvial elbows. These features are related also to the passage, locally tectonic, between the Babadil Gr. and the less erodible Sipahi Fm, both Paleozoic in age. Similar features have also been observed in other areas where a stratigraphic passage between these two formations give rise systematically to relief associated to the Sipahi Fm and to a drainage network sub-parallel to bedding. Local geological and structural setting passively drives drainage network, usually of sub-parallel or trellis type, with some main fluvial tracts cutting through the structures and many low order streams running along structures/bedding trend.

All these features are thus derived from differential erosion and morpho-selection.

Fluvial terraces are present at different height in the Yanışlı, Büyükeceli and Sipahili Valley, where flights of a fill-cut and strath terraces, elevated above the present valley floor, are recognizable.

In [6/75] the presence of some lineaments identified as “previously un-mapped faults” in the near region area is highlighted. These are:

x) the western end of 40 km long NE-SW trending lineament, divided into three 13 km long segments;

y) a 5 km long NW-SE lineament, running along the Büyükeceli Valley.

The former is a straight feature almost corresponding to the Büyükeceli overthrust whose marked geomorphological evidence is due, as already explained, to morphoselection. The NW-SE oriented lineament runs exactly along the Büyükeceli Valley: no evidence of faulting/deformation has been detected along this supposed fault. It has to be noted that there is a perfect matching between the structural features running perpendicularly to the valley and surveyed on both its sides,

suggesting that no displacement/deformation has occurred along a structure buried below the Büyükeceli Valley.

NW Sector – the Plateau

This area is divided, just north of the southern margin of the plateau, by the present-day water divide, however past traces of southward directed drainage system are still recognizable at the southern fringe of the plateau and in some spot areas of the south-eastern sector.

The plateau is mainly dissected by the Sipahili Valley, whose basin is partially excavated inside the plateau region and whose eastern branch isolates some mesa south of the plateau.

Description of the Highlighted Lineaments

The analysis is addressed in recognizing all possibly capable faults in the near regional area, tentatively determining their latest movements and evidence of segmentation. Recent (Late Pleistocene to Holocene) surface faulting should be still recognizable, considering particularly conservative climatic and morphologic framework of the area. Climatic arid conditions and the scarce amount of vegetation are particularly favorable for the application of this technique in fault displacement detecting. Map of identified lineaments is shown in Figure 6/6.6.

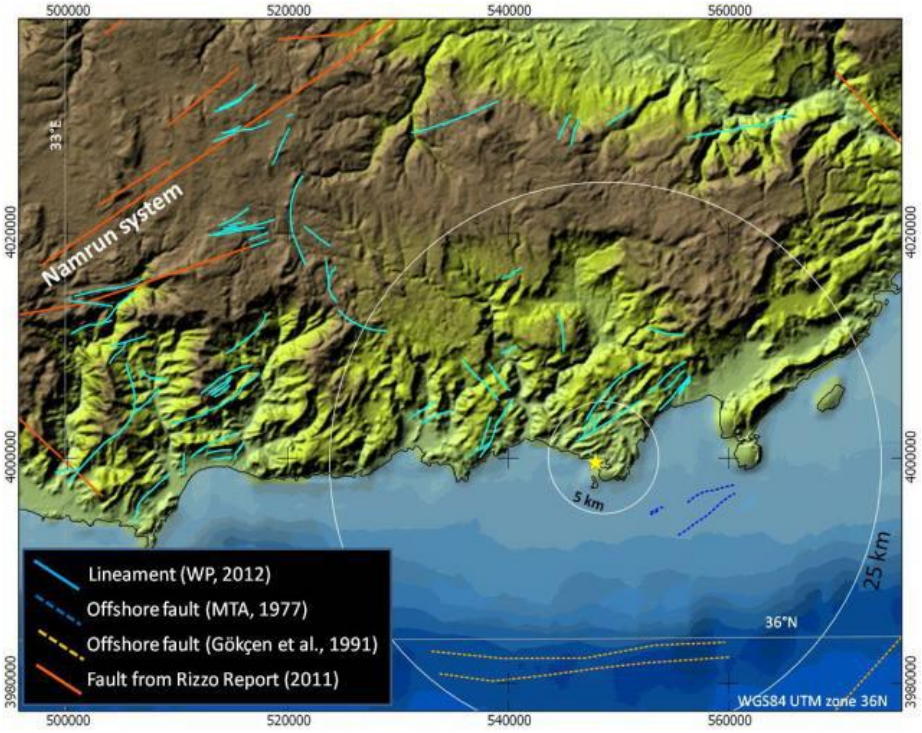

Figure 6/6.6 – Map of identified lineaments. The location of the "Namrun FZ" is hypothetical.

No evidence for recent surface faulting can be definitively associated to any regional fault. Several lineaments have been identified, based on their morphological evidence and freshness of the planar features.

To better illustrate the main results achieved during this analysis and to depict the general morphotectonic framework of the near regional area, 29 points of interest have been described in the following explanatory notes. These features are mapped in Figure 6/6.5. The nearest distance of the feature to the site is provided for each point of interest.

17) In the vicinity of the Hırmanlı village, there is a peculiar landform due to a recent relative uplift of this coastal sector. The alluvial fan delta is now dissected from the drainage system which in turn erodes this landform. Local streams run parallel in a north-south direction and then make a series of abrupt right-angle deviations, aligned just along the remnants of the dissected fan apex. The fan is differentially tilted to the SE, as highlighted by dipping measurements reported by large scale geological maps, [6/57 and 6/55] 15° to the SE in the apex sector and 8° at the south-eastern fringe of the fan. Bedrock is locally NW dipping thus a fan deposition upon a pre-existing flatiron-like feature cannot be inferred. Structurally there is a NE-SW trending syncline north of the fan and a sub-parallel anticline, whose structural culmination is just below this fan, running buried under the sediments of the valley. Nevertheless, the observed differential tilting does not seem consistent with amplification of these folds.

It has to be underlined that the present upstream catchment is under-dimensioned with respect to the fan, which seems to be related to an abandoned southward draining hydrological system, as also suggested by the presence of some paleo-rivers north of this site. The fan age has not been estimated through absolute dating although Demirtaşli & Genç [6/57 and 6/55] report Pliocene-Quaternary age for this feature. Minimum distance to the site: 7 km.

18) At the outlet of a small SW-NE trending valley an alluvial fan is presently crossed by a stream which is actively feeding the fan itself. A hundred meters to the north a relatively deep gully, incised into the fan is completely disconnected from any upstream sector and now represent a tract of a beheaded valley. If the stream deviation has to be related with tectonic causes, then a tilting of this sector has to be considered, with a differential uplift of the northern sector (where the stream was actively incising until uplift has defeated the water erosive power) with respect to the southern one (where the stream has been deviated). Uniform uplift of the whole outlet area could not explain this feature. It has to be underlined that also other non-tectonic process could have been considered for this feature. Minimum distance to the site: 40 km.

19) This lineament, 13 km long, presents a strong morphologic expression, underlined by aligned saddles, crest splitting, aligned valleys and counterslope scarps. In the central sector

it crosses an intramountain depression, developed into the outcropping Paleozoic units. This lineament could be probably related to passively inherited stratigraphic contacts or to the presence of a cataclastic zone, associated to faulting, more prone to erosion. No Quaternary covers has been detected that can prove or definitively rule out a recent activity of this recognized lineament. Minimum distance to the site: 42 km.

20) This lineament is a fault detected based on the angular unconformity between the bedding of adjacent zones. No morphologic expression is associable with this fault. Minimum distance to the site: 42 km.

21) These sub-parallel NE-SW trending short lineaments were identified based on alignment of sub-parallel rectilinear valleys and saddles. No Quaternary covers has been detected that can prove or rule out a recent activity of these recognized lineaments. Minimum distance to the site: 35 km.

22) This 10 km long, ENE-WSW directed lineament, is marked by a north-dipping plane, morphologically expressed by a continuous series of aligned saddles, counterslope scarps and crest splitting. Bedding is sub-parallel to this feature on its both sides. No Quaternary covers has been detected that can prove or rule out a recent activity of this lineament. Minimum distance to the site: 32 km.

23) This is a 5 km long lineament, marked by a clear curved alignment of saddles and secondary valleys, crosscutting the E-W trending tightly folded Paleozoic rocks. No Quaternary covers have been detected that can prove or rule out recent activity of this lineament. Minimum distance to the site: 33 km.

24) This lineament is 3 km long, N-S directed W-dipping planar feature, recognized based on a strong alignment between two rectilinear valleys on the opposite sides of a mesa and a trench, crossing the flat area aligned with these valleys. No Quaternary covers have been detected that can prove or rule out a recent activity of this lineament. Minimum distance to the site: 10 km.

25) Along the eastern branch of the Sipahili Valley, 15 km upstream from the river outlet, several flights of elevated fill & cut terraces are recognizable. These terraces are located in a tract where the valley widens and closes between the plateau to the north and a mesa to the south. The aggradational and subsequent erosive phase (or phases) that intersected this valley tract cannot be examined in details but the good preservation of the terraces, on both valley sides, allow a good reconstruction of at least two different aggradational valley floors, separated by at least two periods of incision, including the present one. The alluvial terrace,

preserved 2 km to the SE and described in detail in point 12, testify to an older and more elevated aggradational valley floor. These terraces point to the recent regional uplift of this region, as discussed in the previous sections. Minimum distance to the site: 13 km.

26) This lineament is a fault detected based on the angular unconformity between the bedding of adjacent zones. No morphologic expression is associable with this fault. Minimum distance to the site: 12 km.

27) This fluvial terrace is now drained by a small stream, running WNW-ESE and connecting to the drainage of the Sipahili Valley. There is a short valley tract (500 m long) upstream of this terrace with no catchment upstream (beheaded valley). Just north of this terrace a N-S directed and south-dipping paleoriver could be detected over some flat and elevated area. Farther north other paleoriver tracts are still recognizable, still showing a southward confluence. This fluvial terrace has to be probably related to an ancient paleo-drainage system, draining to the south from the plateau area, which was locally infilling the valley floor. After an important phase of uplift and regional folding of the whole Taurides domain, drainage has been locally inverted and the newly developed southward draining system (south of the elevated area now occupied by the plateau) started to deeply incise bedrock and older alluvial covers. Fluvial piracy caused abandonment of ancient valley floors and general rearrangement of the catchments. Similar observations are reported also for the westernmost sector of the Taurides by Monod et al. (2006) [6/157]. In this case the ancient valley floor has been cut by the newly developed drainage, definitively disconnecting the terrace area by the upstream sectors. Minimum distance to the site: 12 km.

28) These are some 1 to 5 km long, ENE-WSW oriented lineaments, located upon the plateau sector. Bedding is generally horizontal and thus high dipping or sub-vertical planes, like the ones depicted by these sub-parallel lineaments, have to be related to secondary planar structures. These lineaments are identified based on alignment of rectilinear crests and elongated closed small basins (sag-ponds). The northernmost lineament crosscuts a small intramountain basin whose sediments texture seems to abruptly change along the lineament. Minimum distance to the site: 37 km.

29) A NW-SE directed 3 km long lineament, marked by a clear counterslope scarp running along a marked morphological scarp due to fluvial erosion. Probably this lineament is the remnant of an ancient paleo-river rectilinear tract, sub-parallel to the present one, deeply incising the ancient valley floor. Minimum distance to the site: 31 km.

30) This is an 8 km long, convex eastward lineament, marked by a continuous succession of saddles, crest splitting and counterslope scarps. Probably this lineament has to be related to the remnants of an ancient paleo-drainage system, now completely rejuvenated and rearranged. No Quaternary cover has been detected that can prove or rule out a recent activity of this lineament. Minimum distance to the site: 31 km.

31) This lineament is a fault detected based on the angular unconformity between the bedding of adjacent zones. A deep entrenched canyon is locally cutting through rocky spurs. This feature has to be related to the remnants of an ancient paleo-drainage system, now completely rejuvenated and rearranged. Minimum distance to the site: 40 km.

32) This is a 6 km long, ENE-WSW directed lineament, aligned with the rectilinear southern side of a small intramountain basin. The lineament is marked by long rectilinear aligned crests and seems to be related to a change in the texture of the sediments infilling the basin. Minimum distance to the site: 42 km.

33) These sub-parallel NW-ward convex lineaments have been detected based on alignments of small crests and counterslope scarps. Morphoselection can be advocated for these features. Minimum distance to the site: 46 km.

34) This is an 8 km long, ENE-WSW directed lineament, developing in sub-horizontal dipping bedrock detected based on the presence of a recognized sub-vertical fault/fracture plane with a clear geomorphological expression. No Quaternary covers has been detected that can prove or rule out a recent activity of this lineament. Minimum distance to the site: 33 km.

35) An eastward convex, 9 km long lineament has been detected based on the alignment of small crests and counterslope scarps. Probably this lineament is the remnant of an ancient paleoriver drainage system, now completely re-juvenated and rearranged. Minimum distance to the site: 23 km.

36) These two small lineaments have been detected based on the presence of two sub-parallel small valleys, aligned with other two incisions on the opposite side of the main valley floor. No Quaternary covers has been detected that can prove or rule out a recent activity of this lineament. Minimum distance to the site: 28 km.

37) This small lineament is marked by a rectilinear entrenchment running along the water divide on the NW flank of the main valley. There is a clear morphological evidence for this lineament but no Quaternary cover has been detected and gravitational processes seem to be more probably responsible for this type of feature. Minimum distance to the site: 30 km.

38) This is an E-W trending, 10 km long lineament, highlighted by the concordant alignment of fluvial elbows (with a right step-over), low order streams, counterslope scarps and crest splitting. Plane attitude is sub-vertical. Minimum distance to the site: 30 km.

39) These are a series of straight lineaments, NE-SW trending, corresponding to the Büyükeceli and Koçaşlı overthrusts whose marked geomorphological evidence is due to morphoselection. Minimum distance to the site: 3 km.

40) This 5 km long, NW-SE trending lineament is highlighted by the alignment of counterslope scarps and rectilinear incisions on the opposite valley floor. Minimum distance to the site: 11 km.

41) These 3 km long, NE-SW trending lineaments have been detected based on the alignment of fluvial elbows, counterslope scarps and saddles. Deep-seated gravitational processes seem to be more probably responsible for this type of feature. Minimum distance to the site: 15 km.

42) These 3 to 5 km long, NE-SW trending lineaments have been detected based on the alignment of fluvial elbows, counterslope scarps and saddles. Their marked geomorphological evidence is probably due, consistent with bedding attitude and with structures trend, to morpho-selection. Minimum distance to the site: 10 km.

43) A small doubtful NE dipping high-angle plane feature crosscuts a water divide 1.5 km NW of the site. The origin of this fresh-looking but certainly minor feature, being recognizable in the photos for a length of only 250 m, should be verified in the field. Minimum distance to the site: 1.5 km.

44) Fluvial terraces recognized in the site vicinity area, as well as the reincised alluvial fans, testify a recent uplift of this sector. In the Yanisli Valley a series of staircase fluvial terraces, both of fill & cut and strath origin, have been recognized. These fluvial terraces, in such sea-proximal areas, are typically the result of the direct interaction between cyclic rise and fall of sea-level and the uplift of the coastal sector, the latter allowing ancient valley floors to be cut by subsequent fluvial erosion. Minimum distance to the site: 4 km.

45) This lineament is a fault detected based on the angular unconformity between the bedding of adjacent zones. No morphologic expression is associable with this fault. Minimum distance to the site: 13 km.

No major tectonic lines appear to cross the near region, as described above. Some of the lineaments traced outside the 25 km radius may be connected to the Namrun Fault System, which runs about 40 km northwest of the site according to the recent mapping of the area.

6.6.3 MARINE SURVEY

In 1976 MTA (Geophysics Dpt., Dr. M. Boztaş) has recorded 613 km of high resolution seismic lines near the Akkuyu site with its vessel Sismik-1 [6/159]. The work was commissioned by TEK (Turkish Electricity Authority) within the framework of the studies for characterizing the Akkuyu site. The track lines, approximately east-west and NNW-SSE-trending, were recorded with spacing of 500 m within a distance of 5 km from the site and a spacing of 1 km from 5 to 10 km (Figure 6/6.7). The lines started at a distance of 500 m off the coast. The purpose, apart from building a bathymetry map, was to search for any evidence of active faulting, by mapping fault ruptures and other signs of disturbance, such as gravity collapses and warping. Two different systems were utilized, one less penetrative but with higher resolution for water depths shallower than 70 m (resolution 40-60 cm) and another one (air gun) for larger depths (attained resolution of 1 m).

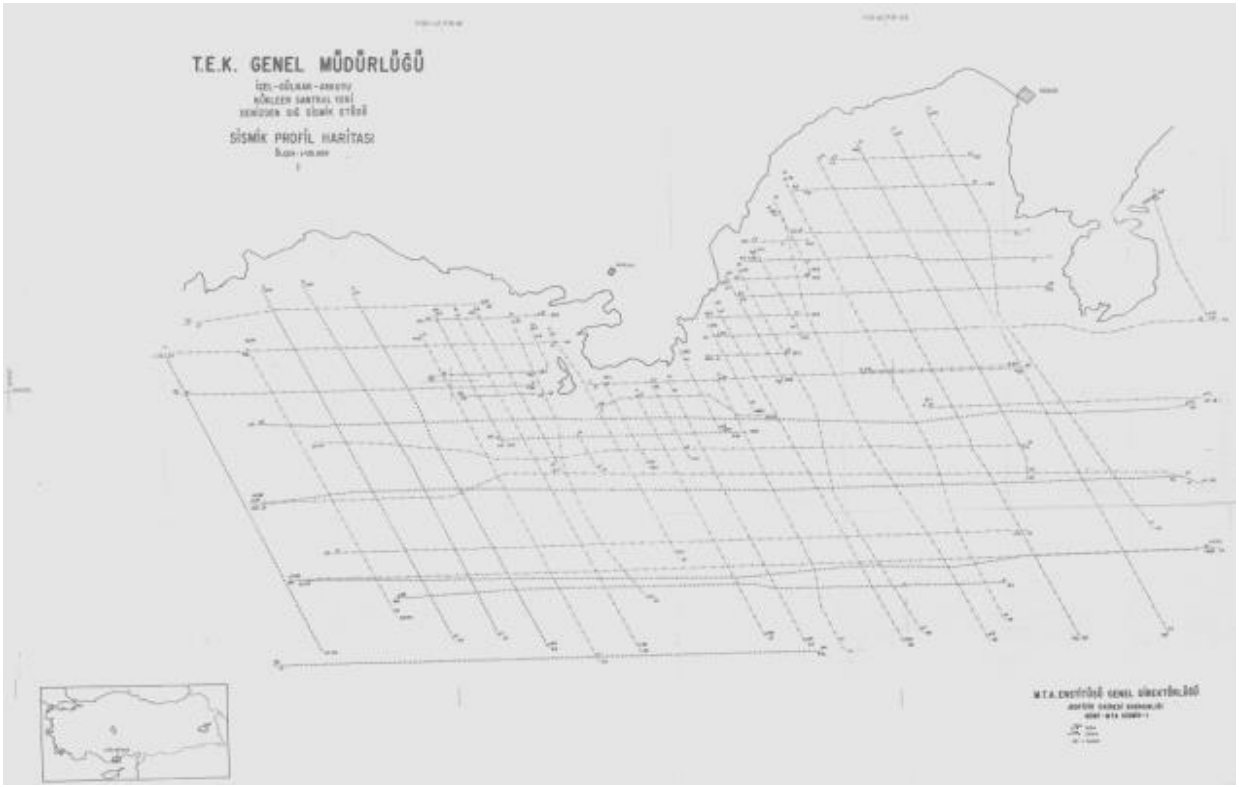

Figure 6/6.7 – Grid of seismic lines in the MTA report of 1977 [6/159]

The study area can be divided in three basins: eastern (Ovacık), central and western. The main results are given below (Figure 6/6.8):

a) In the Ovacık basin, there is a north-south drop of ca. 30 m in the sea bottom, which is interpreted as a fault-controlled erosion scarp continuing the fault visible inland.

Minor faulting and slumping features are also recognized, but with small offset and lacking lateral continuity. In the southeast edge of the explored basin, at a minimum distance of 7 km from the site, graben features were mapped with evidence of faulting propagating to the surface and offset reaching 1.5 m. This feature has been investigated by the recent offshore high-resolution seismic reflection campaign performed by WorleyParsons in 2011 [6/244] and summarized below.

b) The central basin shows a number of unconformities, partly cut by deep erosional features, but no evidence of dislocations.

c) The western basin shows reefal structures near shore and local disturbances due to an increase in the overburden pressure. There are also domal structures, interpreted as likely caverns, and minor faulting visible only in the upper layers and not laterally continuous.

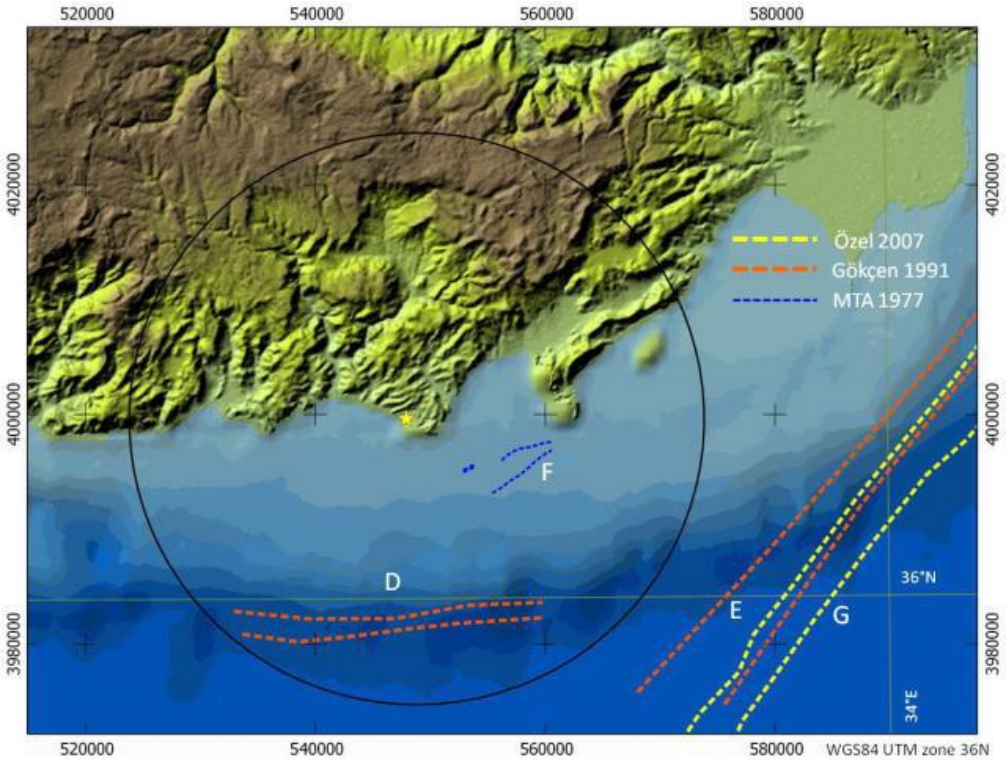

Figure 6/6.8 – Active offshore faults inside and close to the Near Region area of the Akkuyu site, according to various sources. The faults labeled "F", only 7 km from the site, are now excluded by the most recent seismic investigation [6/244]

In the offshore area south of the site, a geophysical campaign has been conducted during November 2011 covering a maximum distance from the coast of approximately 25 km at a water depth approaching 400 m. Data acquisition was carried out by Fugro Ltd, while Anatolian

Geophysical (AG) has performed the data processing and interpretation [6/244]. The acquired data were:

1) multibeam and side-scan sonar tracks, to obtain a detail mapping of the sea floor;
2) sub-bottom profiles, to detail the most superficial Quaternary stratigraphy;
3) 2-D high resolution seismic reflection lines, to search for possible evidence of faulting in the deeper stratigraphic units.

The seismic data acquisition parameters are summarized in Figure 6/6.9. In total, about 420 kilometers of seismic lines were recorded, distributed on 30 traverses, with a grid composed of 18 traverses in the NW-SE direction (Akkuyu NPP100 series) with spacing 1 kilometer, and 12 in the NE-SW direction (Akkuyu NPP200 series) with spacing 2 kilometers.

The interpreted lines were obtained by prestack time migration and prestack depth migration. The relative amplitudes were preserved so that the reflector amplitudes on the image sections are proportional to the velocity contrast across layer boundaries. Section lengths vary from nearly 20 to 6 kilometers each.

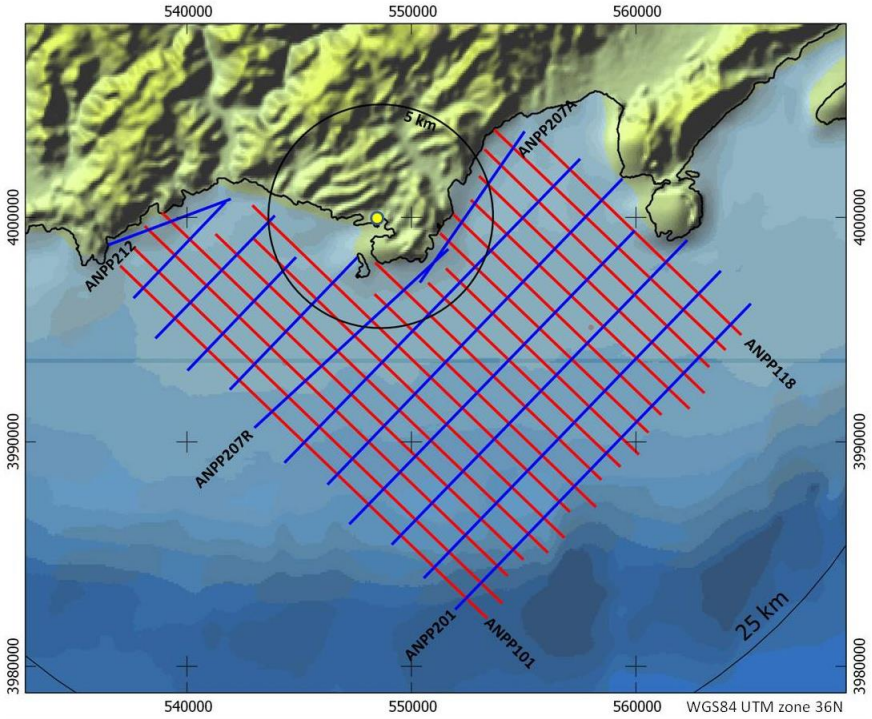

Figure 6/6.9 – Map of traverses of offshore 2-D seismic survey compared with the extensions of site vicinity (5 km) and near regional (25 km) areas [6/244]

The following list of observations made on the seismic sections has been made:

(1) In all the sections, the top-Basement rock can be clearly identified which is mid-Devonian dolomitic limestone (labeled as B) associated with the Alanya Massif on land. As a result

of the basement uplift, several major normal faults are observed, but only affecting the basement itself.

(2) The basement uplift has caused folding and faulting on the sedimentary sequence immediately above (labeled as T).

(3) A major unconformity within the Pliocene sequence can also be clearly identified in these sections (labeled as U). The tectonically induced folding and faulting (T) caused by the basement uplift has affected the sedimentary sequence below the unconformity (U) but not above.

(4) Basement-induced displacements (labeled as A) at the sea-bottom sediments and sea-bottom morphology (E) associated with rapid deposition which runs over the gravity sliding effect are observed.

(5) Gravity induced deformation (C) beyond the shelf edge along the dipping water bottom is observed.

(6) The marked difference in reflection strength between the sub-bottom Plio-Quaternary sequence (Q) and the deeper Pliocene sequence (P) is observed.

(7) The top-Basement (B) shows extremely rugged topography associated with an erosional surface carved by deep channels and canyons.

(8) Change in reflection character along the top-Basement is observed which may be associated with possible build-up of reefs on top of the mid-Devonian basement. The basement rock outcrops at the Akkuyu NPP Site. In contrast, the top-basement is represented by a sharp event (B) as moving up to the higher basement elevations close to the shoreline, where the reef limestone may have been eroded.

(9) Major faulting caused by the basement uplift but only affecting the basement itself is observed.

Figure 6/6.10 reproduces a representative choice of interpreted seismic sections. Only pre-stack time migrated (PSTM) lines are shown. The whole set of lines, as well as the corresponding prestack depth migrated (PSDM) lines, can be found in the WorleyParsons report [6/244]. The sections are shown down to 1.2 seconds, approximately corresponding to a depth of 1 000 meters.

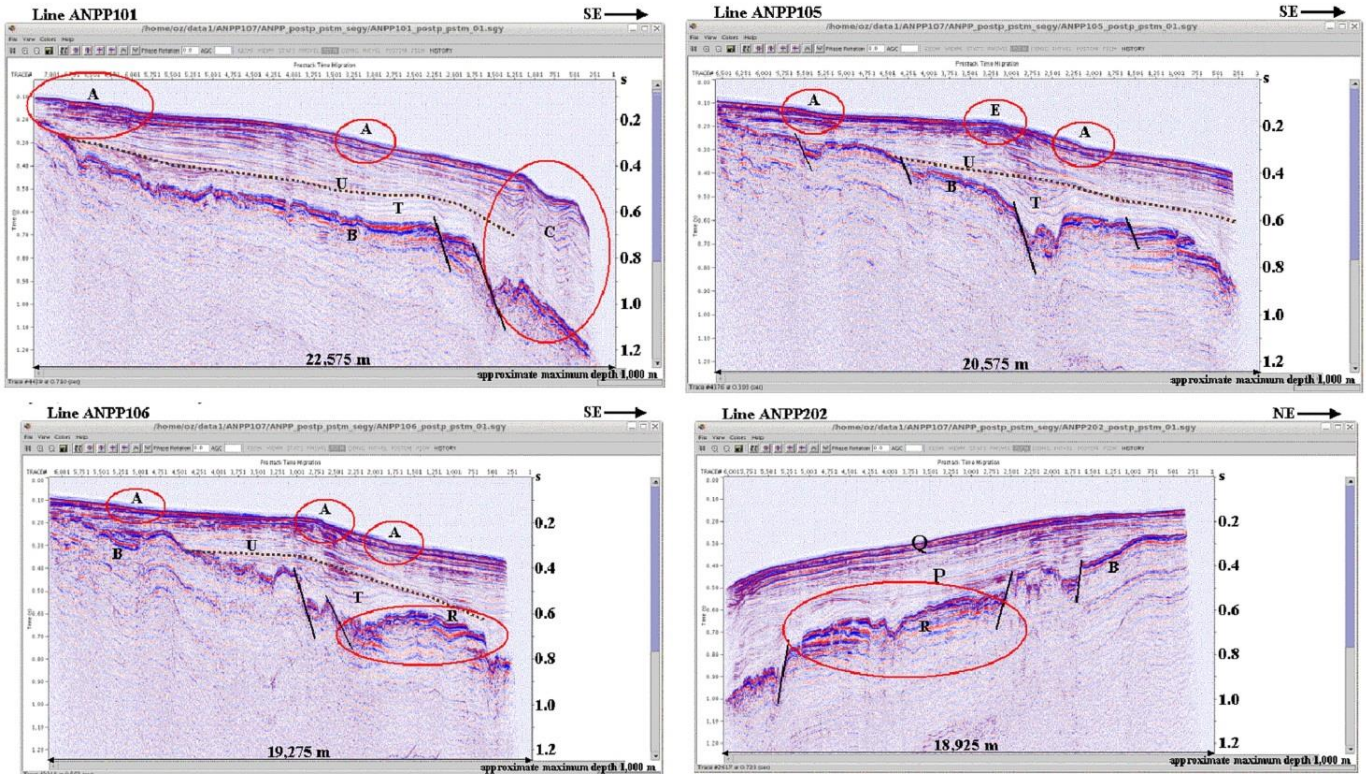

Figure 6/6.10 – Samples of pre-stack time-migrated (PSTM) seismic lines. Q - Quaternary, P - Pliocene, A - basement-induced displacements, B - top of basement, C – gravityinduced deformation, E - morphology associated to rapid deposition, R - possible reef limestone, T - folding and faulting induced by basement uplift, U – unconformity [6/244]

Based on the observations made on the PSTM sections along the 100-series of lines in the NWSE direction and the 200-series of lines in the SW-NE direction, the time- and depth-structure maps produced by picking the depositional unit boundaries from the PSTM sections and the PSDM sections, the following structural history can be constructed for the survey area:

(1) The basement rock, which constitutes the Alanya Massif on land, consists of mid-Devonian fractured dolomitic limestone. Over a long period of geologic times, this formation was subjected to intensive erosion giving rise to an extremely rugged topography.

(2) The basement uplift then took place, which accelerated the erosional process - carving deep canyons and channels in the basement rock.

(3) The basement uplift also caused en-echelon normal faulting that affected the basement topography.

(4) Following the subsequent Lower-Pliocene transgression, rapid deposition of sediments formed the first depositional unit on top of the basement rock (Unit 1).

(5) The basement uplift continued and thus caused severe deformation within the depositional unit above in the form of faulting and folding (T).

(6) A regression took place, which caused rapid erosion of a significant portion of the depositional unit just above the basement rock and formed the mid-Pliocene unconformity (U).

(7) Subsequent transgression formed two additional depositional units on top of the unconformity (Units 2 and 3) during the Upper-Pliocene and the last depositional unit (Unit 4) during the Plio-Quaternary.

(8) Additionally, tectonic activity ceased after the formation of the middle Pliocene unconformity.

(9) During the Upper-Pliocene and Quaternary, the deposited sediments were subjected to basement induced deformations (A and E) and gravity induced deformations (C).

(10) Although some faulting has occurred as a result of the compaction-induced and gravityinduced deformations that reach up to the sea bottom; nevertheless, these faults are not in any manner attributable to active tectonics. Moreover, the sub-bottom profiler sections do not imply any neotectonic disturbance

In conclusion, it can be stated that no tectonic activity exists in the project area since mid-Pliocene up to the present time. The mid-Pliocene unconformity defines the geologic time boundary between the active tectonics before that is primarily in the form of basement uplift and the inactive period after.

6.6.4 SITE VICINITY SURVEY

High-precision marine seismic survey was performed within the 5-km sea area in 2011 (see Section 6.2). According to the results of survey a channel-like structure (micrograben type) was revealed in the bottom sediment layer in the paleorelief buried surface. It can be the result of excavation of a river or what is more likely a faulting activity. The revealed structure does not deform the recent sediment deposits, so it is concluded that it has no recent activity.

In the site vicinity/site area, the landscape is characterized by small hills and very gentle rounded slopes without irregularities or other geomorphic evidence that could suggest tectonic dislocation of the topographic surface in geologically recent time. The site vicinity (5 km radius) and site area (1 km^2) around the Akkuyu NPP site is given in Figure 6/6.11.

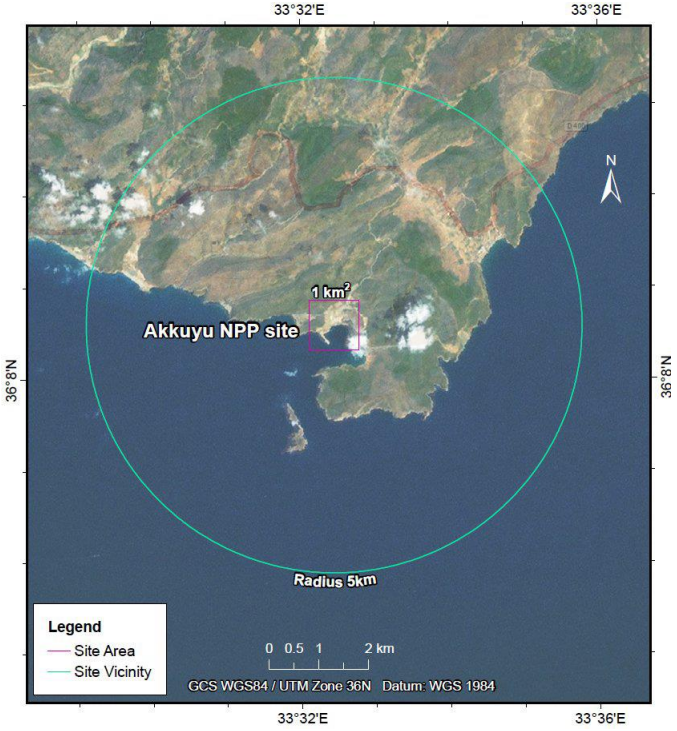

Figure 6/6.11 – The site vicinity (5 km radius) and site area (1 km^2) around the Akkuyu NPP site

Series of fault investigations were carried out at the Akkuyu NPP site and at the area which lies within approximately 10 km radius around the site which is beyond the IAEA recommended distance for site vicinity scale investigations of 5km. Detailed geological map (Akkuyu Sheet) of the site in a scale 1:5000 was used for dedicated fault displacement hazard analysis.

The geological reconnaissance and mapping performed during the new site investigation campaigns were based on this mapping and the work of Demirtaşlı, [6/56]. The recent investigations conducted by Envy and Worley Parsons pointed out other unmapped geological structures in the vicinity and site areas.

The following tectonic structures were found in the site vicinity/area:

Normal faults

The Akkuyu Fault is an E-W trending normal fault that dips 60° north [6/56]. The sense of movement on the fault has been inferred based on the nature of its east-west trending fault plane and juxtaposition of formations across the fault. The block to the north of the Akkuyu fault was downthrown by ~ 200 m bringing the Db6 and Db4 members of the Büyükeceli Formation into contact with the younger Akdere Formation (Da) [6/56]. The Akkuyu fault was encountered in the excavated trenches T5, T6, T7 and T8, with trenches T5 and T8 showing that that the Akkuyu Fault did not have any effect on the Plio-Quaternary talus breccia.

To the west, the Akkuyu Fault is offset left-laterally by the Aksaz Bay Fault. Borehole investigations made in the Aksaz Bay alluvium revealed that the continuation of the Akkuyu Fault exists under the Alluvium in an E-W direction [6/56].

The Tepeköy Fault is a normal fault trending in a NNE-SSW direction with a fault plane dipping 65° towards the west [6/56]. Since it has no effect on the Tertiary Tepekoy Formation it is therefore assessed to be older than the Miocene [6/56].

Tear Faults

Shear faults trend in two general directions NNW-SSE and NNE-SSW [96]. The NNE-SSW trending faults are more prominent than the NNW-SSE trending faults. They show clear right or left lateral strike-slip movements. However, some of these shear faults are older than E-W trending Akkuyu fault as they are truncated by it [6/56]. These strike-slip faults have been assumed as pre-late Permian Variscan orogeny related. However, other strike-slip faults are observed that clearly offset Permian and Triassic formations which are assumed to be pre-Jurassic, related to the Eocimmerian Orogeny [6/56]. None of these faults have been observed affecting any Quaternary deposits.

The NNW-SSE fault trend is observed in the orientation of numerous micro-tectonic features such as joints and fractures in the outcropping Devonian rocks [6/223 and 6/225].

Subsurface data from borings, test pits and geophysical evidence also indicate faults of this orientation that are not expressed on the surface [6/56].

Joints

The dominant orientations of joints are:

- NNW-SSE
- NNE-SSW
- NE-SW
- SE-NW

The NE-SW orientation of joints is the most abundant with dips varying from steep to moderate. There is also a noticeable set of joints in the WSW-ENE direction but it is not as abundant as the other four orientations.

These orientations of joint sets are in general agreement with the joint orientations derived from both surface and subsurface studies during the early investigations of the Akkuyu Site and the Sothern tectonic region [6/56, 6/223 and 6/225].

Folds:

The main folding axis of the folds in the southern region trends approximately in a NE-SW direction while North of the site area, a major anticline and syncline pair exist which are called Büyükeceli Anticline and Büyükeceli Syncline. In the center of the Büyükeceli lies the oldest structure, ENE-WSW trending Akkuyu Anticline which was displaced by strike-slip faults.

Overthrusts:

The most persistent and important overthrust in the Site Vicinity is the Büyükeceli overthrust which runs in a NE-SW direction over a distance of 20 km, dipping 40° to northwest [6/56]. Its southern extent traverses the northwestern portion of the Site Vicinity where it forms the boundary between the Intermediate and Southern tectonic regions. Stratigraphic constraints indicate that the age of the Büyükeceli overthrust is Late Eocene [6/56 and 6/93].

The Koçaşlı Overthrust runs parallel to the Büyükeceli Overthrust thrusting the Sipahili Formation over the Babadil Group [6/56 and 6/93]. Since it appears likely that both the Büyükeceli and Koçaşlı overthrusts belong to the same tectonic system, they must both be older than the Late Jurassic.

The Sarnıç Overthrust trends in a NE-SW direction until it is terminated by NNE-SSW trending Tepeköy fault approximately 2 km south of the village of Tepeköy [6/56 and 6/93]. Since the Tepeköy Fault is a normal fault which is older than Early Miocene, the Sarnıç fault has been assessed to be older than Miocene, i.e. older than 20 million years [6/56 and 6/93].

The Taşlık Overthrust trends in a SW-NE direction one kilometer to the north of the Site, within the Site Area. Along it various members of the Büyükeceli Formation have been thrusted over the Kırtıldağı Formation, The Taşlık Overthrust has been accepted as the conjugate of the Gökgedik overthrust having moved during the main phase of folding of Eocimmerian orogeny approximately 160 million years ago [6/56 and 6/93].

The Gökgedik Overthrust trends in a general NW-SE direction, 2km east of the site. It is well exposed at the bay 1 km south of the Gökgedik hill and is cut by multiple NE-SW trending strike slip faults on Gökgedik Hill [6/56]. As mentioned above, the Gökgedik Fault is thought to have moved during the Eocimmerian orogeny [6/56].

The Aksaz Bay Fault is known to be a thrust fault with a strike slip component based on trenching investigations. Previously this NNW-SSE trending fault was assumed to be a left lateral strike-slip fault which clearly displaces the Akkuyu Fault [6/56 and 6/93]. The Aksaz Fault is covered by the Quaternary alluvium of Aksaz Bay.

Eight shallow investigation boreholes drilled in this alluvium as well as trench excavations, show that the Akzas fault has not affected the Quaternary deposits [6/56].

An detailed aerial photo-interpretation of the site vicinity and site area has been performed by WorleyParsons in 2011 to complete the database and support the fault displacement hazard assessment. Three different aerial photograph coverages have been analyzed. Site vicinity analysis made use of approximately 1:15000 scale black and white coverage, acquired in 1984.

This is composed of two different flight paths, acquired in the E-W direction, covering about 97% of the inland site vicinity area (Figure 6/6.12).

Average lateral overlapping is 65% in E-W direction and 40 % in the N-S direction, ensuring an optimal 3D coverage of the investigated area. The site vicinity area not covered by this photo series has been analyzed through 1:30000 scale black and white coverage. This series has also been used to investigate in deeper detail some selected areas of the near region area.

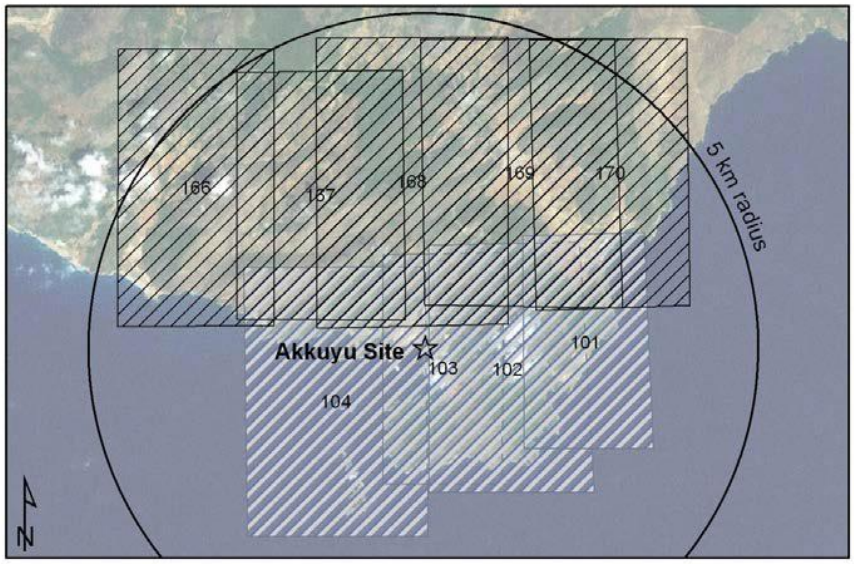

Figure 6/6.12 – Air-photo coverage for Site Vicinity Area. Original photo scale 1:15000 [6/242]

Figure 6/6.13 presents the morphotectonic map developed as a result of the investigation, showing the geomorphic features along identified faults and lineaments.

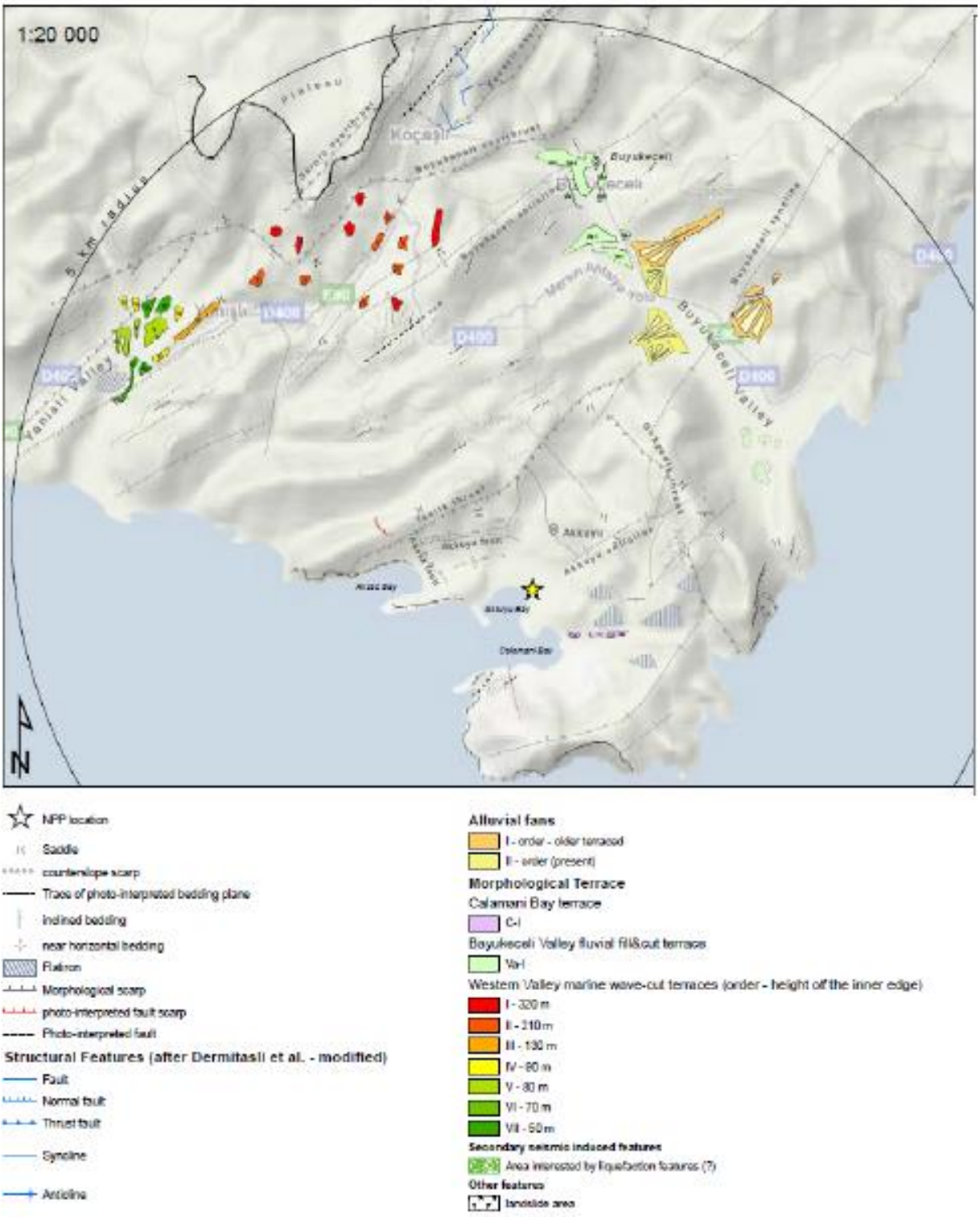

Figure 6/6.13 – Morphotectonic map of the site vicinity area [6/242]

South of the main overthrusts, folding is dominating and drives the structural forms of the landscape. Bedding is often easily recognizable at medium scale through photo-interpretation and alternating different textures and colors on the analyzed images highlight different types of rocks.

Along fold flanks, where competent strata are alternating with more erodible ones, aligned flatirons, derived from eroded hogback or cuesta, are recognizable. These features are often underlined also by counterslope scarps in the upslope sector and subsequent thalweg, following the bedding plane, along their sides. Parallel or trellis drainage pattern is dominant, driven by subparallel folding, high angle homoclinalic slopes.

North of the Sarnıç overthrust Triassic to Jurassic units unconformably overlie the Paleozoic succession. The outcropping Mesozoic sequence is morphologically underlined by an elevated, flat lying and faintly corrugated area, constituting a plateau resting in the NW sector of the site vicinity area, along the left flank of the Yanışlı Valley. A high cliff marks the borders of this plateau: on the SW and west side it is quite ondulated in map view, testifying a prolungated phase of erosion. On the SE side the plateau margin runs straight along a NE-SW direction since the morphological plateau scarp is located along the Sarnıç overthrust itself, close to the Kocaşlı village. A few hundreds of meters SE of the Sarnıç overthrust the passage of the Kocaşlı overthrust is underlined by a subparallel valley, and by the alignment of some fluvial elbows. These features are related to the passage, locally tectonic, between the Babadıl Gr. and the less erodible Sipahili Fm. Similar features have also been observed in other areas where a stratigraphic passage between these two formations give rise systematically to relief associated to the Sipahili Fm and to a drainage network sub-parallel to the bedding.

All these features are thus derived from differential erosion and morpho-selection. No evidence of fault capability has been detected related to the main regional faults (Taşlık thrust and Gökgedik thrust) in the core of the Büyükeceli anticline and near the site.

Fluvial terraces are present at different heights in the Yanışlı Valley and in the Büyükeceli Valley. A flight of a fill-cut terrace, elevated at about 20-30 m above the present valley floor is present near Büyükeceli town. The left side of the valley is also characterized by the presence of terraced alluvial fans.

Concerning the potential hazard for surface tectonic deformation, recent (Late Pleistocene to Holocene) surface faulting events should have been still recognizable if present, considering particularly the conservative climatic and morphologic framework of the area. As stated before, no evidence for recent surface faulting can be associated to any regional fault. In particular, a recent movement along the Taşlık thrust or the Akkuyu fault should have been well recognizable by a counterslope scarp which is not the case. Only a small scale uncertain plane feature, found 1.5 km NW of the site, crosscutting the watershed located just north of the Taşlık thrust, could be very remotely associated with surface faulting effects. This is a NE dipping high-angle plane that could be followed for about 250 m in length. This could eventually be the surface expression of a

secondary fault linked to the medium scale folds belonging to the Büyükeceli anticlinorium. It is planned to investigate in more detail this feature (through exploratory trenches) in the confirmatory phase analysis of the Akkuyu site.

Fluvial terraces recognized in the site vicinity area, as well as the reincised alluvial fans, indicate a recent uplift of this sector. A more detailed analysis of these terraces will be useful in order to tentatively date the relic surfaces, measure more precisely terrace height and thus estimate an average uplift of this sector and compare it with available data in literature (e.g. 0.2 mm/yr [6/51]; 0.1 mm/yr [6/53].

Site area according to the IAEA SSG-9 [6/113] should include the entire area covered by the nuclear power plant (i.e. under the control of plant management), which is typically considered as one square kilometer (Figure 6/6.14).

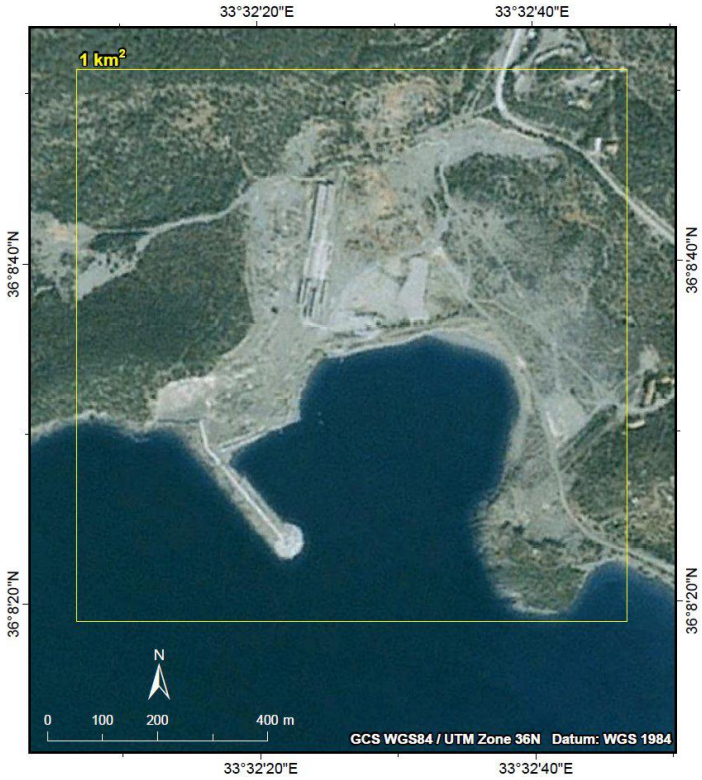

Figure 6/6.14 – Akkuyu Site Area map

The past geological investigations are considered valid studies that represent important input in the Akkuyu NPP site database.

In 1954, M. Blumenthal conducted the first geological study in 1:100 000 scale across the area between Silifke and Anamur (sheet number: Silifke 143/2) to assemble the geological map of Turkey. Between 1966 and 1981, E. Demirtaşlı mapped the region in 1:25 000 scale and compiled geological map sheets of Silifke (P31d1, P31d2 and P31c1). In 1976, detailed geological studies

focused on the Akkuyu NPP site provided five geological map sheets in 1:10 000 scale (P31b1 No.1-4, P30c2 No.3).

In the following years, Geological Department of the Mineral Research and Exploration Institute of Turkey (MTA) with a group of geologists led by E. Demirtaşlı mapped the Akkuyu NPP site in 1:5000 and 1:1000 scales and divided the Büyükeceli Formation into eight members (Figure 6/6.15). During these local geological investigations, all the structural features such as unconformities, folds, faults and joints have been studied to reveal the tectonic characteristics of the area [6/56]. In order to identify the most recent tectonic activity in the site, a total of ten trenches were opened on the prominent faults (Akkuyu and Aksaz faults), on the Quaternary deposits and across the planned foundation of the Akkuyu Nuclear Power Plant. The obtained results which revealed no sign of recent tectonic activity were later compiled in the final site geology report [6/225].

In 1986, another detailed geological study was conducted by Middle East Technical University for the Çamalanı region which was considered for a second NPP unit [6/155].

Extensive excavations carried out during 1980’s created excavated surfaces with steep cut slopes and large filled sections at the site. Along these sections, old geological maps representing the situation independent of artificial effects can be used to infer the subsurface that is now covered.

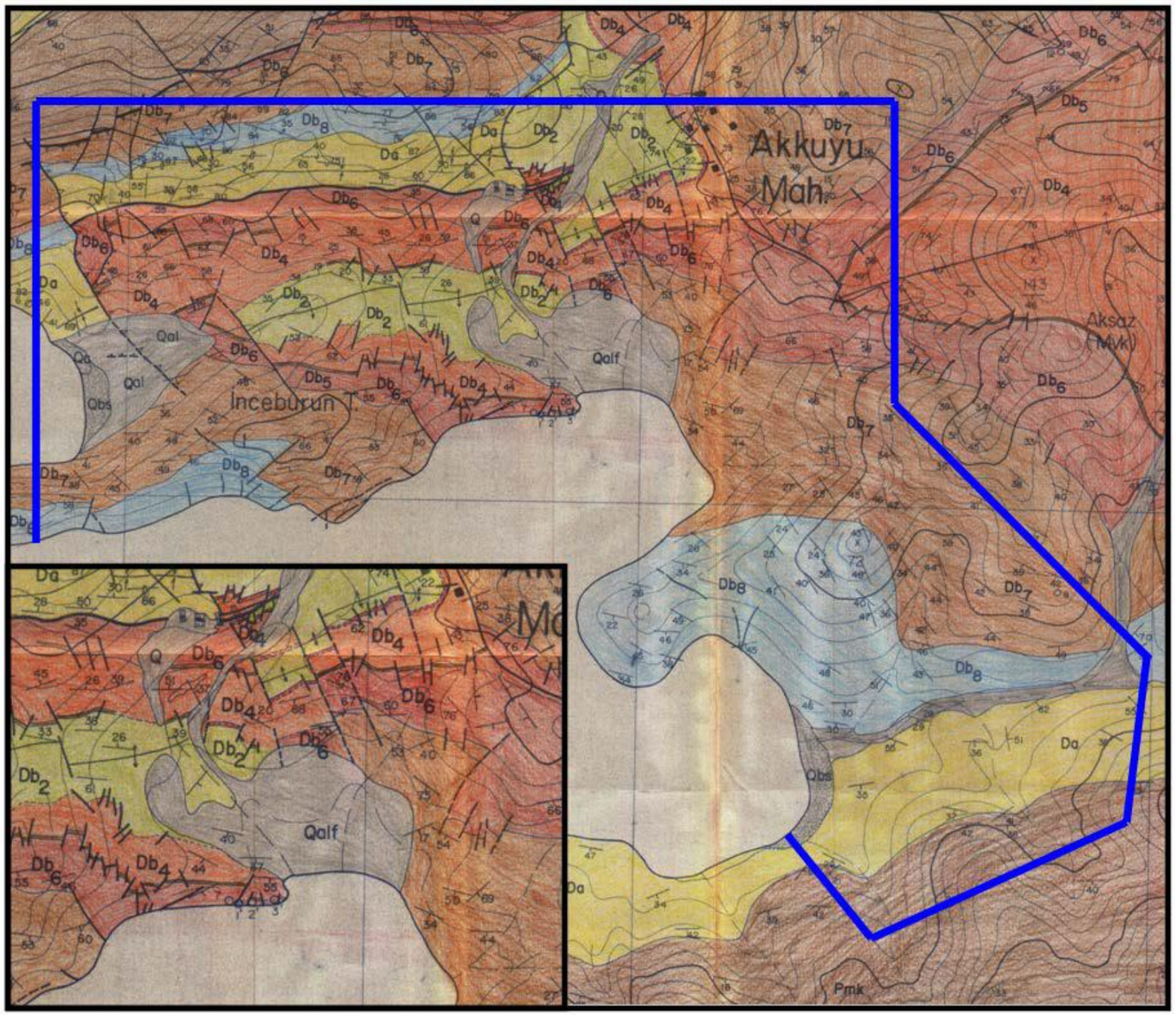

Quaternary	Qc	Caliche
	Qbs	Beach sand
	Qal	Alluvium
	Qaf	Alluvial fan deposits
Plio-Quaternary	PQb	Talus breccia
Triassic	Trk	Kusyuvasıtepe
Upper Permian	Pmk	Kırtıldağı Formation: Wackestone, quartzite, packstone
Upper Devonian	Da	Akdere Formation: Limestone, quatzitic sandstone, wackestone
Middle Devonian – Buyukeceli Formation	Db8	Fossiliferous dolostone, dolomitic wackestone
	Db7	Quartzitic sandstone, wackestone
	Db6	Megabreccia, wackestone,
	Db5	Wackestone
	Db4	Dolomitic limestone, shale, megabreccia
	Db3	Quartzitic sandstone
	Db2	Wackestone, dolomitic limestone,megabreccia
	Db1	Conglomerate, sandstone, mudstone
		Thrust Fault
		Normal Fault
		Strike-slip fault
		Anticlinal axıs
		Synclinal axis
		Strike and dip

Figure 6/6.15 – The geological map of the Akkuyu NPP site prepared by the MTA team [6/56]. Blue line outlines the study area of this campaign. The figure shows the close-up view of the Akkuyu Bay which is now characterized by newly formed cut and fill sites

6.6.5 PALEOSEISMOLOGICAL INVESTIGATIONS

Ten trench investigations were carried out by METU/EERC 1983 [6/226] in the site area (T1, T2, T3 and T4), along the Akkuyu fault (T5, T6, T7 and T8) and Aksaz Bay fault (T9 and T10). Their location is presented in Figure 6/6.16.

In 2011, four new trenches have been excavated by Envy along the Akkuyu (T1 and T2) and Aksaz (T3 and T4) faults (see location in Figure 6/6.17), taking into account the distribution of Quaternary deposits and site accessibility. The METU trenches were reassessed by Dr. E. Demirtaşlı in 2011 [6/93] with the following conclusions that basically confirm the conclusions of METU/EERC (1983), [6/226].

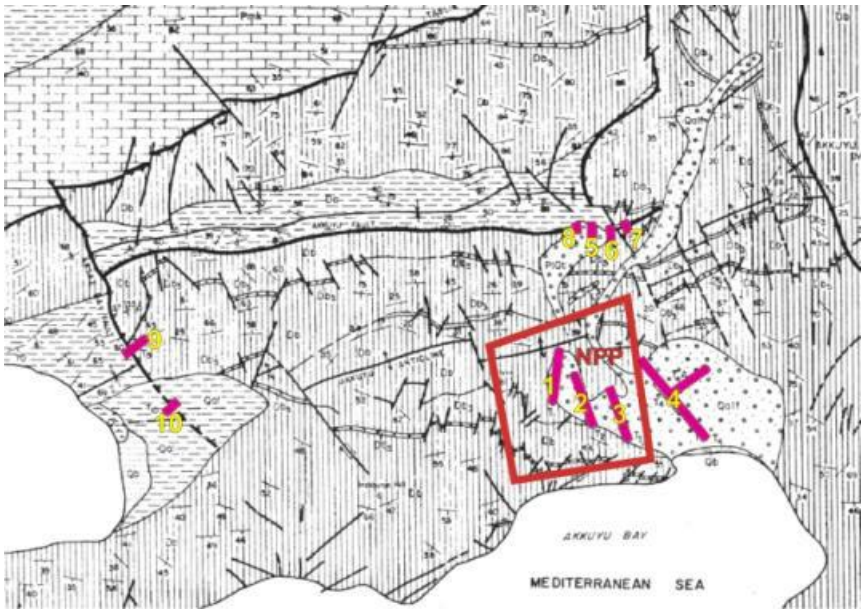

Figure 6/6.16 – Location of the trench sites investigated by METU/EERC 1983 [6/226]

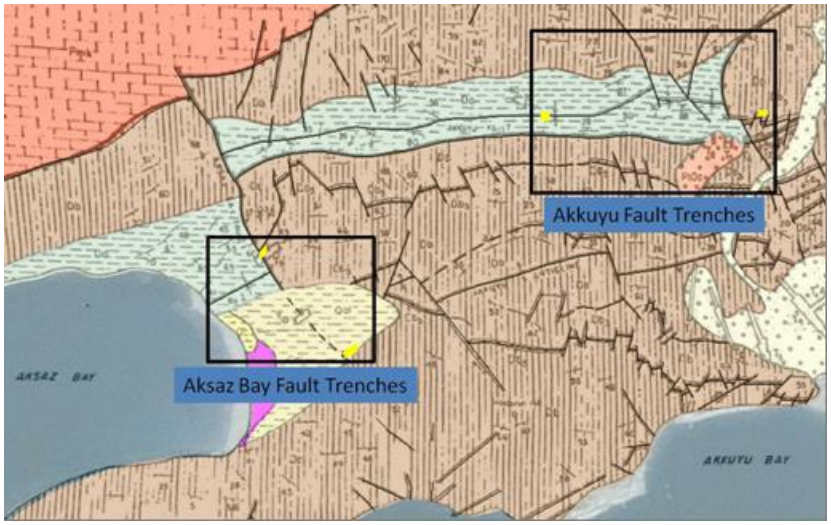

Figure 6/6.17 – Location of the four trenches excavated by Envy, 2011 [6/69]

Akkuyu Fault

Trench T5, METU

Trench T-5 is 14m long, 8m wide and 5m deep. Since the west Wall of the trench T-5 provided more information than the East Wall it was investigated in detail and logged in 1:20 scale (Figure 6/6.18) whereas the east Wall was logged in a scale of 1:50 (Figure 6/6.19). Results obtained from these observations are given below:

- Akkuyu Fault stops upstairs against Plio-Quaternary Breccia (PlQb) and Quaternary Alluvium (Qal);
- Plio-Quaternary breccias and the underlying (Db6) member of the Büyükeceli Formation were subjected to erosion and karstification before the deposition of Quaternary Alluvium;
- Karstic cavities developed in the (Db6) member of the Büyükeceli Formation and in the Plio-Quaternary. Breccias are filled by calcareous cement or red clay. No sign of any tectonic activity such as faults and joints can be seen on these deposits indicating that the tectonism stopped before the karstification.

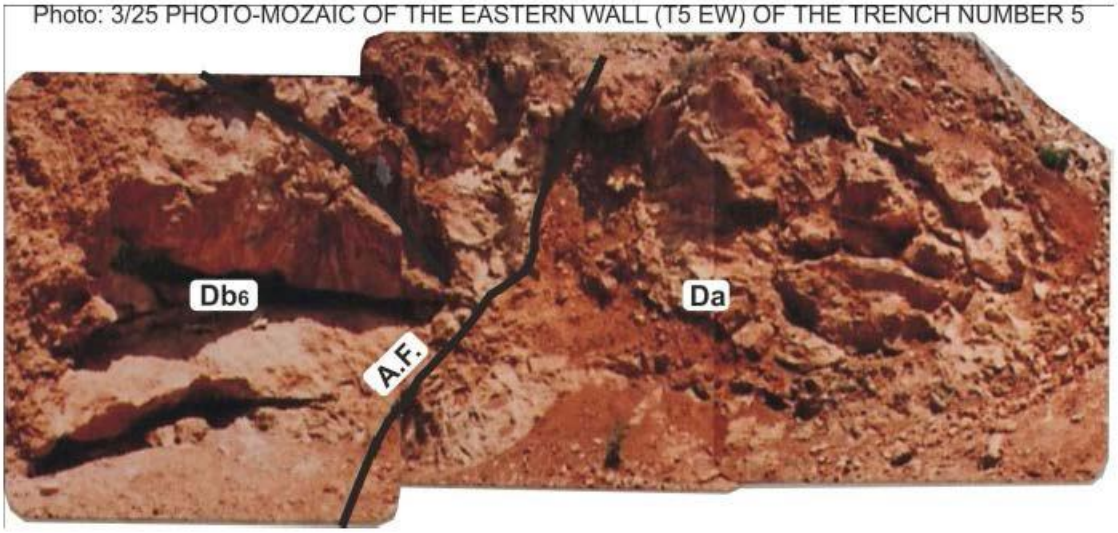

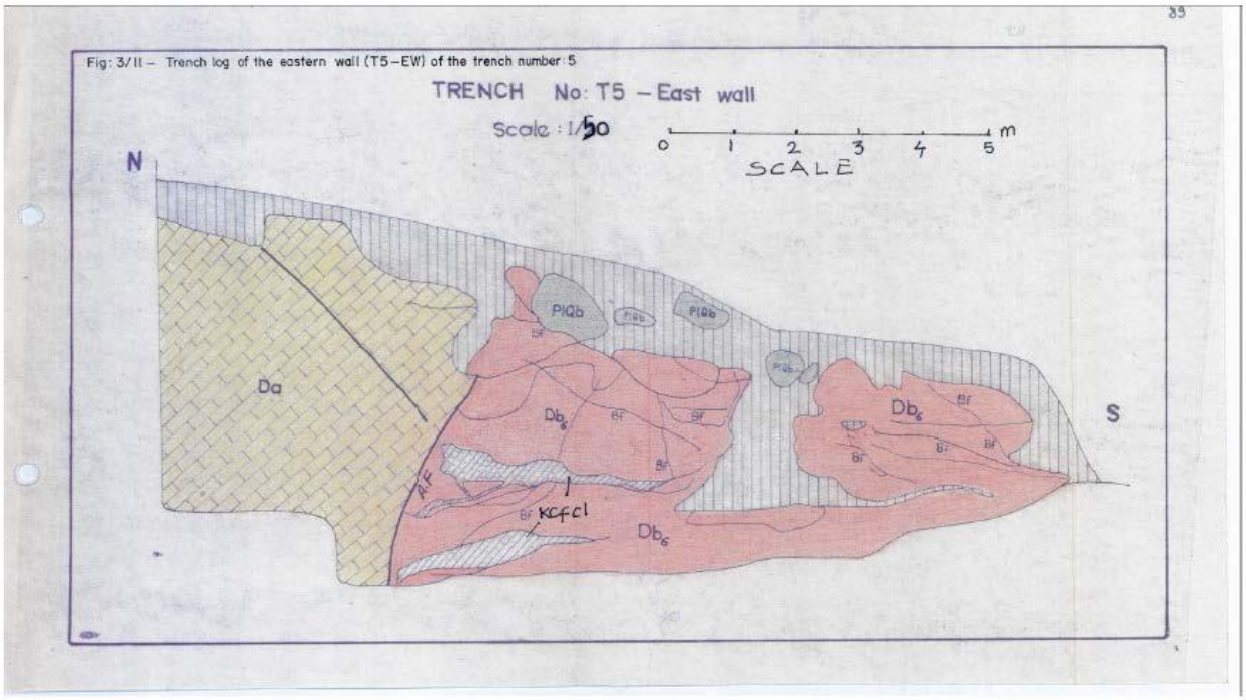

Figure 6/6.18 – Photomosaic and stratigraphic log of the east wall of Trench 5 along Akkuyu Fault [6/93]

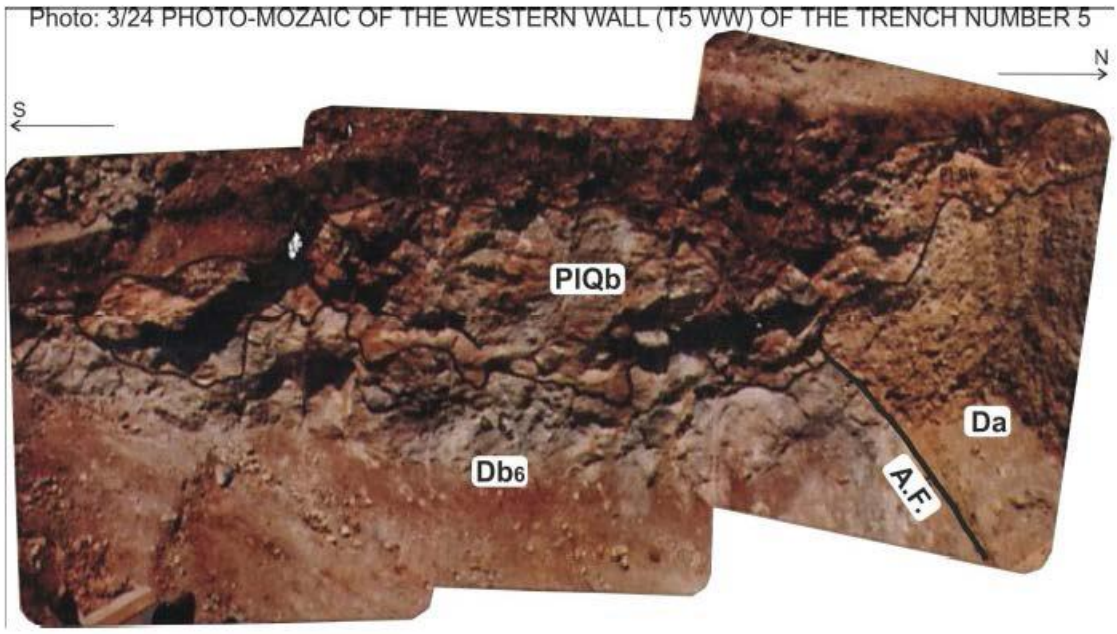

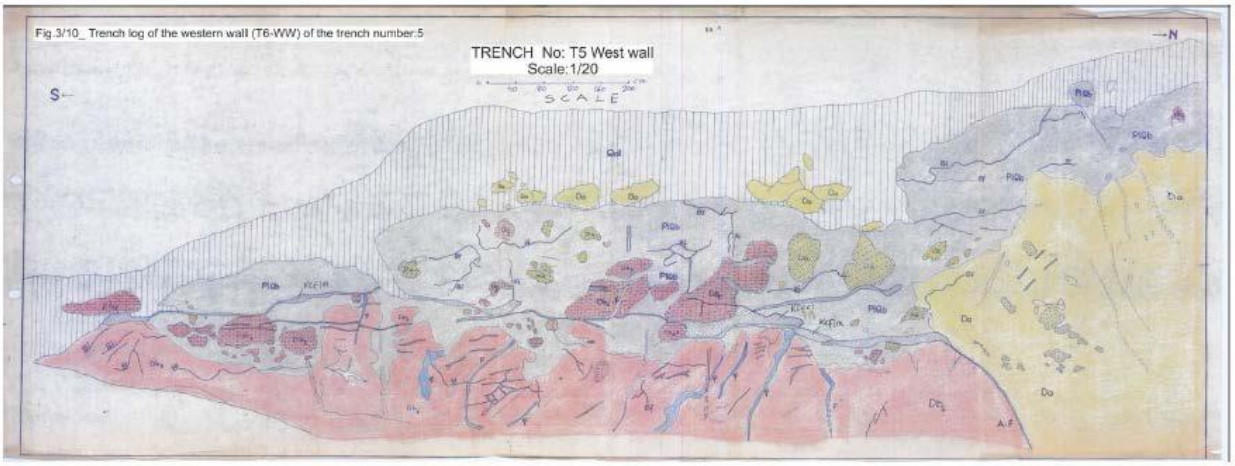

Figure 6/6.19 – Photomosaic and stratigraphic log of the west wall of Trench 5 along Akkuyu Fault [6/93]

Trench T8, METU

Trench T8 is 20m long, 8m wide and 5m deep. It was opened 25m west of trench T-5 where Plio-Quaternary breccias unconformably overlie Büyükeceli and Akdere formations and they

reach their maximum thickness in this locality. This trench was dug in order to investigate the capability of the Akkuyu Fault and demonstrate stratigraphic and structural relationships between Plio-Quaternary breccias and underlying Büyükeceli and Akdere formations. Trench logs of the East wall in scale of 1/20 and a photograph in 1/10 scale are shown in Figure 6/6.20.

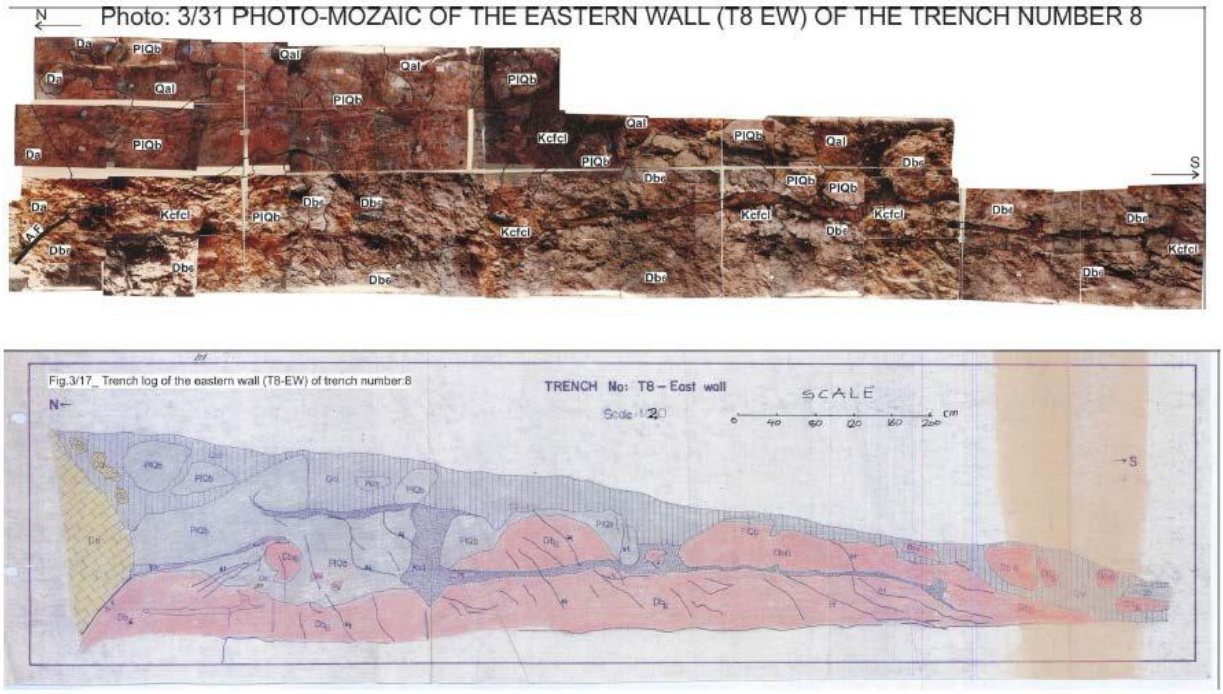

Figure 6/6.20 – Photomosaic and stratigraphic log of the east wall of Trench 8 along Akkuyu Fault [6/93]

Results obtained from the investigation of Trench-T-8 are given below:

- Akkuyu Fault is older than the Plio-Quaternary Breccias and Quaternary Alluvium which unconformably overlie both Plio- Quaternary Breccias, Büyükeceli and Akdere Formations;
- Plio-Quaternary Breccias were subjected to erosion and karstification together with the underlying (Db-6) member of the Büyükeceli Formation before the deposition of young alluvium. Karstic cavities are filled with reddish clay or caliche-like limy deposition which were deposited by lime rich ground water circulating through karstic cavities or open fractures. These cavity filling claystones or limestones form 10-15 meter long, continuous, undisturbed beds indicating that after the karstification event no tectonic activity took place in the Akkuyu Area.

Trench T1, Envy

Observations made at the western wall of the trench are shown in Figure 6/6.21 and results obtained from detailed investigation of trench T1 are listed below:

- Akkuyu Fault is a dip slip (normal) fault that forms the boundary between the member Db6 of the Büyükeceli Formation in the south and the Akdere Formation (Da) in the north. In the trench, it is observed as a zone with two main branches which are characterized by 1 m wide greenish clay (fault clay). According to the fault plane measurements, they trend approximately in E-W direction and dip 50°-60° towards N;
- In the south, the member Db6 is represented by breccia, sandstone and reddish shale which are affected by a series of minor faults sub-parallel to the Akkuyu Fault;
- In the north, the Akdere Formation (Da) is characterized by limestone, calcareous sandstone, siltstone and breccia alternation. At the bottom, it displays steeply dipping joints and some minor karstification;
- At the top, a thin talus and soil cover unconformably overlies the older units and faults. Undisturbed nature of the Quaternary deposits suggests that the site has not been subjected to any recent tectonic activity during Quaternary.

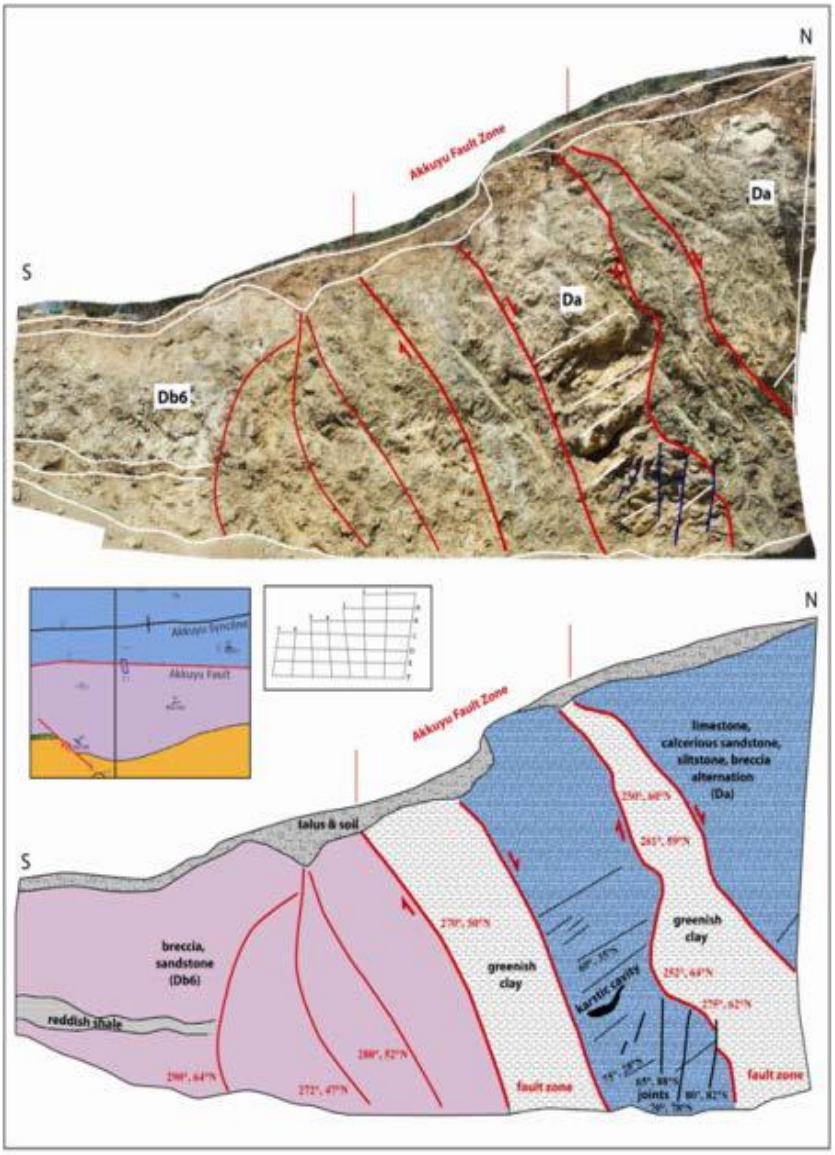

Figure 6/6.21 – Photomosaic and stratigraphic log of the west wall of Trench T1 along Akkuyu Fault. Envy [6/69]

Trench T 2, Envy

Observations made at the western wall of the trench are shown in Figure 6/6.22 and results obtained from detailed investigation of trench T2 are listed below:

- In the trench, Akkuyu Fault cuts the unnamed thrust fault along which the member Db4 of the Büyükeceli Formation is thrusted over the Akdere Formation (Da) and forms the northern boundary of the member Db6 of the Büyükeceli Formation. At the trench, Akkuyu Fault has a WSW-ENE trending fault plane which is dipping 50° towards north. In contrast, the N-S trending unnamed thrust that is dipping 40°-50° towards east displays a wide highly

deformed fault zone containing limestone blocks surrounded by dark greenish clay matrix;

- In the south, the member Db6 is represented by limestone, sandstone, silt and clay alternation and contains a black wackestone bed that is displaced by minor faults. In the north, the member Db4 at the top is light colored massive limestone and Akdere Formation (Da) at the bottom is jointed thick bedded limestone with minor karstification;
- Beside the talus wedge observed over the member Db6, Quaternary deposits are very thin across the trench and unconformably overlie the Akkuyu Fault and older rocks confirming that the site has not been subjected to any recent tectonic activity during Quaternary.

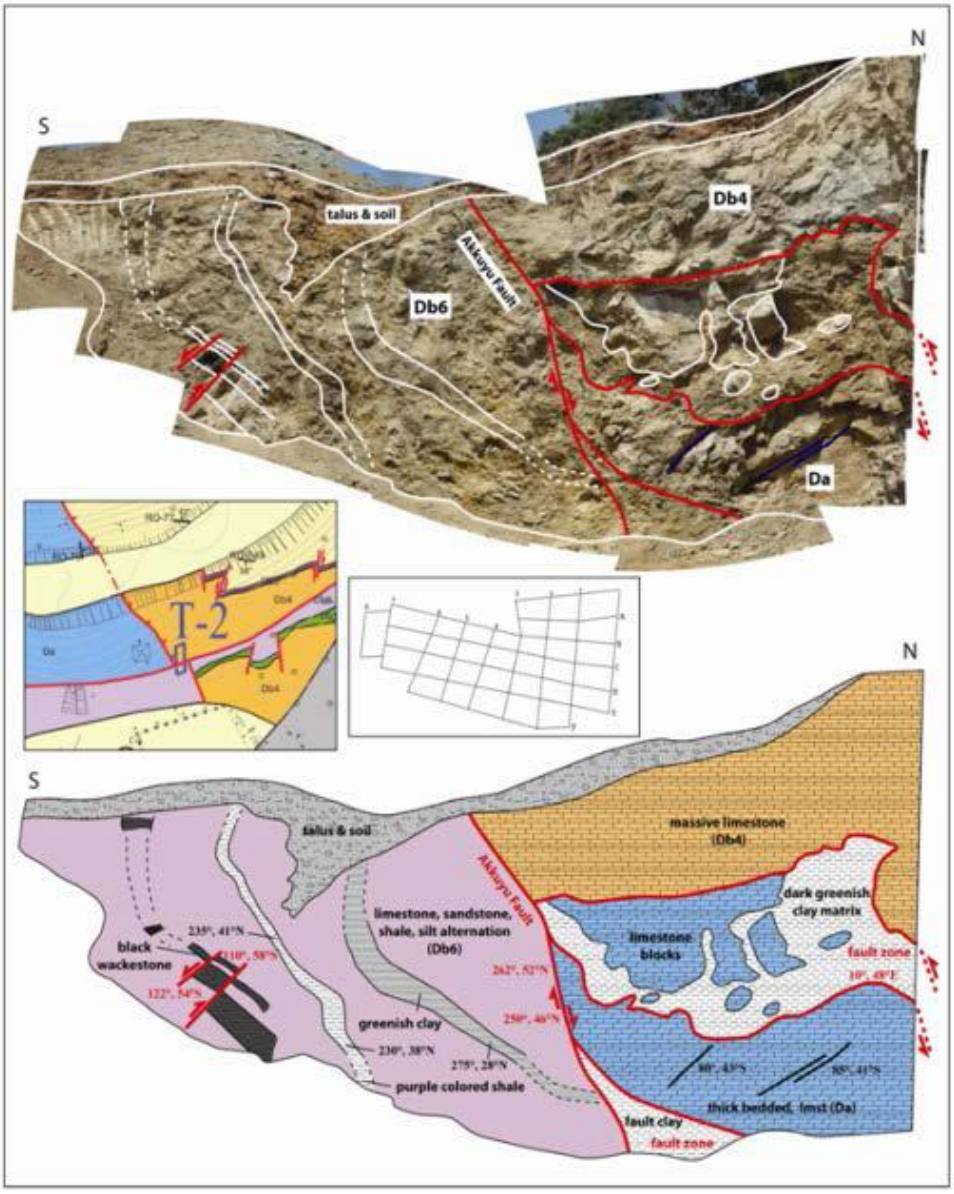

Figure 6/6.22 – Photomosaic and stratigraphic log of the west wall of Trench T2 along Akkuyu Fault. Envy [6/69]

Aksaz Bay Fault

Aksaz Bay Fault trends in the NNW-SSE direction (N30W, 40NE), offsetting both Akkuyu and Taşlik faults. It was first assumed that the Aksaz Bay Fault is a left lateral strike slip fault.

Trench T9, METU

Trench T-9 proved that it is a thrust fault with a strike-slip component along which the member (Db4) of the Büyükeceli Formation thrusted over the Akdere Formation from east to west. Trench T-9 also showed that Aksaz Bay Fault is covered by a thin alluvium layer. Therefore it was decided to open another trench on this fault (Trench-10).

Figures 6/6.23 and 6/6.24 provide the stratigraphic logs of Trench T9.

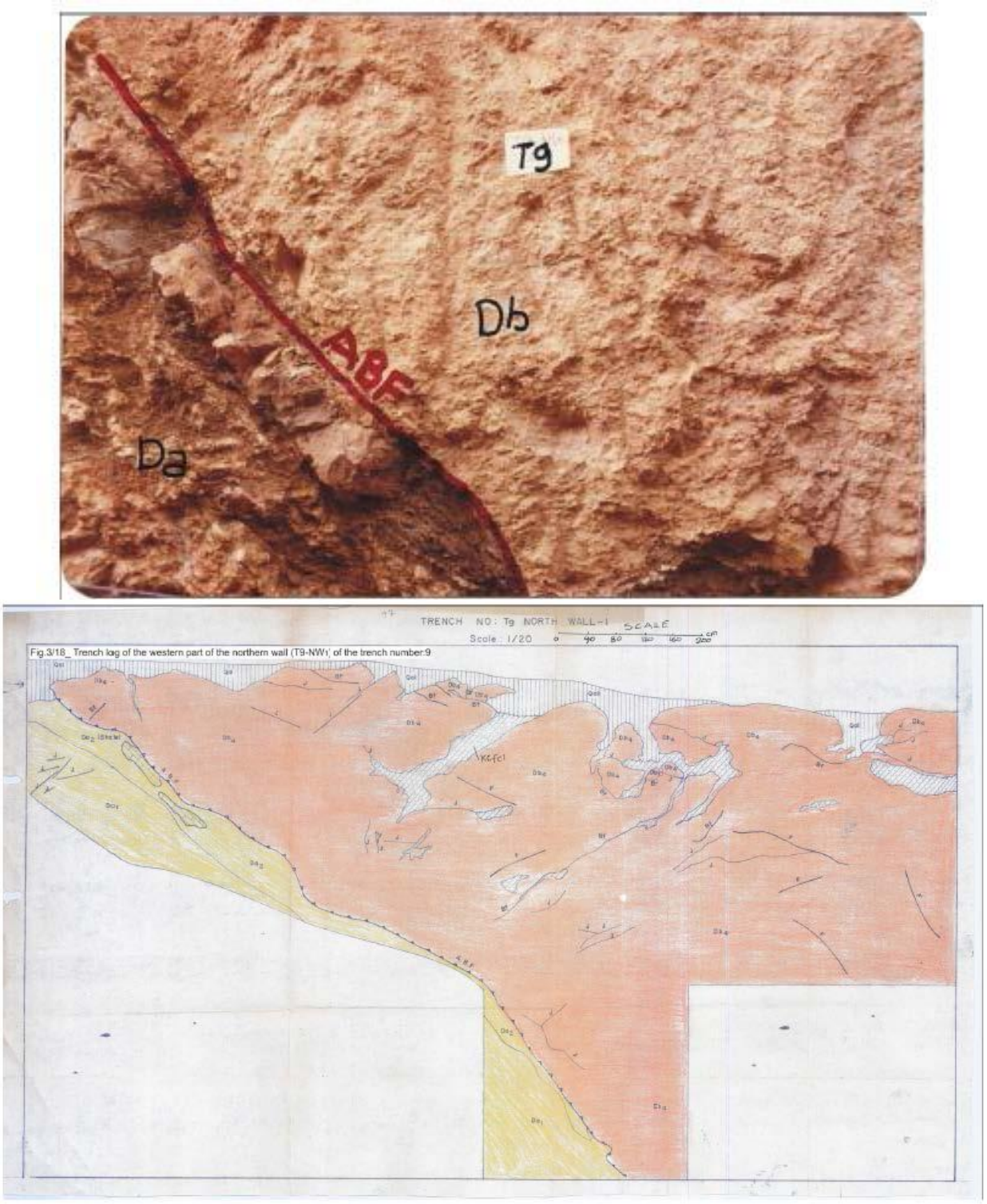

Figure 6/6.23 – Photomosaic and stratigraphic log of the northern wall of T9 along the Aksaz fault, METU/EERC, [6/226]

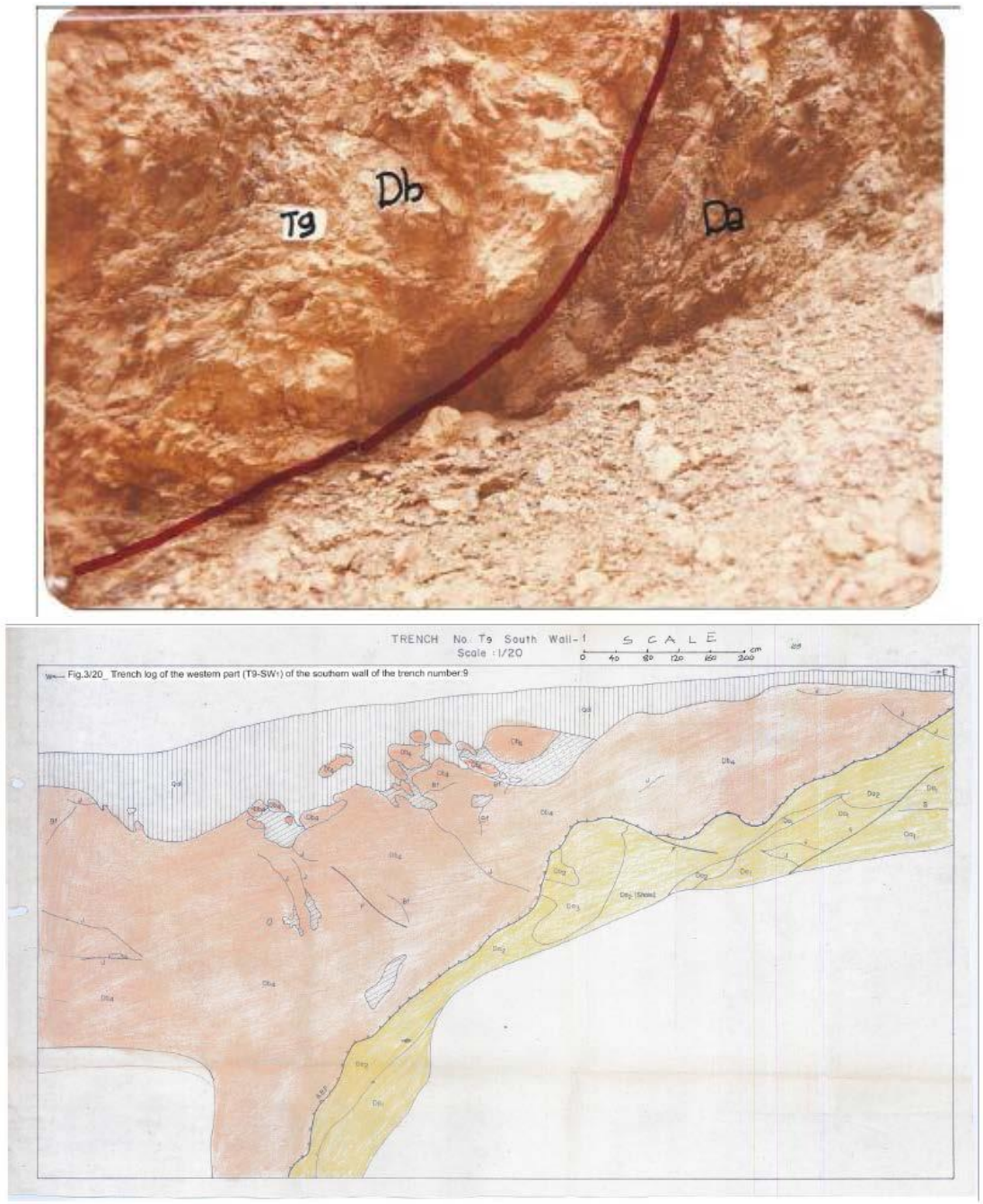

Figure 6/6.24 – Photomosaic and stratigraphic log of the southern wall of T9 along the Aksaz fault, METU/EERC, [6/226]

Trench T10, METU

Trench T-10 was opened on the Aksaz Alluvium. It is 15m long, 4.5m wide and 5m deep. Figure 6/6.25 presents the log of Trench-10 which shows that the Aksaz Bay Fault has no effect on the Aksaz Alluvium cover which includes five different types of lithology:

- A - Top Soil with recent vegetation on it (10-20cm);
- B - Grey, sandy silty soil of no vegetation or plant remains (100cm);

- C- Dark grey silty clay with abundant reed stems and organic matter (80-100cm.);
- D- Yellowish grey, sandy, silty and pebbly clay (50-60cm);
- E- Yellowish brown clay with rare pebbles at top and increasing amount of pebbles of the Akdere Formation near to the bottom (150cm).

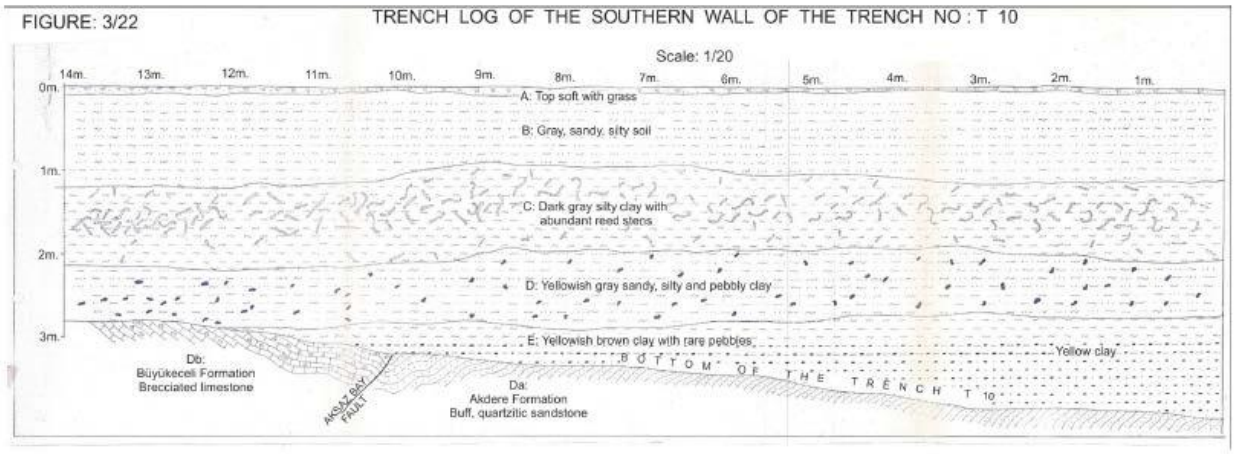

Figure 6/6.25 – Southern wall of T10 along Aksaz Bay Fault, METU/EERC [6/226]

Trench 3, Envy

Observations made at the northwestern wall of the trench are shown in Figure 6/6.26 and results obtained from detailed investigation of trench T3 are listed below. Figure 6/6.27 provides a photograph and log of T3.

- Along the Aksaz Fault, the member Db4 of the Büyükeceli Formation is thrusted towards southwest over the Akdere Formation (Da). The measurements made in the trench indicate that the Aksaz fault plane trends in NW-SE direction with a 30°-45° dip towards NE;
- In the southwest, the Akdere Formation (Da) consists of gently dipping sandstone, siltstone and clay beds. In the northeast, the member Db4 is composed of folded megabreccia;
- At the top, the talus and soil cover displays some variation in thickness due to erosion and unconformably overlies the Aksaz Fault and older units indicating that the site has not been subjected to any recent tectonic activity during the Quaternary.

Figure 6/6.26 – Photo of the Aksaz Fault observed in trench T3. Envy [6/69]

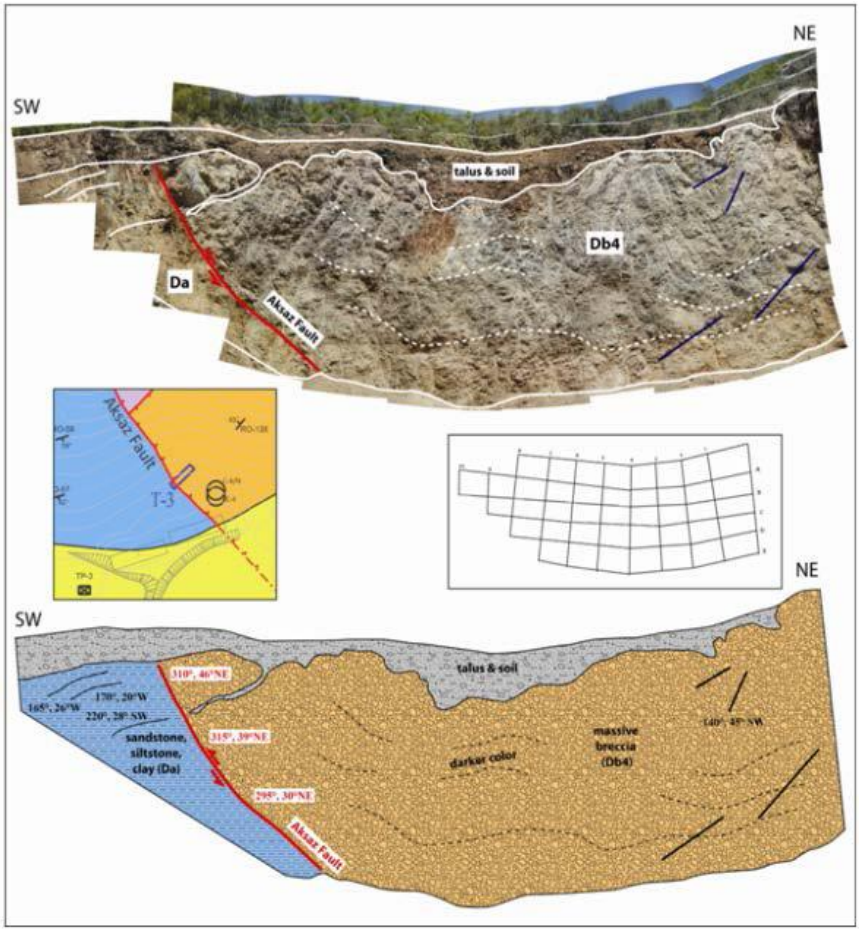

Figure 6/6.27 – Photomosaic and stratigraphic log of the northwestern wall of T3 along the Aksaz fault. Envy [6/69]

Trench 4, Envy

This is the only trench opened on a thick Quaternary alluvium. When excavation exceeded 1 m depth, fresh water started to fill the trench which was pumped out during trench mapping.

Observations at the northwestern wall of the trench are shown in Figure 6/6.28 and results from detailed investigation of trench T4 are listed below:

- Unlike T3, Aksaz Fault is observed as a wide (~2 m) steeply dipping highly deformed shear zone that consists of tectonic multiple faults. At the trench, the NW-SE trending fault zone cuts the member Db7 of the Büyükeceli Formation which is also affected by a series of N-S trending minor faults dipping 40° towards east;
- Across the trench, the member Db7 is composed of E-W trending wackestone, sandstone, silt and breccia that dip towards south and contains calcite veins and joints. In the south, a reddish clay infill ("Terra Rossa") that is formed due to karstification is also observed within the member Db7;
- The Quaternary deposits viewed in T3 which is characterized by thick (~1.5 m) organic reddish-brown soil at the top and loosely consolidated breccia at the bottom, overlies the Aksaz Fault and older units unconformably and is not affected by any recent tectonic activity.

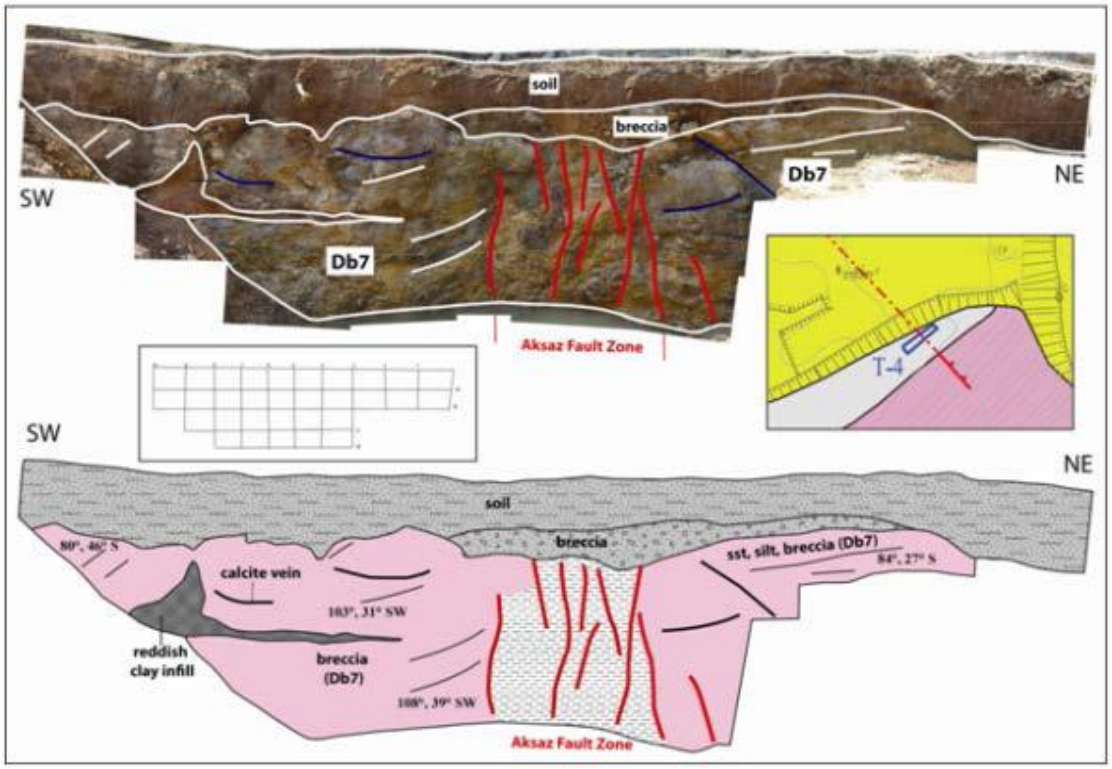

Figure 6/6.28 – Photomosaic and stratigraphic log of the northwestern wall of T4 along the Aksaz fault. Envy [6/69]

According to the results of trench investigations it can be concluded that the faults of the Akkuyu NPP site are not associated with morphological scarps and do not affect the old paleosoil covering the bedrock.

6.6.6 ASSESSMENT OF QUATERNARY SEDIMENTS

Caliche Deposits

Along the coast line of the Çamalanı Bay a series of consolidated and cemented calichified sands (Eolinids) were deposited [6/54]. They contain calcium carbonate tubes or columns being generally in vertical positions (Figures 6/6.29, 6/6.30). They are interpreted as tubular caliche deposits developed in the beach sands which have been transported and deposited either by winds or storm waves. There is a hole inside each tube through which limy sea water rises up by capillary movement due to evaporation and is deposited as calcium carbonate ($CaCO_3$). Leaching of calichified sands by rain give rise to a peculiar appearance of these calichified sands. Deposition of calichified sands was interrupted by the deposition of the alluvial fans advancing to the shore during strong run-off.

Figure 6/6.29 – Intercaletion of calichified sands (Qc1, Qc2) and Quaternary alluvial fans (Qalf1, Qalf2), [6/93]

Figure 6/6.30 – Closer view of tubular calichified sands (Qc2) and Quaternary alluvial fan (Qalf2), [6/93]

Landward transportation and deposition of beach sands over alluvial fans continued and intercalation of calichified sands and alluvial fans took place.

Three different levels of calichified sands in the Çamalanı Bay have been observed and mapped (Figure 6/6.31). The uppermost part of the third caliche zone is 40 m above the sea level. This means that the abrasion platform took place during the deposition of the third caliche zone, 40m above the sea level. According to geomorphologists this elevation corresponds to the Tyrrhenian Terrace which was formed about 125kyrs years ago. Because the sea level at this time

was 8 meters above the present sea-level, this means that the coastal uplifting rate is in the order of 0.25 mm/year that is in agreement with the long term uplifting rate that is 0.2 mm/year [6/51]

Calichified sands have not been affected by faults disturbing the bedrock (Figure 6/6.31).

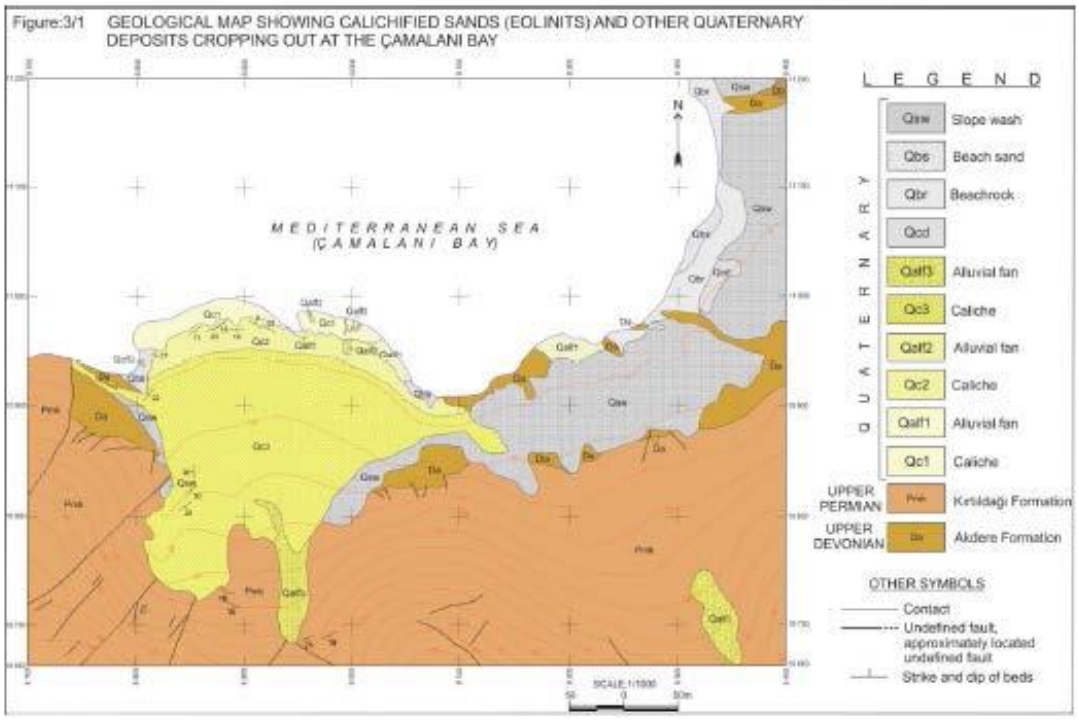

Figure 6/6.31 – Map of calichified sands and other Quaternary deposits at the Çamalanı Bay, [6/93]

Recent alluvial fans (Qalf)

Recent alluvial fan deposits occur in the present fluvial channels forming unconsolidated boulder and pebble size clasts. It has been observed that recent alluvial fans have intercalated with calicified sands (Figure 6/6.29, 6/6.30). They were classified and mapped as Qalf1, Qalf2 and Qalf3 (Figure 6/6.31). They may have been transported by seasonal creeks or by running waters.

Alluvium deposits Qal, presented by gravel soils and sands of different grain size were taped during drilling at the buried channel of the Aksaz paleo-stream.

Slope wash (Qsw)

Slope wash deposits covering gentle slopes consist of angular to subangular material. These unconsolidated and uncemented deposits are transported from the nearest older units. At some places slope wash deposits are so thin that underlying bedrocks can be seen as small inliers.

Beachrock (Qbr)

Beachrocks are generally well exposed along the coast of the Çamalanı Bay (Figure 6/6.31). They are composed of consolidated boulder to pebble size, well-rounded, well cemented materials. Beachrocks have been deposed in swash. Subsequently they have been formed by sea

water evaporation and shortly after cementation. These youngest consolidated conglomerate type sediments are gently inclined to the sea.

Beach sands (Qbs)

Beach sands occur at the shore face of the coastal zone (Figure 6/6.31). These sands are mostly composed of well sorted, white to yellow quarzitic sands.

Coastal dunes (Qsd)

Coastal dunes are found to be limited in extent and about 30 to 40m back of the present coastal zone of the Çamalanı Bay (Figure 6/6.31). They have been deposited by transportation of effective winds.

Suspended old colluvial deposits

Suspended old colluvial sediments can be seen in two places around Akkuyu.

First place is the big cave which is situated at the south of the Kuşyuvası Hill being 15 m above the present day sea level (Figure 6/6.32). Colluvial sediments were deposited in the cave when the sea level was 15m high. According to Fairbridge [6/90] this elevated marine phenomenon corresponds to the time of the Monastrian Terrace which was formed 125 000 years ago. Taking into consideration the above mentioned data, old alluvial fans were deposited before Monastrian Terraces were formed, i.e 125 000 years ago.

Another location where the old colluvial sediments could be seen is the cave situated at the southof the İnceburun Hill.

Figure 6/6.32 – A suspended colluvial fan, 15m above present sea level on the coast of Kuşyuvası Hill [6/93]

Analysis of Quaternary sediment occurrence at the Akkuyu NPP site clearly demonstrates the general neotectonic uplift. That is characteristic feature of the whole Mediterranean Sea coast.

At the same time according to the analysis of Quaternary sediments, there is no evidence of contrast movement indicative of the recent fault activity

6.6.7 CONCLUSIONS ON SURFACE FAULTING POTENTIAL

A capable fault is one of the most important exclusionary features which needs to be considered for the acceptability of a nuclear power plant site.

According to the IAEA SSG-9 *a fault could be considered capable if:*

a) it shows evidence of past movement or movements (such as significant deformations and/or dislocations) of a recurring nature within such a period that it is reasonable to conclude that further movements at or near the surface may occur. In highly active areas, where both earthquake data and geological data consistently reveal short earthquake recurrence intervals, periods of the order of tens of thousands of years (e.g. Upper Pleistocene–Holocene — i.e. the present) may be appropriate for the assessment of capable faults. In less active areas, it is likely that much longer periods (e.g. Pliocene–Quaternary — i.e. the present) are appropriate.

b) If a structural relationship with a known capable fault has been demonstrated such that movement of the one fault may cause movement of the other at or near the surface.

c) If the maximum potential magnitude associated with a seismogenic structure, as determined in the related section , is sufficiently large and at such a depth that it is reasonable to conclude that, in the current tectonic setting of the plant, movement at or near the surface may occur.

Furthermore, for new NPP sites, SSG-9 recommends that:

Where reliable evidence shows that there may be a capable fault with the potential to affect the safety of a plant at a site, the feasibility of design, construction and safe operation of a plant at this site should be re-evaluated and, if necessary, an alternative site should be considered.

In general, the scale of Site Vicinity (~ 5 km radius) is considered to be sufficient for the demonstration of the absence of capable faults. For the Akkuyu NPP site, 5 kms is certainly sufficient because the tectonic features in the near region are not well defined and limited in length and highly segmented.

Regarding the applicable time scale, demonstration of the absence of movement in the Quaternary is also considered sufficient evidence for non-capability.

In relation to requirement (a), numerous investigations have been made in the onshore and offshore site vicinity and also in the near regional area. These investigations include aerial photographs interpretation, field reconnaissance, onshore and offshore geophysical investigations and paleoseismological trenching.

The inland geophysical investigations (see Sections 6.2 and 6.3) revealed no disturbance of the recent lithological layers that may be attributed to surface faulting, i.e. no signs of tectonic deformations were found in the Quaternary sediments (Plio-Quaternary breccias and Quaternary alluvium) that surely are older than the required age coming from the geodynamic setting (interplate) of the Akkuyu site.

The old paleosoil covering the whole site vicinity and near regional areas (the area raised from the sea just after Miocene) has not been faulted and/or showing disturbances or features (like colluvial wedges) that could be attributed to surface faulting.

In relation to requirement (b), faults and folds present in the site vicinity (e.g. Aksaz, Akkuyu, and Taşlık) are well correlated to those related to past orogenesis (Hercinian) and because of that, not capable. In addition the seismicity record (including the Microseismicity records from the 1970s and 1980s) do not reveal any clustering attributable to potential new faults that could be correlated to the capable regional ones.

In relation to requirement (c), it is important to point out that, the historical earthquake catalogue and geological field studies did not provide any evidence of a M>6.5 event in the near region of the site. Taking into account this evidence and the seismotectonic setting of Akkuyu site, a background earthquake of Mmax = 6.5 is considered in the SHA assessment with kinematic parameters not leading to surface faulting.

Commitments

The vast amount of geological, geophysical, seismological and paleoseismological work has clearly demonstrated that there is no potential for surface faulting at the Akkuyu site which may challenge the safe operation of the planned NPP.

Even so, confirmatory studies aiming to expand the region of applicability (i.e. more than 5 kilometers) and the time frame (older than Quaternary) are under way. This can be considered a commitment to be concluded prior to the submission of the next report addressing the site related design basis parameters.

These investigations can be summarized as follows:

- Field check of the features identified in the aerial photointerpretation analysis
- Investigation of the marine terraces in the region of Akkuyu NPP

– A new investigation of the microearthquake activity has started in July 2011 and is currently ongoing. The results from this campaign should be more reliable than those of older campaigns due to the characteristics of the instruments and recording techniques. The data from this network will be used to check the conclusions already made regarding fault capability and reported to TAEK periodically. This can also be considered as a commitment.

6.7 SOIL LIQUEFACTION

One of the most damaging aspects of earthquakes is liquefaction-induced ground failure. Under strong ground shaking, pore water pressure builds up in saturated unconsolidated soils. If the induced shear-strains are large enough over a long enough duration, the pore water pressure can equal or exceed the overburden pressure resulting in a loss of shear strength or soil failure.

The Akkuyu NPP site area is a rock site, with minor Quaternary deposits and rather widespread artificial fill deposits .The only soil covered areas are the Aksaz beach area and the Akkuyu beach area, which are now buried by spoil piles. The alluvium and the spoil piles, because of their high clay contents, are not susceptible to liquefaction.

During the field investigation campaign in 2011-2012 more than 500 boreholes were drilled at the site in a very dense grid. Out of these there are only several boreholes where there is a saturated soil layer with considerable thickness (> 3m).

Table 6/7.1 provides data on boreholes No 223, 246, 247, 272 and 297, the soils observed at these boreholes, their thickness and the groundwater table level.

Table 6/7.1 – Properties of the boreholes

Borehole No	Elevation	Elevation of Groundwater	Soil	
			Type	Existing Depth from ground Surface (m)
223	1.16	-0.34	Quaternary Beach Sand	0.0-7.95
246	0.99	-0.01	Sea Sand	0.0-8.5
247	2.57	-1.93	Fill	0.0-3.0
			Limestone Pebbles and Cobbles	3.0-9.0
272	1.46	0.46	Quaternary Beach Sand	0.0-7.6
297	1.77	0.27	Beach Sand	0.0-0.5
			Clayey Silty Sand	4.0-9.6

Within the observed soil layers Standard Penetration Tests (SPT) and sieve laboratory analysis of soil samples were performed. The results are summarized in Table 6/7.2.

Table 6/7.2 – Summary of field and laboratory test results

Borehole No	Soil Type	SPT N *	Gravel Content G (%)	Sand Content S (%)	Fine Content (F)
223	Quaternary Beach Sand	11,12,19,20, 50+	2.0	70.0	28.0
246	Sea Sand	8,6,13,14,31	0	99.0	1.0
247	Limestone Pebbles and Cobbles	50+,50+,50 +,50+	-	-	-
272	Quaternary Beach Sand	11,12,16,17, 50+	0.0	27.0	73.0
			0.0	99.0	1.0
297	Clayey Silty Sand	18,24,45,50 +	66.0	20.0	14.0

**Uncorrected*

It is obvious that only in one borehole (No.246) out of 5, where soft sediments up to 8 m present water-saturated sea sand the results of standard penetration showed N=6 – 8.

The sea sand deposits in Aksaz bay are local and have countouring according to the results of engineering-geological surveys both in plan and with regards to depth.

The information in these tables demonstrates that the combination SPT N blow count - fine content generally does not imply susceptibility for liquefaction.

Potentially unstable soils under dynamic impact in one borehole only, which is placed on the coast of Aksaz bay do not give a ground to make a conclusion on the hazard of potential liquefaction of the Akkuyu NPP site as a whole.

Most importantly there is no lateral continuity of saturated soil layers which totally excludes a wide spread liquefaction phenomena at Akkuyu NPP site.

In addition all safety related systems, structures and components of the plant will be founded on competent bedrock which will exclude the potential for liquefaction related failures. Hence there is no potential of soil liquefaction at the Akkuyu NPP site that may in any way jeopardize the safety of the NPP.

If the design does not provide for replacement (removal from the soils) of the water-saturated sand all the required laboratory tests of these soils will be conducted to assess the hazard resulted from possible liquefaction in terms of dynamic loads.

In any case, the assessment of the liquefaction potential for the whole site will be made in order to understand and deal with the potential consequences of the failure of non-safety related structures, systems and components. Furthermore, any impact of liquefaction on accessibility and on-site emergency response will be evaluated and considered when the actual NPP infrastructure and emergency plans are developed during the design phase of the project.

6.8 SLOPE STABILITY

The Akkuyu NPP site is located on the seashore and is separated from the surrounding area by hills up to 200 – 250 m high, formed by folded and faulted rock. Average slope of the site area is around 35°. There are no tectonic or erosion scarps at slopes facing the site. The slopes are covered by dense pine forest and thin soil. Thus, there is no risk of slope instability along the natural slopes.

In 1983 [6/223] the Kuşyuvası and Taşlık hills, and also Akkuyu mountain ridge were investigated in the course of detailed examination of the Akkuyu NPP site aimed at determining strata bedding orientation. These studies have revealed that a risk of landslide descent at the Kuşyuvası hill is absent due to the strata bedding orientation (deep into a slope). The stability studies run for the Taşlı k hill proves its stability.

As a result of extensive excavation works performed at the Akkuyu bay area, steep rock cut slopes have been created. Natural slopes facing the sea are in form of vertical cliffs. The rock material is highly sheared, folded, and deformed. Thus, planar, wedge, and even toppling type failures may be expected

In 2012 during the route observations at the Akkuyu NPP site three different modes of rockfall were observed. First one is rockfalls in natural slopes facing seashores at high bedding angles and favorable jointing conditions forming cliffs (Figure 6/8.1). Second mode is observed as rockfalls in cut slopes and slopes of artificial fills forming debris at the foot of these slopes (Figure 6/8.2, 6/8.3, 6/8.4). The final mode is rockfalls or mobilizations in the high angle slopes forming debris (Figure 6/8.5) that can be activated by an earthquake or steady downpour.

As the lithologies are highly deformed, folded and sheared, various slope instabilities could easily be expected at cut slopes. On the other hand, the examination of trench walls made in 1983 and 2011 did not showed any activity, although they were nearly vertical.

Figure 6/8.1 – Rockfall in natural slope facing sea, south slopes of Aksaz hills

Figure 6/8.2 – Rockfall in cut slope facing sea, south slopes of İnceburun

Figure 6/8.3 – Rockfall in cut slope, detachment is seen, not mobilized yet (south slopes of İnceburun)

Figure 6/8.4 – Rockfall in cut slope, detachment is seen, not mobilized yet (south of Akkuyu fault)

Figure 6/8.5 – Rockfalls forming talus

REFERENCE LIST

6/1. Abrahamson, N. and W. Silva (2008) "Summary of the Abrahamson & Silva NGA Ground-Motion Relations" Earthquake Spectra, Volume 24, No. 1, pp. 67–97.

6/2. Agostini S., Doglioni C., Innocenti F., Manetti P., Tonarini S. (2010). On the geodynamics of the Aegean rift. Tectonophysics (2010).

6/3. Akın, U., & Çiftçi, Y. (2011). Structural Discontinuties of Turkey: Geological and Geophysical Analysis (Gravity and Magnetic). General Directorate of Mineral Research and Exploration (MTA).

6/4. Akkar S, Bommer J. Prediction of elastic displacement response spectra in Europe and the Middle East. Earthquake Engng. Struct. Dyn., 2007, v.36, p. 1275–1301.

6/5. Akkar, S. and J.J. Bommer, 2010, "Empirical Equations for the Prediction of PGA, PGV, and Spectral Accelerations in Europe, the Mediterranean Region and the Middle East," Seismological Research Letters, Vol. 81, No. 2, pp. 195-206.

6/6. Aksoy R. and Eren Y. (2004) – The Konya Fault Zone. S.U. Muh.-Mim. Fak. Derg., c.19, s.2, 2004 J. Fac. Eng. Arch. Selcuk Univ., v.19, n.2, 2004

6/7. Aksu A.E., Hall J., and Yaltirak C. (2005). Miocene to Recent tectonic evolution of the eastern Mediterranean: new pieces of the old Mediterranean puzzle. Marine Geology 221, 1-13.

6/8. Aksu, A.E, T.J. Calon, J. Hall, S. Mansfield, D. Yasar (2005), The Cilicia–Adana basin complex, Eastern Mediterranean: Neogene evolution of an active fore-arc basin in an obliquely convergent margin, Marine Geology, 2005. №221, 121–159.

6/9. Allmendinger, R.W., Reilinger, R. & Loveless, J. (2007) Strain and rotation rate from GPS in Tibet, Anatolia, and the Altiplano. Tectonics, 26 (3). Art. No. TC3013.

6/10. Altuncu, S., Yılmazer, M., Kalafat, D., Pınar, A., (2007). A present day evidence for the active tectonics in the inner part of Isparta angle in SW Turkey. International earthquake symposium, Kokaeli 2007

6/11. Ambraseys N., Adams R. (1993) Seismicity of the Cyprus region, Terra, vol. 5, pp. 85-94.

6/12. Ambraseys N.N. Far-field effects of Eastern Mediterranean earthquakes in Lower Egypt. Journal of Seismology 5: 263–268, 2001.

6/13. Ambraseys, N. (2009). Earthquakes in the Mediterranean and Middle East: A Multidisciplinary Study of Seismicity up to 1900. Cambridge, UK: Cambridge University Press. 2009, 968 p.

6/14. Ambraseys, N.N, 1989, Temporary Seismic Quiescence: SE Turkey, Geopyhsical Journal, 96, 311-331.

6/15. Amit R., Zilbermann E., Enzel Y., and N. Porat (2002). Paleoseismic evidence for time dependency of seismic response on a fault system in the southern Arava valley, Dead Sea rift, Israel, Geol. Soc. Am. Bull., 114, 192-206.

6/16. Anastasakis, G., and Kelling, G., 1991, Tectonic connection of the Hellenic and Cyprus arcs and related geotectonic elements: Marine Geology, v. 97, p. 261– 277.

6/17. Aptikaev (2004), Drafting new seismic scale (instead of MSK-64). Research manager, Dr. Ph., Prof. F.F. Aptikaev//Federal target program "Seismic safety of the territory of Russia". Moscow. 2004. P.229.

6/18. Atkinson, G.M. and Boore, D.M., 2006: Earthquake ground-motion prediction equations for Eastern North America, Bull. Seismol. Soc. Am., 96, 2181-2205.

6/19. Atkinson, G.M., and Boore, D.M., 2003, Empirical ground-motion relations for subduction-zone earthquakes and their application to Cascadia and other regions: Bulletin of the Seismological Society of America, v. 93, no. 4, p. 1703–1729.

6/20. Arpat E. and Şaroglu F. (N,D,). The East Anatolian fault system; thoughts on its development. Exploration Institute of Turkey. Vol. xx, 33-39.

6/21. Aydemir A. and Ates A. (2005). Structural interpretation of the Tuzgolu and Haymana Basins, Central Anatolia, Turkey, using seismic, gravity and aeromagnetic data. Earth Planets Space, 58, 951-961.

6/22. Baer G., Sandwell D., Williams S., Bock Y., and Shamir G., (1999). Coseismic deformation associated with the November 1995, Mw = 7.1 Nuweiba earthquake, Gulf of Elat (Aqaba), detected by synthetic aperture radar interferometry. J. Geophys, Res., v. 104, p. 25,221 - 25.232.

6/23. Barka A.A. and Kadinsky-Cade K. (1988) – Strike-slip fault geometry in Turkey and its influence on earthquake activity. Tectonics, 7, 663-684.

6/24. Barka, A., Reilinger, R., Şaroğlu, F. and Şengör, A.M.C. (1995) The Isparta angle: its importance in the neotectonics of the eastern Mediterranean region. Pişkin, Ö., Ergün, M., Savaşcn, G. (ed.). IESCA-1995 Proceedings, 3-17.

6/25. Barka, A. and R. Reilinger (1997) Active Tectonics of the Eastern Mediterranean Region: Deduced from GPS, Neotectonic and Seismicity data. Annali Di Geofisica, Vol. XL, No. 3, June 1997.

6/26. Bartov, Y., Steinitz, G., Eyal, M., Eyal, Y., 1980. Sinistral movement along the Gulf of Aqaba – its age and relation to the opening of the Red Sea. Nature 285, 220-221.

6/27. Bayer Altin T. (2007). Development of drainage and terrace systems in Ecemiş valley, NE of Mediterranean region. Extended Abstract, GEOMED, International Symposium on Geography, Environment and Culture in the Mediterranean Region, Proceedings: 31-43, June 5-8, 2007 Kemer, Antalya-Turkey

6/28. Bayer Altin T. (2008). Ecemiş cayi vadi olugunda polisiklik topografya sekilleri – Polycyclic Topographic Forms in Ecemiş River Valley Turk Cografya Dergisi, Sayi: 50, s.21-36.

6/29. Bazzurro, P. and Cornell, C. A. 1999, "Disaggregation of seismic hazard", Bulletin of the Seismological Society of America 89, 501-520

6/30. Ben-Avraham, Z., Kempler, D. & Ginzburg, A., 1988. Plate convergence in the Cyprian Arc, Tectonophysics, 146, 231–240.

6/31. Bender B., and Perkins D. M., 1987, SEISRISK III: A Computer Program for Seismic Hazard Estimation. U. S. Geological Survey Bulletin 1772. Denver, U. S. Department of the Interior.

6/32. Biryol, C.B., Beck, S.L., Zandt, G., and Ozacar, A.A., 2011, Segmented African lithosphere beneath the Anatolian region inferred from teleseismic p-wave tomography: Geophysical Journal International, v. 184, p. 1037-1057.

6/33. Boccaletti M., Manetti P., Peccerillo A. (1974). The Balkanids as an insta the Hellenids. Geol. Soc. Am. Bull. 85, 1077–1084.

6/34. Bogazici University Earthquake Engineering Reseach Institute. Akkuy. Geotechnical investigations. Istanbul, 1979.

6/35. Bollinger, G.A., F.C. Davison, M.S. Sibol, and J.B. Birch, 1989, "Magnitude Recurrence Relations for the Southeastern United States and its Subdivisions," Journal of Geophysical Research, Vol. 94, No. B3, pp. 2857-2873.

6/36. Bonilla, M.G., Mark,'R.K., and Lienkaemper, V.V., 1984, Statistical relations among earthquake magnitude, surface rupture length, and surface fault displacement: Bulletin of the Seismological Society of America, 74, 2379-2411.

6/37. Boore, D.M. and Atkinson G. M. (2008), "Ground-Motion Prediction Equations for the Average Horizontal Component of PGA, PGV, and 5%-Damped PSA at Spectral Periods between 0.01 s and 10.0 s" Earthquake Spectra, Vol. 24, No. 1, pp: 99–138.

6/38. Bozkur E. (2001). Neotectonics of Turkey – a synthesis. Geodinamica Acta, vol. 14 (1-3), 3-30.

6/39. Boztas M. (1978) – Far distance seismic studies, Içel-Gülnar-Akkuyu, Turkey. MTA (Mineral Research and Exploration Institute), Final Report for TEK (Turkish Electricity Association), 26 p.

6/40. Cagnan Z. and Tanircan G. (2010) – Seismic hazard assessment for Cyprus. Journal of Seismology Volume 14, Number 2, 225-246.

6/41. Calon T.J., Aksu A.E., Hall J. (2005). The Neogene evolution of the Outer Latakia Basin and its extension into the Eastern Mesaoria Basin (Cyprus), Eastern Mediterranean. Marine Geology 221, 61-94.

6/42. Campbell, K. W. and Y. Bozorgnia (2008) "NGA Ground Motion Model for the Geometric Mean Horizontal Component of PGA, PGV, PGD and 5% Damped Linear Elastic Response Spectra for Periods Ranging from 0.01 to 10 s" Earthquake Spectra, Vol. 24, No. 1, pp: 139–171.

6/43. Canitez, N.(1984), Supplement to the Final Seismcity Report of the Akkuyu Nuclear Power Plant Site, Research Report, İstanbul Technical University, Department of Geophysics, Istanbul, Turkey.

6/44. Canitez, N., Eyidogan, H., Buyukaşıkoğlu S., and Ezen, 0., 1989, Microearthquake studies of Akkuyu Nuclear Power Plant Site: Istanbul Technical University Earth Sciences and Resources Research Center, Final Report No. TEK-84-13.

6/45. Catuneanu, O. (2003), Key concepts of sequence stratigraphy: The interplay of base level changes and sediment supply, Geological Association of Canada, Abstracts, 2003

6/46. Cemen I., Goncuoglu M.C. and Dirik K. (1999) – Structural evolution of the Tuzgolu Basin in Central Anatolia, Turkey. The Journal of Geology, 107, p. 603-706.

6/47. Cetin H., Guneylia H., Mayerb L. 2003. Paleoseismology of the Palu-Lake Hazar segment of the East Anatolian Fault Zone, Turkey. Tectonophysics, volume 374, 3-4, 163-197.

6/48. Chiou, B.S:J. and R.R. Youngs (2008) "An NGA Model for the Average Horizontal Component of Peak Ground Motion and Response Spectra" Earthquake Spectra, Vol. 24, No. 1, pp: 173–215.

6/49. Cicek A. and A. Kocyicit (2009). A NNE-trending active graben in the Isparta Angle, SW Turkey: Karamik Graben, its geometry, age and earthquake potential. Trabajos de Geología, Universidad de Oviedo, 29 : 168-174 (2009).

6/50. Cornell, A. (1968) Engineering Seismic Risk Analysis, Bulletin of Seismological Society of America, Vol. 58, No. 5, 1583-1606, October 1968.

6/51. Cosentino D:, Schildgen T. F., Cipollari P., Faranda C., Gliozzi E., Hudácková N., Lucifora S. and M. R. Strecker (2011) - Late Miocene surface uplift of the southern margin of the Central Anatolian Plateau, Central Taurides, Turkey. Geological Society of America Bulletin, B30466.1.

6/52. Cowgill E. (2007) - Neotectonic evidence of active folding in NE Iraq and SE Turkey suggests the Taurus-Zagros thrust belt is underlain by a locked, northeast-dipping megathrust. EGU, Geophysical Research Abstracts, Vol. 9, 04692,

6/53. Demir, T., Yesilnacar, I. and Westaway, R. (2004) - River terrace sequences in Turkey: sources of evidence for lateral variations in regional uplift. Proceedings of the Geologists' Association, 115, 289–311.

6/54. Demirtaşli E. (1984) - Stratigraphic evidence of Variscan and early Alpine tectonics in Southern Turkey. Geological Society London, Special pubblication n° 17, 129-145.

6/55. Demirtaşli E. and M. Genç (1987) - Final Report of the Tectonic Investigation of the Region between Anamur, Gülnar and Mut which Lies to the West and Northwest of the Akkuyu Nuclear Power Plant Site. Turkish Electricity Authority (TEK) Nuclear Power Plants Division.

6/56. Demirtaşli, E. (1982) - "Final Report of the Local Geological Investigations for the Akkuyu Nuclear Power Plant Site, Gulnar Mersin," Mineral Research and Exploration Institute (MTA) Geology Department, Prepared for the Turkish Electricity Authority, July 1982.

6/57. Demirtaşli, E. and M. Genç (1986) - Final Report of the Tectonic Investigation of the Region between the Akkuyu Site, Silifke-Mersin-Tarsus Coastal Area, Adana and Iskenderun Basins, Eçemis Fault Zone, Bolkar Mountains, Ereğli Ulukişla Basin and Eastern Part of the Mut Basin. Turkish Electricity Authority (TEK) Nuclear Power Plants Division. 103 pp.

6/58. Dhont D., Chorowicz J, Yurur T., Froger J.L., Kose O. Gundgdu N. (1988) – Emplacement of volcanic vents and geodynamic of Central Anatolia, Turkey, Journ of Volcanology and Geothermal Research, 85, 33-54.

6/59. Dhont, D., Chorowicz, J., Yurur, T. (1999) The Bolkar Mountains (Central Taurides, Turkey): A Neogene extensional thermal uplift?," Geological Bulletin of Turkey, Vol. 42, Number 2, pp. 69-87. DRAFT Akkuyu Seismic Hazard Assessment Report 112 114545/11 (November 23, 2011)

6/60. Dilek, Y. and Sandvol, E. (2009) Seismic Structure, and Tectonic Evolution of the Anatolian-African Plate Boundary and the Cenozoic Orogenic Belts in the Eastern Mediterranean Region. In: Murphy, J.B., Keppie, J.D., and Hynes, A.J., (Eds.), Ancient Orogens and Modern Analogues, Vol. 327, Geological Society, London, pp. 723-782.

6/61. Dirik K. & M. Göncüoglu C. (1996). Neotectonic Characteristics of Central Anatolia. International Geology Review, vol. 38, 9, pp. 807-817.

6/62. Dirik K, Goncuoglu MC, Kozlu H. (1999). Stratigraphy and pre-Miocene tectonic evolution of the southwestern part of the Sivas Basin, central Anatolia, Turkey. Geological Journal 34: 303-319.

6/63. Doglioni, C., Agostini, S., Crespi, M, Innocenti, F., Manetti, P., Riguzzi, F. and Savasçin, Y. (2002). On the extension in western Anatolia and the Aegean sea. In: Rosenbaum, G.

and Lister, G. S. Reconstruction of the evolution of the Alpine-Himalayan Orogen. Journal of the Virtual Explorer, 8, 161-176.

6/64. EERI-METU, EMCH + Berger Ltd., Basler & Hofmann (1978). NPP Akkiyu, Seismotectonics, Part 1. Berne and Zurich, December 1978.

6/65. EERI-METU, EMCH + Berger Ltd., Basler & Hofmann (1980). Akkuyu NPP, Seismotectonics, Part 2

6/66. EIEI. Akkuyu Nukleer Santral Yeri. Geofizik Arastirmalari/ Sonuc Raporu. 1976.

6/67. Ellenblum R., Marco S., Agnon A., Rockwell T. and Boas A. (1998). Crusader castle torn apart by earthquake at dawn, 20 May 1202. Geology April 1998, v. 26 no. 4 p. 303-306.

6/68. EMCH+BERGER LTD, consulting engineers Berne Switzeland. Geotechnics first unit area (eng) Akkuyu, 1982.

6/69. ENVY (2011) AKKUYU NPP Project. Compiling of Engineering Geological Survey Works. With the implementation of stage II comments. Stage III. AKKUYU NPP Project. ENVY. Ankara, 22.11.2011

6/70. ENVY. Surface geophysical survey. Design stage. Stage III. Ankara, 2013

6/71. ENVY (2011), AKKUYU NPP Project. Geophysical Borehole Surveys. With the implementation of stage II comments. Stage III. ENVY. Ankara, 28.11.2011

6/72. IAEA (2005), Safety Guide. Safety Standards Series. No NS-G-3.6 Geotechnical Aspects of Site Evaluation and Foundations for Nuclear Power Plants, published by IAEA, Vienna, 2005

6/73. ENVY (2011), AKKUYU NPP Project. Surface Geophysical Survey. Stage-II. ENVY. Ankara, 15.09.2011

6/74. ENVY (2011), Report for the Akkuyu Nuclear Power Plant marine hydrological survey works, Stage III, Nov, 2011.

6/75. ENVY (2011), Seismological and seismotectonic investigations of the territory with the implementations of stage II comments. Stage III. Final report of Bogazici University, Kandilli observatory and earthquake research institute. Istanbul. November, 2011.

6/76. ENVY (2012), AKKUYU NPP Project. Engineering-Geological Survey. The well drilling and pumping test methodology for aquifer characterization at Akkuyu nuclear power plant. 2012

6/77. ENVY. Engineering geological survey report. Design stage. Stage III. Ankara, 2012

6/78. ENVY. Integration & analysis of geological & geophysical data. Design stage. Stage III. Ankara, 2012

6/79. ENVY (2012), Report on seismic monitoring at the site and in the nearest region (November 15, 2011 – March 31, 2012). Report of Bogazici University, Kandilli observatory and earthquake research institute. Istanbul. July, 2012.

6/80. ENVY (2012), Report on seismic monitoring at the site and in the nearest region (April 1, 2012 – July 15, 2012). Report of Bogazici University, Kandilli observatory and earthquake research institute. Istanbul. July, 2012.

6/81. ENVY (2012), Report on seismic monitoring at the site and in the nearest region (July 16, 2012 – September 20, 2012). Report of Bogazici University, Kandilli observatory and earthquake research institute. Istanbul. October, 2012.

6/82. ENVY/Eskisehir Osmangazi Univ (2012), Archeoseismological investigations in Seleukeia, Diocaesarea, Olba and Korykos. Stage I. Report by ENVY/Eskisehir Osmangazi Univ., 2012.

6/83. Erdik, M., and Eren, K. (1983). Attenuation of Intensities for Earthquake Associated with the North Anatolian Fault, Middle East Technical University Earthquake Engineering Research Center, Ankara, Turkey.

6/84. Erdik, M., V. Doyuran, P.Gulkan and N. Akkas (1983), A Probabilistic Assessment of the Seismic Hazard in Turkey, METU, EERC Report No: 83-1, March, 1983, Ankara.

6/85. Erdogan S. et al. (2008) - Monitoring of Deformations Along Burdur Fethiye Fault Zone with GPS. Journal of Earthquake Engineering, 12(S2):109–118, 2008.

6/86. Erdoğan, S., M. Sahin, H. Yavasoglu, H. Karaman, T. Erden, S. Bilgi, G. Ruzgar, E. Tari, Z. Coskun, O. Tuysuz, M. Gullu, T. Baybura, Đ. Tiryakioğlu, O. Erdogan, F. Taktak, E. Gokalp, and Y. Boz, 2006, "Monitoring of Deformations Along Fethiye-Burdur Fault Zone (Turkey) with GPS," in "Geodetic Deformation Monitoring: From Geophysical to Engineering Roles," Eds. Sanso, F. and Gil, A. J., International Association of Geodesy Symposia, Springer Berlin Heidelberg, ISBN: 978-3-540-38596-7, pp. 152 – 159, Vol. 131, 2006.

6/87. Erentoz & Ternek eds. (1962) – 1:100000 Geological map of Turkey – Adana Sheet.

6/88. Ergin K., S. Buyukaşıkoğlu (1978), Final Report: Seismicity of Akkuyu Nuclear Power Plant Site and its Vicinity, Research Report, Istanbul Technical University, Department of Geophysics, Istanbul, Turkey.

6/89. Faccenna C., Bellier O., Martinod J., Piromallo C. and Regard V. (2006). Slab detachment beneath eastern Anatolia: A possible cause for the formation of the North Anatolian fault. Earth and Planetary Science Letters 242 (2006) 85– 97.

6/90. Fairbridge, R.W., 1961, Eustatic changes in sea-level. Physics and Chemistry of the Earth, 4:99-185 Londo

6/91. Freund, R., 1965. A model of the structural development of Israel and adjacent areas since Upper Cretaceous times. Geol. Mag. 102, 189–205.

6/92. Garfunkel Z. (2004). Origin of the Eastern Mediterranean Basin: a reevaluation. Tectonophysics, 391, 11-34.

6/93. Geopet Ltd. (2012a). Report of the fault displacement hazard investigations at the Akkuyu NPP site and its vicinity. Demirtasli E., prepared for WorleyParsons, February 2012.

6/94. Geopet Ltd. (2012b). Revised final report related with the tectonic investigations of the region between Akkuyu site, Silifke, Mersin, Taurus coastal area, Ecemis fault zone, Adana and Iskenderun nasins, Misis Mountains area, Clichihan trough, Bolkar Mountains, Eregliulukisla basin and the Eastern part of the Mut basin. Demirtasli E., prepared for WorleyParsons, March 2012

6/95. Gokçen, S., Kelling, G., Ulug, A., and Gokçen, N., (1991). Neotectonic structural features in the Alanya-Mersin shelf area, Jeofizik, 1991, №5, 3-12 (in Turkish).

6/96. Gomez, F., Meghraoui, M., Darkal, A. N., Sbeinati, R., Darawcheh, R., Tabet, C., Khawlie, M., Charabe, M., Khair, K., and Barazangi, M. (2001). Coseismic displacements

along the Serghaya Fault; an active branch of the Dead Sea fault system in Syria and Lebanon. Journal of the Geological Society 158, 405-408.

6/97. Gosatomnadzor (2001), NP-031-01 Norms of designing aseismic nuclear power plants. Moscow, Gosatomnadzor of Russia, 2001.

6/98. Graizer V., Kalkan E. Prediction of spectral acceleration response ordinates based on PGA attenuation // Earthquake Spectra. 2009. V. 25. P. 39-69.

6/99. Grunthal, G., 1998, European macroseismic scale, European Seismological Commission, Sub-commission on Engineering Seismology, Working Group Macroseismic scales, Luxembourg, 99 pp.

6/100. Guidoboni E. and Comastri A. (1997). The large earthquake of 8 August 1303 in Crete: seismic scenario and tsunami in the Mediterranean area. Journal of Seismology, Vol. 1, N. 1, 55-72

6/101. Gulen L., (1999). Seismic activity in the Cyprus region preceding major earthquakes in Turkey, in: Proceedings of the International Conference on Earthquake Hazard and Risk in the Mediterranean Region, H. Gökçekuş (editor), EHRMR'99, vol.1, Near East University Publ., Lefkoşa, 189-199.

6/102. Gulen, L., A. Barka, M. N. Toksoz (1987). Continental collision and related complex deformation: Maraş Triple Junction and surrounding structures, southeastern Turkey, Yerbilimleri (Bull. Earth Sci. Applica. and Res. Center, Hacettepe Univ.), 14, 319-336.

6/103. Hall, J., Aksu, A. E., Yaltırak, C., and Winsor, J. D. (2009). Structural architecture of the Rhodes Basin: A deep depocentre that evolved since the Pliocene at the junction of Hellenic and Cyprus Arcs, eastern Mediterranean. Marine Geology 258, 1-23.

6/104. Hall, J., Hubscher, C., Ehrhardt, A., Dehghani, A., Holz, S., Louden, K., Aksu, A., and Schattner, U. (2010) - From subduction to collision: the role of the Eratosthenes Seamount in the Eastern Mediterranean. Tectonic Crossroads: Evolving Orogens of Eurasia-Africa-Arabia. GSA Meeting 2010.

6/105. Hamouda A.Z. (2006). Numerical computations of 1303 tsunamigenic propagation towards Alexandria, Egyptian Coast, J. African Earth Sci., 44, p. 37-44

6/106. Harvard CMT Project Global CMT Catalog (1976-2010), Harvard University, Cambridge, MA, USA.

6/107. Hempton M.R. and Dewey J.F. (1981) Structure and tectonics of the Lake Hazar pull-apart basin, SE Turkey, Transactions, American Geophysical Union, EOS, 62, 1033.

6/108. Herak, Milan, and V. T Stringfield (1972) Karst, Important Karst Regions of the Northern Hemisphere: Edited by M. Herak and V. T. Stringfield. Amsterdam: Elsevier Pub. Co., 1972.

6/109. Hofstetter R., Klinger Y., Amrat A.Q., Rivera L., and Dorbath L. (2007). Stress tensor and focal mechanisms along the Dead Sea fault and related structural elements based on seismological data: Tectonophysics, v. 429, p. 165-181.

6/110. IAEA (1985), Licensing considerations related to seismicsafety for the Akkuyu nuclear power plant by Aybars Gurpinar, IAEA Expert. Report to the Government of Turkey. December 17, 1984- January 11, 1985.

6/111. IAEA (1985), Review of geological and seismological aspects of Akkuyu site. Report to the Government of Turkey. IAEA-TA-2366. 23 May, 1986.

6/112. IAEA (1996), Yılmaz Bektur, Seismic catalogue of Turkey, 1996 International Atomic Energy Agency (IAEA), Nuclear Safety Department, Turkish Atomic Energy Authority(TAEA), Ankara, 1996.

6/113. IAEA (2010), Specific Safety guide No SSG-9 Seismic Hazard in site evaluation for Nuclear Installations, published by IAEA, Vienna, 2010.

6/114. Imprescia P., S. Pondrelli, G. Vannucci & S. Gresta, (2011). Regional centroid moment tensor solutions in Cyprus from 1977 to the present and seismotectonic implications, J. Seismol., DOI 10.1007/s10950-011-9254-7.

6/115. Inan S., (1993) Morphotectonic and structural characteristics of the Kızılırmak fault zone, Proc. 8th Geol. Cong. Turkey, 321–328.

6/116. International Seismological Centre (ISC), 2011, ISC On-line Bulletin, Thatcham, United Kingdom, Website: <http://www.isc.ac.uk>, Date accessed: 6 April 2011.

6/117. IPE RAS (2011) Elaboration of seismic hazard assessment alternative model for the NPP "Akkuyu" installation site in Turkey based on seismological and seismotectonic conditions. IPE RAS report. Moscow, November 2011.

6/118. Ipek, M., Z. Uz, and U. Gulu, 1965, "Earthquake Regions in Turkey Based on Seismological Data", Technical Report, Istanbul Technical University, Institute of Seismology Doglioni in Turkish].

6/119. IRIS dataset. http://www.iris.edu/hq

6/120. Jackson J. and McKenzie D., 1984, Active tectonics of the Alpine-Himalayan Belt between western Turkey and Pakistan. Geophys. J. R. Astr. Soc., 77, 185-264.

6/121. Jaffey N., Robertson A. (2005) - Non-marine sedimentation associated with oligocene-recent exhumation and uplift of the central Taurus Mountains, S Turkey. Sedimentary Geololy, 173, 53–89.

6/122. Jaffey, N. and A.H.F. Robertson (2001), New Sedimentological and Structural Data from the Ecemiş Fault Zone, Southern Turkey: Implications for its Timing and Offset and the Cenozoic Tectonic Escape of Anatolia, Journal of the Geol. Soc., London, v.158, pp.367-378

6/123. Jeolojik. Geophysical log report of the bore holes. Ankara, 1978.

6/124. Jolivet, L. (2001). A comparison of geodetic and finite strain pattern in the Aegean, geodynamic implications. Earth Planet. Sci. Lett. 187, 95–104.

6/125. Kalafat, D., Y. Güneş, K. Kekovalı, M. Kara, P. Deniz, M. Yılmazer (2011). Bütünleştirilmiş Homojen Türkiye Deprem Kataloğu (1900-2010; M≥4.0). A revised and extended earthquake catalogue for Turkey since 1900, M≥4.0., 640p. Bogazici University Publication.

6/126. Karabacak (2010). Geological, geomorphological and archeaseismological observations along the Cibyra fault and their implications for the Regional Tectonics of SW Turkey. Turkish Journal of Earth Sciences, vol. 20, pp. 429-447.

6/127. Keller, E.A. and Pinter, N., 1996, Active Tectonics, Englewood Cliffs, New Jersey, Prentice Hall Inc. 338 pp.

6/128. Ketin (1966) - Tectonic units of Anatolia, Bull. Miner. Res. Explor. Inst. Turk. 66 (1966), pp. 23–34.

6/129. Khair, K., 2001, "Geomorphology and Seismicity of the Roum Fault as one of the Active Branches of the Dead Sea Fault System in Lebanon", Journal of Geophysical Research, Vol. 106, No. B3, pp. 4233-4245.

6/130. Kissel, C., Laj, C., Poisson, A., G̈or̈ur, N.,(2003) Paleomagnetic reconstruction of the Cenozoic evolution of the Eastern Mediterranean. Tectonophysics 362,199–217.

6/131. Klinger, Y., J.P. Avouac, L. Dorbath, N. Abou Karaki, and N. Tisnerat, 2000b, "Seismic Behavior of the Dead Sea Fault along the Araba Valley, Jordan," Geophysical Journal International, Vol. 142, pp. 769-782.

6/132. Klinger, Y., J.P. Avouac, N. Abou Karaki, L. Dorbath, D. Bourles, J.L. Reyss, 2000a, "Slip Rate on the Dead Sea Transform Fault in Northern Araba Valley (Jordan)," Geophysical Journal International, Vol. 142, pp. 755-768.

6/133. Kocyigit A. and Beyhan A. (1998). A new intracontinental transcurrent structure: the Central Anatolian Fault Zone, Turkey. Tectonophysics, 284, 317-336.

6/134. Koçyigit A., Özacar A., 2003. Extensional Neotectonic Regime through the NE Edge of the Outer Isparta Angle, SW Turkey: New Field and Seismic Data. Turkish Journal of Earth Sciences (Turkish J. Earth Sci.), Vol. 12, 2003, pp. 67-90.

6/135. Koçyiğit, A. & Deveci, Ş., (2007). A N-S-trending active extensional structure, the Şuhut (Afyon) graben: commencement age of the extensional neotectonic period in Isparta Angle, SW Turkey. Turkish Journal of Earth Sciences 16, 391-416.

6/136. Kohketsu. K., The extended reflectivity method for synthetic near-field seismograms, J. Phys. Earth, 33, 121-131, 1985.

6/137. Konstantinou K.I. and Melis N.S. (2008). High-Frequency Shear-Wave Propagation across the Hellenic Subduction Zone. Bull. Seismol. Soc. Am. 98 (2), 797–803

6/138. Kopf, A. (2003). The Mediterranean Ridge: A mass balance across the fastest growing accretionary complex on Earth. Journal of Geophysical Research 108.

6/139. Kreemer C. and Chamot-Rooke N. (2004). Contemporary kinematics of the southern Aegean and the Mediterranean Ridge. Geophys. J. Int. (2004) 157, 1377–1392.

6/140. Kuge, K., Source modeling using strong-motion waveforms: Toward automated determination of earthquake fault planes and moment-release distributions, Bull. Seismol. Soc. Amer., 93, 639-654, 2003.

6/141. Le Beon M., Klinger Y., Agnon A., Dorbath L., Baer G., Meriaux A.S., Ruegg J.C., Charade O., Finkel R., and Ryerson F. (2006). Geodetic versus geologic slip rate along the Dead Sea, Seismological Society of America Annual Meeting, San Francisco.

6/142. Le Beon M., Klinger Y., Amrat A.Q., Agnon A., Dorbath L., Baer G., Ruegg G., Charade J.C. and Mayyas O. (2008). Slip rate and locking depth from GPS profiles across the southern Dead Sea transform. Journ of Geophys. Res. Solid Earth., v. 113.

6/143. Le Pichon, X., Angelier, J., (1979). The Hellenic arc and trench system: a key to the neotectonic evolution of the eastern Mediterranean area. Tectonophysics 60, 1–42.

6/144. Leonard M., (2010). Earthquake Fault Scaling: Self-Consistent Relating of Rupture Length, Width, Average Displacement, and Moment Release. Bull. Seismol. Soc. Am., 100, 1971-1988.

6/145. Marco, S., Hartal, M., Hazan, N., Lev, L., and Stein, M., 2003, Archaeology, history, and geology of the A.D. 749 earthquake, Dead Sea transform: Geology, v. 31, p. 665-668

6/146. Mart, Y. and Ryan, W.B.F. (2003). The Complex Tectonic Regime of Cyprus Arc: A Short Review. Israel Journal of Earth Sciences, 51: 117-134.

6/147. Mart, Y., Ryan, W. (2003) - The tectonics of Cyprus Arc: a model of complex continental collision. EGS-AGU-EUG Joint Assembly, Abstracts from the meeting held in Nice, France, 6-11 April 2003.

6/148. Mc Clusky (2003), Reilinger R., Mahmoud S., Ben Sari D. and Tealeb A.. GPS constraints on Africa (Nubia) and Arabia plate motions. Geophys. J. Int., 155-126-138

6/149. McClusky, S., S. Balassanian, A. Barka, C. Demir, S. Ergintav, ˙I. Georgiev, O. Gurkan, M. Hamburger, K. Hurst, H. Kahle, K. Kastens, G. Kekelidze, R. King, V. Kotzev, O. Lenk, S. Mahmoud, A. Mishin, M. Nadariya, A. Ouzounis, D. Paradissis, Y. Peter, M. Prilepin, R. Reilinger, I. Sanli, H. Seeger, A. Tealeb, M. N. Toksoz, and G. Veis, Global Positioning System constraints on plate kinematics and dynamics in the eastern Mediterranean and Caucasus, J. Geophys. Res., 105(B3), 5695–5719, 2000

6/150. McGuire R. K. Probabilistic Seismic Hazard Analysis and Design Earthquakes: Closing the Loop // Bul. Seismol. Soc. Am. 1995. V. 85(5). P. 1275-1284.

6/151. McGuire, R., 1976. FORTRAN Computer Program for Seismic Risk Analysis, U.S. Geol. Surv. Open-File Rep. 76-67, U.S., Rep. 1-90.

6/152. McKenzie, D. P. 1978. Active tectonism in the Alpine– Himalayan belt: the Aegean Sea and the surrounding regions (tectonics of the Aegean region). Geophysical Journal of the Royal Astronomical Society 55, 217–54.

6/153. McKenzie, D.P, 1972, Active tectonics of the Mediterranean region: Geophys.J.R.Astro.Soc., 30, 109-185.

6/154. METU (1989) Doyuran, V., P. Gulkan and A. Kocyigit, Seismotectonic evaluation of the Akkuyu Nuclear Power Plant site. METU/GGRC, Aug., 1989.

6/155. METU, 1986, Akkuyu II (Camalanı) Nuclear Power Plant, Detailed Site Investigation Report, Earthquake Engineering Research Center, Ankara, Turkey.

6/156. METU, EERI (1979) Earthquake resistant design parameters for the Akkuyu nuclear plant site. Part 1. Report No. 79-4 July, 1979

6/157. Monod O., Kuzucuoglu C. and Okay A. (2006) - A Miocene Palaeovalley Network in the Western Taurus (Turkey). Turkish Journal of Earth Sciences (Turkish J. Earth Sci.), Vol. 15, 2006, pp. 1-23.

6/158. Morishita M. Measuring of the dispersion of individuals and analysis of the distribution patterns// Memorie Fac. Sci. Kyushu Univer. Ser. E. 1959, Vol. 2, .p. 215-235.

6/159. MTA (1977) (Mineral Research and Exploration Institute) – Offshore fault investigation using a high resolution reflection technique, Içel-Gülnar-Akkuyu, Turkey. MTA (Mineral Research and Exploration Institute), Report of Boztas M. for TEK (Turkish Electricity Association), 31 p.

6/160. MTA (1977), Geophysics department of the MTA. Report on the gravity investigations on the NPP site at Akkuyu Turkey, 1977.

6/161. Muhelberger W.R. and Gordon M.B. (1987) - Observations on the complexity of the east anatolian fault, Turkey. Journal of Structural Geology, vol. 9, Issue 7, 1987, Pages 899–903.

6/162. Muir-Wood, R., "From Global Seismotectonics to Global Seismic Hazard", Annali di Geofisica, v.36, pp.153-169, 1993.

6/163. Musson, R. M. W., (2000). Intensity-based Seismic Risk Assessment, Soil Dynamics and Earthquake Engineering, Vol. 20, 353-360.

6/164. MTA. Maden TETKIK VE ARAMA Enstitusu. Icel-Gülnar-Akkuyu. Nukleer Energi Santral Yeri. Rezistivite Calismalari Raporu. Ankara, 1977.

6/165. N.V. Shebalin, S.S. Arefiev, V.Yu.Vasiliev, R.E. Tatevosyan. From seismic sites to seismic structures.//Edited by ASUSSR. Physics of the earth. 1991. No.9, p.20-28.

6/166. Nakamura, Y., A method for dynamic characteristics estimation of subsurface using microtremor on ground surface, Quarterly Report of the Railway Technical Research Institute, 1989, vol. 30, c. 25-33.

6/167. Niemi T.M., Zhang H., Atallah M. and Harrison B.J. (2001). Late Pleistocene and Holocene slip rate of the Northern Wadi Araba fault, Dead Sea transform, Jordan. Journal of Seismology., v. 5, p. 449-474.

6/168. NUREG-0712 Safety Evaluation Report Related to the Operation of San Onofre Nuclear Generating Station, Units 2 and 3, dated February 1981.

6/169. Nutzmann G. A simple finite element method for modeling one-dimension water flow and solute transport in variably saturated soils. Acta Hydrophys., 1991

6/170. Okay, A.I. and Tüysüz, O. (1999) - Tethyan sutures of northern Turkey. In "The Mediterranean Basins: Tertiary extension within the Alpine orogen" (eds. B. Durand, L. Jolivet, F. Horváth and M. Séranne), Geological Society, London, Special Publication 156, 475-515.

6/171. Okay, A.İ. (2008) Geology of Turkey: A synopsis. Anschnitt. 21: 19–42.

6/172. Okyar, M., Ergin, M., & Evans, G. (2005). Seismic stratigraphy of Late Quaternary sediments of western Mersin Bay shelf, (NE Mediterranean Sea). Marine Geology, 220(1-4), 113-130

6/173. Orgulu G. Akta M., Trkelli N., Sandvol E. and Barazangi M. (2003) – Contribution to the seismotectonics of Eastern Turkey from moderate and small size events. Geophysical Research Letters, 30, doi 10.1029/203GL018258.

6/174. Ozaner F.S., Tufekci K.D., (1988) Geomorphology and recent tectonics of the Sqarkıs.la–Gemerek area and its surroundings, J. Geomorph. 16, 53–60.

6/175. Ozel E., Ulug A., and Pekcentinoz (2007). Neotectonic aspects of the northern margin of the Adana – Cilica submarine basin, NE Mediterranean. J. Earth. Sci. 116, 2, April 20117, 113-124.

6/176. Özeren MS, Holt WE (2010) The dynamics of the eastern Mediterranean and eastern Turkey. Geophys J Int 183:1165–1184

6/177. Ozsain E. and Dirik K. (2011) - The role of oroclinal bending in the structural evolution of the Central Anatolian Plateau: evidence of a regional changeover from shortening to extension. Geologica Carpathica, Volume 62, Number 4 / August 2011, 345-359.

6/178. Papadimitriou, E. E. and Karakostas, V. G. (2006) Earthquake generation in Cyprus revealed by the evolving stress field. Tectonophysics, 423: 61-72.

6/179. Papazachos, B. C. and Ch. A. Papaioannou, 1999, "Lithospheric Boundaries and Plate Motions in the Cyprus Area", Tectonophysics, Vol. 308, pp. 193-204.

6/180. Papazachos, B.C., Karakostas, V.G., Papazachos, C.B., Scordilis, E.M. (2000). The geometry of the Wadati-Benioff zone and lithospheric kinematics in the Hellenic arc. Tectonophysics 319, 275–300.

6/181. Perincek, D., and H. Kozlu (1984). Geological Investigation of the Elbistan - Goksun - Sariz Area, International Symposium on the Geology of the Taurus Belt. The Geological Society of Turkey, Special Publication, pp. 181-198.

6/182. Perinçek, D., Y. Gunay, H. Kozlu, New observation on strike-slip faults in East and Southeast Anatolia, 7th Biannual Petroleum Congress of Turkey, Proceeding, pp. 89-103 Ankara (Türkçe).

6/183. Pilidou S., Priestley K., Jackson J. and Maggi A. (2004). The 1996 Cyprus earthquake: a large, deep event in the Cyprian Arc. Geophys. J. Int., 158, 85-97.

6/184. Piper ,J.D.A.,Gürsoy ,H. and Tata R, O (2002). Palaeo-magnetism and magnetic properties of the Cappadocian ignimbrite succession, central Turkey and Neogene tectonics of the Anatolian collage. Journal of Volcanology and Geothermal Research 117

6/185. Power, M., Chiou, B., Abrahamson, N., Bozorgnia, Y., Shantz, T. and Roblee, C. (2008). An overview of the NGA project. Earthquake Spectra 24, 3–21.

6/186. Provision on NPP sites (Official gazette No. 27176. Publishing date 21.03.2009), Turkey.

6/187. Rast, B., and Saegesser, R., 1980, On the systematics in defining seismic zones: Proceedings of the Seventh World Conference on Earthquake Engineering, Istanbul, Turkey, Geoscience Aspects, Part I., 261-268.

6/188. Reasenberg, P.A., 1985: Second-order moment of Central California seismicity. J Geophys Res., 90, 5479–5495.

6/189. Reilinger et al. (2006). GPS constraints on continental deformation in the Africa-Arabia-Eurasia continental collision zone and implications for the dynamics of plate interactions. J. Geophys. Res., Vol. 111, BO5411, doi: 10.1929/2005JBOO4051, p. 1-26.

6/190. Robertson A.H.F., Clift P.D., Degnan P.J., Jones G. (1991). Palaeogeographic and palaeotectonic evolution of the eastern Mediterranean Neotethys. In: Channell, J.E.T., Winterer, E.L., Jansa, L.F. (Eds.), Palaeogeography and Paleoceanography of Tethys: Palaeogeog., Palaeoclim., Palaeoecol., vol. 87, pp. 289–343.

6/191. Robertson, A.H.F. (1998). Mesozoic-Tertiary tectonic evolution of the easternmost Mediterranean area: integration of marine and land evidence. In: Robertson, A.H.F., Eneis, K.C., Richter, C. and Camerlenghi, A. (eds.), Proceed.Ocean Drilling Prog., Scientific Results, 160, 723-782.

6/192. Rumpker G., T. Ryberg, G. Bock and the DESERT Seismology Group (2003). Boundary-layer mantle flow under the Dead Sea Transform fault inferred from seismic anisotropy, Nature, 425, 497–501, doi:10.1038/nature01982.

6/193. S. Arefiev, R.E. Tatevosyan, N.V. Shebalin. Method of measurement of the seismic mode parameters. Innovation. 1989. Application No. 4610030/31-25 of 27.12.90, Moscow, G01V1/00 class.

6/194. S.M. Zverev. Crustal blocks and fractures of the Levant basin. Edited by Svetoch Plus, 2010, p.224.

6/195. Saroglu F., Emre O. and Kuscu I. (1992) – The East Anatolian Fault zone of Turkey. Annales Tectonicae, 99 – 125.

6/196. Satır Erdag D., Tuysuz, O., Akyuz, H.S. (2009) - Ecemiş Fay zonu"num morfotektoniy ozellikleri ve morfometrik analizi. itudergisi/d muhendislik Cilt:8, Sayi:5, 67-79.

6/197. Scordilis, E.M., 2006, "Empirical Global Relations Converting MS and mb to Moment Magnitude," Journal of Seismology, Vol. 10, pp. 225-236.

6/198. Selcuk A.S. & Gokten E. (2011). Neotectonic characteristics of the Inonu-Eskisehir Fault System in the Kaymaz (Eskisehir) Region: influence on the development of the Mahmudiye – Cifteler-Emridag Basin. Turkish Journal of Earth Sciences (Turkish J. Earth Sci. 2011). Doi: 10.3906/yer-0910-30.

6/199. Sengor A. and Yılmaz, Y. (1981). Tethyan evolution of Turkey: a plate tectonic approach, Tectonophysics, 75, 181-241,

6/200. Sengor, A.M.C., Gortir, N., and Şaroglu, F (1985). Strike-slip faulting and related basin formation in zones of tectonic escape: Turkey as a case study, In: Strike-slip Faulting and Basin Formation, K. Biddle and N. Christie-Blick (editors), Special Publication 37, Society of Economic Paleontologists and Mineralogists, Tulsa, Oklahoma.

6/201. Serpelloni E., Vannucci G., Pondrelli S., Argnani A., Casula G., Anzidei M., Baldi P. and GasperiniP. (2007). Kinematics of the Western Africa-Eurasia plate boundary from focal mechanisms and GPS data. Geophys. J. Int. (2007) 169, 1180–1200.

6/202. Sesetyan K., Durukal E., Demircioglu, M.B. and Erdik M., 2005, "A Revised Intensity Attenuation Relationships for Turkey", EGU.

6/203. Seyrek E. (2008). Post-Miocene tectonic evolution of Alidag anticline, Adiyaman, Turkey. Thesis, Graduate School of Natural and Applied Sciences of METU, 115 pp.

6/204. Slemmons, D.B. and CM. dePolo (1986), Determination of earthquake Size, in Proc. of te Conf. XXIV: A Workshop on "Probabilistic Earthquake Hazard Assessments", USGS Open File Report 86-185, Reston, Virginia.

6/205. Slemmons, D.B. and D.H. Chung (1982), Maximum Credible Earthquake Magnitude for the Calevras and Hayward Fault Zones, California, California Division Mines and Geology, Special Publication No: 62, pp. 115-124.

6/206. Sobolev, S. V., Petrunin, A. G., Garfunkel, Z., Babeyko, A. Y. (2003). Thermo-mechanical model of the Dead Sea Transform. Earth and Planetary Science Letters, 238, 1-2, 78-95.

6/207. Stampfli, G.M., and Borel, G.D. (2002). A plate tectonic model for the Paleozoic and Mesozoic constrained by dynamic plate boundaries and restored synthetic ocean isochrons. Earth Planet. Sci. Lett. 196, 17–33.

6/208. Stepp, J. C., (1973). "Analysis of completeness of the earthquake sample in the Puget Sound area", S.T. Handing (Editor), Contributions to Seismic Zoning. NOAA Tech. Rep. ERL 267-ESL 30, U.S. Dep. of Commerce.

6/209. Strasser, F.O., M.C. Arrango, and J.J. Bommer, 2010, "Scaling of the Source Dimensions of Interface and Intraslab Subduction-zone Earthquakes with Moment Magnitude," Seismological Research Letters, Vol. 81, No. 6, pp. 941-950.

6/210. Tan O., Tapirdamaz M.C and Yoruk A. (2008). The Earthquake catalogues for Turkey. Turkish Journal of Earth Sciences, 17, 405-418.

6/211. Taymaz T., Yilmaz Y., and Dilek Y. (2007). The geodynamics of the Aegean and Anatolia: introduction. Geological Society, London, Special Publications 2007, v. 291, p. 1-16, doi: 10.1144/SP291.1.

6/212. TEK (1975) AKKUYU NNP DSI Hydrogeological investigation of submarine springs. Ankara., 1973

6/213. TEK (1975), NED-I-14, Nuclear power plant. Site report, November 1975.

6/214. TEK (1976) NED-I-16, Nuclear power plant. Revised site report, April-1976.

6/215. TEK (1978), Microearthquake study in Akkuyu region (field recording in summer 1977). Project No. TEC-77-01. Final report. ITU. Istanbul, July, 1978.

6/216. TEK (1978), Second microearthquake study in Akkuyu region (field recording in spring 1978). Project No. TEC-77-01.2. Progress report № 1. Istanbul, August, 1978.

6/217. TEK (1978), Seismicity of Akkuyu nuclear power plant site and its vicinity. Project No. TEC-77-02. Final report. ITU. Istanbul, October, 1978.

6/218. TEK (1979), AKKUYU NNP DSI Hydrogeological investigation II. Part progress report. Ankara, 1979

6/219. TEK (1981), AKKUYU NNP. DSI. Geophysical log report in relevant whith unit I, additional drilled wells in the Akkuyu nuclear power plant, 1981.

6/220. TEK (1982), AKKUYU NNP DSI Hydrogeological investigation final report. Ankara 1982

6/221. TEK (1982), Crosshole survey (Turkish). Ankara, 1982.

6/222. TEK (1983), "Akkuyu Nuclear Power Plant: Detailed Site Investigations Report", Turkish Electricity Authority, Nuclear Power Plants Division, NSD-I-29, Turkey, June 1983.

6/223. TEK (1983), AKKUYU NNP Detailed Site Investigation Report. Geotechnics – first unit», part 2, annex 5, 1983

6/224. TEK (1987), Microearthquake studies in Akkuyu nuclear plant site. Project No. TEC-84-11. Final report. ITU. Istanbul, November, 1987.

6/225. TEK, (1983a), Akkuyu Nuclear Power Plant, Detailed Site Investigation Report, Local Geology and Site Geology, Part-II, Annex: 3-4, Nuclear Power Plants Division, Ankara.

6/226. TEK, METU, EERC (1983) Akkuyu nuclear power plant design basis earthquake ground motion. Turkish Electricity Authority, METU/EERC. Ankara. May,1983.

6/227. TEK/KOERI (1990) Akkuyu nuclear power plant design basis ground motion. Report № 90-2. Turkish Electricity Authority, KOERI Bogazici University. Istanbul. May, 1990.

6/228. Ten Veen, J.H., Woodside, M., Zitter, T.A.C., Dumont, J.F., Mascle, J., Volkonskaia, A. (2004) Neotectonic evolution of the Anaximander Mountains at the junction of the Hellenic and Cyprus Arcs. Tectonophysics 391, 35–65.

6/229. Tezcan S., Durgunoğlu T., Acar Y. Akkuyu Nuclear Power Plant, Mersin, Turkey. Geotechnical Investigations. Vol. 1-4. Istanbul, Boğaziçi Üniversity, Earthquake Engineering Research Institute, 1979

6/230. Tibi, R., J. Blanco, and A. Fatehi, 2011, "An Alternative and Efficient Cluster-Link Approach for Declustering of Earthquake Catalogs," Seismological Research Letters, Vol. 82, No. 4, pp. 509-518.

6/231. Ucer, B. and Erdik, M., 1988, Seismicity of the Akkuyu NPP Site and surrounding area: Department of Earthquake Engineering, Kandilli Observatory and Earthquake Research Institute, Bogazici University, Istanbul.

6/232. University of Athens (UOA), 2011, Online Seismological Catalogues, Seismological Laboratory, University of Athens, Greece, Website: http://dggsl.geol.uoa.gr/en_index.html, Accessed: September 27, 2011.

6/233. Van Hinsbergen, D. J. J., Edwards, M. A. & Govers, R. (eds)(2009) Collision and Collapse at the Africa–Arabia–Eurasia Subduction Zone. The Geological Society, London, Special Publications, 311, 1–7.

6/234. Wdowinski, S., Y. (2004) Bock, G. Baer, L. Prawirodirdjo, N. Bechor, S. Naaman, R. Knafo, Y. Forrai, and Y. Melzer (2004). GPS measurements of current crustal movements along the Dead Sea Fault, J. Geophys. Res., 109, B05403, doi:10.1029/2003JB002640.

6/235. Wdowinski, S., Z. Ben-Avraham, R. Arvidsson, and G. Ekstrom, 2006, "Seismotectonics of the Cyprian Arc," Geophysical Journal International, Vol. 164, pp. 176-181.

6/236. Weber, M. (2009), Abu-Ayyash, K., Abueladas, A., Agnon, A., Alasonati Tasárová, Z., Al-Zubi, H., Babeyko, A., Bartov, Y., Bauer, K., Becken, M., Bedrosian, P.A., Ben-Avraham, Z., Bock, G., Bohnhoff, M., Bribach, J., Dulski, P., Ebbing, J., El-Kelani, R., Förster, A., Förster, H.-J., Frieslander, U., Garfunkel, Z., Goetze, H.J., Haak, V., Haberland, C., Hassouneh, M., Helwig, S., Hofstetter, A., Hoffmann-Rothe, A., Jäckel, K.H., Janssen, C., Jaser, D., Kesten, D., Khatib, M., Kind, R., Koch, O., Koulakov, I., Laske, G., Maercklin, N., Masarweh, R., Masri, A., Matar, A., Mechie, J., Meqbel, N., Plessen, B., Möller, P., Mohsen, A., Oberhänsli, R., Oreshin, S., Petrunin, A., Qabbani, I., Rabba, I., Ritter, O., Romer, R.L., Rümpker, G., Rybakov, M., Ryberg, T., Saul, J., Scherbaum, F., Schmidt, S., Schulze, A., Sobolev, S.V., Stiller, M., Stromeyer, D., Tarawneh, K., Trela, C., Weckmann, U., Wetzel, U. and Wylegalla, K. (2009). DESERT Dead Sea Rift Transect: an interdisciplinary research project to study the Dead Sea Transform. STR 09/08.

6/237. Weichert, D.H., 1980, "Estimation of the Earthquake Recurrence Parameters for Unequal Observation Periods for Different Magnitudes," Bulletin of the Seismological Society of America, Vol. 70, No. 4, pp. 1337-1346.

6/238. Wells D.L., and K.J. Coppersmith, 1994, "New Empirical Relationships Among Magnitude, Rupture Length, Rupture Width, Rupture Area, and Surface Displacement, Bulletin of the Seismological Society of America, Vol. 84, pp. 974-1002.

6/239. Westaway R. (1994). Present-day kinematics of the Middle East and eastern Mediterranean. Journ of Geophys. Res., vol. 99, NO. B6, PP. 12,071-12,090, 1994, doi:10.1029/94JB00335

6/240. Westaway R. (1999). Comment on "A new intracontnental transcurrent structure: the Central Anatolian Fault Zone, Turkey", by A. Kocygit and A. Beyhan, Tectonophysics, 314, 469-479.

6/241. Westaway, R. (2004). Kinematic consistency between the Dead Sea Fault Zone and the Neogene and Quaternary left-lateral faulting in SE Turkey. Tectonophysics, 391(1-4), 203-237.

6/242. WorleyParsons (2011), Akkuyu NPP Fault Displacement Hazard Analysis – Photointerpretation Analysis – Site Vicinity Area, version 0, 19 December 2011.

6/243. WorleyParsons (2011), Initial Seismic Input to be provided to the General Designer. Rizzo report prepared for WorleyParsons Nuclear Services JSC. TNPP-00-SV-REP-RU-0039-R0. December 2011.

6/244. WorleyParsons (2012) Report on the Offshore Geophysical Investigations - confirmation of no capable faulting in the offshore area of the Site vicinity, revision 0, 29 February 2012.

6/245. WorleyParsons (2012), Akkuyu NPP Photointerpretation Analysis – Near Region, version 0, 14 January 2012.

6/246. WorleyParsons (2012), Independent Review of the Seismic Hazard Assessment of Akkuyu NPP Site. Final Report. TNPP-00-SV-REP-EN-0061-R1. WorleyParsons, 08 June 2012

6/247. Yetis C. (1978). Geology of the Camardi (Nigde) region and the characteristics of the Ecemis Fault Zone between Maden Bogazi and Kamisli. Istanbul University Fen Fakultesi Mec. Series B, 43, 41-61.

6/248. Yilmaz H., Over S. and Ozden S. (2006). Kinematics of the East Anatolian Fault Zone between Turkoglu (Kahramanmaras) and Celikhan (Adiyaman), eastern Turkey. Earth Planets Space, 58, 1463–1473, 2006.

6/249. Yilmaz Y, Can Genç S., Gürer F., Bozcu M., Yilmaz K., Karacik Z., Altunkaynak S., and Elmas A. (2000). When Did the Western Anatolian Grabens Begin to Develop? In: Bozkurt E., Winchester JA. & Piper J.D.A. (eds). Tectonics and magmatism in Turkey and the suorrounding area. Geological Society London, Sp. Publ., 173, 353-384.

6/250. Youngs, R.R., S.J. Chiou, W.J. Silva, and J.R. Humphrey, 1997, “Strong Ground Motion Attenuation Relationships for Subduction Zone Earthquakes,” Seismological Research Letters, Seismological Society of America, Vol. 68, No. 1, pp. 58-73.

6/251. Zhao, John X., Jian Zhang, Akihiro Asano, Yuki Ohno, Taishi Oouchi, Toshimasa Takahashi, Hiroshi Ogawa, Kojiro Irikura, Hong K. Thio, Paul G. Somerville, Yasuhiro Fukushima, and Yoshimitsu Fukushima, 2006, “Attenuation Relations of Strong Ground Motion in Japan Using Site Classification Based on Predominant Period”, Bulletin of the Seismological % Society of America, Vol. 96, No. 3, pp. 898-913, June 2006.